JACC
Basic to Translational Science

A Journal of the American College of Cardiology

EDITORIAL CONSULTANTS

JACC
Basic to Translational Science
A Journal of the American College of Cardiology

CORRESPONDENCE FOR AMERICAN COLLEGE OF CARDIOLOGY

All correspondence for the College, other than that related to *JACC: Basic to Translational Science* should be sent to Resource Center, American College of Cardiology, 2400 N Street, NW, Washington, DC 20037

Instructions For Authors

JACC: Basic to Translational Science, an open access journal, serves a forum for advancing the field Translational Cardiovascular Medicine, and as a platform for accelerating the translation of novel scientific discoveries into new therapies that improve clinical outcomes for patients affected with or at risk for Cardiovascular Disease. Thematic areas of interest include pre-clinical research; clinical trials; personalized medicine; novel drugs, devices, and biologics; proteomics, genomics and metabolomics; and early phase clinical trial methodology.

We request that all manuscripts be submitted online at http://www.jaccsubmit-basicts.org

Manuscript submissions should conform to the guidelines set forth in the ''Uniform Requirements for Manuscripts Submitted to Biomedical Journals: Writing and Editing for Biomedical Publication,'' available from http://www.ICMJE.org and most recently updated in April 2010.

English language help service: Upon request, Elsevier will direct authors to an agent who can check and improve the English of their paper (before submission). Please contact authorsupport@elsevier.com for further information.

The *JACC* Journals use a single-blind peer-review process. Papers are assigned an Associate Editor, who can assign up to two peer-reviewers, although more can be assigned if necessary.

AUTHOR ENQUIRIES

For enquiries relating to the submission of articles or to articles currently under review, please contact the *JACC: Basic to Translational Science* editorial office at jaccbts@acc.org. For information on articles that have been accepted for publication, please visit Elsevier's Authors Home at www.elsevier.com/authors. Elsevier's Authors Home also provides the facility to track accepted articles and set up e-mail alerts to inform you of when an article's status has changed, as well as detailed artwork guidelines, copyright information, frequently asked questions, and more. Authors can order copies of the issue in which their article appears at a discounted rate; please contact Elsevier Health Sciences Division, Subscription Customer Service, 3251 Riverport Lane, Maryland Heights, MO 63043, Tel: 1-800-654- 2452, E-mail: journalscustomerservice-usa@elsevier.com.

EXCLUSIVE SUBMISSION/PUBLICATION POLICY

Manuscripts are eligible for review only under the conditions that they are not under consideration elsewhere and that the data presented have not appeared on the Internet or have not been previously published (including symposia, proceedings, transactions, books, articles published by invitation, or preliminary publications of any kind except abstracts not exceeding 400 words).

COPYRIGHT

Upon acceptance of an article, authors will be asked to complete an 'Exclusive License Agreement' (for more information see http://www.elsevier.com/OAauthoragreement). Permitted third party reuse of open access articles is determined by the author's choice of user license (see http://www.elsevier.com/openaccesslicenses). As an author you (or your employer or institution) have certain rights to reuse your work. For more information on author rights please see http://www.elsevier.com/copyright.

FUNDING BODY AGREEMENTS AND POLICIES

Elsevier has established a number of agreements with funding bodies which allow authors to comply with their funder's open access policies. Some authors may also be reimbursed for associated publication fees. To learn more about existing agreements please visit http://www.elsevier.com/fundingbodies. After acceptance, open access papers will be published under a noncommercial license. For authors requiring a commercial CC BY license, you can apply after your manuscript is accepted for publication.

OPEN ACCESS

This is an open access journal: all articles will be immediately and permanently available for everyone to read and download without cost. Permitted third party (re)use is defined by the following Creative Commons user licenses (see http://www.elsevier.com/openaccesslicenses):

Creative Commons Attribution-NonCommericial-NoDerivs (CC BY-NC-ND)—For non-commercial purposes, lets others distribute and copy the article, and to include in a collective work (such as an anthology), as long as they credit the author(s) and provided they do not alter or modify the article.

If you need to comply with your funding body policy you can apply for a CC-BY license after your manuscript is accepted for publication.

To provide open access, this journal has an open access fee (also known as an article publishing charge, aka APC) which needs to be paid by the authors or on their behalf, e.g., by their research funder or institution. The open access fee for full articles is $3,200 for members of the American College of Cardiology and $3,400 for non-members, excluding taxes. The open access fee for research letters is $1,600 for members of the American College of Cardiology and $1,700 for non-members, excluding taxes. Learn more about Elsevier's pricing policy: http://www.elsevier.com/openaccesspricing.

RELATIONSHIP WITH INDUSTRY POLICY

Authors are required to disclose any relationship with industry and other relevant entities—financial or otherwise—within the past 2 years that might pose a conflict of interest in connection with the submitted article in both the cover letter and on the title page. All sources of funding for the work should be acknowledged in a footnote on the title page, as should all institutional affiliations of the authors (including corporate appointments). Other kinds of associations, such as consultancies, stock ownership, or other equity interests or patent-licensing arrangements, should be disclosed to the Editors in the cover letter at the time of submission. If no conflict of interest exists, please state this in the cover letter and on the title page. Relationship with industry guidelines apply to authors of all the following: Original Research Papers, State-of-the-Art Papers, Editorials and Viewpoints, Images, Editorial Comments, and Letters to the Editor.

ALL FORMS ARE NOW SIGNED AND SUBMITTED ELECTRONICALLY. Once a manuscript is accepted, the authors will be sent links to complete electronic Copyright Transfer and Relationship with Industry forms. Only the corresponding author may electronically sign the copyright form; however, ALL AUTHORS ARE REQUIRED TO ELECTRONICALLY SIGN A RELATIONSHIP WITH INDUSTRY FORM. Once completed, a PDF version of the form is e-mailed to the author. Authors can access and confirm receipt of forms by logging into their account online. Each author will be alerted if his/her form has not been completed by the deadline. The *JACC* Journals program prefers the term Relationships with Industry and Other Entities as opposed to the term Conflict of Interest, because, by definition, it does NOT necessarily imply a conflict. When all relationships are disclosed with the appropriate detail regarding category and amount, and managed appropriately for building consensus and voting, the *JACC* Journals program believes that potential bias can be avoided and the final published document is strengthened since the necessary expertise is accessible.

Only authors appearing on the final title page will be sent a form. YOU CANNOT ADD AUTHORS AFTER ACCEPTANCE OR ON PROOFS. After a paper is sent to the publisher, the links to the electronic forms will no longer be active. In this case, authors will be sent links to download hard

copy forms that they may mail or fax to the *JACC: Basic to Translational Science* office.

ETHICS

Studies should be in compliance with human studies committees and animal welfare regulations of the authors' institutions and Food and Drug Administration guidelines.

Human studies must be performed with the subjects' written informed consent. Authors must provide the details of this procedure and indicate that the institutional committee on human research has approved the study protocol. If radiation is used in a research procedure, the radiation exposure must be specified in the Methods. Clinical trials should be registered.

Studies on patients or volunteers require ethics committee approval and informed consent which should be documented in your paper. Patients have a right to privacy. Therefore, identifying information, including patients' images, names, initials, or hospital numbers, should not be included in videos, recordings, written descriptions, photographs, and pedigrees unless the information is essential for scientific purposes and you have obtained written informed consent for publication in print and electronic form from the patient (or parent, guardian or next of kin where applicable). If such consent is made subject to any conditions, the editorial office must be made aware of all such conditions.

Written consents must be provided to the editorial office on request. Even where consent has been given, identifying details should be omitted if they are not essential. If identifying characteristics are altered to protect anonymity, such as in genetic pedigrees, authors should provide assurance that alterations do not distort scientific meaning and editors should so note. If such consent has not been obtained, personal details of patients included in any part of the paper and in any supplementary materials (including all illustrations and videos) must be removed before submission. Animal investigation must conform to the ''Position of the American Heart Association on Research Animal Use,'' adopted by the AHA on November 11, 1984. If equivalent guidelines are used, they should be indicated. The AHA position includes: 1) animal care and use by qualified individuals, supervised by veterinarians, and all facilities and transportation must comply with current legal requirements and guidelines; 2) research involving animals should be done only when alternative methods to yield needed information are not possible; 3) anesthesia must be used in all surgical interventions, all unnecessary suffering should be avoided and research must be terminated if unnecessary pain or fear results; and 4) animal facilities must meet the standards of the American Association for Accreditation of Laboratory Animal Care (AAALAC).

The *JACC* Journals has an ethics committee comprised of 7 members, which oversees quality control and will look into the issues of concern, if any.

AUTHORSHIP/COVER LETTER

Each author must have contributed significantly to the submitted work. If there are more than 4 authors, the contribution of each must be substantiated in the cover letter. If authorship is attributed to a group (either solely or in addition to 1 or more individual authors), all members of the group must meet the full criteria and requirements for authorship. To save space, if group members have been listed in *JACC: Basic to Translational Science*, the article should be referenced rather than reprinting the list. The Editors consider authorship to include all of the following: 1) conception and design or analysis and interpretation of data, or both; 2) drafting of the manuscript or revising it critically for important intellectual content; and 3) final approval of the manuscript submitted. Participation solely in the collection of data does not justify authorship but may be appropriately acknowledged in the Acknowledgment section.

Manuscripts must be submitted with a cover letter stating: 1) the paper is not under consideration elsewhere; 2) none of the paper's contents have been previously published; 3) all authors have read and approved the manuscript; and 4) the full disclosure of any potential conflict of interest (see ''Relationship With Industry Policy''). Exceptions must be explained. If there is no conflict of interest, this should also be stated in the cover letter.

The corresponding author should be specified in the cover letter. All editorial communications will be sent to this author. The corresponding author will be whom we contact for submission queries.

GENERAL GUIDELINES FOR SUBMISSION OF ORIGINAL RESEARCH PAPERS

JACC: Basic to Translational Science is not restricted to page length, however the Editors prefer that manuscripts not exceed 5,500 words (including references and figure legends). Note that if you are asked to revise your paper an alternate word limit may be specified by the Editors. Illustrations and tables should be limited to those necessary to highlight key data. Please provide gender-specific data, when appropriate, in describing outcomes of epidemiologic analyses or clinical trials; or specifically state that no gender-based differences were present.

The manuscript should be arranged as follows: 1) title page; 2) structured abstract and key words; 3) condensed abstract; 4) abbreviations list; 5) text; 6) acknowledgments (if applicable); 7) Funding Sources 8) references; 9) figure titles and legends; and 10) tables.

OTHER PAPER CATEGORIES

The following information should be noted for these paper types:

STATE-OF-THE-ART PAPERS. The Editors will consider both invited and volunteered review articles. Such manuscripts must adhere to preferred length guidelines of no more than 5,000 words and require an unstructured abstract, a central illustration and a list of 3-4 brief (15 words or fewer for each bullet, or 85 characters for each bullet) bullet points that highlight the main message of the review. The first bullet should provide the translational/clinical context or background that establishes the relevance or need for this review. The second bullet should speak to the main message and focus of the review, including any recommendations made by the authors. The final bullet should summarize where the field needs to move forward from this point. Authors should detail in their cover letters how their submission differs from existing reviews on the subject.

Example of bullet points:

- The acute inflammatory response is a critical mechanism for host defense, whereas the resolution of inflammation is equally important for tissue homeostasis by delimiting the destructive effects of chronic inflammation.
- This review will discuss the role of the activation of the G-protein coupled formyl peptide receptor 2 (ALX/FPR2) in terms of regulating the resolution of inflammation following tissue injury, and will specifically focus on the role of lipid mediators in activating the ALX/FPR2 receptor.
- Additional studies will be required to clarify whether activation of the ALX/FPR2 receptor can be used therapeutically to prevent chronic inflammation, scar tissue formation following acute tissue injury.

LEADING EDGE TRANSLATIONAL RESEARCH articles are discrete, highly significant, innovative or novel findings reported in a shorter format of 3,500 words or fewer in length. Editors will review for interest within seven (7) days of submission. These may be invited or volunteered manuscripts.

TRANSLATIONAL PERSPECTIVES. Although usually invited, succinct opinion pieces relevant to a specific aspect of translational medicine will also be considered for *JACC: Basic to Translational Science*. They should not exceed 2,500 words and should have no more than a total of 2 figures and tables than 5 references.

RESEARCH LETTERS. Both Research Letters and Letters to the Editor are published under the heading "Letters." *JACC: Basic to Translation Science* will publish a limited number of research letters that are tightly focused on a new or novel research observation. Research letters will generally be solicited by the Editors; however, authors can also submit original investigations of a focused nature as a research letter. Research Letters should be submitted online at www.jaccsubmit-basictr.org. They should not exceed 1000 words, including references and figure legend, with no more than 5 references, one Figure (in no more than 2 parts) or one simple Table. A title page is required. Online or Supplemental Material is not permitted.

LETTERS TO THE EDITOR AND REPLIES. *JACC: Basic to Translation Science* will publish a limited number of letters that focus on a specific manuscript that has appeared in the journal. Letters must be submitted within 3 weeks of the issue date of the article. *JACC: Basic to Translation Science* does not consider letters to the editor on review articles, editorials, or any correspondence, including research letters. Letters should be submitted online at www.jaccsubmit-basictr.org. They should not exceed 500 words, including references and figure legend, with no more than 5 references, one Figure (in no more than 2 parts) or one simple Table. A title page is required with a unique title of 15 words or less that does not include the title of the original research paper. Replies will generally be solicited by the Editors.

MANUSCRIPT CONTENT

TITLE PAGE

Include the full title, authors' names (including full first name and middle initial and degrees), total word count, and a brief title of no more than 15 words. List the departments and institutions with which the authors are affiliated, and indicate the specific affiliations if the work is generated from more than one institution (use superscript letters [a, b, c, d], and so on). Also provide information on grants, contracts, and other forms of financial support, and list the cities and states of all foundations, funds and institutions involved in the work. Include any relationship with industry (see "Relationship With Industry Policy"). If there are no relationships with industry, this should be stated. Under the heading, "Address for correspondence," give the full name and complete postal address of the author to whom communications, author proofs, and reprint requests should be sent. Also provide telephone and fax numbers and an email address for the corresponding author.

STRUCTURED ABSTRACT

Provide a structured abstract of no more than 250 words, presenting essential data in 5 paragraphs introduced by separate headings in the following order: Objectives, Background, Methods, Results, and Conclusions. Use complete sentences. All data in the abstract must also appear in the manuscript text or tables. For general information on preparing structured abstracts, see "Haynes RB, Mulrow CD, Huth EJ, Altman DG, Gardner MJ. More informative abstracts revisited. Ann Intern Med 1990;113:69-76." An unstructured abstract is appropriate for review articles.

For accepted papers, authors will be asked to provide a list of bulleted highlights and a summary to replace the abstract (see Visual Abstract instructions below).

CONDENSED ABSTRACT

Provide a condensed abstract of no more than 100 words, stressing clinical implications, for the expanded table of contents. Include no data that do not also appear in the manuscript text or tables.

TEXT

The text should be structured as Introduction, Methods, Results, and Discussion. Use headings and subheadings in the Methods, Results, and particularly, Discussion sections. Every reference, figure, and table should be cited in the text in numerical order according to order of mention.

The abbreviations of common terms (e.g., ECG, PTCA, CABG) or acronyms (GUSTO, SOLVD, TIMI) may be used in the manuscript. On a separate page following the condensed abstract, list the selected abbreviations and their definitions (e.g., TEE = transesophageal echocardiography). The Editors may determine which lesser known terms should not be abbreviated. Please consult "Uniform Requirements for Manuscripts Submitted to Biomedical Journals: Writing and Editing for Biomedical Publication," available from http://www.ICMJE.org and most recently updated in April 2010, for appropriate use of units of measure.

STATISTICS

All publishable manuscripts will be reviewed for appropriateness and accuracy of statistical methods and statistical interpretation of results. We subscribe to the statistics section of the "Uniform Requirements for Manuscripts Submitted to Biomedical Journals: Writing and Editing for Biomedical Publication," available from http://www.ICMJE.org and most recently updated in April 2010. In the Methods section, provide a subsection detailing the statistical methods, including specific methods used to summarize the data, methods used for hypothesis testing (if any), and the level of significance used for hypothesis testing. When using more sophisticated statistical methods (beyond *t* tests, chi-square, simple linear regression), specify the statistical package, version number, and nondefault options used. For more information on statistical review, see "Glantz SA. It is all in the numbers. J Am Coll Cardiol 1993;21:835-7."

PERSPECTIVES

The authors should delineate clinical implications and translational outlook recommendations for their manuscripts. These should be listed in the manuscript after the Text and before the Acknowledgments and References. Please review the examples provided below. The implications describe the consequences of the study for current practice. The translational outlook identifies the potential barriers to clinical translation, emphasizing directions for additional research.

Clinical Competencies. Competency-based learning in cardiovascular medicine addresses the 6 domains promulgated by the Accreditation Council on Graduate Medical Education (ACGME) and endorsed by the American Board of Internal Medicine (Medical Knowledge, Patient Care and Procedural Skills, Interpersonal and Communication Skills, Systems-Based Practice, Practice-Based Learning, and Professionalism) (www.acgme.org/acgmeweb). The ACCF has adopted this format for its competency and training statements, career milestones, lifelong learning, and educational programs. The ACCF also has developed tools to assist physicians in assessing, enhancing, and documenting these competencies (www.acc.org/Lifelong-Learning-and-MOC/Resources/Competencies).

Authors are asked to consider the clinical implications of their report and identify applications in one or more of these competency domains that could be used by clinician readers to enhance their competency as professional caregivers.

This applies not only to physicians in training, but to the sustained commitment to education and continuous improvement across the span of their professional careers.

Translational Outlook. Translating biomedical research from the laboratory bench, clinical trials or global observations to the care of individual patients can expedite discovery of new diagnostic tools and treatments through multidisciplinary collaboration. Effective translational medicine facilitates implementation of evolving strategies for prevention and treatment of

disease in the community. The Institute of Medicine identified two areas needing improvement: testing basic research findings in properly designed clinical trials and, once the safety and efficacy of an intervention has been confirmed, more efficiently promulgating its adoption into standard practice (Sung NS, Crowley WF, Genel M. The meaning of translational research and why it matters. JAMA 2008;299:3140-3148).

The National Institutes of Health (NIH) has recognized the importance of translational biomedical research, emphasizing multifunctional collaborations between researchers and clinicians to leverage new technology and accelerate the delivery of new therapies to patients (www.ncats.nih.gov/about/about.html).

Authors are asked to place their work in the context of the scientific continuum, by identifying impediments and challenges requiring further investigation and anticipating next steps and directions for future research.

VISUAL ABSTRACT

A visual abstract is a single, concise, pictorial summary of the main findings of the article. Our in-house medical illustrators will create the final printable versions of these figures in consultation with the Editor-in-Chief and the authors. The visual abstract is specially designed to be placed at the beginning of the article and is accompanied by 3-5 "bulleted highlights" and a short summary written by the author and ultimately replaces the written abstract. See examples of articles with visual abstracts:

Example #1: http://basictranslational.onlinejacc.org/content/1/1-2/3

Example #2: http://basictranslational.onlinejacc.org/content/1/1-2/32

ACKNOWLEDGMENTS

Acknowledgments or appendices should be concise. Signed letters of permission from all individuals listed in the acknowledgments must be submitted to *JACC: Basic to Translational Science*.

REFERENCES

Identify references in the text by Arabic numerals in parentheses on the line. The reference list should be typed double-spaced on pages separate from the text. The references should be numbered consecutively in the order in which they are mentioned in the text.

Do not cite personal communications, manuscripts in preparation, or other unpublished data in the references; however, these may be included in the text in parentheses. *Do not cite abstracts that are older than 2 years.* Identify abstracts by the abbreviation "abstr" in parentheses. If letters to the editor are cited, identify them with the word "letter" in parentheses.

Use *Index Medicus* (National Library of Medicine) abbreviations for journal titles. It is important to note that when citing an article from the *JACC: Basic to Translational Science*, the correct citation format is J Am Coll Cardiol Basic Trans Science.

Use the following style and punctuation for references:

Periodical

List all authors if 6 or fewer, otherwise list the first 3 and add et al.; do not use periods after the authors' initials. Please do provide inclusive page numbers as in example below.

5. Glantz SA. It is all in the numbers. J Am Coll Cardiol 1993; 21:835-7.

Doi-based citation for an article in press

If the ahead-of-print date is known, provide as in example below.

16. Winchester D, Wen X, Xie L, et al. Evidence for pre-procedural statin therapy: meta-analysis of randomized trials. J Am Coll Cardiol 2010 Sept 28 [E-pub ahead of print], http://dx.doi.org/10.1016/j.jacc.2010.09.028.

If the ahead-of-print date is unknown, omit as in example below.

16. Winchester D, Wen X, Xie L, et al. Evidence for pre-procedural statin therapy: meta-analysis of randomized trials. J Am Coll Cardiol 2010 [E-pub ahead of print], http://dx.doi.org/10.1016/j.jacc.2010.

Chapter in book

Provide authors, chapter title, editor(s), book title, publisher location, publisher name, year, and inclusive page numbers.

27. Meidell RS, Gerard RD, Sambrook JF. Molecular biology of thrombolytic agents. In: Roberts R, editor. Molecular Basis of Cardiology. Cambridge, MA: Blackwell Scientific Publications, 1993:295-324.

Online media

Provide specific URL address and date information was accessed.

10. Henkel J. Testicular Cancer: Survival High With Early Treatment. FDA Consumer magazine [serial online]. January-February 1996. Available at: http://www.fda.gov/fdac/features/196_test.html. Accessed August 31, 1998.

Material presented at a meeting but not published

Provide authors, presentation title, full meeting title, meeting dates, and meeting location.

20. Eisenberg J. Market forces and physician workforce reform: why they may not work. Paper presented at: Annual Meeting of the Association of Medical Colleges; October 28, 1995; Washington, DC.

FIGURE LEGENDS

Figure legends should be typed double-spaced on pages separate from the text; figure numbers must correspond with the order in which they are mentioned in the text.

ALL FIGURES MUST HAVE A TITLE AS WELL AS A CAPTION.

For example, Figure 1: Title - Caption, etc.

All abbreviations used in the figure should be identified either after their first mention in the legend or in alphabetical order at the end of each legend.

All symbols used (arrows, circles, etc.) must be explained.

If previously published figures are used, written permission from the original publisher is required. See STM Guidelines for details: http://www.stm-assoc.org/permissions-guidelines. Cite the source of the figure in the legend.

FIGURES

Figures and graphs submitted in electronic format should be provided in EPS or TIF format. Graphics software such as Photoshop and Illustrator, NOT presentation software such as Powerpoint, CorelDraw, or Harvard Graphics, should be used to create the art. Color images must be at least 300 DPI. Gray scale images should be at least 300 DPI. Line art (black and white or color) should be at least 1200 DPI and combinations of gray scale images and line art should be at least 1200 DPI. Lettering should be of sufficient size to be legible after reduction for publication. The optimal size is 12 points. Symbols should be of a similar size. Figures should be no smaller than 13 cm× 18 cm (5″ × 7″). Please do not reduce figures to fit publication layout. If the manuscript is accepted for publication, the publisher will re-size the figures accordingly.

ALL FIGURES MUST HAVE A TITLE AND A LEGEND.

Our editors encourage authors to submit figures in color, as we feel it improves the clarity and visual impact of the images. If your original submission contains any line art or black and white figures that you would like to change to color, please email the revised color figures to the *JACC: Basic to Translational Science* editorial office during the revision process. Be sure to include correspondence, with the manuscript number, explaining the change.

Decimals, lines, and other details must be strong enough for reproduction.

Designate special features with arrows. All symbols, arrows, and lettering on halftone illustrations must contrast with the background.

TABLES

Tables should be typed double-spaced on separate sheets, with the table number and title centered above the table and explanatory notes below the table. Use Arabic numbers. Table numbers must correspond with the order cited in the text.

ALL TABLES MUST HAVE A TITLE.

Abbreviations should be listed in a footnote under the table in alphabetical order. Footnote symbols should appear in the following order: *, †, ‡, §, ||, ¶, #, **, ††, etc.

Tables should be self-explanatory, and the data presented in them should not be duplicated in the text or figures. If previously published tables are used, written permission from the copyright holder (typically the original publisher) is required. Cite the source of the table in the legend.

VIDEO REQUIREMENTS

Inclusion of videos in the published paper is at the discretion of the Editors.

1. Video submissions for viewing online should be one of the following formats: Audio Video Interleave (.avi), MPEG (.mpg), or Quick Time (.qt, .mov).

   AVI files can be displayed via Windows Media Player

   MPEG files can be displayed via Windows Media Player

   http://www.microsoft.com/windows/windowsmedia

   http://www.microsoft.com/windows/windowsmedia/players.aspx

   Quick Time files require Quick Time software (free) from Apple, http://www.apple.com/quicktime/download/index.html
2. Videos should be brief (<2-5 min). Longer videos will require longer download times and may have difficulty playing online. Videos should be restricted to the most critical aspects of your research. A longer procedure can be restructured as several shorter videos and submitted in that form.
3. It is advisable to compress files to use as little bandwidth as possible and to avoid overly long download times. Video files should be no larger than 5 megabytes. This is a suggested maximum. If files are larger please contact the *JACC: Basic to Translational Science* office.
4. A video legends page giving a brief description of the content of each video should be included in the manuscript. Please note that ALL videos must be linked to figures or panels of a figure(s).
5. If your paper is accepted for publication you may wish to supply the editorial office with several different resolutions of your video files. This will allow viewers with slower connections to download a lower resolution version of your video.

It is important to note that when citing an article from *JACC: Basic to Translational Science*, the correct citation format is J Am Coll Cardiol Basic Trans Science

JACC: BASIC TO TRANSLATIONAL SCIENCE
PUBLISHED BY ELSEVIER ON BEHALF OF THE AMERICAN COLLEGE OF CARDIOLOGY FOUNDATION.

VOL. 4, NO. 1, 2019

LEADING EDGE TRANSLATIONAL RESEARCH

Neutrophil Subsets, Platelets, and Vascular Disease in Psoriasis

Heather L. Teague, PhD,[a] Nevin J. Varghese, BS,[a] Lam C. Tsoi, PhD,[b] Amit K. Dey, MD,[a] Michael S. Garshick, MD,[c] Joanna I. Silverman, BA,[a] Yvonne Baumer, PhD,[a] Charlotte L. Harrington, BA,[a] Erin Stempinski, MS,[a] Youssef A. Elnabawi, BS,[a] Pradeep K. Dagur, PhD,[a] Kairong Cui, PhD,[a] Ilker Tunc, PhD,[a] Fayaz Seifuddin, MSc,[a] Aditya A. Joshi, MD,[a] Elena Stansky, BS,[a] Monica M. Purmalek, BS,[d] Justin A. Rodante, PA,[a] Andrew Keel, DNP,[a] Tarek Z. Aridi, BS,[a] Carmelo Carmona-Rivera, PhD,[d] Gregory E. Sanda, BS,[a] Marcus Y. Chen, MD,[a] Mehdi Pirooznia, MD, PhD,[a] J. Philip McCoy, Jr, PhD,[a] Joel M. Gelfand, MD,[e,f] Keji Zhao, PhD,[a] Johann E. Gudjonsson, MD, PhD,[b] Martin P. Playford, PhD,[a] Mariana J. Kaplan, MD,[d] Jeffrey S. Berger, MD,[c] Nehal N. Mehta, MD[a]

VISUAL ABSTRACT

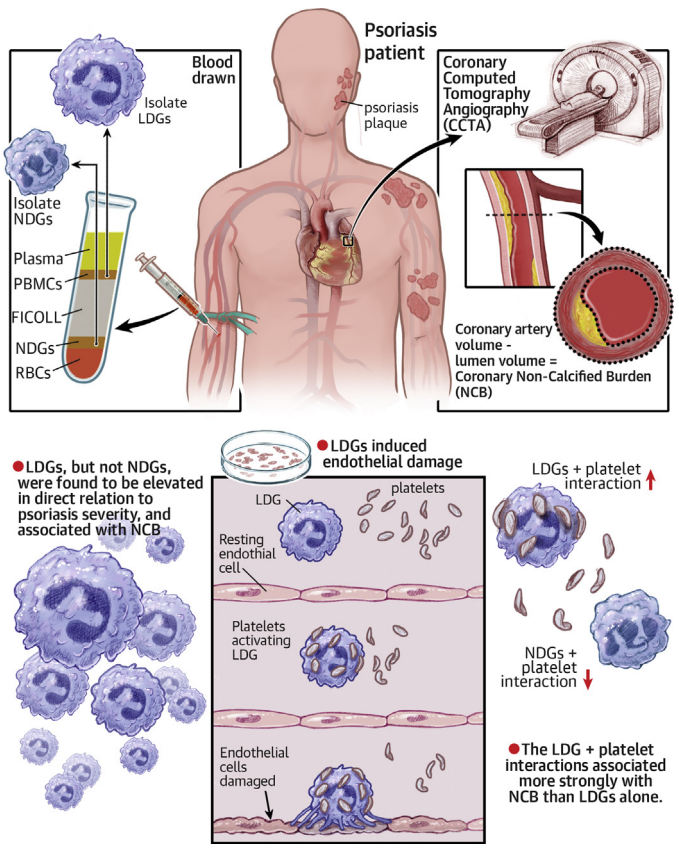

Teague, H.L. et al. J Am Coll Cardiol Basic Trans Science. 2019;4(1):1-14.

HIGHLIGHTS

- **LDGs are a subset of neutrophils that were elevated in psoriasis and associated with the severity of disease.**
- **In psoriasis, LDGs associated with noncalcified coronary plaque burden beyond cardiovascular risk factors and *in vitro*, induced endothelial cell damage.**
- **Compared to normal-density granulocyte neutrophils, platelet-associated biological pathways were upregulated in LDGs, suggesting enhanced platelet adherence to the LDG surface.**
- **LDGs co-localized with platelets in circulation, and the LDG-platelet interaction associated more strongly with non-calcified coronary burden by coronary CTA compared to LDGs alone.**

ISSN 2452-302X https://doi.org/10.1016/j.jacbts.2018.10.008

JACC: BASIC TO TRANSLATIONAL SCIENCE VOL. 4, NO. 1, 2019
FEBRUARY 2019:1–14

ABBREVIATIONS AND ACRONYMS

CCTA = coronary computed tomography angiography

CVD = cardiovascular disease

FDR = false discovery rate

HAoEC = human aortic endothelial cell

LDG = low-density granulocyte

MI = myocardial infarction

NCB = noncalcified coronary plaque burden

NDG = normal-density granulocyte

NET = neutrophil extracellular trap

PASI = psoriasis area severity index

SLE = systemic lupus erythematosus

TB = total coronary plaque burden

SUMMARY

Psoriasis is an inflammatory skin disease associated with increased cardiovascular risk and serves as a reliable model to study inflammatory atherogenesis. Because neutrophils are implicated in atherosclerosis development, this study reports that the interaction among low-density granulocytes, a subset of neutrophils, and platelets is associated with a noncalcified coronary plaque burden assessed by coronary computed tomography angiography. Because early atherosclerotic noncalcified burden can lead to fatal myocardial infarction, the low-density granulocyte–platelet interaction may play a crucial target for clinical intervention.

Psoriasis is a chronic inflammatory, immune-mediated skin disease that affects 2% to 3% of the adult U.S. population (1-3). Psoriasis is associated with detrimental effects beyond the skin; it significantly reduces the quality of life through emotional and physical complications (4). Most concerning, multiple studies have demonstrated that psoriasis patients have increased susceptibility to early-onset atherosclerosis and its ensuing complications, including myocardial infarction (MI), stroke, and cardiovascular mortality beyond traditional cardiovascular disease (CVD) risk factors (1,2,5,6). CVD is the leading cause of mortality in psoriasis, especially in patients with severe psoriasis (7,8).

The immune response plays a pivotal role in the development of atherosclerosis, with neutrophils playing an important role in plaque progression (9-11). Circulating neutrophil frequency is reported to be a potential biomarker of CVD (12), and in inflammatory diseases such as systemic lupus erythematosus (SLE), rheumatoid arthritis, and HIV, neutrophils are associated with accelerated atherogenesis (13-15). Circulating neutrophils in psoriasis exhibit an activated phenotype, and the inflammatory neutrophil protein calprotectin (S100A8/A9) is elevated in psoriasis (16). Moreover, S100A8/A9 is related to vascular disease. Neutrophils are the foremost immune cells to infiltrate the papillary layer and subepidermal zone of the skin before psoriatic lesion formation, which suggests they may be a potential link between early-onset CVD and psoriasis (17). The distinct subset of neutrophils termed low-density granulocytes (LDGs) are of particular interest. LDGs are neutrophils purified from the less dense peripheral blood mononuclear cell (PBMC) fraction after density gradient centrifugation (18-20) and are associated with CVD in chronic inflammatory disease states (19,21). LDGs have an enhanced capacity to spontaneously form neutrophil extracellular traps (NETs), a cell death process termed

From the [a]National Heart, Lung, and Blood Institute, National Institutes of Health, Bethesda, Maryland; [b]Department of Dermatology, University of Michigan, Ann Arbor, Michigan; [c]Department of Medicine, Division of Cardiology, New York University School of Medicine, New York, New York; [d]Systemic Autoimmunity Branch, National Institute of Arthritis and Musculoskeletal and Skin Diseases, National Institutes of Health, Bethesda, Maryland; [e]Department of Dermatology, Perelman School of Medicine, Philadelphia, Pennsylvania; and the [f]Department of Biostatics, Epidemiology, and Informatics, Perelman School of Medicine, Philadelphia, Pennsylvania. This study was supported by the National Heart, Lung, and Blood Institute Intramural Research Program (HL006193-02). This research was also made possible through the National Institutes of Health (NIH) Medical Research Scholars Program, a public-private partnership supported jointly by the NIH and generous contributions to the Foundation for the NIH from the Doris Duke Charitable Foundation (DDCF Grant #2014194), the American Association for Dental Research, the Colgate-Palmolive Company, Genentech, Elsevier, and other private donors. Dr. Mehta was supported National Institutes of Health Intramural Research Program (Z01 HL-06193). Dr. Gelfand has received honoraria and served as a consultant for Coherus (Data and Safety Monitoring Board), Dermira, Janssen Biologics, Merck (Data and Safety Monitoring Board), Novartis Corp., Regeneron, Dr. Reddy's labs, Sanofi, and Pfizer Inc.; has received research grants from Abbvie, Janssen, Novartis Corp., Regeneron, Sanofi, Celgene, and Pfizer Inc.; has received payment for continuing medical education work related to psoriasis that was supported indirectly by Lilly and Abbvie; and he is a co-patent holder of resiquimod for treatment of cutaneous T-cell lymphoma. Dr. Gudjonsson has received research grants from SunPharma and AbbVie; and has served on the advisory boards for Novartis, Kirn, and MiRagen. Dr. Mehta has received research grants from Abbvie, Janssen, Novartis Corp, and Celgene. All other authors have reported that they have no relationships relevant to the contents of this paper to disclose.

All authors attest they are in compliance with human studies committees and animal welfare regulations of the authors' institutions and U.S. Food and Drug Administration guidelines, including patient consent where appropriate. For more information, visit the *JACC: Basic to Translational Science* author instructions page.

Manuscript received September 4, 2018; revised manuscript received October 29, 2018, accepted October 31, 2018.

NETosis, which is characterized by the extracellular release of chromatin material bound to proteins present in neutrophil granules (22-24). However, the stimulus that activates the spontaneous NETosis mechanism in LDGs in inflammatory diseases remains unclear.

Activated platelets have been described to play a role among the various stimuli known to induce NETs (25-27). Platelet activation characterized by the expression of platelet activation molecules (e.g., CD36) is associated with atherosclerosis and other inflammatory conditions (25,26). Although platelets are involved in NET formation, only a few studies have investigated this in nonchronic inflammatory states (25,26). Furthermore, when spontaneous NETosis occurred at a higher frequency in a small preliminary study, it was not studied, but the reason may be related, in part, to unexplored neutrophil–platelet interactions (28).

In the present study, we aimed to characterized LDGs and normal-density granulocytes (NDGs) in psoriasis. Our goal was to understand the potential relationship between neutrophil subsets and the presence of early coronary artery disease in humans with psoriasis. We hypothesized that LDGs would be associated with psoriasis skin disease severity and early noncalcified coronary plaque burden (NCB) as assessed by coronary computed tomography angiography (CCTA). Subsequently, we identified the interaction between LDGs and platelets as a prospective mechanism that stimulated increased LDG NETosis, which resulted in endothelial damage.

METHODS

STUDY POPULATION. Study approval for the cohort study was obtained from the Institutional Review Board of the National Heart, Lung, and Blood Institute in accordance with the principles of Declaration of Helsinki. This study reported the baseline visits of patients recruited longitudinally and consecutively into 2 ongoing protocols from January 2013 to May 2017 (Supplemental Figure 1). To be included in the study, psoriasis patients were required to have a formal diagnosis of psoriasis confirmed by a health care provider. All patients underwent CCTA to assess coronary plaque burdens, as described previously (29). Psoriasis skin disease severity was assessed with the psoriasis area and severity index (PASI) score and was measured as published (30). The PASI score combines the severity of lesions and the area affected into a single score, considering erythema, induration, and desquamation within each lesion. A combination of isolation and flow cytometry was used to determine the frequencies of LDGs and NDGs for each patient. Exclusion criteria for healthy control subjects included a history of systemic inflammatory or vascular disease, active infectious disease, uncontrolled hypertension, and overweight to obese individuals (body mass index >30 kg/m^2). In total, 81 psoriasis patients and 36 healthy control subjects were enrolled with comprehensive CCTA data (Supplemental Figure 1). Strengthening the Reporting of Observational Studies in Epidemiology (STROBE) guidelines were followed for reporting the findings of our observational study (31).

ACQUISITION OF CCTA. All patients underwent CCTA on the same day as the blood draw, using the same computed tomography scanner (320-detector row Aquilion ONE ViSION, Toshiba, Japan).

ANALYSIS OF CCTA. A single, blinded reader (blinded to treatment and time of scan) evaluated coronary plaque characteristics across each of the main coronary arteries at >2 mm using dedicated software (QAngio CT, Medis Medical Imaging Systems, Leiden, the Netherlands) (32,33). Results of the automated contouring were also reviewed on transverse reconstructed cross sections of the artery on a section-by-section basis at 0.5-mm increments. Lumen attenuation was adaptively corrected on an individual scan basis using gradient filters and intensity values within the artery.

LABORATORY PROCEDURES. For detailed methods see the Supplemental Methods section.

WHOLE BLOOD PROCESSING AND IMMUNOPHENOTYPING. Briefly, lysed whole blood cells or ficoll-separated PBMCs were incubated for 30 min in a 10-color antibody cocktail (Supplemental Table 1) and acquired on a BD Biosciences LSRII flow cytometer using DIVA 6.1.2 software (BD Bioscience, San Jose, California). We determined the frequency of LDGs by quantitating the percentage of $CD14^{lo}CD15^{hi}CD10^{hi}$ cells in the PBMC fraction by flow cytometry and used the complete blood count to determine the frequency of LDGs per microliter.

RNA SEQUENCING ANALYSIS. Paired NDGs or LDGs ($n = 50{,}000$) were isolated from 7 psoriasis patients. We performed quantile normalization and used limma (34) for differential expression analysis to identify genes that were dysregulated between the NDG and LDG subsets, controlling for the individual and batch effects. The false discovery rate (FDR) was used for multiple testing, and significant differentially expressed genes had a FDR ≤ 0.1 and $|\log2(\text{fold change})| \geq 1.5$. We then identified functions or gene ontologies that were enriched among differentially

TABLE 1 Baseline Characteristics of Psoriasis Patients and Healthy Control Subjects

	Psoriasis (n = 81)	Healthy Control Subjects (n = 36)	p Value
Demographic and clinical characteristics			
Age, yrs	49.1 ± 12.9	33.6 ± 12.6	<0.001‡
Males	52 (64)	22 (61)	0.75
Hypertension	18 (22)	3 (8)	0.07
Hyperlipidemia	25 (31)	5 (14)	0.05
Type 2 diabetes	7 (9)	1 (3)	0.25
Body mass index, kg/m^2	28.5 ± 5.2	24.1 ± 3.1	<0.001‡
Current smoker	6 (7)	2 (6)	0.71
Lipid treatment	18 (22)	1 (3)	0.008†
Clinical and laboratory values			
Total cholesterol, mg/dl	185.3 ± 37.9	170.8 ± 31.3	0.02*
High-density lipoprotein, mg/dl	56.6 ± 19.8	61.3 ± 16.2	0.11
Low-density lipoprotein, mg/dl	105.7 ± 29.1	91.2 ± 25.9	0.006†
Triglycerides, mg/dl	101.0 (79.0–142.0)	83.5 (72.0–97.5)	0.02*
C-reactive protein	2.2 (0.9–4.1)	0.7 (0.5–1.6)	<0.001‡
Framingham risk score	2.0 (1.0–4.0)	1.0 (1.0–1.0)	<0.001‡
Absolute neutrophil count, K/μl	3.9 ± 1.2	3.1 ± 1.2	<0.001‡
Psoriasis characteristics			
Psoriasis area severity index score	7.4 (3.4–11.8)		
Systemic treatment	8 (10)		
Cytokines characterization			
Tumor necrosis factor-α	1.30 (0.85–1.85)	1.00 (0.65–1.36)	0.045*
Interleukin-6	1.32 (0.74–2.13)	0.70 (0.41–1.07)	0.006†
Interleukin-1β	0.13 (0.08–0.16)	0.10 (0.04–0.14)	0.08*
Interleukin-18	390 (307–543)	300 (220–449)	0.01*
Interleukin-17A	1.60 (0.88–2.85)	0.73 (0.30–1.03)	<0.001‡
Coronary CT angiography			
Total burden, mm^2 (×100)	1.12 ± 0.43	0.93 ± 0.27	<0.001‡
Noncalcified burden, mm^2 (×100)	1.10 ± 0.43	0.91 ± 0.27	<0.001‡
Dense-calcified burden, mm^2 (×100)	0.006 (0.002–0.023)	0.009 (0.004–0.017)	0.31

Values are mean ± SD, n (%), or median (interquartile range). The p values were calculated by using an unpaired Student's *t*-test or Mann-Whitney U test for continuous variables and Pearson's chi-square test for categorical variables. Significance set at *p < 0.05, †p < 0.01, and ‡p < 0.001.

CT = computed tomography.

expressed genes, and FDR ≤0.1 was used to declare significance. All graphical illustrations and RNA-seq analyses were conducted using custom scripts and libraries implemented in R (R Foundation, Vienna, Austria).

STATISTICAL ANALYSIS. Summary statistics were presented as mean ± SD for normally distributed variables, medians and interquartile range were used for non-normally distributed continuous variables, and frequencies were used for categorical variables. Normality was assessed by skewness and kurtosis. Parametric variables were compared between groups using Student's *t*-test, whereas the Mann-Whitney U test was performed for nonparametric variables. Dichotomous variable comparisons were done using Pearson's chi-square test. Unadjusted regression analyses were performed to evaluate for potential relationships between LDG frequency and coronary plaque burden, and regression results were represented as standardized beta-coefficients with p values. We conducted multivariable linear regression analyses to evaluate the association of coronary plaque burden with LDG and NDG frequency. These analyses were adjusted for traditional CVD risk as assessed by the Framingham 10-year risk, body mass index, type 2 diabetes, treatment with statins, and treatment with systemics. Results were presented with 95% confidence intervals, where applicable, and p values <0.05 were considered statistically significant. Statistical analyses were performed with STATA version 12.0 (StataCorp, College Station, Texas).

RESULTS

CLINICAL CHARACTERISTICS OF STUDY PARTICIPANTS. We summarized the characteristics of our study population in Table 1. The study cohort consisted of 81 consecutively recruited psoriasis patients and 36 healthy control subjects for LDG and NDG frequency comparisons (Table 1, Supplemental Figure 1). The psoriasis cohort was middle aged (49.1 ± 12.9 years), with a slight male predominance (64%), and a low CV risk as assessed by Framingham 10-year risk (median: 2; interquartile range: 1 to 4). The median PASI score was 7.4 (interquartile range: 3.4 to 11.8), which was consistent with moderate psoriasis skin disease severity (Table 1).

CIRCULATING LDG COUNTS IN PSORIASIS ARE ASSOCIATED WITH PSORIASIS SKIN DISEASE SEVERITY. Both LDG and NDG subsets were elevated in psoriasis patients compared with healthy control subjects (1.3- and 2.0-fold, respectively) (Figure 1A). The frequency of circulating LDGs was associated with psoriasis severity (PASI: β = 0.28; p = 0.01), which remained significant after adjustment for body mass index, psoriasis treatment, and absolute neutrophil count (β = 0.26; p = 0.03) (Figure 1B). However, an association between NDG frequency and psoriasis skin disease severity was not detected (β = −0.006; p = 0.92) (Figure 1C). We then compared the surface markers of LDGs and NDGs in psoriasis to LDGs and NDGs from healthy control subjects (Figure 1D) and observed a significant elevation in CD15 in healthy control and psoriasis LDGs compared with both healthy control and psoriasis NDGs. This was concomitant with a reduction in CD11b on psoriasis LDGs and NDGs compared with healthy control NDGs (Figure 1E). CD62L was significantly downregulated on psoriasis LDGs compared with both psoriasis and healthy control NDGs (Figure 1E). Increased shedding of CD62L might indicate that psoriasis LDGs were in a

FIGURE 1 LDGs Are Elevated in Psoriasis Patients and Are Associated With Psoriasis Severity

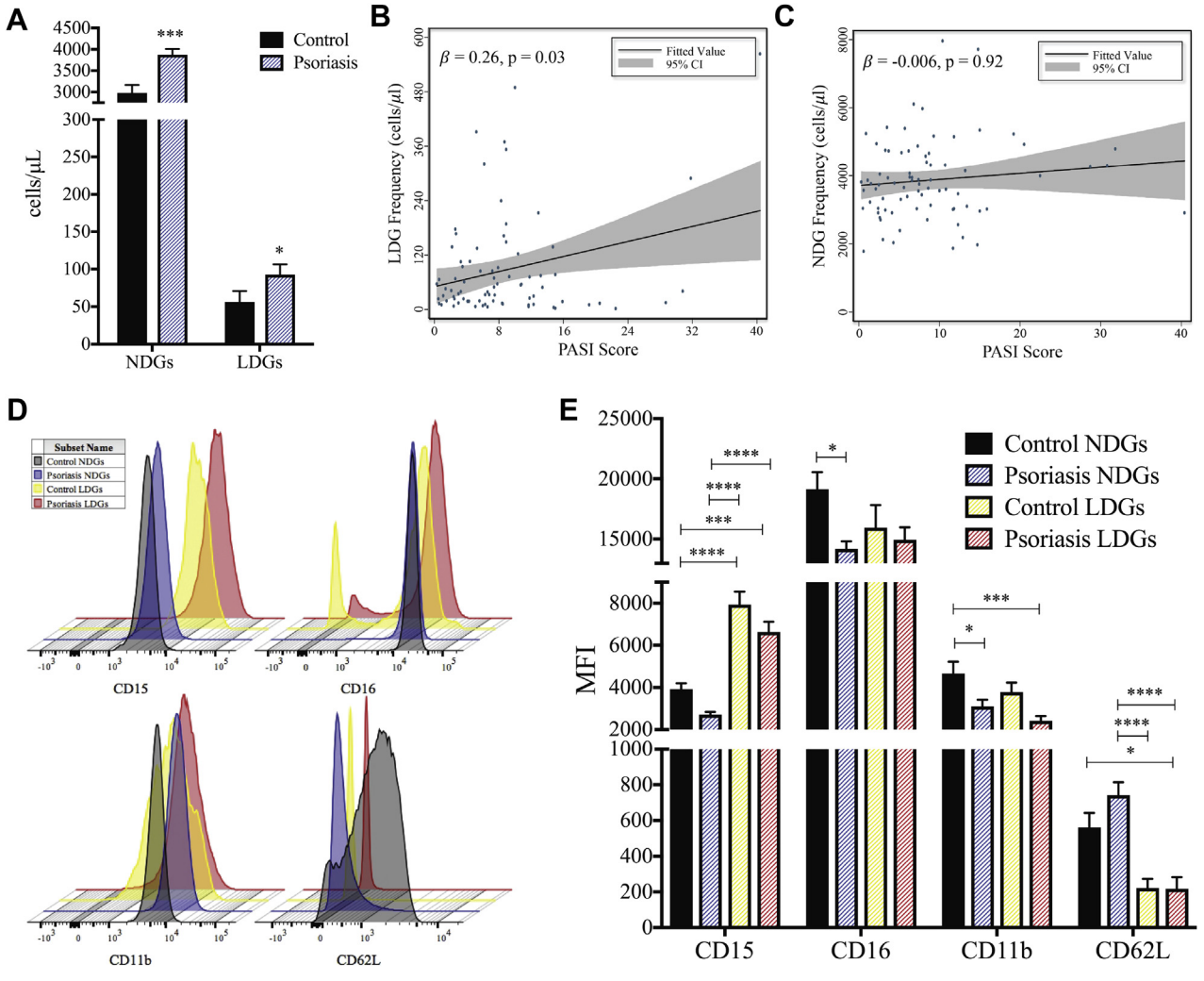

(A) Normal-density granulocyte (NDG) and low-density granulocyte (LDG) frequencies were determined by flow cytometry and are elevated in psoriasis patients (n = 81) compared with healthy control subjects (n = 36). Data are represented as mean ± SEM. The Mann-Whitney test was performed, and significance was set at *p < 0.05* and ***p < 0.001. Regression analyses between **(B)** LDGs but not **(C)** NDGs are associated with the psoriasis area severity index (PASI) score for the psoriasis cohort (n = 81). **(D)** Surface marker expression of NDGs and LDGs was analyzed by flow cytometry and **(E)** showed a significant elevation in CD15 on psoriasis LDGs compared with healthy control and psoriasis NDGs, as well as lower CD11b and CD62L expression on psoriasis LDGs compared with healthy control LDGs. Data are represented as mean ± SEM. Significance was established by 1-way analysis of variance (ANOVA) and a Tukey's multiple comparisons test set at *p < 0.05, ****p < 0.001, and ****p < 0.0001. MFI = median fluorescence intensity.

higher state of activation compared with NDGs. No change in the surface expression of CD15, CD16, CD11b, or CD62L was observed when comparing LDGs from psoriasis patients with LDGs from healthy control subjects (Figure 1E).

NCB IN PSORIASIS ASSOCIATES WITH LDG COUNTS. Evidence of early coronary atherosclerosis in psoriasis patients is driven by an increase in NCB (Table 1). Moreover, total coronary plaque burden (TB) and NCB within 3 major epicardial coronary arteries were positively associated with LDG frequency (β = 0.18; p = 0.005), which persisted beyond adjustment for traditional CVD risk factors and lipid treatment (TB: β = 0.13; p = 0.026) (NCB: β = 0.13; p = 0.019) (Figure 2A). Furthermore, no association was observed between NDG frequency and TB, as well as NCB, even when adjusted for traditional risk factors (TB: β = −0.003; p = 0.98; NCB: β = −0.03; p = 0.76) (Figure 2B).

LDGs INDUCE APOPTOSIS IN HUMAN AORTIC ENDOTHELIAL CELLS. Because psoriasis LDGs were associated with NCB compared with psoriasis NDGs,

FIGURE 2 LDGs and Their NETs Induce Endothelial Cell Damage

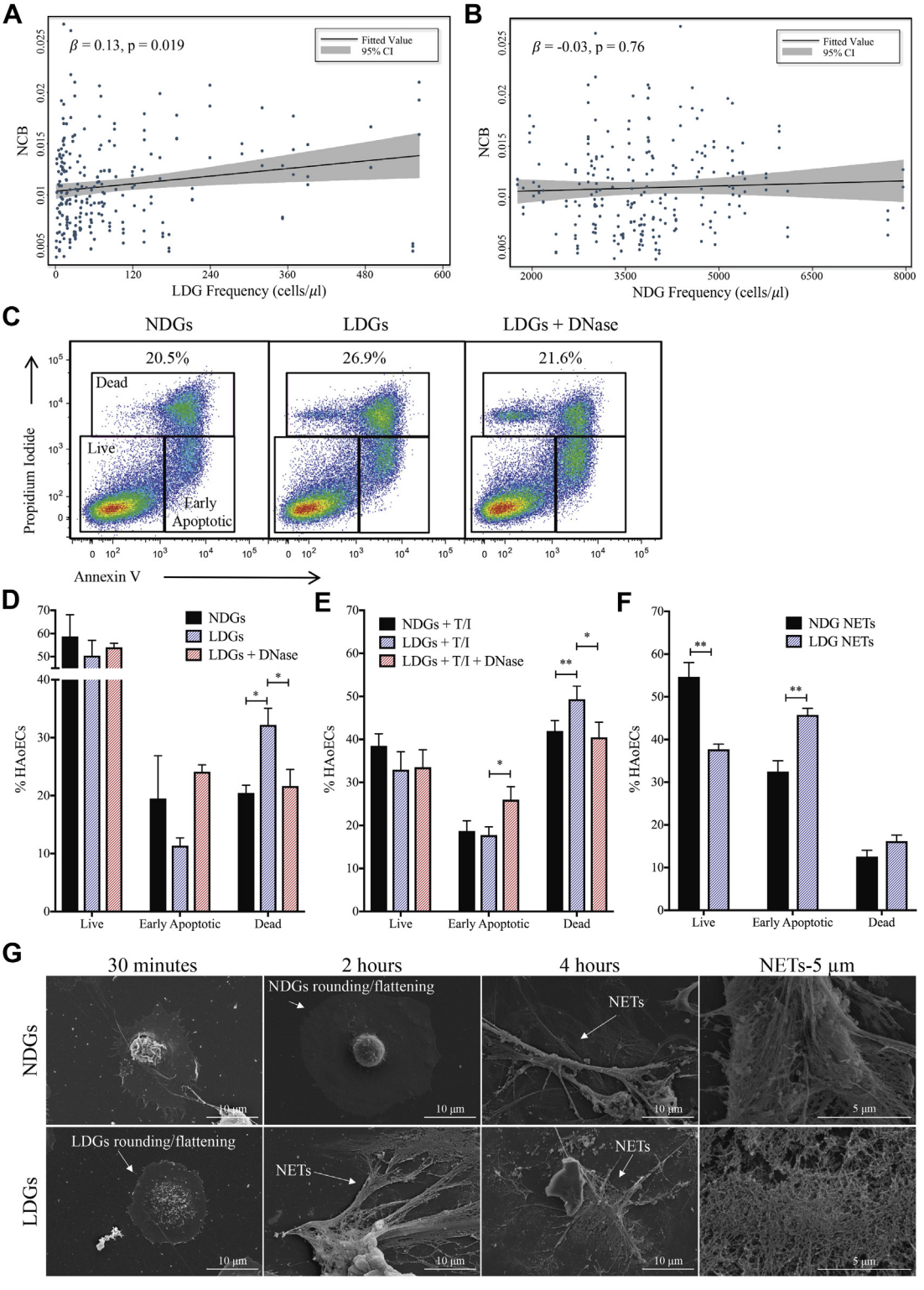

Continued on the next page

we hypothesized that LDGs from psoriasis and their NETs would exert enhanced cytotoxic effects on human aortic endothelial cells (HAoECs) compared with psoriasis NDGs. To normalize activation between LDGs and NDGs from psoriasis due to the isolation process, we sorted both LDGs and NDGs following an identical gating strategy (Supplemental Figure 2). We then measured the cytotoxic potential of psoriasis LDGs compared with psoriasis NDGs by quantifying the percentage of apoptotic $CD146^{+}$ HAoECs via flow cytometry in a co-culture system (**Figure 2C**). LDGs (2:1, LDGs-to-HAoECs) led to an increase in the percentage of apoptotic HAoECs by 1.6-fold compared with the same number of NDGs (**Figure 2D**). To further support our hypothesis that HAoEC death might have been due be to LDG-derived NET formation, HAoECs were simultaneously treated with DNase and LDGs. DNase-treated co-cultures led to a 1.5-fold decrease in the percentage of HAoEC deaths comparable with NDGs, which resulted in increased HAoECs in the early apoptotic stage compared with LDGs alone (**Figure 2D**). To further mimic the psoriasis-like inflammatory state, HAoECs were pre-treated with tumor necrosis factor-α and interferon-γ, followed by psoriasis LDGs or NDGs (35). LDGs further increased the percentage of HAoEC death upon activation (**Figure 2E**).

We next measured the cytotoxic potential of NETs harvested from psoriasis LDGs and NDGs, which contain NET-associated proteins and fragmented DNA, on HAoECs. Upon treatment of HAoECs with LDG or NDG NETs, normalized to 50 μg of either LDG or NDG NET-associated proteins, we determined that HAoECs treated with LDG NETs showed a 32% reduction in live HAoECs concomitant with a 1.4-fold increase in early apoptotic cells compared with NDG NET-associated proteins (**Figure 2F**). No difference was detected in the percentage of dead HAoECs subsequent to LDG and NDG NET treatments (**Figure 2F**). This suggested that the mechanism by which LDGs exerted cytotoxic effects might, in part, rely on the cellular interaction between LDGs and HAoECs or intact DNA. To visualize the NETosis process between psoriasis LDGs and NDGs, we acquired scanning electron microscopy images of NET formation over time. Nonstimulated LDGs formed NETs by the 2-h timepoint compared with psoriasis NDGs stimulated with phorbol 12-myristate 13-acetate (PMA), which is an inducer of NETosis. NETs were not observed until 4 h (**Figure 2G**). We observed the initial stages of NETosis, characterized by rounding and flattening at 30 min for LDGs and 2 h for NDGs (24).

RNA SEQUENCING OF LDGs COMPARED WITH NDGs REVEALS UPREGULATION OF GRANULE PROTEINS AND ADHESION MOLECULES. To understand the relationship between psoriasis LDGs and NCB, which is a relationship not observed with psoriasis NDGs, we studied RNA expression between these neutrophil subsets derived from 7 patients with active psoriasis. By comparing the transcriptomes between LDGs and NDGs, we determined that 1,076 (Supplemental Table 1) were differentially expressed (**Figure 3A**). The volcano plots showed a separation of genes corresponding to NDGs relative to LDGs (**Figure 3B**). Functional analyses revealed that gene pathways that were differentially expressed between LDGs and NDGs were clustered in leukocyte activation ($p = 1 \times 10^{-10}$; FDR $= 3 \times 10^{-8}$) and cell activation ($p = 2 \times 10^{-10}$; FDR $= 4 \times 10^{-8}$) (**Figure 3C**). In addition, the granule proteins were upregulated at the gene level in LDGs (**Figure 3D and 3E**), which is a mechanism that typically stops before release from the bone marrow (36). Transmission electron microscopy further confirmed this finding, demonstrating LDGs had more electron-dense granules that corresponded with primary granules (**Figure 3F**) (37). Concomitant with increased granule proteins, we observed that the adhesion molecules intercellular adhesion molecule-2, integrin subunit alpha M (ITGAM), and integrin alpha subunit L (ITGAL) were upregulated in LDGs (**Figure 3D**).

CO-LOCALIZATION OF LDGs WITH PLATELETS CORRELATE WITH NCB. A stark difference in RNA sequencing between LDG and NDG data was the presence of platelet-associated biological pathways upregulated in the LDG samples compared with NDGs (**Figure 4A**). Therefore, we investigated the

FIGURE 2 Continued

(A) Psoriasis LDGs but not **(B)** psoriasis NDGs are associated with noncalcified coronary plaque burden (NCB) in psoriasis ($n = 81$). **(C)** Representative flow cytometry plots from the cytotoxicity assay show **(D)** psoriasis LDGs ($n = 7$) increase apoptosis of human aortic endothelial cells (HAoECs) compared with psoriasis NDGs ($n = 5$), an effect abrogated by DNase treatment ($n = 4$). Data are represented as mean ± SEM. Significance established by a 1-way ANOVA and a Tukey's multiple comparisons test set at *$p < 0.05$, **$p < 0.01$, and ***$p < 0.0001$. **(E)** Cytotoxicity of HAoECs pre-treated with tumor necrosis factor-α and interferon-γ is further increased by LDGs. Data are represented as means ± SEM. Significance established by 1-way ANOVA and a Tukey's multiple comparisons test and set at *$p < 0.05$ and **$p < 0.01$. **(F)** HAoECs were incubated for 18 h with NDG neutrophil extracellular trap (NET) associated ($n = 5$) or LDG-NET associated proteins ($n = 5$), and apoptosis was quantified using flow cytometry. Data are represented as mean ± SEM. Significance established by unpaired 2-tailed Student's *t*-test and set at **$p < 0.01$. **(G)** Scanning electron microscopy images of the formation of NETs from NDGs and LDGs over time subsequent to purification. CI = confidence interval; T/I = tumor necrosis factor alpha/interferon gamma; other abbreviations as in **Figure 1**.

FIGURE 3 Granule Proteins and Adhesion Molecules Are Upregulated in LDGs Compared With NDGs at the Gene Level

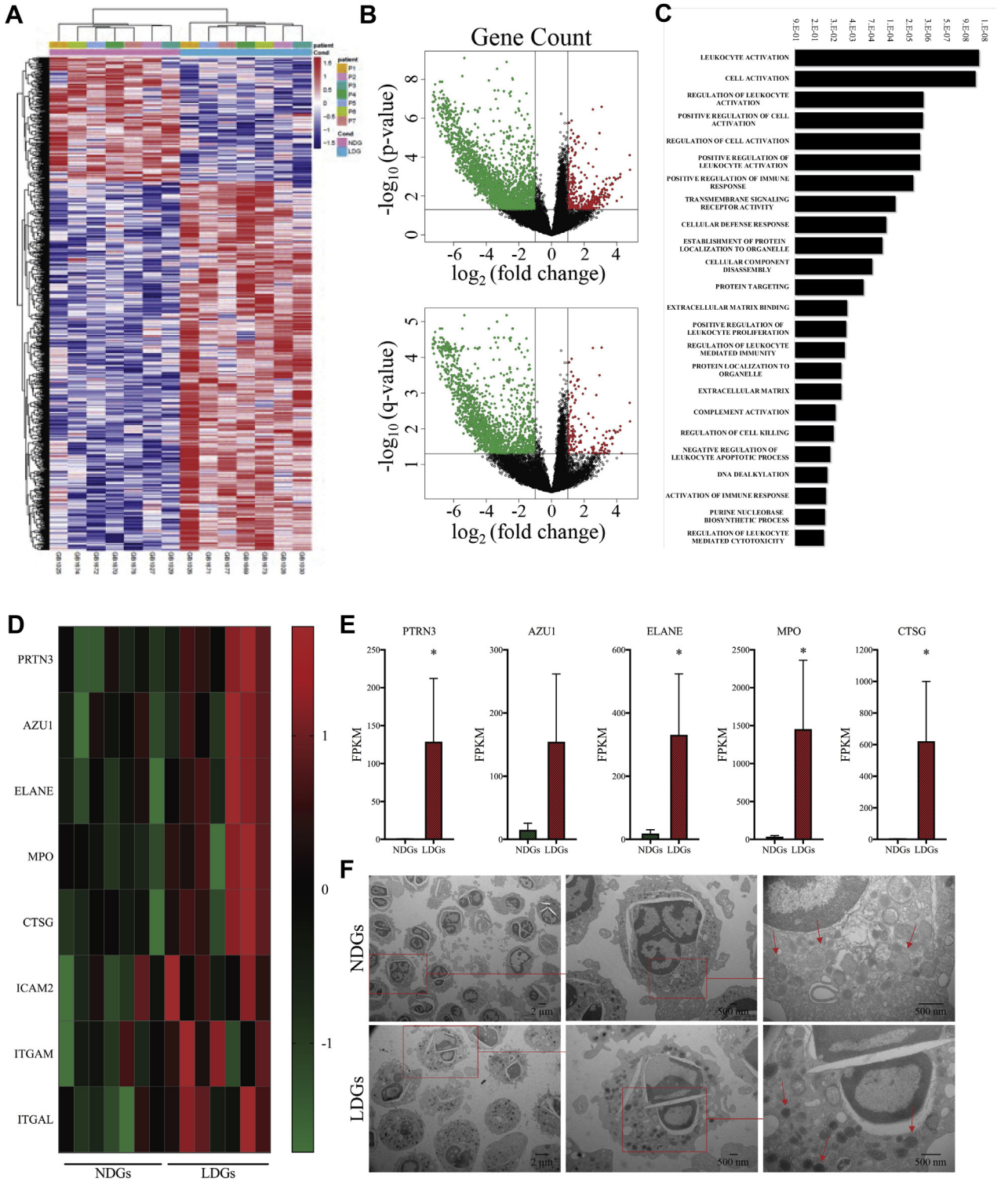

Continued on the next page

relationship of platelets and LDGs as a potential link to the positive association between LDGs and NCB. From the transcriptome data, we observed a clear upregulation of platelet-specific biological processes in the LDG sample, clustered in pathways that included platelet alpha granules ($p = 4 \times 10^{-5}$; FDR $= 2 \times 10^{-3}$), platelet activation ($p = 2 \times 10^{-3}$; FDR $= 3 \times 10^{-2}$), platelet alpha granule lumen ($p = 3 \times 10^{-3}$; FDR $= 6 \times 10^{-2}$), platelet activation signaling and aggregation ($p = 4 \times 10^{-3}$; FDR $= 7 \times 10^{-2}$), and platelet degranulation ($p = 6 \times 10^{-3}$; FDR $= 9 \times 10^{-2}$) (Figure 4A). These were selected pathways because they were not the most significant from the biological pathways list. To understand neutrophil–platelet interactions, we tested the frequency of neutrophil platelet aggregates and found an upregulation of neutrophil platelet aggregates in psoriasis (Figure 4B). We then focused on a subset of those genes and determined that CD40 and SELP (platelet-specific receptors that bind to CD40LG and SELPLG on neutrophils), as well as CD40LG and SELPLG were upregulated in LDGs, which suggested increased adhesion between platelets and LDGs (Figure 4C). We measured CD36 expression because CD36 promoted thrombosis, and we determined that CD36 expression was upregulated on LDGs compared with NDGs (Figures 4C and 4D) and were also associated with NCB (Figure 4E). After measuring the percentage of LDGs or NDGs that aggregated with platelets in psoriasis using flow cytometry (Figure 4F), we determined that the NDG platelet aggregation was highly variable, and there was no difference in the percentage of aggregates compared with LDGs when considering the mean (Figure 4G). However, the percentage of LDG platelet aggregates had a positive linear association with NCB, and this association was specific to LDGs (Figure 4H). Scanning electron microscopy images confirmed the presence of platelets that adhered to LDGs, a finding that was not observed in the NDG samples (Figure 4I).

SPONTANEOUS NETosis OF LDGs IS ASSOCIATED WITH PLATELET FREQUENCY. In addition to our previously described findings, the product of LDGs and platelets in circulation were also correlated with NCB beyond traditional risk factors ($\beta = 0.27$; $p < 0.001$) (Figure 5A). This finding was similar to the association between LDGs and NCB (Figure 2A); however, the association between LDG platelet aggregates and NCB was more robust. Consistent with previous data, this association was attenuated and not significant with the product of NDGs and platelets ($\beta = 0.11$; $p = 0.12$) (Figure 5B). Lastly, we confirmed that LDGs had increased spontaneous NETosis (Figures 5C and 5D) and determined that the percentage of LDGs to spontaneously form NETs was associated with the frequency of circulating platelets ($\beta = 0.78$; $p = 0.022$) (Figure 5E).

DISCUSSION

We demonstrated the following: 1) an increase in LDG frequency was associated with psoriasis severity and TB, specifically NCB, in psoriasis beyond in vitro traditional risk factors for CVD; 2) the frequency of NDGs, the dominant neutrophil subset, was not associated with TB or NCB; 3) psoriasis LDGs might exert a cytotoxic effect on endothelial cells compared with NDGs, similar to SLE; and 4) the amount of CD36 gene expression, a platelet gene, in LDGs and the percentage of circulating platelet LDG aggregates were associated with early atherosclerotic NCB. These findings suggested that in an inflammatory environment platelets might potentially interact with LDGs and promote vascular damage. These observations suggested that the adherence of LDG to platelets might be an important link between psoriasis skin disease severity and early atherogenesis, as well as represented a potential target for treatment of both diseases in the future.

Neutrophils are critical to the development of psoriasis, and a reduction in circulating neutrophils is accompanied by regression of psoriatic plaque development (38). Our previous study reported an increased circulating frequency of activated neutrophils, as defined by lower CD62L and CD16 surface expression, in psoriasis patients compared with healthy control subjects (16). When we focused on biologic-naïve psoriasis patients and the different

FIGURE 3 Continued

RNA sequencing analysis was completed on 50,000 LDGs relative to NDGs from psoriasis patients. **(A)** Differentially expressed genes (n = 1,076) were identified between NDGs and LDGs from psoriasis patients (n = 7). NDGs are the reference, as are upregulated genes in LDGs. **(B)** The volcano plot shows clear separation between NDGs and LDGs. The upregulated **(red)** and downregulated **(green)** transcriptomes are NDGs, as LDGs are the reference sample. **(C)** The gene ontology biological process analysis highlighted biological processes that were differentially expressed between NDGs and LDGs. Significance was established by false discovery rate (FDR). **(D)** Granule proteins are upregulated in all patients (n = 7) and when normalized and by **(E)** FPKM values (n = 7). Data are represented as means ± SEM. Significance was established by the unpaired Mann-Whitney Student's *t*-test and set at *p < 0.05. **(F)** Transmission electron microscopy images of LDGs and NDGs show LDGs had more electron dense granules. AZU1 = azurocidin 1; CTSG = cathepsin G; ELANE = neutrophil elastase; FPKM = fragments per kilobase of transcripts per million; ICAM2 = intercellular adhesion molecule 2; ITGAL = integrin subunit alpha L; ITGAM = integrin subunit alpha M; MPO = myeloperoxidase; P = patient; PRTN3 = proteinase 3; other abbreviations as Figures 1 and 2.

FIGURE 4 Upregulated Genes in LDGs Show Increased Binding to Platelets

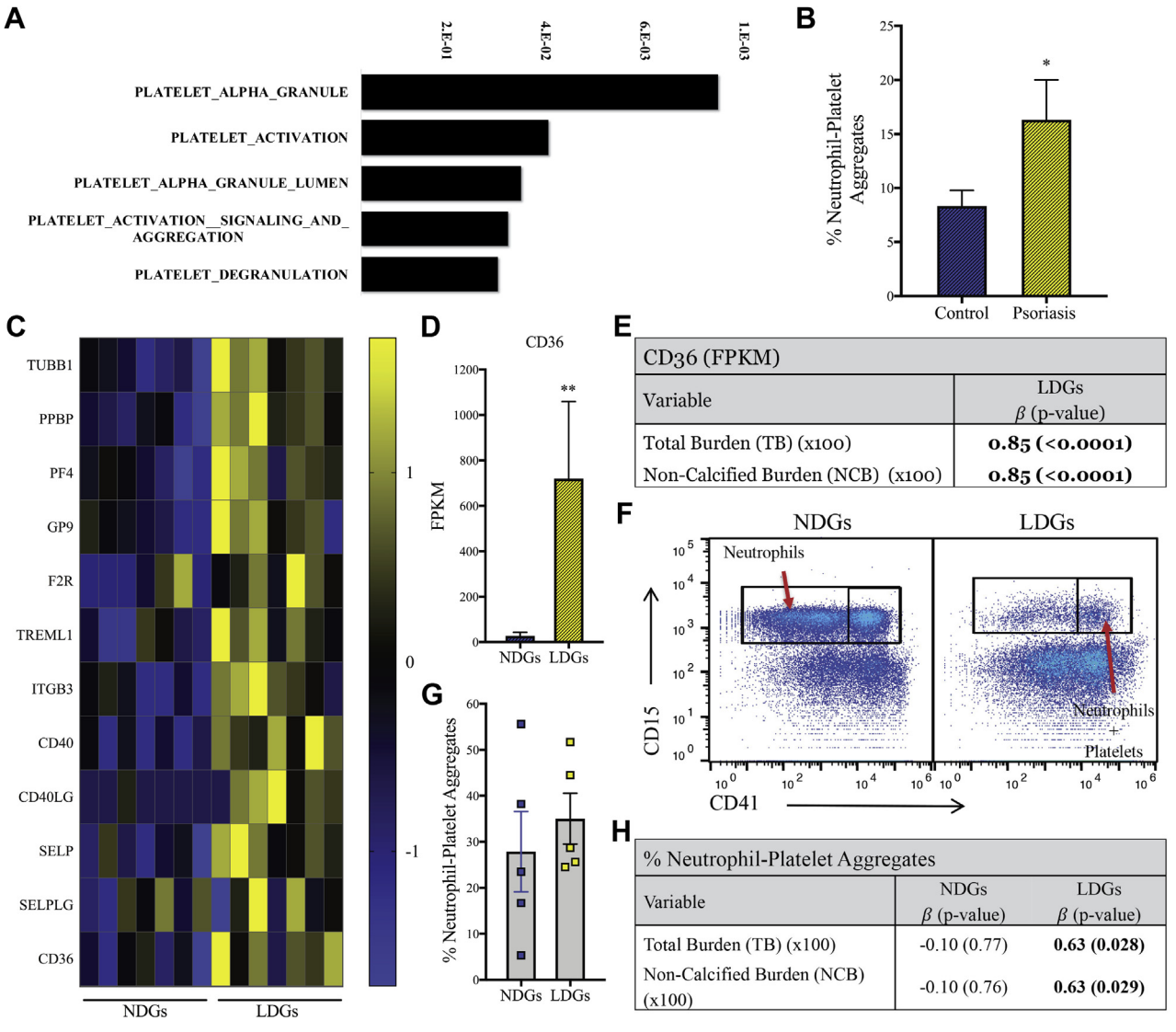

E

CD36 (FPKM)	
Variable	LDGs β (p-value)
Total Burden (TB) (x100)	**0.85 (<0.0001)**
Non-Calcified Burden (NCB) (x100)	**0.85 (<0.0001)**

H

% Neutrophil-Platelet Aggregates		
Variable	NDGs β (p-value)	LDGs β (p-value)
Total Burden (TB) (x100)	-0.10 (0.77)	**0.63 (0.028)**
Non-Calcified Burden (NCB) (x100)	-0.10 (0.76)	**0.63 (0.029)**

RNA sequencing analysis shows an **(A)** upregulation of platelet-specific biological pathways in psoriasis LDGs versus psoriasis NDGs. Significance was established by FDR. **(B)** Neutrophil platelet aggregates were increased in psoriasis patients (n = 12) compared with matched control subjects (n = 10). Data are represented as mean ± SEM. Significance was established by the unpaired Mann-Whitney Student's *t*-test and set at *p < 0.05. **(C)** The platelet-specific transcriptomes were upregulated in LDGs compared with NDGs (n = 7). **(D)** The platelet receptor, CD36, was highly upregulated in LDGs, and the FPKM values were associated with **(E)** NCB (n = 7). **(F)** Flow cytometry plots show **(G)** aggregates of NDGs or LDGs with platelets and the percentages of platelets LDG aggregates are **(H)** highly associated with NCB. **(I)** Scanning electron microscopy images of NDGs and LDGs demonstrate platelet LDG aggregates. Scale bar: 10 μm. CD40LG = CD40 ligand; F2R = coagulation factor II thrombin receptor; GP9 = glycoprotein IX platelet; ITGB3 = integrin subunit beta 3; PF4 = platelet factor 4; PPBP = pro-platelet basic protein; SELP = selectin P; SELPLG = selectin P ligand; TREML1 = triggering receptor expressed on myeloid cells like 1; TUBB1 = tubulin beta 1 class VI; other abbreviations as in Figures 1 to 3.

FIGURE 5 Percentage of LDGs to Spontaneously Form NETs Is Associated With Circulating Platelet Counts

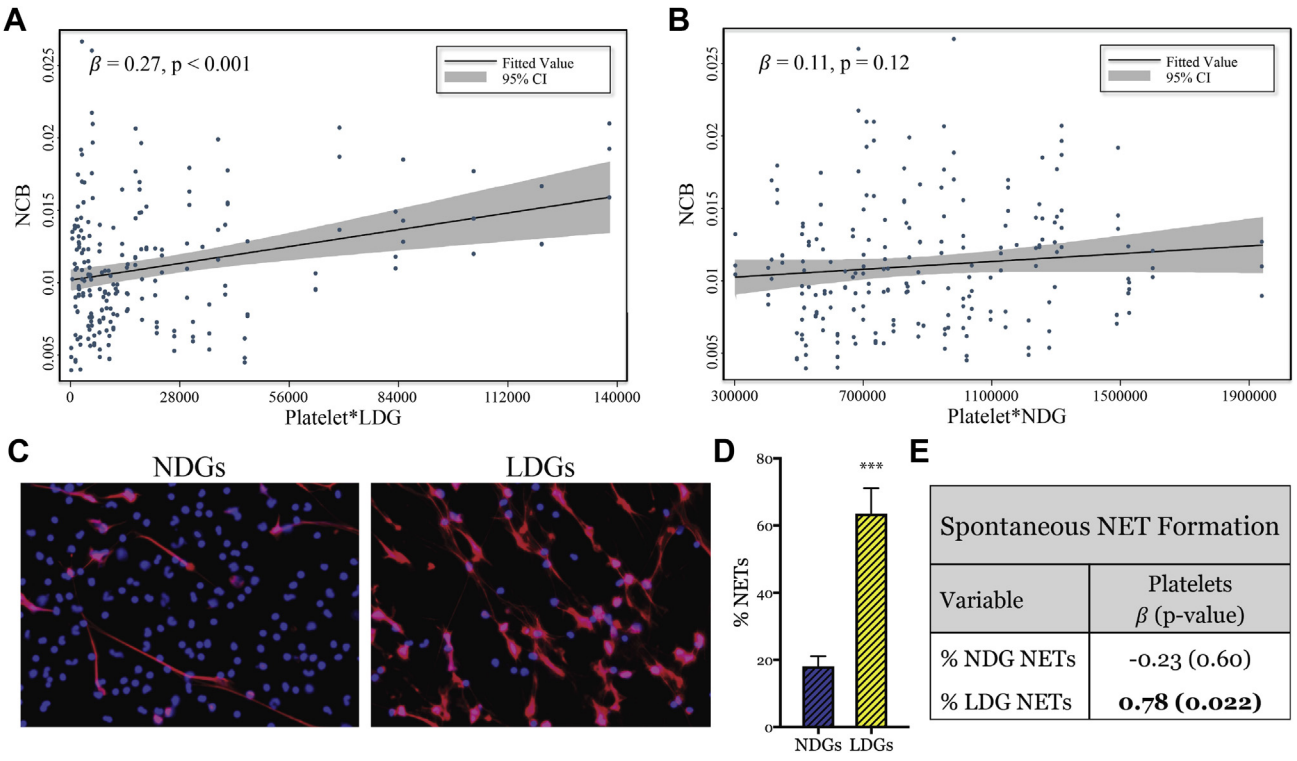

(A) The product of platelets and LDGs in circulation is associated with NCB; however, **(B)** this relationship is absent with the product of platelets and NDGs. **(C)** LDGs spontaneously form NETs at a **(D)** higher frequency than NDGs (n = 9). Data are represented as mean ± SEM. Significance was established by an unpaired Mann-Whitney Student's *t*-test and set at ***p < 0.001. **(E)** The percentage of LDGs (n = 8) to undergo spontaneous NETosis is associated with the frequency of circulating platelets. Abbreviation as in Figures 1 to 3.

neutrophil subsets in this study, we determined that CD62L expression on LDGs was significantly lower compared with both healthy control and psoriasis NDGs. We found CD62L expression to be decreased on LDGs compared with NDGs. Although both CD16 and CD62L mark a heightened activation state, only CD62L was reduced on LDGs compared with NDGs in psoriasis. This might, in part, be a result of the formation of LDG platelet aggregates. Neutrophil platelet aggregation in resting neutrophils reduces CD62L expression, and primes neutrophils for adhesion (39). This might explain why only the LDGs were associated with psoriasis severity and psoriatic comorbidities. In addition, this positive relationship between LDG frequency and psoriasis severity suggested that LDGs might potentially be a clinical target for treating psoriasis.

Neutrophils are increasingly being recognized as significant contributors to the pathogenesis of CVD. Neutrophil frequency was a predictor of coronary events (40), and more recently, this frequency was involved in early atherosclerotic plaque development (41). To understand if the development of in vivo atherogenesis is related to neutrophils, we leveraged CCTA as a reliable, noninvasive imaging technique to detect atherosclerotic plaque composition in coronary arteries. Comprehensive plaque characterization permitted us to directly assess and correlate TB and NCB with the frequencies of both neutrophil subsets in circulation. Similar to psoriasis severity, we found a positive linear relationship between LDGs and TB in the major coronary arteries, primarily driven by NCB. Furthermore, these activated neutrophils might, in part, be responsible for early damage to both the epidermis and endothelium.

We hypothesized that early plaque formation evidenced by the increase in NCB in psoriasis was potentially related to the cytotoxic effects of LDGs by 2 factors. First, LDG NETs themselves are more cytotoxic than NDG NETs, and second, LDGs form NETs spontaneously; therefore, the amount of circulating NETs in psoriasis was increased due to increased

LDGs. NETs are known to play a role in atherosclerotic plaque development independently of autoimmunity; NETs are released from neutrophils in response to cholesterol-crystal priming, and within the atherosclerotic lesion, NETs are localized to cholesterol-rich areas (42). Impairments in DNA clearance by DNase I were described in autoimmunity and might lead to an enhanced half-life of immunogenic material present in NETs, further exacerbating endothelial damage. When endothelial cells were treated with isolated NETs from LDGs or NDGs, we did not observe an increase in endothelial cell apoptosis from LDG NETs. However, the early stage of apoptosis was elevated by LDG-NET treatment compared with NDG NETs, and there was a significant reduction in live HAoECs. Endothelial cell apoptosis required a cell–cell interaction. Notably, DNase I treatment abrogated the cytotoxic effect of LDGs, which suggested that endothelial cell death was not induced by LDGs independent of NET formation. Studies focused on the effects of NETs showed multiple outcomes. At lower concentrations of NETs normalized to DNA content, NETs that contained fragmented DNA were not as potent at activating human pulmonary artery endothelial cells (43). However, at significantly higher DNA concentrations, fragmented DNA induced endothelial cell apoptosis to the same extent as intact DNA (44). In the present study, the NDG and LDG NETs were composed of NET-associated proteins and fragmented DNA. In addition, we normalized the HAoEC treatments to protein content as opposed to DNA concentrations. This might explain the lack of apoptotic HAoECs subsequent to LDG NET treatment.

To understand the enhanced cytotoxicity of LDGs compared with NDGs, we completed RNA sequencing of paired LDGs and NDGs derived from biologic-naïve psoriasis patients with severe, active skin disease and identified a potential mechanistic target driving the spontaneous NETosis of LDGs. First, RNA sequencing data showed that LDGs were activated, which was demonstrated by the differential biological pathways corresponding to leukocyte activation, cell activation, regulation of leukocyte activation, positive regulation of cell activation, and regulation of cell activation. These data are in agreement with the decrease in surface expression of CD62L observed on the LDG surface compared with both healthy and psoriasis NDGs. Second, we determined that P-selectin and P-selectin ligand transcriptomes were upregulated in LDGs compared with NDGs. P-selectin is a platelet-specific receptor that is upregulated on activated platelets and binds to the P-selectin ligand on neutrophils. Concomitantly, CD40 and CD40 ligand were upregulated in the LDG sample. This is of interest because activated platelets are reported to induce NET formation from neutrophils in acute lung injury and sepsis (25-27). Furthermore, for the neutrophil inflammatory response to fully ensue, stimulation through the P-selectin ligand is required and drives neutrophil migration (45). Blockade of P-selectin ligand signaling altered neutrophil migration and protected mice against thromboinflammatory injury (45). Although it was clear that the interaction of platelets and neutrophils through P-selectin and P-selectin ligand is essential, it was shown that high-mobility group box-1 on platelets directs neutrophils to undergo NETosis (27). High mobility group box-1 expression increases on the platelet surface upon activation and elicits NET formation through a receptor for advanced glycation end products, a process that is independent of toll-like receptor-4 (27).

We determined that the frequency of LDGs co-localized with platelets had a linear association with early NCB. This observation was further strengthened by a significant association between the fragments per kilobase of transcript per million reads of CD36 in the LDG sample and NCB. The CD36 reads were most likely contributed by platelets co-localized with LDGs because our samples were immunophenotyped by flow cytometry to exclude other cell populations that might express CD36. Combined, our data highlighted a potential role for the LDG–platelet interactions in early atherogenesis. It was possible that the association between the percentage of LDGs to spontaneously form NETs and platelet counts was driven by an increase in activated platelets in psoriasis. Further investigations are required to validate this hypothesis and decipher a biological mechanism by which platelets contribute to NET formation in psoriasis. Recent studies provided insight into which LDGs undergo spontaneous NETosis (46,47). Spontaneous NETosis in isolated SLE LDGs occurs within 50 min. This was reported to occur by a mitochondrial reactive oxygen species–dependent mechanism (47). A similar NETosis timeframe was observed when neutrophils were treated with platelet activating factor. Because the adherence of platelets to LDGs might stimulate the release of platelet activating factor, and the NETosis timeframe seen in our studies was similar, we proposed that platelet activating factor was involved in the mechanism of LDG-dependent NETosis.

This study could be extended to other autoinflammatory pathologies such as SLE. In SLE patients, activated platelets enhance the interferon response, and platelet depletion in an SLE murine

model significantly improved disease measures and survival (48).

STUDY LIMITATIONS. There were important limitations to our study. This was an observational study; therefore, it was subjected to potential for confounders and needs experimental follow-up. We also acknowledged that our control group was not adequately matched to our psoriasis group, which was a limitation. Thus, our results should be interpreted with caution. Our plaque characterization and quantification by CCTA was used as a surrogate marker for atherosclerosis, although intravascular ultrasound would be the gold standard to prove these findings (49). In vitro characterization studies are lacking and will be conducted to determine potential drivers of neutrophil platelet aggregation. The RNA sequencing should be followed up with validation studies of protein content and include control samples to determine if LDGs from healthy control subjects have a similar RNA signature compared with psoriasis LDGs. In addition, future studies using single cell RNA sequencing to better characterize our findings and validation studies should be conducted.

CONCLUSIONS

We demonstrated that LDG frequency is elevated in psoriasis and is related to skin disease severity and NCB. Our in vitro studies showed that psoriasis LDGs were cytotoxic to the endothelium following direct contact. This study identified the interactions between LDGs and platelets as a mechanistic focus of future studies to determine how spontaneous NETosis of LDGs might be partly dependent upon platelets. Furthermore, this LDG–platelet interaction might provide a potential therapeutic target in the future to reduce atherosclerosis in psoriasis.

ACKNOWLEDGMENTS The authors would also like to thank the National Heart, Lung, and Blood Institute Electron Microscopy Core for their contribution to the scanning electron microscopy images.

ADDRESS FOR CORRESPONDENCE: Dr. Nehal N. Mehta, Cardiovascular and Pulmonary Branch, NHLBI, 10 Center Drive, CRC, Room 5-5140, Bethesda, Maryland 20892. E-mail: nehal.mehta@nih.gov.

PERSPECTIVES

COMPETENCY IN MEDICAL KNOWLEDGE: Neutrophils have been shown to play an important role in the development early-onset atherogenesis, especially in inflammatory disease states. In addition, a distinct subset of neutrophils termed LDGs are shown to be associated with cardiovascular disease in chronic inflammatory diseases. Finally, the inter-relationship of LDG, platelets, and CCTA-derived early NCB highlights the potential role of LDG–platelet interaction as a driver in chronic inflammatory disease–associated atherosclerosis.

TRANSLATIONAL OUTLOOK 1: Studies in vitro should focus on the effect of antiplatelet therapy on neutrophil–platelet aggregate interactions.

TRANSLATIONAL OUTLOOK 2: Studies in vivo should deplete platelets in pre-clinical models to understand if neutrophil platelet aggregates and atherosclerosis are reduced.

REFERENCES

1. Prodanovich S, Kirsner RS, Kravetz JD, Ma F, Martinez L, Federman DG. Association of psoriasis with coronary artery, cerebrovascular, and peripheral vascular diseases and mortality. Arch Dermatol 2009;145:700–3.

2. Mehta NN, Azfar RS, Shin DB, Neimann AL, Troxel AB, Gelfand JM. Patients with severe psoriasis are at increased risk of cardiovascular mortality: cohort study using the General Practice Research Database. Eur Heart J 2010;31:1000–6.

3. Rachakonda TD, Schupp CW, Armstrong AW. Psoriasis prevalence among adults in the United States. J Am Acad Dermatol 2014;70:512–6.

4. Meyer N, Paul C, Feneron D, et al. Psoriasis: an epidemiological evaluation of disease burden in 590 patients. J Eur Acad Dermatol Venereol 2010; 24:1075–82.

5. Brauchli YB, Jick SS, Miret M, Meier CR. Psoriasis and risk of incident myocardial infarction, stroke or transient ischaemic attack: an inception cohort study with a nested case-control analysis. Br J Dermatol 2009;160:1048–56.

6. Gelfand JM, Neimann AL, Shin DB, Wang X, Margolis DJ, Troxel AB. Risk of myocardial infarction in patients with psoriasis. JAMA 2006;296:1735–41.

7. Yeung H, Takeshita J, Mehta NN, et al. Psoriasis severity and the prevalence of major medical comorbidity: a population-based study. JAMA Dermatol 2013;149:1173–9.

8. Abuabara K, Azfar RS, Shin DB, Neimann AL, Troxel AB, Gelfand JM. Cause-specific mortality in patients with severe psoriasis: a population-based cohort study in the U.K. Br J Dermatol 2010;163: 586–92.

9. Hansson GK. Inflammation, atherosclerosis, and coronary artery disease. N Engl J Med 2005;352: 1685–95.

10. Soehnlein O. Multiple roles for neutrophils in atherosclerosis. Circ Res 2012;110:875–88.

11. Naruko T, Ueda M, Haze K, et al. Neutrophil infiltration of culprit lesions in acute coronary syndromes. Circulation 2002; 106:2894–900.

12. Arbel Y, Finkelstein A, Halkin A, et al. Neutrophil/lymphocyte ratio is related to the severity of coronary artery disease and clinical outcome in patients undergoing angiography. Atherosclerosis 2012;225:456–60.

13. Kaplan RC, Kingsley LA, Sharrett AR, et al. Ten-year predicted coronary heart disease risk in HIV-infected men and women. Clin Infect Dis 2007;45:1074–81.

14. Kim CH, Al-Kindi SG, Jandali B, Askari AD, Zacharias M, Oliveira GH. Incidence and risk of heart failure in systemic lupus erythematosus. Heart 2017;103:227–33.

15. Giles JT, Post WS, Blumenthal RS, et al. Longitudinal predictors of progression of carotid

atherosclerosis in rheumatoid arthritis. Arthritis Rheum 2011;63:3216–25.

16. Naik HB, Natarajan B, Stansky E, et al. Severity of psoriasis associates with aortic vascular inflammation detected by FDG PET/CT and neutrophil activation in a prospective observational study. Arterioscler Thromb Vasc Biol 2015;35:2667–76.

17. Chowaniec O, Jablonska S, Beutner EH, Proniewska M, Jarzabek-Chorzelska M, Rzesa G. Earliest clinical and histological changes in psoriasis. Dermatologica 1981;163:42–51.

18. Hacbarth E, Kajdacsy-Balla A. Low density neutrophils in patients with systemic lupus erythematosus, rheumatoid arthritis, and acute rheumatic fever. Arthritis Rheum 1986;29:1334–42.

19. Carmona-Rivera C, Kaplan MJ. Low-density granulocytes: a distinct class of neutrophils in systemic autoimmunity. Semin Immunopathol 2013;35:455–63.

20. Denny MF, Yalavarthi S, Zhao W, et al. A distinct subset of proinflammatory neutrophils isolated from patients with systemic lupus erythematosus induces vascular damage and synthesizes type I IFNs. J Immunol 2010;184:3284–97.

21. Nakou M, Knowlton N, Frank MB, et al. Gene expression in systemic lupus erythematosus: bone marrow analysis differentiates active from inactive disease and reveals apoptosis and granulopoiesis signatures. Arthritis Rheum 2008;58:3541–9.

22. Brinkmann V, Reichard U, Goosmann C, et al. Neutrophil extracellular traps kill bacteria. Science 2004;303:1532–5.

23. Urban CF, Ermert D, Schmid M, et al. Neutrophil extracellular traps contain calprotectin, a cytosolic protein complex involved in host defense against Candida albicans. PLoS Pathog 2009;5:e1000639.

24. Fuchs TA, Abed U, Goosmann C, et al. Novel cell death program leads to neutrophil extracellular traps. J Cell Biol 2007;176:231–41.

25. McDonald B, Urrutia R, Yipp BG, Jenne CN, Kubes P. Intravascular neutrophil extracellular traps capture bacteria from the bloodstream during sepsis. Cell Host Microbe 2012;12:324–33.

26. Caudrillier A, Kessenbrock K, Gilliss BM, et al. Platelets induce neutrophil extracellular traps in transfusion-related acute lung injury. J Clin Invest 2012;122:2661–71.

27. Maugeri N, Campana L, Gavina M, et al. Activated platelets present high mobility group box 1 to neutrophils, inducing autophagy and promoting the extrusion of neutrophil extracellular traps. J Thromb Haemost 2014;12:2074–88.

28. Lin AM, Rubin CJ, Khandpur R, et al. Mast cells and neutrophils release IL-17 through extracellular trap formation in psoriasis. J Immunol 2011;187:490–500.

29. Salahuddin T, Natarajan B, Playford MP, et al. Cholesterol efflux capacity in humans with psoriasis is inversely related to non-calcified burden of coronary atherosclerosis. Eur Heart J 2015;36:2662–5.

30. Langley RG, Ellis CN. Evaluating psoriasis with psoriasis area and severity index, psoriasis global assessment, and lattice system physician's global assessment. J Am Acad Dermatol 2004;51:563–9.

31. von Elm E, Altman DG, Egger M, et al. Strengthening the Reporting of Observational Studies in Epidemiology (STROBE) statement: guidelines for reporting observational studies. BMJ 2007;335:806–8.

32. Lerman JB, Joshi AA, Chaturvedi A, et al. Coronary plaque characterization in psoriasis reveals high-risk features that improve after treatment in a prospective observational study. Circulation 2017;136:263–76.

33. Kwan AC, May HT, Cater G, et al. Coronary artery plaque volume and obesity in patients with diabetes: the Factor-64 study. Radiology 2014;272:690–9.

34. Ritchie ME, Phipson B, Wu D, et al. Limma powers differential expression analyses for RNA-sequencing and microarray studies. Nucleic Acids Res 2015;43:e47.

35. Mehta NN, Teague HL, Swindell WR, et al. IFN-gamma and TNF-alpha synergism may provide a link between psoriasis and inflammatory atherogenesis. Sci Rep 2017;7:13831.

36. Theilgaard-Monch K, Jacobsen LC, Borup R, et al. The transcriptional program of terminal granulocytic differentiation. Blood 2005;105:1785–96.

37. Bainton DF, Farquhar MG. Origin of granules in polymorphonuclear leukocytes. Two types derived from opposite faces of the Golgi complex in developing granulocytes. J Cell Biol 1966;28:277–301.

38. Toichi E, Tachibana T, Furukawa F. Rapid improvement of psoriasis vulgaris during drug-induced agranulocytosis. J Am Acad Dermatol 2000;43:391–5.

39. Peters MJ, Dixon G, Kotowicz KT, Hatch DJ, Heyderman RS, Klein NJ. Circulating platelet-neutrophil complexes represent a subpopulation of activated neutrophils primed for adhesion, phagocytosis and intracellular killing. Br J Haematol 1999;106:391–9.

40. Horne BD, Anderson JL, John JM, et al. Which white blood cell subtypes predict increased cardiovascular risk? J Am Coll Cardiol 2005;45:1638–43.

41. Quillard T, Araujo HA, Franck G, Shvartz E, Sukhova G, Libby P. TLR2 and neutrophils potentiate endothelial stress, apoptosis and detachment: implications for superficial erosion. Eur Heart J 2015;36:1394–404.

42. Warnatsch A, Ioannou M, Wang Q, Papayannopoulos V. Inflammation. Neutrophil extracellular traps license macrophages for cytokine production in atherosclerosis. Science 2015;349:316–20.

43. Aldabbous L, Abdul-Salam V, McKinnon T, et al. Neutrophil extracellular traps promote angiogenesis: evidence from vascular pathology in pulmonary hypertension. Arterioscler Thromb Vasc Biol 2016;36:2078–87.

44. Saffarzadeh M, Juenemann C, Queisser MA, et al. Neutrophil extracellular traps directly induce epithelial and endothelial cell death: a predominant role of histones. PLoS One 2012;7:e32366.

45. Sreeramkumar V, Adrover JM, Ballesteros I, et al. Neutrophils scan for activated platelets to initiate inflammation. Science 2014;346:1234–8.

46. Gupta S, Chan DW, Zaal KJ, Kaplan MJ. A High-throughput real-time imaging technique to quantify NETosis and distinguish mechanisms of cell death in human neutrophils. J Immunol 2018;200:869–79.

47. Lood C, Blanco LP, Purmalek MM, et al. Neutrophil extracellular traps enriched in oxidized mitochondrial DNA are interferogenic and contribute to lupus-like disease. Nat Med 2016;22:146–53.

48. Duffau P, Seneschal J, Nicco C, et al. Platelet CD154 potentiates interferon-alpha secretion by plasmacytoid dendritic cells in systemic lupus erythematosus. Sci Transl Med 2010;2:47ra63.

49. Park HB, Lee BK, Shin S, et al. Clinical feasibility of 3D automated coronary atherosclerotic plaque quantification algorithm on coronary computed tomography angiography: comparison with intravascular ultrasound. Eur Radiol 2015;25:3073–83.

KEY WORDS cardiovascular disease, low-density granulocytes, neutrophils, platelets, psoriasis

APPENDIX For an expanded Methods section as well as supplemental tables and figures, please see the online version of this paper.

JACC: BASIC TO TRANSLATIONAL SCIENCE VOL. 4, NO. 1, 2019

MINI FOCUS ON SGLT2 INHIBITORS

SGLT2 Inhibitor, Canagliflozin, Attenuates Myocardial Infarction in the Diabetic and Nondiabetic Heart

Ven G. Lim, MBChB,[a,*] Robert M. Bell, PhD,[a,*] Sapna Arjun, PhD,[a] Maria Kolatsi-Joannou, PhD,[b] David A. Long, PhD,[b] Derek M. Yellon, PhD, DSc[a]

JACC: BASIC TO TRANSLATIONAL SCIENCE CME/MOC/ECME

This article has been selected as this month's *JACBTS* CME/MOC/ECME activity, available online at http://www.acc.org/jacc-journals-cme by selecting the *JACC* Journals CME/MOC/ECME tab.

Accreditation and Designation Statement

The American College of Cardiology Foundation (ACCF) is accredited by the Accreditation Council for Continuing Medical Education (ACCME) and the European Board for Accreditation in Cardiology (EBAC) to provide continuing medical education for physicians.

The ACCF designates this Journal-based CME/MOC/ECME activity for a maximum of 1 AMAPRA Category 1 Credit or 1 EBAC Credit. Physicians should only claim credit commensurate with the extent of their participation in the activity.

Successful completion of this CME activity, which includes participation in the evaluation component, enables the participant to earn up to 1 Medical Knowledge MOC point in the American Board of Internal Medicine's (ABIM) Maintenance of Certification (MOC) program. Participants will earn MOC points equivalent to the amount of CME credits claimed for the activity. It is the CME activity provider's responsibility to submit participant completion information to ACCME for the purpose of granting ABIM MOC credit.

SGLT2 Inhibitor, Canagliflozin, Attenuates Myocardial Infarction in the Diabetic and Nondiabetic Heart will be accredited by the European Board for Accreditation in Cardiology (EBAC) for 1 hour of External CME credits. Each participant should claim only those hours of credit that have actually been spent in the educational activity. The Accreditation Council for Continuing Medical Education (ACCME) and the European Board for Accreditation in Cardiology (EBAC) have recognized each other's accreditation systems as substantially equivalent. Apply for credit through the post-course evaluation.

Method of Participation and Receipt of CME/MOC/ECME Certificate

To obtain credit for JACBTS: Basic to Translational Science CME/MOC/ECME, you must:

1. Be an ACC member or JACBTS subscriber.
2. Carefully read the CME/MOC/ECME-designated article available online and in this issue of the *journal*.
3. Answer the post-test questions. At least 2 questions provided must be answered correctly to obtain credit.
4. Complete a brief evaluation.
5. Claim your CME/MOC/ECME credit and receive your certificate electronically by following the instructions given at the conclusion of the activity.

CME/MOC/ECME Objective for This Article: Upon completion of this activity, the learner should be able to: 1) discuss the effects of treatment with canagliflozin on myocardial infarct size among diabetic ZDF and non-diabetic ZL rats; 2) examine the guideline recommendations for prevention of acute myocardial infarction in patients with diabetes mellitus; and 3) define the potential applications of canagliflozin on cardiovascular health among people with or at risk for cardiovascular disease.

CME/MOC/ECME Editor Disclosure: CME/MOC/ECME Editor L. Kristin Newby, MD, is supported by research grants from Amylin, Bristol-Myers Squibb Company, GlaxoSmithKline, Sanofi, Verily Life Sciences (formerly Google Life Sciences), the MURDOCK Study, NIH, and PCORI; receives consultant fees/honoraria from BioKier, DemeRx, MedScape/The-Heart.org, Metanomics, Philips Healthcare, Roche Diagnostics, CMAC Health Education & Research Institute; serves as an Officer, Director, Trustee, or other fiduciary role for the AstraZeneca HealthCare Foundation and the Society of Chest Pain Centers (now part of ACC); and serves in another role for the American Heart Association and is the Deputy Editor of *JACC: Basic to Translational Science*.

Author Disclosures: Janssen-Cilag provided funding support for this study and the formulated treatment diets for the long-term oral administration study and the treatment drug for the ex vivo administration study. Dr. Bell is supported by the National Institute of Health (NIHR) University College London Biomedical Research Centre (BRC) and work is supported by the British Heart Foundation (PG/18/10/33550). Dr. Long's laboratory is supported by a Medical Research Council (MR/P018629/1), Diabetes UK (13/0004763, 15/0005283), Kidney Research UK (RP36/2015), and by the NIHR BRC at Great Ormond Street Hospital for Children NHS Foundation Trust and University College London. Prof. Yellon has served on a global advisory board for Novo Nordisk. All other authors have reported that they have no relationships relevant to the contents of this paper to disclose.

Medium of Participation: Online (article and quiz).

CME/MOC/ECME Term of Approval

Issue Date: February 2019
Expiration Date: January 31, 2020

From [a]The Hatter Cardiovascular Institute, University College London, London, United Kingdom; and the [b]Developmental Biology and Cancer Programme, UCL Great Ormond Street Institute of Child Health, London, United Kingdom. *Drs. Lim and Bell contributed equally to this work and are joint first authors. Janssen-Cilag provided funding support for this study and the

ISSN 2452-302X https://doi.org/10.1016/j.jacbts.2018.10.002

JACC: BASIC TO TRANSLATIONAL SCIENCE VOL. 4, NO. 1, 2019
FEBRUARY 2019:15–26

SGLT2 Inhibitor, Canagliflozin, Attenuates Myocardial Infarction in the Diabetic and Nondiabetic Heart

Ven G. Lim, MBChB,[a,*] Robert M. Bell, PhD,[a,*] Sapna Arjun, PhD,[a] Maria Kolatsi-Joannou, PhD,[b] David A. Long, PhD,[b] Derek M. Yellon, PhD, DSc[a]

VISUAL ABSTRACT

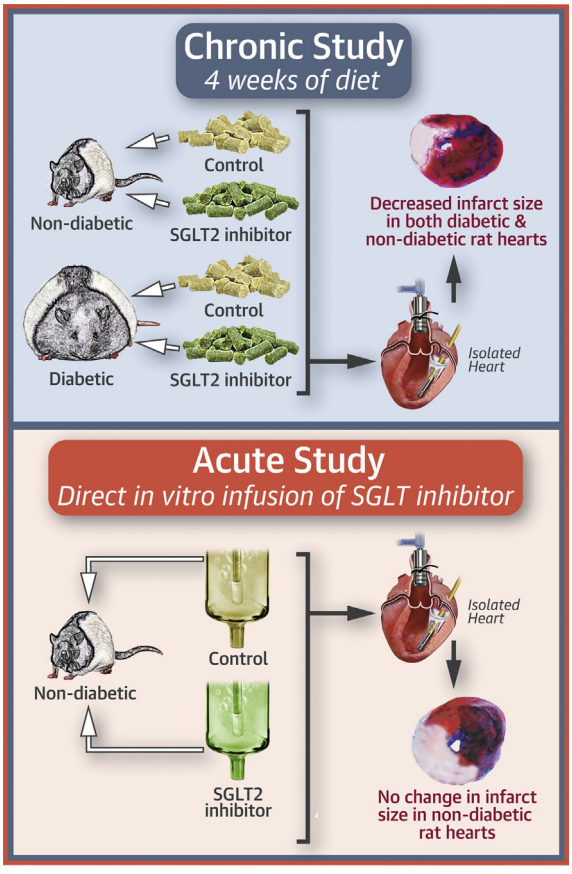

Lim, V.G. et al. J Am Coll Cardiol Basic Trans Science. 2019;4(1):15–26.

HIGHLIGHTS

- **Long-term SGLT2 inhibition with dietary canagliflozinin diabetic *and* nondiabetic rats attenuates myocardial ischemia/reperfusion injury ex vivo.**
- **This suggests that the improvement in myocardial infarct size by SGLT2 inhibition may occur independent of the glycemic status.**
- **Canagliflozin improved hyperglycemia in diabetic rats but importantly did not cause hypoglycemia in nondiabetic rats.**
- **Short-term perfusion of the nondiabetic heart with canagliflozin, solubilized in the Langendorff perfusion buffer, had no impact on the myocardial infarct size.**

formulated treatment diets for the long-term oral administration study and the treatment drug for the ex vivo administration study. Dr. Bell is supported by the National Institute of Health (NIHR) University College London Biomedical Research Centre (BRC) and work is supported by the British Heart Foundation (PG/18/10/33550). Dr. Long's laboratory is supported by a Medical Research Council (MR/P018629/1), Diabetes UK (13/0004763, 15/0005283), Kidney Research UK (RP36/2015), and by the NIHR BRC at Great Ormond Street Hospital for Children NHS Foundation Trust and University College London. Prof. Yellon has served on a global advisory board for Novo Nordisk. All other authors have reported that they have no relationships relevant to the contents of this paper to disclose.

All authors attest they are in compliance with human studies committees and animal welfare regulations of the authors' institutions and Food and Drug Administration guidelines, including patient consent where appropriate. For more information, visit the *JACC: Basic to Translational Science* author instructions page.

Manuscript received August 29, 2018; revised manuscript received October 11, 2018, accepted October 11, 2018.

SUMMARY

The authors hypothesized that despite similar cardiovascular event rates, the improved cardiovascular survival from sodium glucose transporter 2 (SGLT2) inhibition, seen clinically, could be via a direct cytoprotective effect, including protection against myocardial ischemia/reperfusion injury. Langendorff-perfused hearts, from diabetic and nondiabetic rats, fed long-term for 4 weeks with canagliflozin, had lower infarct sizes; this being the first demonstration of canagliflozin's cardioprotective effect against ischemia/reperfusion injury in both diabetic and nondiabetic animals. By contrast, direct treatment of isolated nondiabetic rat hearts with canagliflozin, solubilized in the isolated Langendorff perfusion buffer, had no impact on infarct size. This latter study demonstrates that the infarct-sparing effect of long-term treatment with canagliflozin results from either a glucose-independent effect or up-regulation of cardiac prosurvival pathways. These results further suggest that SGLT2 inhibitors could be repurposed as novel cardioprotective interventions in high-risk cardiovascular patients irrespective of diabetic status. (J Am Coll Cardiol Basic Trans Science 2019;4:15–26)

ABBREVIATIONS AND ACRONYMS

DMSO = dimethyl sulfoxide

NHE = sodium hydrogen exchange

NS = not significant

SGLT2 = sodium glucose transporter 2

ZDF = Zucker Diabetic Fatty

ZL = Zucker Lean

The remarkable cardiovascular benefits of sodium/glucose co-transporter 2 (SGLT2) inhibitors are now well recognized in high-risk type 2 diabetic patients following the landmark clinical trials, EMPA-REG OUTCOME (Empagliflozin Cardiovascular Outcome Event Trial in Type 2 Diabetes Mellitus) (1) and CANVAS (CANagliflozin CardioVAScular Assessment Study) (2), and is further supported by positive outcome data from DECLARE-TIMI 58 trial (Multicenter Trial to Evaluate the Effect of Dapagliflozin on the Incidence of Cardiovascular Events-Thrombolysis In Myocardial Infarction 58) announced at the recent European Society of Cardiology World Congress. These studies, both designed as noninferiority investigations mandated by the regulatory authorities, revealed an unexpected benefit and superiority over existing standard diabetic care, with a significant reduction of cardiovascular mortality. Equally remarkably, this reduction in cardiovascular mortality was seen notably early—within 1 to 2 months—following the introduction of the respective SGLT2 inhibitor. The mechanism underlying the reduction in cardiovascular mortality is not clear and has been subject to much conjecture: seemingly, improvements in blood sugar control were comparatively minor and improvements in terms of diuresis, weight loss, and blood pressure reduction inadequate to fully explain the differences observed. Indeed, many, including ourselves, have speculated a potential pleiotropic beneficial effect for this class of glucose-lowering therapy (3–5).

The hypothesis that SGLT2 inhibitors may have pleiotropic effects appears to be supported by other observations from the clinical trial data, not least that SGLT2 inhibition appears to have minimal impact upon the cardiovascular event rate—be it myocardial infarction or stroke, admissions with unstable angina or the need for a coronary revascularization procedure (1,2). As such, there appears to be minimal impact of SGLT2 inhibition upon macrovascular (arterial atheromatous) disease—but overall, despite experiencing the same frequency of cardiovascular events, survival nonetheless appears to be better in those taking SGLT2 inhibitors, a benefit that strikingly manifests within the first few months of treatment.

Cellular injury, necrosis, and programmed cell death (apoptosis, necroptosis, autophagy) are important pathophysiological features of a number of maladaptive processes in the heart, including myocardial ischemia and heart failure (6). We therefore hypothesized that despite a similar cardiovascular event rate from events such as acute myocardial ischemia, the improved cardiovascular survival arising from SGLT2 inhibition was through direct myocardial cytoprotection. In a rat, this can be tested in an experimental model of injurious ischemia/reperfusion injury, whereby diabetic animals treated with an SGLT2 inhibitor would be anticipated to have smaller myocardial infarcts. Moreover, if the cardiovascular benefits of SGLT inhibitors are genuinely pleiotropic, we hypothesized that the benefits of SGLT2 inhibition would also be found in those without diabetes.

In designing our experiments, we observed that whereas the survival curves in the EMPA-REG and CANVAS trials separate quickly, it still takes weeks to see the survival curves diverge. As such, we undertook to treat both diabetic and nondiabetic rats for a period of 4 weeks. Moreover, because treatment with an SGLT2 inhibitor will invariably affect circulating blood glucose at the time of myocardial infarction in vivo, we harvested the hearts and undertook the

FIGURE 1 Characterization of the ZL and ZDF Phenotypes

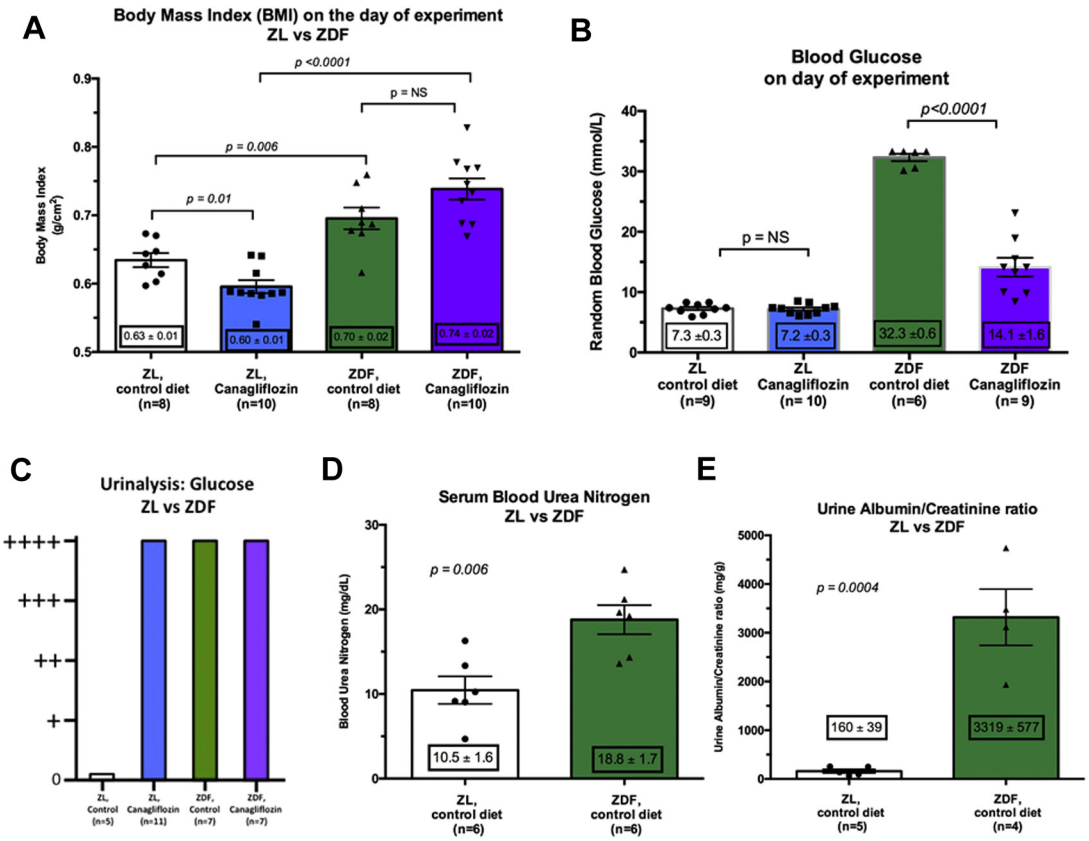

(A) Body weight index. The diabetic ZDF rats were significantly larger than the nondiabetic ZL rats. Canagliflozin administration in the ZL led to a significant reduction in body mass index that was absent in the ZDF diabetic rats. n = 8 to 10 per group. **(B)** Random glucose concentration on day of experiment. As expected, ZDF diabetic rats had significantly higher blood glucose concentrations compared to the nondiabetic ZL controls ($p < 0.0001$; n = 6 to 9 per group). Canagliflozin had no impact upon blood glucose in the ZL group (p = NS; n = 9 to 10 per group), but significantly reduced glucose in the diabetic ZDF rats ($p < 0.0001$; n = 6 to 9 per group). **(C to E)** Renal manifestations of diabetes in the ZDF rats. **(C)** Urine glucose, measured by urinalysis strip test. No glucosuria was detectable in the control ZL rats, but there was significant glucosuria in ZL rats on canagliflozin. As expected, significant glucosuria was found in both ZDF control and canagliflozin-treated groups. **(D)** Blood urea nitrogen was significantly higher in the ZDF rats compared with the nondiabetic ZL: 11 ± 2 mg/dl versus 19 ± 2 mg/dl (p = 0.006, n = 6 per group). **(E)** A similar pattern was observed in the urine albumin/creatinine ratio—the diabetic ZDF rats demonstrating a significantly higher albumin excretion compared with the nondiabetic ZL rat: 160 ± 39 mg/g versus 3,319 ± 577 mg/g (p = 0.0004; n = 4 to 5 per group). ZDF = Zucker Diabetic Fatty; ZL = Zucker Lean.

experiments in an ex vivo Langendorff model, with perfused glucose concentration controlled in all experiments.

Finally, we wished to ascertain whether the SGLT2 inhibitor would have a direct, cardioprotective effect in the isolated heart, and to this end, we undertook a further group of experiments with "acute" exposure to the SGLT2 inhibitor, with the drug added to the Langendorff perfusate throughout the perfusion protocol.

Using the SGLT2 inhibitor, canagliflozin, in a reverse-translational study, we found that long-term pre-administration over 4 weeks led to a significant attenuation of myocardial infarct size in both diabetic Zucker Diabetic Fatty (ZDF) and nondiabetic Zucker Lean (ZL) rats. This observation may have significant impact for future translational studies in the repurposing of this new class of glucose-lowering drugs in all patients, irrespective of diabetic status, with high-risk cardiovascular disease.

METHODS

For a detailed description of all methods, see the Supplemental Appendix. In brief, ZL and ZDF rats were monitored weekly with random blood glucose

FIGURE 2 **Impact of Canagliflozin in Nondiabetic ZL and Diabetic ZDF Rats**

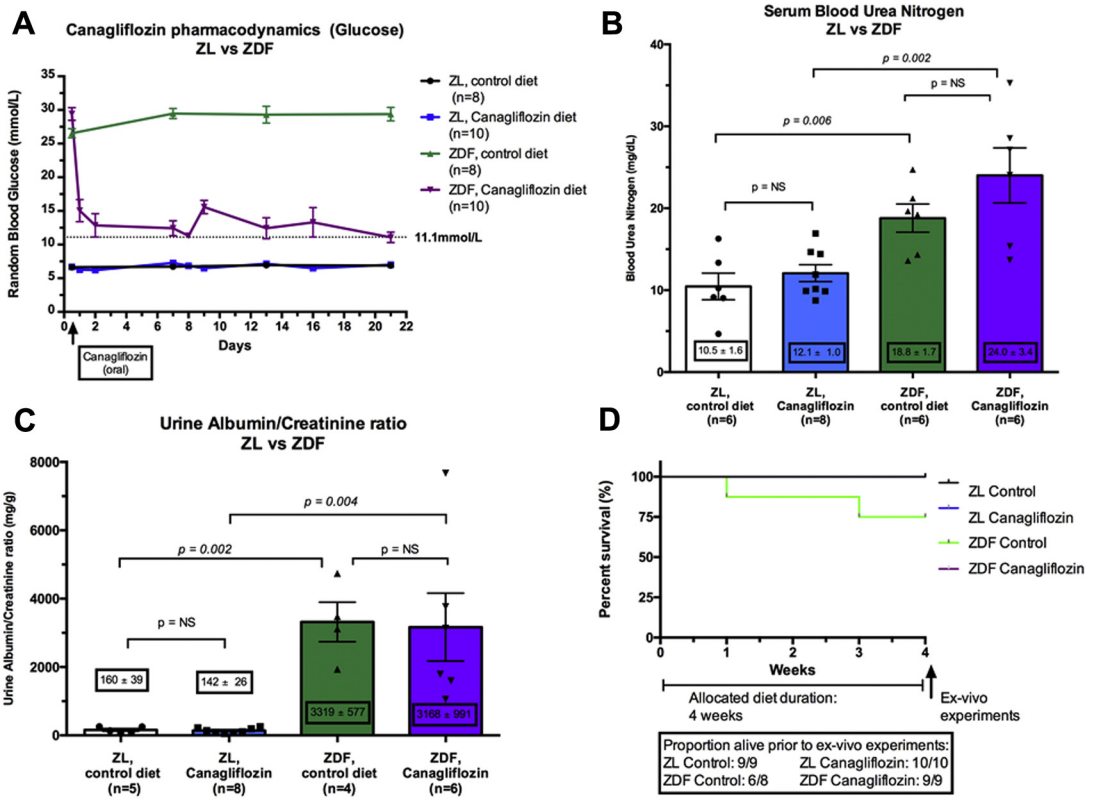

(A) Canagliflozin had a rapid and sustained impact upon circulating blood glucose in the diabetic ZDF rats compared with the untreated animals. By contrast, canagliflozin had no impact upon circulating blood glucose in the nondiabetic ZL rats ($p = 0.002$; $n = 8$ to 10 per group). **(B)** After 4 week's treatment, canagliflozin had little impact upon blood urea nitrogen in either ZL or ZDF rats ($p = NS$; $n = 6$ to 8 per group). **(C)** As with BUN, there was little impact from 4-week oral canagliflozin administration in either ZL or ZDF rats upon albumin/creatinine ratios ($p = NS$; $n = 4$ to 8 per group). **(D)** Kaplan-Meier survival curve. Two animals, both in the control diabetic ZDF group, had to be euthanized for severe urinary sepsis. All other groups completed without events. Abbreviations as in Figure 1.

assessment, and fed either standard or high-fat chow, either fortified with canagliflozin or without (control) for a period of 4 weeks before harvesting the heart and Langendorff perfusion. All feeds, both with and without drug, were prepared by Research Diets (New Brunswick, New Jersey) based on the diet formulations provided by Janssen Research and Development (Springhouse, Pennsylvania). Using this formulation, the canagliflozin-fortified feed results in a circulating canagliflozin concentration (10 μmol/l) equivalent to that found in human subjects taking maintenance canagliflozin, 300 mg daily (7). Different diets were used for nondiabetic ZL and diabetic ZDF rats to account for the quantity of food eaten by these rats: the details of these feeds are detailed in the Supplemental Appendix.

Animals used for the acute administration of canagliflozin were nondiabetic Sprague-Dawley rats where canagliflozin (Janssen Research and Development) or vehicle, dimethyl sulfoxide (DMSO) (0.05% DMSO, Sigma Aldrich, Poole, United Kingdom) was perfused throughout the Langendorff experiment.

RANDOMIZATION. All experiments were block randomized. Analysis was performed by 2 blind observers and arbitrated by a third independent adjudicator if required. Once all results were available, the data were unblinded and analyzed.

STATISTICAL ANALYSIS. All analyses were performed using GraphPad Prism version 6 (GraphPad Software, San Diego, California). The specific statistical test used is reported next to each result. An unpaired *t*-test was used for 2 independent groups of continuous variables and a 1-way analysis of variance with Tukey's multiple comparison test for 3 or more independent groups. Data are presented as mean ± SEM. N values are either displayed in the

FIGURE 3 A CONSORT-Style Diagram for Infarct Assessment in the 4-Week Administration Study

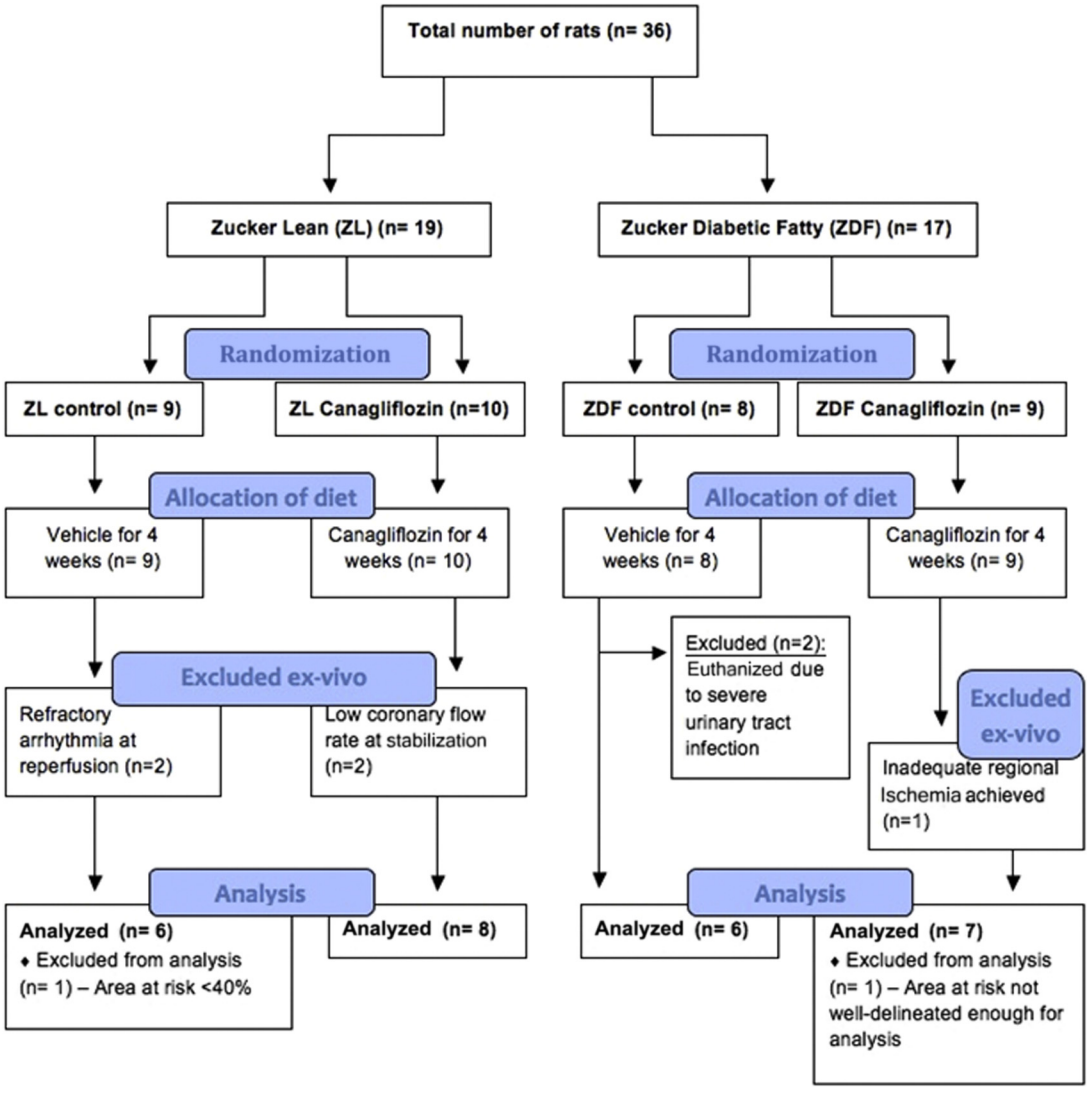

Thirty-six animals were started into the study, of which 29 completed through to analysis. Reasons for and timings of animal exclusions shown in all groups. Pre priori exclusion criteria are shown in the Supplemental Appendix. Abbreviations as in **Figure 1**.

figure or described in the figure legend for each experiment. A significance level of 5% ($\alpha = 0.05$) and 80% power ($\beta = 0.20$) were used. Statistical significance was reported if p was <0.05 and results where p was >0.05 were reported as nonsignificant.

RESULTS

CHARACTERIZATION OF THE ZDF DIABETIC PHENOTYPE. To ensure that our ZDF rats represented a reasonable facsimile of the diabetic cohort represented within the EMPA-REG and CANVAS studies, we undertook characterization of the nondiabetic ZL and diabetic ZDF rats. We found, as expected, that the ZDF rats were obese and hyperglycemic (**Figures 1A and 1B**) and hyperglucosuric (**Figure 1C**). In addition, the ZDF rats were found to have evidence of end-organ manifestations of their diabetes, as represented by abnormal renal function and albuminuria (**Figures 1C and 1D**). We are therefore confident that the ZDF represents a reasonable approximation of the human obese type 2 diabetic phenotype with significant and established diabetes at the time of experimentation.

Unexpectedly, we found that diabetic rats treated with canagliflozin were heavier than untreated

diabetic rats; the expected weight loss from the calorific depletion associated with SGLT2-dependent glycosuria was, however, observed in the canagliflozin-treated nondiabetic ZL rats. Growth curves are shown in Supplemental Figure 1: the control-diet diabetic ZDF rats started heavier than the nondiabetic ZL rats, but failed to gain significant weight over the 4 weeks of feeding. By contrast, nondiabetic ZL rats gained weight in a linear fashion over the same 4-week period. Interestingly, the pattern and rate of weight gain seen in nondiabetic rats were mirrored in diabetic ZDF rats fed with canagliflozin, suggesting a healthier animal concomitant with better-controlled diabetes, an interpretation fitting with empirical observations of these animals' physical condition.

CHARACTERIZATION OF THE EFFICACY OF CANAGLIFLOZIN IN LOWERING CIRCULATING GLUCOSE. To ensure that oral administration of canagliflozin, via fortification of the chow, was an effective antihyperglycemic intervention in our rat model, we observed the random glucose profile in both nondiabetic ZL and diabetic ZDF rats throughout the treatment lead-in period. We found that canagliflozin was highly effective in lowering blood glucose concentrations in the ZDF rats within a short period from the onset of oral drug administration. Significantly improved blood glucose control was evident throughout the canagliflozin treatment course compared with control, with random blood glucose of 16 ± 4 mmol/l versus 29 ± 1 mmol/l, respectively (p = 0.002) (**Figure 2A**).

Importantly, canagliflozin had no impact upon circulating glucose in the nondiabetic ZL rats, with equivalent blood glucose being recorded in both groups (p = NS) (**Figure 2A**). Importantly, we found no evidence of hypoglycemia in either canagliflozin treatment group, despite the presence of significant glucosuria in the canagliflozin-treated nondiabetic ZL rats (**Figure 1C**).

Interestingly, there was no attenuation of renal dysfunction in the diabetic canagliflozin-treated group (p = NS) (**Figures 2B and 2C**). Unfortunately, our urinalysis assay saturates at glucose levels in excess of 110 mmol/l, but higher urinary glucose would be anticipated in this group (**Figure 1C**). With respect to animal mortality, only 2 deaths were recorded—both animals were euthanized for severe urinary tract infection, and these events were found to occur only in animals in the untreated control diabetic ZDF group (**Figures 2D and 3**). The impact of diabetes and canagliflozin upon un-paced heart rate and liver: body weight ratio are summarized in Supplemental Figures 3 and 4, respectively.

FIGURE 4 Infarct Size Reduction Following Long-Term 4-Week Oral Administration of Canagliflozin

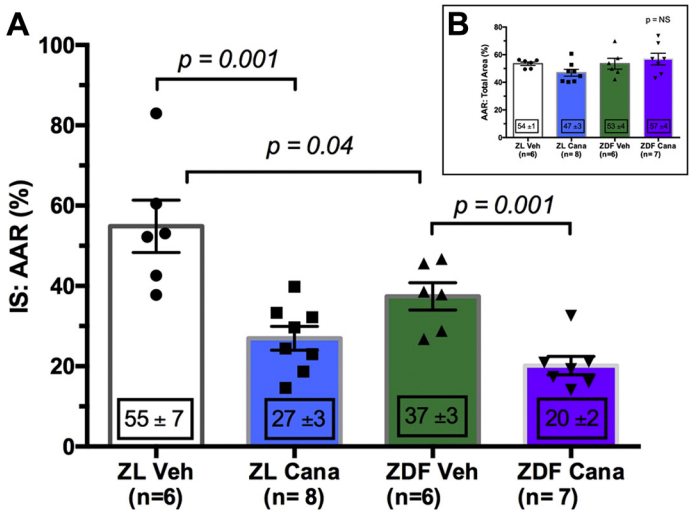

(A) In both diabetic ZDF and nondiabetic ZL rats, we found a significant reduction of infarct size compared with control. In nondiabetic rats, infarct size was reduced from 55 ± 7% to 27 ± 3% (p = 0.001; n = 6 to 8 per group). In the diabetic ZDF rats, a similar reduction of infarct size was also observed with infarct size reducing from 37 ± 3% to 20 ± 2% (p = 0.001; n = 6 to 8). There was a modest, but significant, difference in infarct size between control diet–treated ZL and ZDF rats (p = 0.04). **(B)** Area at risk in all groups was equivalent (p = NS; n = 6 to 8 per group). Cana = canagliflozin; IS:AAR = infarct size/area at risk ratio; ND = nonsignificant; Veh = vehicle; other abbreviations as in **Figure 1**.

IMPACT OF 4-WEEK ORAL CANAGLIFLOZIN ON MYOCARDIAL INFARCT SIZE. For this investigation, we used 36 animals. Of these, 9 had to be excluded for reasons summarized in **Figure 3**. Twenty-seven animals completed the full experimental protocol.

We found a small, but significant, difference between myocardial infarct size in the control arms of the diabetic ZDF and the nondiabetic ZL rat heart groups (p = 0.04) (**Figure 4A**, Supplemental Figure 2). This difference is expected in Langendorff-perfused hearts where glucose is the sole energy substrate (see review [8]). We found that canagliflozin, mirroring the important data by Andreadou et al. (9) in the mouse, significantly reduced myocardial infarct size in diabetic ZDF rats. Infarct size relative to the control chow-fed ZDF rats was significantly attenuated, from 37 ± 3% to 20 ± 2% of the area at risk (p = 0.001) (**Figure 4A**). Importantly, canagliflozin also significantly abrogated myocardial injury in the nondiabetic ZL rats, reducing infarct size from

FIGURE 5 Infarct Sizes Following Short-Term Ex-Vivo Administration in Nondiabetic Sprague-Dawley Rats

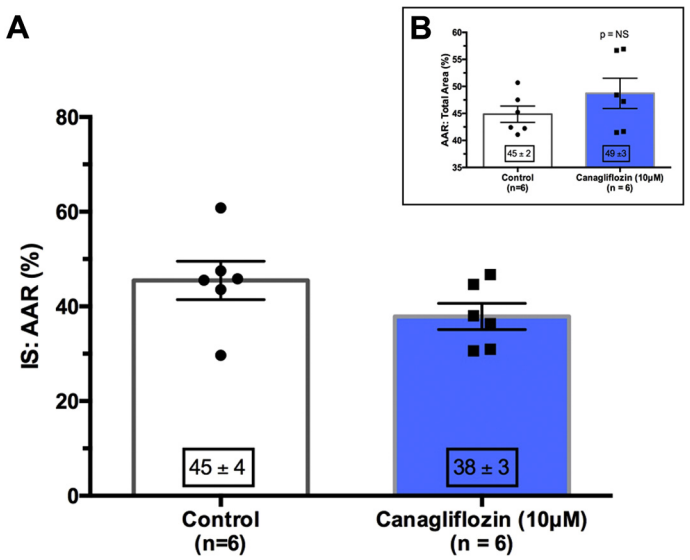

(A) In contrast to the cardioprotective effect of 4-week oral administration of canagliflozin, we found no evidence of infarct reduction with short-term, ex-vivo administration of canagliflozin: infarct sizes of 45 ± 4% versus 38 ± 3% ($p = NS$, $n = 6$ per group) in the vehicle control group. **(B)** There was no difference in the area at risk in either of the treatment groups (DMSO vehicle control versus canagliflozin; $p = NS$; $n = 6$ per group). DMSO = dimethyl sulfoxide; other abbreviations as in Figures 1 and 4.

55 ± 7% to 27 ± 3% ($p = 0.001$) (Figure 4A). The areas at risk in all control and treatment groups were similar with no statistical difference (Figure 4B). The impact of canagliflozin upon coronary flow and left ventricular developed pressure are summarized in Supplemental Figures 5 and 6, respectively.

EFFECT OF SHORT-TERM ADMINISTRATION OF CANAGLIFLOZIN AT THE TIME OF ISCHEMIA/REPERFUSION INJURY. To ascertain whether acute administration of canagliflozin is protective against injurious ischemia/reperfusion injury in the nondiabetic rat, we subjected the isolated Sprague-Dawley rat heart to ischemia/reperfusion injury in the presence of vehicle (0.05% DMSO) or 10 μmol/l canagliflozin throughout the perfusion protocol (during 40-min stabilization, 35-min regional ischemia, and throughout the 2 h of reperfusion). The concentration used is equivalent to the plasma concentration of canagliflozin in diet-fed ZDF rats (7). Baseline characteristics were identical between groups: both demonstrating a nondiabetic level of random blood glucose and identical anthropological measurements between groups (Supplemental Table 1). No rats had to be excluded from this study, and all rat data were included in the final analysis.

Of note, short-term, ex-vivo canagliflozin failed to significantly alter infarct size, with treatment versus control of 38 ± 3% versus 45 ± 4%, respectively ($p = 0.15$) (Figure 5A). There was no difference in the area at risk between any of the groups (Figure 5B).

DISCUSSION

Our study provides the first evidence to our knowledge that long-term oral administration of canagliflozin over a period of 4 weeks is cardioprotective, ameliorating myocardial infarct size in both diabetic *and* nondiabetic rats, independent of glucose concentration at the time of ischemia/reperfusion injury. The latter observation, that canagliflozin-induced protection in the nondiabetic rat, is particularly noteworthy: a clinically available SGLT2 inhibitor, canagliflozin, appears to have a cardiovascular and cardioprotective role that extends beyond (and probably also independent of) its intended indication in the management of hyperglycemia in type 2 diabetes mellitus.

LONG-TERM ORAL CANAGLIFLOZIN ATTENUATES MYOCARDIAL INFARCTION IN THE DIABETIC RAT. In the diabetic ZDF rats, attenuating the extent of myocardial necrosis hints towards a novel mechanism underlying the significant reduction of cardiovascular mortality found in the clinical outcome studies, EMPA-REG and CANVAS (1,2). Although the clinical data reveal no evidence that SGLT2 inhibitors reduce the number of cardiovascular events such as acute coronary syndromes, they may reduce the myocardial injury that occurs as a consequence of these events. A reduction of myocardial necrosis may thus improve both the immediate and long-term survivability of acute myocardial infarction and reduce the progression into ischemic cardiomyopathy and heart failure—a hypothesis that warrants further investigation.

Interestingly, the protection from long-term ingestion of canagliflozin was found in hearts that were removed and perfused, ex vivo, with a perfusate that contained a fixed concentration of glucose (11 mmol/l). We designed the experiments this way intentionally to avoid potential confounding the effects of glucose-lowering by canagliflozin at the time of ischemia/reperfusion injury. Moreover, Langendorff perfusion removes, through washout, other metabolic substrates that may confound canagliflozin administration (e.g., hepatic generation of ketones (10), as discussed further later in the text) are excluded as a potential mechanism of cardioprotection. Moreover, that these explanted hearts were protected, despite 40 min of crystalloid

washout before ischemia, suggests a mechanism that imbues a "memory," potentially through the recruitment of signaling pathways. And if a signaling pathway, it is a pathway whose efficacy, unlike that of ischemic conditioning (11), is seemingly not affected by the presence of significant diabetes (the severity of the diabetic phenotype confirmed by evidence of the development of nephropathy). One such mechanism may be through a Jak-STAT3 pathway, as suggested by Iliodromitis's group (9)—but there may be others.

LONG-TERM ORAL CANAGLIFLOZIN ATTENUATES MYOCARDIAL INFARCTION IN THE NONDIABETIC RAT. Although the observation that canagliflozin attenuates infarct size in the diabetic rat is important, the principal novelty in this study comes from our data in the nondiabetic group of animals. We observe that long-term oral canagliflozin administration significantly reduces myocardial infarct size in the nondiabetic ZL rat heart. These data have 3 provocative implications:

1. The potentially paradigm-shifting observation that SGLT2 inhibitors may be repurposed for the management of high-risk nondiabetic patients with significant pre-existing cardiovascular disease.
2. Canagliflozin is not a pure diabetic drug, and possesses pleiotropic effects that extend beyond purely lowering serum glucose.
3. The cardioprotective effect of canagliflozin is only manifest when administered orally over a period of weeks, which challenges current thinking in terms of mechanisms that appear to extend beyond a direct effect upon either the myocardium or kidney.

EX-VIVO CANAGLIFLOZIN FAILS TO PROTECT THE NONDIABETIC RAT HEART. In contrast to the long-term oral administration, the short-term administration of canagliflozin, ex vivo, administered at a concentration of 10 μmol/l (equivalent to the circulating concentration in patients taking canagliflozin, 300 mg once daily [7]) throughout the perfusion protocol, failed to reduce infarct size. This concentration of canagliflozin is also equivalent to a rat steady-state circulating serum canagliflozin concentration from oral digestion of drug, and a concentration that is sufficient to inhibit both SGLT2 and SGLT1, but insufficient to abrogate GLUT (glucose transporter) activity (12). The observation that short-term ex vivo administration of canagliflozin fails to protect the isolated heart may provide some further clues to the potential mechanism of action, because it appears to preclude a direct-acting cardioprotective effect of the drug upon the myocardium. Administering the drug ex vivo removes any confounding endocrine effects that the drug might elicit from any other organ system in vivo, as might occur in our long-term administration model. Thus, in the absence of infarct attenuation from ex vivo administration of canagliflozin, it would appear that the cardioprotective effect of SGLT inhibition is unlikely to be through the drug acting directly upon the myocardium itself and hints toward an endocrine (and downstream signaling) or metabolic effect to explain the beneficial effect of long-term oral administration of canagliflozin. However, our data appear not to support a metabolic effect: in our long-term canagliflozin model, the protection was seen ex vivo with a sole metabolic substrate: glucose at a concentration of 11 mmol/l. This makes preferential energy-substrate switching, as proposed in the ketone hypothesis (10), unlikely as an explanation for the cardioprotection observed. Following explantation and Langendorff perfusion of the heart, ketones will be rapidly washed out of the coronary circulation because the crystalloid-perfused Langendorff model is associated with far higher coronary flows than found in vivo (13). Thus, ketones will rapidly fall to negligible levels within the myocardium, and are unlikely to supplant the plentiful supply of glucose as the heart's primary fuel source in the Langendorff perfused model. Of course, we have not excluded the role of endogenous myocardial glycogenesis, but interestingly, long-term SGLT2 inhibition leads to diminution of kidney and liver glycogen stores (14). The role of glycogen in myocardial ischemia reperfusion injury is complex—canonical succinate synthesis through gluconeogenesis during myocardial ischemia is likely beneficial, but potentially deleterious during reperfusion through reversal of complex II of the mitochondrial transport chain (15). The impact of glycogen depletion on myocardial injury would be interesting to study further.

The sodium hydrogen exchange (NHE) hypothesis appeared to be a strong and attractive contender to explain the cardioprotection in our long-term canagliflozin administration studies (16,17). Previous investigations using cariporide and amiloride in animal models reveal highly efficacious anti-ischemic benefits of NHE inhibition against myocardial infarction, particularly when administered before the onset of myocardial ischemia (18–21). Thus, we had anticipated the short-term ex vivo study to provide further evidence of infarct size limitation. Indeed, in the excellent study from Zuurbier's group (17), with 3 μmol/l canagliflozin, they demonstrated highly effective attenuation of NHE activity. Given the

similarity in concentration of canagliflozin in our and in Zuurbier's cell-based model, we were surprised that we found no protection in our ex-vivo model. Might the protective effects of long-term administration of canagliflozin be mediated through NHE inhibition? Encouragingly, protection was observed in both diabetic and nondiabetic animals as expected. However, with 40 min of washout before induction of ischemia, it seems somewhat unlikely that significant quantities of canagliflozin would remain within the heart. Our data would therefore appear to suggest that the observed protection from long-term administration of canagliflozin is less likely to be mediated through NHE inhibition, but perhaps through another pleiotropic pathway capable of triggering a "memory" effect through activation of signaling cascades. Already identified candidate pathways include the aforementioned Jak/STAT3 pathway (9) that may also help attenuate oxidative stress and fibrotic myocardial remodeling (22) or perhaps through AMPK (23) (also found in kidney to reduce ischemia/reperfusion injury [24]), although these are not hypotheses that we have yet tested.

Finally, SGLT2 inhibitors have been found to imbue significant protection in the vasculature of diabetic ZDF rats, with preservation of endothelial function. This endothelial protection appears to be mediated through attenuation of long-term glucotoxicity and amelioration of oxidative stress (25). This could translate into myocardial protection ex vivo, but we did not find significant differences in coronary flow in our model between canagliflozin-treated versus control-treated animals (data shown in the Supplemental Appendix). Moreover, if the protection were mediated primarily as a mechanism designed to abrogate glucotoxicity, this hypothesis fails to explain why canagliflozin protects the nondiabetic heart. However, it would be interesting to repeat these experiments in the nondiabetic ZL rat to see whether the cytoprotective phenotype is evident in the absence of injurious elevated blood glucose.

CANAGLIFLOZIN-MEDIATED CARDIOPROTECTION APPEARS INDEPENDENT OF CIRCULATING GLUCOSE. As expected, we found canagliflozin to be highly effective at reducing circulating blood glucose in our diabetic rat model. Although we did not see the random blood glucose level in canagliflozin-treated diabetic ZDF rats fall into the nondiabetic range, the drug was nonetheless still highly effective at reducing infarct size, suggesting that complete restoration of random blood glucose into the "normal" nondiabetic range is unnecessary to imbue the cardioprotection observed. Moreover, canagliflozin failed to have an impact on circulating blood glucose levels in the nondiabetic animals: random glucose levels were identical in both nondiabetic control and canagliflozin-treated rats. There are 2 observations in respect to this data: 1) that canagliflozin can be administered to nondiabetic animals without fear of triggering potentially injurious hypoglycemia; and 2) that lowering blood glucose is not a prerequisite for attenuation of myocardial infarct size. Therefore, glucose lowering in the diabetic ZDF animals is a good biomarker of canagliflozin-mediated SGLT2 inhibition, but the in vivo lowering of glucose is not conditional for the triggering of infarct-size reduction when the heart is explanted and perfused ex vivo. Furthermore, as alluded to above, as the hearts were maintained with a perfused glucose concentration of 11 mmol/l throughout perfusion, any confounding effect of differences in circulating glucose concentration is effectively removed from our experiment.

Finally, it is also interesting to observe that long-term oral canagliflozin is equally protective in both nondiabetic and diabetic animals. This contrasts with the majority of cardioprotective interventions whose efficacy is blunted in the presence of the diabetic phenotype (11). This, therefore, leads us to speculate that the mechanisms of protection are different from, and potentially additive to, more established experimental models of myocardial protection, such as ischemic or pharmacological conditioning. If this were to be the case, then it offers the opportunity to augment myocardial protection through combined therapeutic approaches at the time of presentation of an acute coronary syndrome, to optimize patient outcome.

ABSENCE OF RENOPRESERVATION. In establishing our diabetic model, we wanted to determine the severity of the diabetic phenotype. The SGLT2 outcome studies have all been performed in models of established type 2 diabetes mellitus, and typically in patients with high cardiovascular risk. We therefore wanted to ascertain whether our model displayed characteristics of diabetic end-organ damage in the form of albuminuria. Our diabetic ZDF rats did indeed display evidence of significant albuminuria at the point at which the hearts were harvested for ex vivo Langendorff perfusion. The lack of any meaningful difference between the canagliflozin-fed and control ZDF rats is not, however, unexpected. The renoprotective effects of SGLT2 inhibition typically take many months to manifest (2,26), which contrasts with the comparatively rapid separation of the cardiovascular outcome curves. We designed our study primarily as an investigation into cardioprotection; a study with renoprotection as a

primary endpoint would likely mandate a much longer duration of drug treatment.

DIABETIC COMPLICATIONS. It was initially surprising that the only serious, life-threatening complication found during our long-term study was infective. As might have been anticipated, the source of infection was, in both cases, urinary tract. However, these 2 events were in the nontreated control diabetic ZDF rats and not in animals treated with canagliflozin. In total, 2 animals in the control ZDF group had to be euthanized for serious sepsis; neither of the canagliflozin-treated groups (diabetic or nondiabetic) had evidence of septic complications. Both diabetic ZDF groups had significant glycosuria, whereas the untreated control ZDF also had significant hyperglycemia. The sepsis, therefore, is much more likely to be secondary to the uncontrolled diabetes in the control animals, whereas the infective risk associated with canagliflozin-induced glucosuria was easily managed by simple animal husbandry and hygiene methods. No animal deaths were found related to cardiovascular causes, but our study was not powered for this endpoint, nor was it run for a sufficient period for such complications to become manifest.

STUDY LIMITATIONS. In designing our studies, we accepted a number of compromises. To avoid the confusion that may ensue with polypharmacy, we did not treat the control diabetic animals to manage their hyperglycemia. These animals displayed high levels of glycemia, and 2 animals had septic complications that were rapidly identified and managed. We therefore feel that prolonging the duration of study beyond 4 weeks as designed would not have been feasible. However, the infarct size data are compelling: administering canagliflozin, irrespective of diabetic status, resulted in a pronounced reduction of myocardial infarct size.

As all diabetic patients in the clinical outcome studies were undertaken in the presence of antihyperglycemic agents, a future study may be constructed at the outset to include diabetic animals managed with metformin, the backbone of contemporary type 2 diabetic management. Indeed, this may well be mandated in any future study designed to look at cardiovascular complications and renal outcomes where much longer treatment periods would need to be considered.

We do not believe that the severity of the diabetes had an adverse impact upon the outcome of our study; in fact, the infarct size of the diabetic animals was entirely in line with previous short-term studies in other diabetic models (such as streptozocin-treated or Goto-Kakizaki lean diabetic rats) and from our own group and others (27,28). However, having established that canagliflozin is cardioprotective, it would be useful to demonstrate that this protective phenotype is reproducible on top of existing strategies for managing elevated blood sugar.

Interestingly, it is well recognized that diabetic hearts, when Langendorff-perfused with glucose as the sole substrate, will have a smaller infarct size compared with the nondiabetic heart under the same conditions (see review [8]). Although a reductionist approach in metabolic substrate provision has its limitations, there are advantages in that we have excluded other potential metabolic substrates that have been postulated (such as ketone bodies). From our data, future more in-depth analysis of the myocardial metabolome may be undertaken, and for example, the impact of any glycogen depletion that may result from long-term SGLT2 inhibition, investigated.

Finally, our short-term canagliflozin study was performed in Sprague Dawley rats, rather than the ZL strain. Neither strain of rat are diabetic. Both strains reveal similar infarct sizes when subjected to 35 min of regional ischemia and 2 h reperfusion. Although there are differences between individual strains of murine and rat models, and their sensitivity to myocardial ischemia/reperfusion injury, given baseline similarities in infarct size, we would have expected canagliflozin to be as protective in Sprague Dawley rats as the ZL. The absence of protection observed is, therefore, informative, but minor strain differences cannot be completely excluded.

CONCLUSIONS

We demonstrate that long-term oral administration of canagliflozin results in significant reduction in myocardial infarct size, irrespective of glucose lowering or the presence of diabetes. This protection appears not to be mediated via a direct effect of canagliflozin upon the myocardium, but via an intermediate signaling mechanism that has yet to be identified. Our study, therefore, provides new insights into the potential cardiovascular benefits of SGLT2 inhibition and even points to a potential and important translational repurposing of these drugs to reduce cardiovascular mortality in nondiabetic patients.

ADDRESS FOR CORRESPONDENCE: Prof. Derek M. Yellon, The Hatter Cardiovascular Institute, University College London, 67 Chenies Mews, London WC1E 6HX, United Kingdom. E-mail: d.yellon@ucl.ac.uk.

PERSPECTIVES

COMPETENCY IN MEDICAL KNOWLEDGE: SGLT2 inhibitors are known to improve cardiovascular outcomes in high-risk diabetic patients. We demonstrate for the first time that SGLT2 inhibitors attenuate infarct size in both diabetic *and* nondiabetic rats. This class of antihyperglycemic drug, therefore, appears to have cardioprotective properties that extend beyond their ability to lower circulating blood glucose.

TRANSLATIONAL OUTLOOK 1: Long-term SGLT2 inhibition is cardioprotective, reducing myocardial infarct size following injurious myocardial ischemia. This is a favorable characteristic for a diabetic therapy, supporting their use in diabetic patients with high risk of, or established, cardiovascular disease.

TRANSLATIONAL OUTLOOK 2: Our data suggest that infarct limitation is also seen in nondiabetic animals, raising the tantalizing potential for repurposing these drugs to improve cardiovascular outcomes in all high-risk cardiovascular patients, irrespective of diabetic status.

REFERENCES

1. Zinman B, Wanner C, Lachin JM, et al. Empagliflozin, cardiovascular outcomes, and mortality in type 2 diabetes. N Engl J Med 2015;373:2117–28.

2. Neal B, Perkovic V, Mahaffey KW, et al. Canagliflozin and cardiovascular and renal events in type 2 diabetes. N Engl J Med 2017;377:644–57.

3. Pioli MR, Ritter AMV, Modolo R. Unsweetening the heart: possible pleiotropic effects of SGLT2 inhibitors on cardio and cerebrovascular alterations in resistant hypertensive subjects. Am J Hypertens 2018;31:274–80.

4. Bell RM, Yellon DM. SGLT2 inhibitors: hypotheses on the mechanism of cardiovascular protection. Lancet Diabetes Endocrinol 2018;6:435–7.

5. Ahmed HM, Khraishah H, Cho L. Cardioprotective anti-hyperglycemic medications: a review of clinical trials. Eur Heart J 2018;39:2368–75.

6. Moe GW, Marin-Garcia J. Role of cell death in the progression of heart failure. Heart Fail Rev 2016;21:157–67.

7. Devineni D, Curtin CR, Polidori D, et al. Pharmacokinetics and pharmacodynamics of canagliflozin, a sodium glucose co-transporter 2 inhibitor, in subjects with type 2 diabetes mellitus. J Clin Pharmacol 2013;53:601–10.

8. Whittington HJ, Babu GG, Mocanu MM, Yellon DM, Hausenloy DJ. The diabetic heart: too sweet for its own good? Cardiol Res Pract 2012; 2012:845698.

9. Andreadou I, Efentakis P, Balafas E, et al. Empagliflozin limits myocardial infarction in vivo and cell death in vitro: role of STAT3, mitochondria, and redox aspects. Front Physiol 2017;8:1077.

10. Mudaliar S, Alloju S, Henry RR. Can a shift in fuel energetics explain the beneficial cardiorenal outcomes in the EMPA-REG OUTCOME study? A unifying hypothesis. Diabetes Care 2016;39: 1115–22.

11. Sack MN, Murphy E. The role of comorbidities in cardioprotection. J Cardiovasc Pharmacol Ther 2011;16:267–72.

12. Kuriyama C, Xu JZ, Lee SP, et al. Analysis of the effect of canagliflozinon renal glucose reabsorption and progression of hyperglycemia in Zucker diabetic Fatty rats. J Pharmacol Exp Ther 2014; 351:423–31.

13. Sutherland FJ, Hearse DJ. The isolated blood and perfusion fluid perfused heart. Pharmacol Res 2000;41:613–27.

14. Ataqeldiyeva K, Fujita Y, Yanagimachi T, et al. Sodium-glucose cotransporter 2 inhibitor and a low carbohydrate diet affect gluconeogenesis and glycogen content differently in the kidney and the liver of non-diabetic mice. PLoS One 2016;11: e0157672.

15. Zhang J, Wang YT, Miller JH, Day MM, Munger JC, Brookes PS. Accumulation of succinate in cardiac ischemia primarily occurs via canonical Krebs cycle activity. Cell Rep 2018;23: 2617–28.

16. Baartscheer A, Schumacher CA, Wust RC, et al. Empagliflozin decreases myocardial cytoplasmic Na(+) through inhibition of the cardiac Na(+)/H(+) exchanger in rats and rabbits. Diabetologia 2017;60:568–73.

17. Uthman L, Baartscheer A, Bleijlevens B, et al. Class effects of SGLT2 inhibitors in mouse cardiomyocytes and hearts: inhibition of Na(+)/H(+) exchanger, lowering of cytosolic Na(+) and vasodilation. Diabetologia 2018;61:722–6.

18. Avkiran M, Marber MS. Na(+)/H(+) exchange inhibitors for cardioprotective therapy: progress, problems and prospects. J Am Coll Cardiol 2002; 39:747–53.

19. Klein HH, Pich S, Bohle RM, Lindert-Heimberg S, Nebendahl K. Na(+)/H(+) exchange inhibitor cariporide attenuates cell injury predominantly during ischemia and not at onset of reperfusion in porcine hearts with low residual blood flow. Circulation 2000;102:1977–82.

20. Hale SL, Kloner RA. Effect of combined K(ATP) channel activation and Na(+)/H(+) exchange inhibition on infarct size in rabbits. Am J Physiol Heart Circ Physiol 2000;279:H2673–7.

21. Mirkovic S, Seymour AM, Fenning A, et al. Attenuation of cardiac fibrosis by pirfenidone and amiloride in DOCA-salt hypertensive rats. Br J Pharmacol 2002;135:961–8.

22. Lee TM, Chang NC, Lin SZ. Dapagliflozin, a selective SGLT2 Inhibitor, attenuated cardiac fibrosis by regulating the macrophage polarization via STAT3 signaling in infarcted rat hearts. Free Radic Biol Med 2017;104:298–310.

23. Hawley SA, Ford RJ, Smith BK, et al. The Na+/glucose cotransporter inhibitor canagliflozin activates AMPK by inhibiting mitochondrial function and increasing cellular AMP levels. Diabetes 2016; 65:2784–94.

24. Chang YK, Choi H, Jeong JY, et al. Dapagliflozin, SGLT2 inhibitor, attenuates renal ischemia-reperfusion injury. PLoS One 2016;11:e0158810.

25. Steven S, Oelze M, Hanf A, et al. The SGLT2 inhibitor empagliflozin improves the primary diabetic complications in ZDF rats. Redox Biol 2017; 13:370–85.

26. Wanner C, Inzucchi SE, Lachin JM, et al. Empagliflozin and progression of kidney disease in type 2 diabetes. N Engl J Med 2016;375:323–34.

27. Whittington HJ, Harding I, Stephenson CI, et al. Cardioprotection in the aging, diabetic heart: the loss of protective Akt signalling. Cardiovasc Res 2013;99:694–704.

28. Korkmaz-Icoz S, Lehner A, Li S, et al. Mild type 2 diabetes mellitus reduces the susceptibility of the heart to ischemia/reperfusion injury: identification of underlying gene expression changes. J Diabetes Res 2015;2015:396414.

KEY WORDS cardioprotection, diabetes, ischemia-reperfusion injury, myocardial infarction, SGLT2 inhibitor

APPENDIX For an expanded Methods section as well as supplemental figures and tables, please see the online version of this paper.

Go to http://www.acc.org/jacc-journals-cme to take the CME/MOC/ECME quiz for this article.

JACC: BASIC TO TRANSLATIONAL SCIENCE VOL. 4, NO. 1, 2019

MINI FOCUS ON SGLT2 INHIBITORS

Empagliflozin Improves Diastolic Function in a Nondiabetic Rodent Model of Heart Failure With Preserved Ejection Fraction

Kim A. Connelly, MBBS, PhD, Yanling Zhang, MD, Aylin Visram, BSc, Andrew Advani, BSc, MBChB, PhD, Sri N. Batchu, PhD, Jean-François Desjardins, MSc, Kerri Thai, BSc, Richard E. Gilbert, MBBS, PhD

VISUAL ABSTRACT

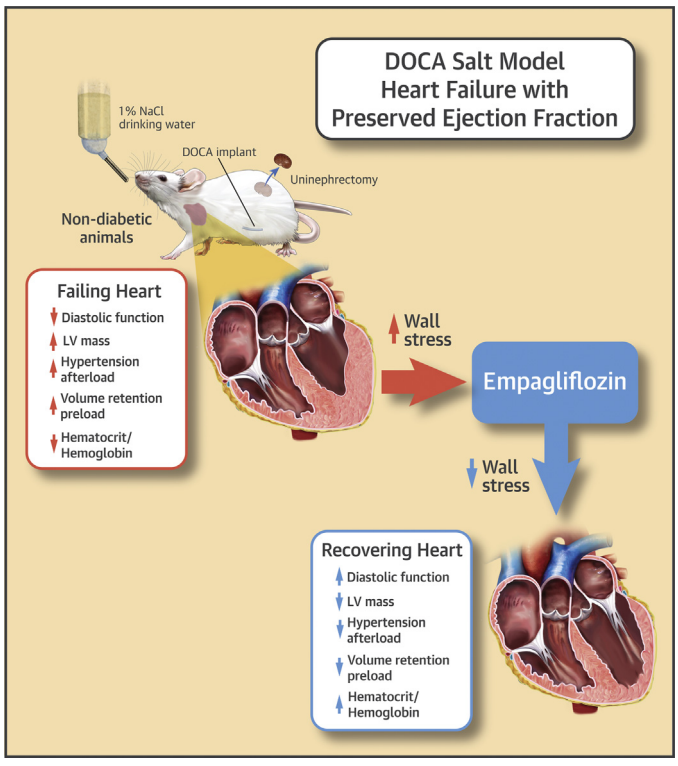

Connelly, K.A. et al. J Am Coll Cardiol Basic Trans Science. 2019;4(1):27–37.

HIGHLIGHTS

- This study evaluated the impact of the sodium-glucose–linked co-transporter-2 inhibitor, empagliflozin, on cardiac function and structure in a nondiabetic model of heart failure with preserved ejection fraction in the deoxycorticosterone acetate salt-sensitive rat.
- Deoxycorticosterone acetate rats developed hypertension, left ventricular hypertrophy, and diastolic dysfunction as measured by the time constant of relaxation, Tau.
- Empagliflozin therapy, which did not significantly reduce blood pressure, increased hematocrit, reduced left ventricular and cardiomyocyte hypertrophy, and reduced wall stress, which led to improved diastolic function (shortening of Tau).
- Empagliflozin treatment did not modify molecular markers of metabolism or hypertrophy, nor did it significantly affect key proteins involved in myocardial calcium handling.
- This study concluded that the sodium-glucose–linked co-transporter-2 inhibitor, empagliflozin, in a nondiabetic model of heart failure with preserved ejection fraction improved cardiac diastolic function and reduced wall stress primary through a reduction in cardiac preload, and also altered hemodynamics.

ISSN 2452-302X https://doi.org/10.1016/j.jacbts.2018.11.010

JACC: BASIC TO TRANSLATIONAL SCIENCE VOL. 4, NO. 1, 2019
FEBRUARY 2019:27–37

ABBREVIATIONS AND ACRONYMS

ANP = atrial natriuretic peptide

DOCA = deoxycorticosterone acetate

GADPH = glyceraldehyde 3-phosphate dehydrogenase

HF = heart failure

HFpEF = heart failure with preserved ejection fraction

HFrEF = heart failure with reduced ejection fraction

LV = left ventricular

SGLT2i = sodium-glucose–linked co-transporter-2 inhibitor

UNX = uninephrectomy

SUMMARY

Recent studies send an unambiguous signal that the class of agents known as sodium-glucose–linked co-transporter-2 inhibitors (SGLT2i) prevent heart failure hospitalization in patients with type 2 diabetes. However, the mechanisms remain unclear. Herein the authors utilize a rodent model of heart failure with preserved ejection fraction (HFpEF), and demonstrate that treatment with the SGLT2i empagliflozin, reduces left ventricular mass, improving both wall stress and diastolic function. These findings extend the observation that the main mechanism of action of empagliflozin involves improved hemodynamics (i.e., reduction in preload and afterload) and provide a rationale for upcoming trials in patients with HFpEF irrespective of glycemic status. (J Am Coll Cardiol Basic Trans Science 2019;4:27–37)

Despite significant advances in cardiovascular diagnostics and therapeutics, heart failure (HF) remains a common condition with significant morbidity and considerable mortality; regardless of underlying etiology, approximately 25% of those hospitalized will die (1). Although there have been major advances with multiple therapeutic agents of proven benefit in HF with reduced ejection fraction (HFrEF), heart failure with preserved ejection fraction (HFpEF) lacks evidence-based therapies (2).

SEE PAGE 38

Sodium-glucose–linked co-transporter-2 inhibitors (SGLT2is) increase urinary glucose excretion off-loading energy, lower plasma glucose and reduce body weight, as well as inducing modest diuresis that assists in blood pressure reduction. In addition to its antihyperglycemic actions, recent cardiovascular outcome studies have demonstrated a reduction in HF hospitalizations (3,4). Although the importance of these trials cannot be overstated, their outcomes are mostly unexpected. It is uncertain whether this drug class may provide similar benefit in both HFpEF and HFrEF or in only 1 of these conditions. Moreover, the magnitude of the effect of this therapy on HF hospitalization and the rapidity of its onset suggest that the cardioprotective properties of SGLT2is are greater than their ability to lower glucose. These findings have led not only to speculation as to how this antihyperglycemic drug class might exert its salutary effects but have also led to consideration that they may be also effective in the nondiabetic setting.

Recognizing the limited cardiac function data available from the aforementioned cardiovascular outcome trials in diabetes and the unmet clinical need in treating HFpEF, we sought to determine the effects of SGLT2 inhibition in HFpEF in the nondiabetic setting using a well-established animal model of the disease.

METHODS

ANIMALS. Experiments were conducted in 8-week old male Sprague-Dawley rats according to standard protocol for the deoxycorticosterone acetate (DOCA) hypertensive salt model, in which implants were prepared by mixing 200 mg of mineralocorticoid in

From the Keenan Research Centre, Li Ka Shying Knowledge Institute, St. Michael's Hospital, Toronto, Ontario, Canada. This study was supported by research grants from the St. Michael's Hospital Foundation, an investigator-initiated grant from Boehringer Ingelheim, as well as from the Canada Research Chair program (awarded to Dr. Gilbert). Dr. Connelly is supported by a new investigator reward from the CIHR and an early researcher award from the Ministry of Ontario. Dr. Advani is supported by a Diabetes Investigator Award from Diabetes Canada. Drs. Connelly, Advani, and Gilbert are listed as inventors on a patent application by Boehringer Ingelheim on the use of DPP-4 inhibitors in heart failure. Dr. Connelly has received research grants from AstraZeneca and Boehringer Ingelheim; has received travel support from Boehringer Ingelheim; and has received honoraria for speaking engagements and ad hoc participation in advisory boards from AstraZeneca, Boehringer Ingelheim, Sevier, Merck, Novo Nordisk, and Janssen. Dr. Advani has received research support from AstraZeneca and Boehringer Ingelheim. Dr. Gilbert is a shareholder in Certa, OccuRx, and Fibrocor Therapeutics; has received research grants from AstraZeneca and Boehringer Ingelheim; has received travel support from AstraZeneca; and has received honoraria for speaking engagements and ad hoc participation in advisory boards from AstraZeneca, Boehringer Ingelheim, and Janssen. All other authors have reported that they have no relationships relevant to the contents of this paper to disclose.

All authors attest they are in compliance with human studies committees and animal welfare regulations of the authors' institutions and Food and Drug Administration guidelines, including patient consent where appropriate. For more information, visit the *JACC: Basic to Translational Science* author instructions page.

Manuscript received May 1, 2018; revised manuscript received November 13, 2018, accepted November 14, 2018.

silicone rubber (5). Implanted rats then received 1% sodium chloride as drinking water, whereas uninephrectomy (UNX) rats were given tap water. One week later, rats were randomized to receive either empagliflozin mixed in chow (0.35 mg/g, gift of Boehringer Ingelheim, Ingelheim, Germany) or a control diet that coincided with DOCA implantation.

Four weeks after DOCA implantation, rats underwent echocardiography and cardiac catheterization. All procedures were performed in the research vivarium under anesthesia using 2.5% isoflurane. Systolic blood pressure was measured in conscious animals using an occlusive tail-cuff plethysmograph (Powerlab, ADInstruments, Colorado Springs, Colorado) (6). Before the animals were killed, they were housed in metabolic cages, and 24-h urine collections were obtained for measurement of glucose, sodium, and ß-OH butyrate excretion. Animals then underwent echocardiography and cardiac catheterization as described in the following. After these procedures, animals were killed, and their hearts were harvested for structural and molecular measurements. Tibial length was measured to provide a morphometric index for cardiac hypertrophy and lung weight (7). All animals were housed with 2 per cage at the St. Michael's Hospital Animal Research Vivarium in a temperature-controlled (22°C) room with a 12-h light/dark cycle and ad libitum access to commercial standard rat chow.

All animal studies were approved by the St. Michael's Hospital Animal Care Committee in accordance with the Guide for the Care and Use of Laboratory Animals (National Institute of Health Publication No. 85-23, revised 1996).

ECHOCARDIOGRAPHY. Transthoracic echocardiography was performed, as previously described (8), under light anesthesia (1% isoflurane supplemented with 100% oxygen) before the animals were killed. Images were acquired using a high-frequency ultrasound system (Vevo 2100, MS-250 transducer, Visualsonics, Toronto, Ontario, Canada). Two-dimensional, long-axis images of the left ventricle (LV) in parasternal long- and short-axis views with M-mode measurements at mid-papillary muscle level and linear dimensions were analyzed offline (Vevo 2100 software, version 1.8) using the standard leading edge-to-leading edge technique by a single investigator, who was blinded to treatment. The percentage of fractional shortening (FS%) was calculated according to the formula: FS% = (LVIDd - LVIDs)/LVIDd × 100, where LVIDd and LVIDs are end-diastolic diameter and end-systolic diameter, respectively, as previously described. LV wall stress (σ) was calculated by the equation: $\sigma = PR_i/2h(1 + h/2R_i)$, where P = systolic pressure, R_i = LV inner diameter (LVID), and h = LV wall thickness (9). Three consecutive cardiac cycles were averaged for all analyses.

CARDIAC CATHETERIZATION. Cardiac catheterization was performed as previously published (6). Briefly, rats were anesthetized with 2% isoflurane, intubated using a 14-gauge catheter, and ventilated using a pressure-controlled ventilator (TOPO ventilator, Kent Scientific, Torrington, Connecticut). Adequacy of anesthesia was assessed by lack of response to surgical manipulation and loss of muscular tone. Rats were placed in the supine position on a water circulating heating pad and a 2-F pressure–volume catheter (SPR-838, Millar Instruments, Inc., Houston, Texas) was inserted into the right carotid artery and advanced into the LV, and pressure–volume loops were generated. All pressure–volume loops were obtained with the ventilator turned off for 5 to 10 s and the animal apneic.

Data were acquired and recorded with a MPVS ultra data acquisition system (Millar Instruments) and LabChart Pro software (CHART 8.1 ADInstruments Inc., Colorado Springs, Colorado) under steady-state conditions and following inferior vena cava occlusion (pre-load reduction). Conductance signals acquired with the Millar catheter were calibrated with the estimated LV volumes derived from echocardiography by using a 2-point calibration method, and matching LV maximal and minimal conductance signals and end-diastolic and end-systolic volume were measured in the long-axis view. Using the pressure conductance data, functional parameters were then calculated, as previously reported (10).

HISTOPATHOLOGY. The extent of cardiac myocyte hypertrophy was determined on hematoxylin and eosin–stained sections, as previously reported (7). In brief, stained sections were scanned digitally by high resolution microscopy (Ultra-Resolution Digital Scanning System, Aperio Technologies Inc., Vista, California), and images were analyzed with NDP view2 software (Hamamatsu Photonics, Hamamatsu City, Japan). Cardiac myocytes with elliptical nuclei in the transverse section were selected. Diameter measurements were taken membrane-to-membrane across the narrowest point crossing the nucleus. The average diameter of 30 to 50 myocytes per animal was measured, as previously described (11).

WESTERN BLOTTING. For preparation of cytosolic fraction, heart tissues were minced and homogenized in homogenization buffer containing sucrose (250 mM), Tris-hydrogen chloride (10 mM),

TABLE 1 Animal Characteristics

	UNX + Control	UNX + Empa	DOCA + Control	DOCA + Empa
Body weight (g)	542 ± 25	490 ± 13*	423 ± 13	352 ± 9*†
LV weight/TL (mg/mm)	22 ± 1	20 ± 0	31 ± 1*	25 ± 1†
LW/TL (mg/mm)	39 ± 1	37 ± 1	44 ± 1*	38 ± 1†
Right kidney weight/TL (mg)	51 ± 1	62 ± 1*	104 ± 5*	90 ± 3*†
Food intake (g/24 h)	32 ± 2	31 ± 1	26 ± 2*	25 ± 1*
Water intake (ml/24 h)	19 ± 5	42 ± 4*	151 ± 14*	228 ± 25*†
Urine volume (ml/24 h)	28 ± 4	49 ± 5*	150 ± 13*	219 ± 24*†

Values are mean ± SEM. n = 7 to 8 in uninephrectomy (UNX) control and UNX empagliflozin (Empa) groups; n = 16 and 15 in deoxycorticosterone acetate (DOCA) control and Emp groups, respectively. *p < 0.05 versus UNX control group. †p < 0.05 versus DOCA control group.

LV weight/TL = left ventricular weight/tibial length; LW/TL = lung weight/tibial length ratio.

ethylenediaminetetraacetic acid (1 mM), sodium orthovanadate (1 mM), sodium flouride (1 mM), and a protease inhibitor cocktail (12). Immunoblotting of heart homogenates was performed on nitrocellulose membranes with antibodies in the following concentrations: phosphorylated phospholamban (phospho-PLN, Ser16) 1:1,000 (A285); Sarcoplasmic reticulum uptake Ca2+-ATPAase (SERCA2a) 1:1,000 (IID8F6); phospho-PLN (Thr17) 1:1,000 (#sc-17024, Santa Cruz Biotechnology, Dallas, Texas), phosphorylated Ca2+/calmodulin-dependent protein kinase II (CAMKII) 1:1000 (#sc-32289, Santa Cruz Biotechnology), total CAMKII 1:1000 (#sc-5306, Santa Cruz Biotechnology), Peroxisome proliferator-activated receptor gamma coactivator 1-alpha -PGC-1alpha 1:1,000 (#ab54481, Abcam Cambridge, Massachusetts), Peroxisome proliferator-activated receptor gamma coactivator 1-beta (PGCß) 1:1000 (#ab176328 Abcam), Glyceraldehyde-3-Phosphate Dehydrogenase (GAPDH) 1:5000 (#2118s, Cell signalling Technology, Danvers, Massachusetts) (12). Densitometry was performed using Image J version 1.39 (National Institutes of Health, Bethesda, Maryland).

FIGURE 1 Time Course for Systolic Blood Pressure

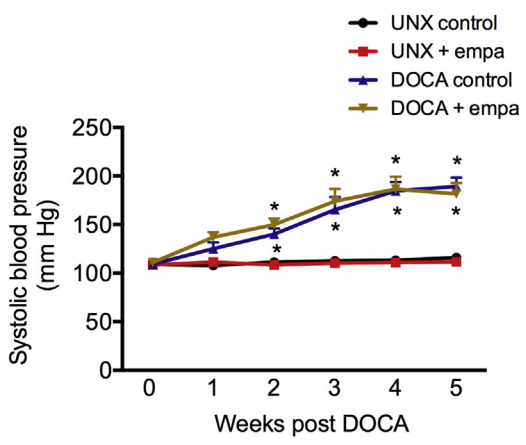

Time course for systolic blood pressure. n = 16 and 15 in deoxycorticosterone acetate (DOCA) control and empagliflozin (empa) groups, respectively. n = 7 to 8 in uninephrectomy (UNX) control and UNX empa groups. *p < 0.05 versus UNX + vehicle.

GENE EXPRESSION. The abundance of atrial natriuretic peptide (ANP), collagen 1/III, CD 36, PGC1α and β, Glut 1 and 4, hexokinase, pyruvate kinase, pyruvate dehydrogenase, carnitine palmitoyltransferase, uncoupling protein-3, nuclear respiratory factor-1, phosphoglucomutase-1, long-chain acyl-CoA dehydrogenase, GAPDH, pyruvate dehydrogenase E1-α subunit, ribosomal protein L13A (rRPL13a), and peroxisome proliferator–activated receptor-α were assessed by measuring their mRNA by quantitative real-time polymerase chain reaction in LV tissue stored at −80°C (10). In brief, SYBR Green (Life Technologies Corporation, Thermo Fisher, Waltham, Massachusetts) green-based measurement of gene expression was performed on the QuantStudio 7 Flex Real-Time PCR System (Applied Biosystems, Foster City, California) according to the manufacturer's instructions using the pre-designed sequence-specific primers from Integrated DNA Technologies (Coralville, Iowa). Data were analyzed using the Applied Biosystems Comparative Computer Tomography method. See Supplemental Table 1 for primers.

STATISTICAL ANALYSIS. Data are expressed as means ± SEM, unless otherwise specified. Between-group differences were analyzed by 2-way analysis of variance with Fisher's least significance difference post hoc test. Statistical analysis was performed using GraphPad Prism 6 for Mac OS X (GraphPad Software Inc., San Diego, California). A p value of <0.05 was regarded as statistically significant.

RESULTS

ANIMAL CHARACTERISTICS. Compared with UNX control rats, DOCA salt rats demonstrated significant reductions in both body weight and food intake, as well as hypertension, that developed 2 weeks after DOCA initiation (**Table 1, Figure 1**). Water intake and urine output also increased in parallel. Empagliflozin administration to DOCA salt animals further reduced body weight compared with control rats, without affecting food intake. DOCA salt animals displayed

increased heart weight and lung weight when indexed to tibial length, which was reduced with empagliflozin (Table 1). Both water intake and urine output were increased in proportion to each other in rats that had received empagliflozin in both control and DOCA salt settings.

LABORATORY PARAMETERS. Hematocrit and hemoglobin were lower in DOCA salt animals compared with control animals, and although these were not normalized to levels seen in control rats, hematocrit and hemoglobin were both substantially higher among DOCA salt rats that received empagliflozin (Table 2). Plasma sodium and 24-h urinary sodium excretion were increased in DOCA salt rats, although neither was affected by empagliflozin administration (Table 2).

Regardless of assignment to control or DOCA salt groups, animals that received empagliflozin showed substantial glucosuria, and, although still within the normoglycemic range, plasma glucose in DOCA salt rats was lower in those that received empagliflozin (Table 2). Urinary excretion of ß-OH-butyrate was higher in DOCA salt animals than that in control animals and did not differ

TABLE 2 Laboratory Parameters

	UNX + Control	UNX+ Empa	DOCA + Control	DOCA + Empa
Hct (%)	42.1 ± 0.7	41.0 ± 0.6	32.1 ± 1.8*	36.5 ± 0.8*†
Hb (g/l)	138.6 ± 1.9	136.6 ± 2.7	108.7 ± 4.6*	121.5 ± 3.6*†
U Na (mmol/l)	79.6 ± 12.0	44.6 ± 4.7	147.5 ± 16.0*	127.6 ± 13.4*
U Na (mmol/d)	2.03 ± 0.31	2.19 ± 0.33	22.3 ± 3.19*	26.6 ± 3.08*
P Na (mmol/l)	133.6 ± 0.7	135.6 ± 0.6	140.5 ± 0.7*	141.7 ± 0.5*
P Glu (mmol/l)	6.18 ± 0.19	5.91 ± 0.18	6.34 ± 0.13	5.71 ± 0.12*†
U Glu (mmol/l)	1.05 ± 0.58	60.0 ± 0.0*	0.9 ± 0.18	41.91 ± 4.38*†
U Glu (mmol/d)	0.03 ± 0.02	2.9 ± 0.31*	0.15 ± 0.04	8.15 ± 0.75*†
HbA_{1c} (%)	4.92 ± 0.18	4.66 ± 0.07	4.02 ± 0.02*	4.12 ± 0.10*
BHB (µmol/d)	1.65 ± 0.34	3.70 ± 0.41	13.43 ± 1.35*	15.18 ± 1.30*

Values are mean ± SEM. *p < 0.05 versus UNX + control group. †p < 0.05 versus DOCA + control group.
BHB = β-hydroxybutyrate; Glu = glucose; Hb = hemoglobin; Hct = hematocrit; Na = sodium; P = plasma; U = urine; other abbreviations as in Table 1.

FIGURE 2 Representative Echocardiograms

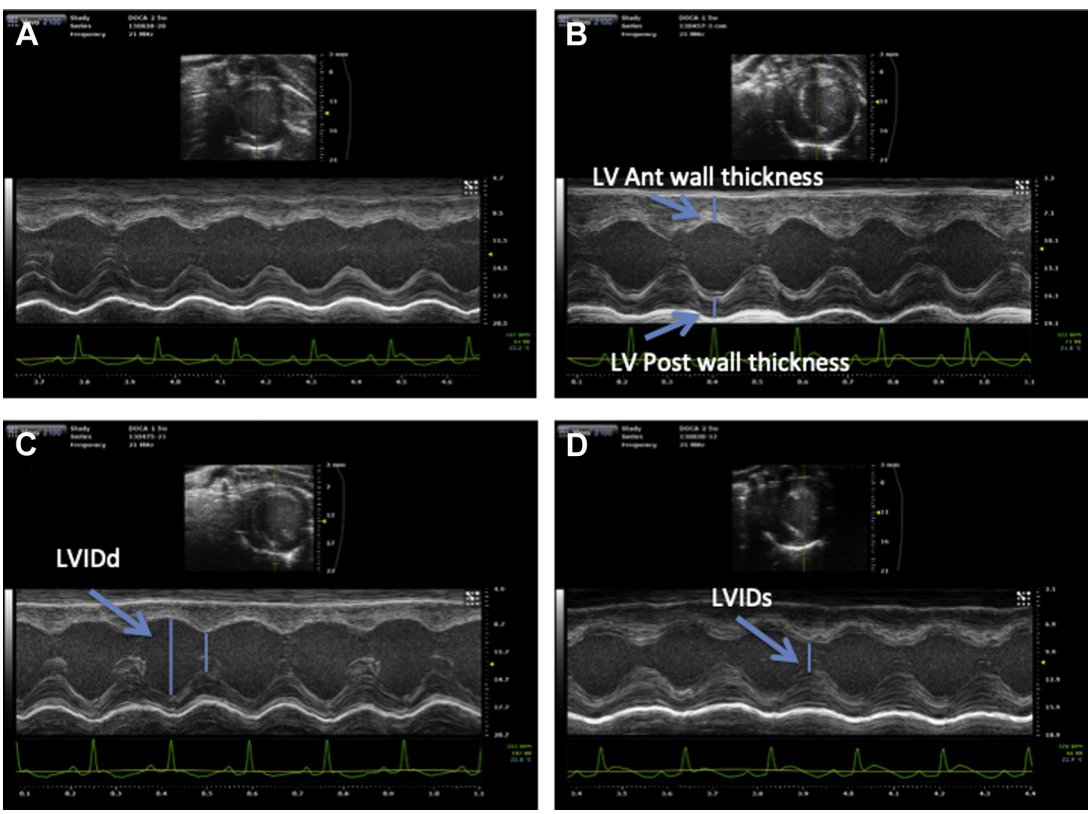

Representative echocardiograms (M-MODE) in **(A)** UNX + control, **(B)** UNX + empagliflozin, and **(C)** UNX + DOCA + control, and **(D)** UNX + DOCA + empa. Both left ventricular internal diameter systole (LVIDs) and wall thickness were reduced by empa in DOCA salt rats. *p < 0.05 versus UNX treated with vehicle. LVIDd = left ventricular internal diameter diastole; other abbreviations as Figure 1.

JACC: BASIC TO TRANSLATIONAL SCIENCE VOL. 4, NO. 1, 2019
FEBRUARY 2019:27–37

TABLE 3 Cardiac Function as Assessed by Echocardiography and Conductance Catheterization

	UNX + Control	UNX + Empa	DOCA + Control	DOCA + Empa
EF (%)	80 ± 2	80 ± 2	84 ± 2*	88 ± 1*
LVIDd (mm)	8.2 ± 0.3	8.1 ± 0.2	7.9 ± 0.2	7.3 ± 0.2*
LVIDs (mm)	4.0 ± 0.2	4.0 ± 0.2	3.5 ± 0.3	2.9 ± 0.2*†
LV mass corr. (mg)	1053 ± 57	975 ± 22	1520 ± 90*	1164 ± 51†
LVPWs (cm)	0.35 ± 0.01	0.35 ± 0.01	0.45 ± 0.02*	0.43 ± 0.01*
SBP (mm Hg)	116 ± 1	112 ± 2	188 ± 6*	182 ± 6*
Wall stress, σ (g/cm^2)	58 ± 5	61 ± 5	73 ± 6*	53 ± 4†
HR (beats/min)	370 ± 10	327 ± 10	334 ± 6*	334 ± 8*
EDP (mm Hg)	11 ± 1	12 ± 2	11 ± 1	11 ± 1
dP/dt_{max} (mm Hg/s)	6,557 ± 451	6,664 ± 324	6,092 ± 494	6,599 ± 377
dP/dt_{min} (mm Hg/s)	−7,596 ± 441	−7,387 ± 317	−5,580 ± 546*	−6,505 ± 548
EDPVR (mm Hg/μl)	0.017 ± 0.004	0.019 ± 0.003	0.024 ± 0.003	0.023 ± 0.002
Tau (ms)	11.5 ± 0.2	12.7 ± 0.7	15.1 ± 0.4*	13.5 ± 0.6*†

Values are mean ± SEM. n = 7 to 8 in UNX control and UNX Empa groups; n = 15 in DOCA control and Empa groups, respectively. *p < 0.05 versus UNX + vehicle. †p < 0.05 versus DOCA + vehicle.

dP/dt_{min} = maximal rate of pressure decline; EDP = end-diastolic pressure; EDPVR = end-diastolic pressure–volume relationship; EF = ejection fraction; HR = heart rate; LVIDd = left ventricular internal diameter in diastole; LVIDs = left ventricular internal dimension in systole; LV mass corr. = left ventricular mass corrected; LVPWs = left ventricular posterior wall in systole; SBP = systolic blood pressure; other abbreviations as in Table 1.

according to treatment assignment to empagliflozin or vehicle (Table 2).

ECHOCARDIOGRAPHY. DOCA salt rats demonstrated preserved EF with increased wall thickness and LV mass compared with control rats (Figure 2, Table 3).

FIGURE 3 Steady-State Pressure–Volume Loops

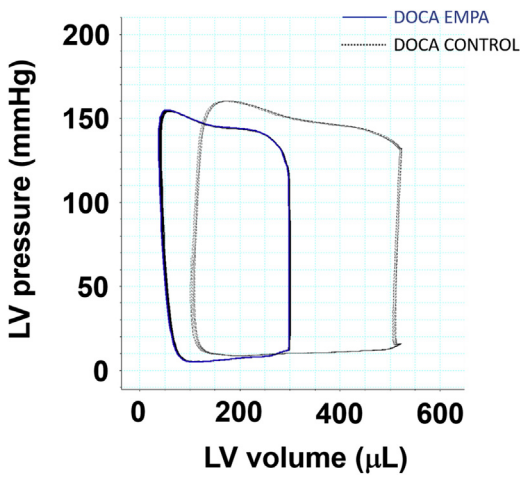

Empa-treated UNX + DOCA salt animals display a leftward shift with a reduction in end-diastolic volume **(blue curve)** compared with the UNX + DOCA salt control animals **(gray curve)**. Abbreviations as in Figures 1 and 2.

Empagliflozin therapy reduced LV end-systolic dimension, LV mass, and posterior wall thickness (Table 3).

CONDUCTANCE CATHETERIZATION. A high-fidelity LV pressure manometer was used to assess diastolic function. DOCA salt administration prolonged Tau and reduced dp/dt_{min}, which indicated impaired diastolic relaxation; these abnormalities were both ameliorated by empagliflozin (Table 3). Similarly, wall stress that was increased in DOCA salt rats was reduced with empagliflozin. In contrast, late diastolic relaxation, as assessed by the end-diastolic pressure–volume relationship, was not increased by DOCA salt and was unaffected by empagliflozin (Table 3, Figure 3).

HISTOLOGY. In keeping with the observed morphometric changes, DOCA salt rats demonstrated increased cardiomyocyte size compared with control rats, which was significantly reduced by empagliflozin therapy (Figure 4). Furthermore, DOCA salt treatment increased perivascular and interstitial LV fibrosis compared with control vehicle. Empagliflozin therapy did not affect the extent of LV fibrosis in either the perivascular or interstitial compartments.

MOLECULAR STUDIES. To assess the mechanism in which early active energy-dependent relaxation was improved with empagliflozin therapy, we assessed a range of proteins involved in calcium handling and the hypertrophic response. There was no significant change in SERCA2A content, nor in the total and/or phosphorylated phospholamban expression at either pSer16 or pThr17 sites. Furthermore, we assessed total and phosphorylated calcium and/or calmodulin-dependent protein kinase II to better elucidate the change in cardiomyocyte hypertrophy and identification of LV hypertrophy. There was no significant change seen with either DOCA or empagliflozin administration (Supplemental Figure 1).

DOCA salt treatment increased ANP, collagen 1, and III mRNA compared with control vehicle ($p < 0.05$). Empaglifozin treatment had no effect on collagen 1/III or ANP mRNA (Figure 5).

Because of the surprising absence of altered protein expression in key cardiac calcium handling proteins, we went on to assess whether the observed functional benefits were secondary to improved myocardial energetics. As a result, we performed RTq polymerase chain reaction on a panel of genes known to be involved in metabolism. UNX + DOCA had minimal effect on gene expression of the metabolic

FIGURE 4 Stained Sections

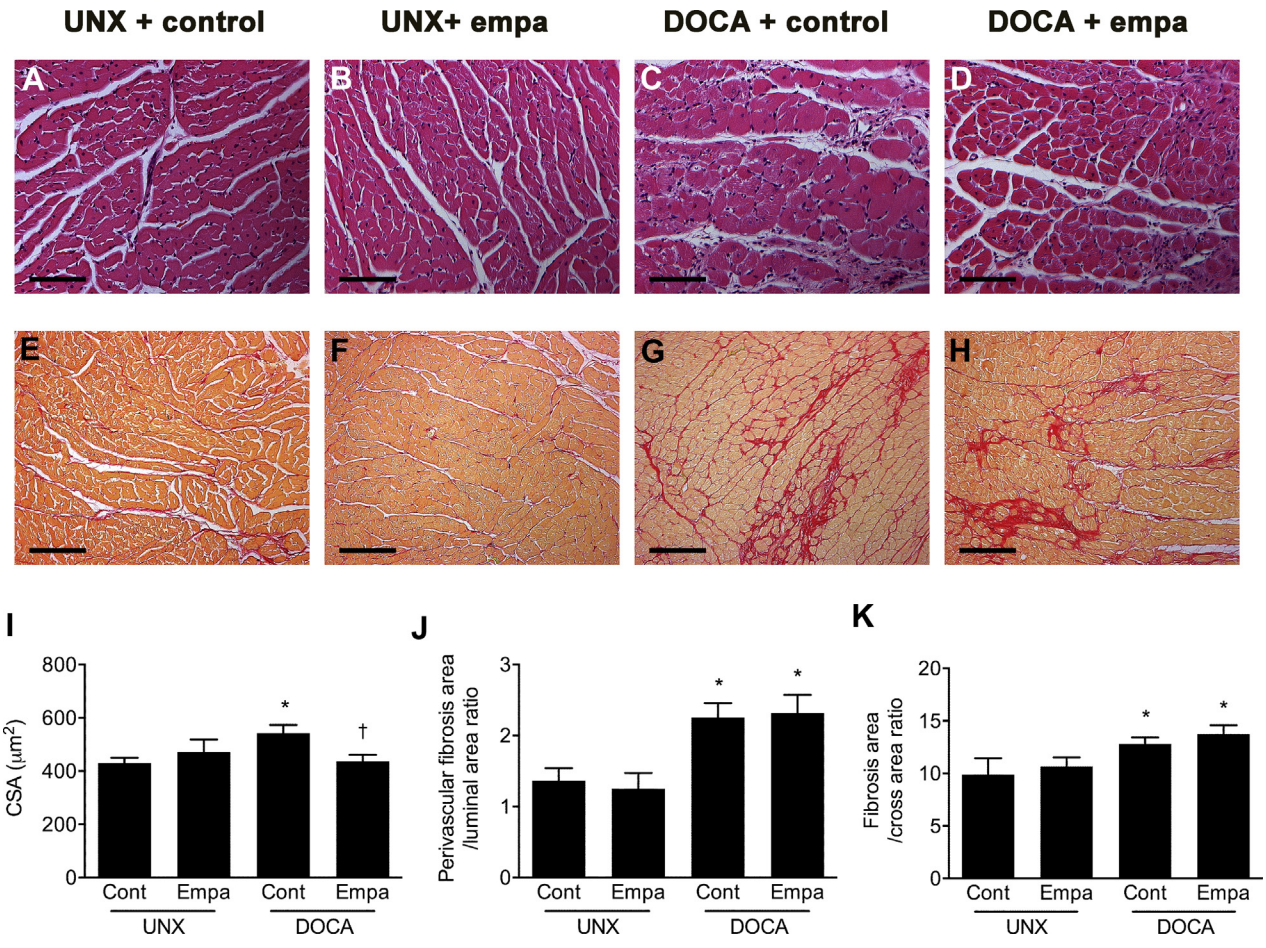

(A to D) Representative hematoxylin and eosin and **(E to H)** picrosirius red stained sections. Hearts of UNX + DOCA salt rats showed evidence of **(I)** myocyte hypertrophy, together with both **(J and K)** perivascular and interstitial fibrosis. Empa reduced cardiomyocyte size in UNX + DOCA animals but had no effect on either interstitial or perivascular fibrosis. n = 7 to 8 in UNX control and UNX empa groups; n = 16 and 15 in DOCA control and empa groups, respectively. *p < 0.05 treated with UNX + control. †p < 0.05 treated with UNX + DOCA + control. CSA = cross-sectional area; other abbreviations as in Figure 1.

genes presented (Supplemental Figure 2). However, there was a significant reduction in both PGC1α and fatty acid protein and/or CD36 expression that was improved by empagliflozin therapy ($p < 0.05$). The changes in mRNA expression were not accompanied by changes in protein abundance (Supplemental Figure 1).

DISCUSSION

Despite significant advances in the treatment of HFrEF, HFpEF lacks evidence-based therapies. We used a model of hypertension-induced HFpEF, the DOCA salt rat that demonstrates the cardinal manifestations of HFpEF. Without significantly affecting either blood pressure or glycemia, the SGLT2i, empagliflozin, reduced LV mass and attenuated the increased wall stress and impaired diastolic function that develop in this nondiabetic disease model.

Administration of the mineralocorticoid, DOCA, in combination with dietary salt loading increased cardiac afterload, which created pathological changes that are highly reminiscent of human hypertensive heart disease, with increased LV mass, cardiomyocyte hypertrophy, cardiac interstitial fibrosis, and impaired diastolic function (13). From a pathophysiological perspective, the requirement of the LV to approximate aortic pressure in systole increases intraventricular wall stress that can be further exacerbated by chamber dilatation. To mitigate an

FIGURE 5 Heart Collagen 1 and III, ANP mRNA Levels

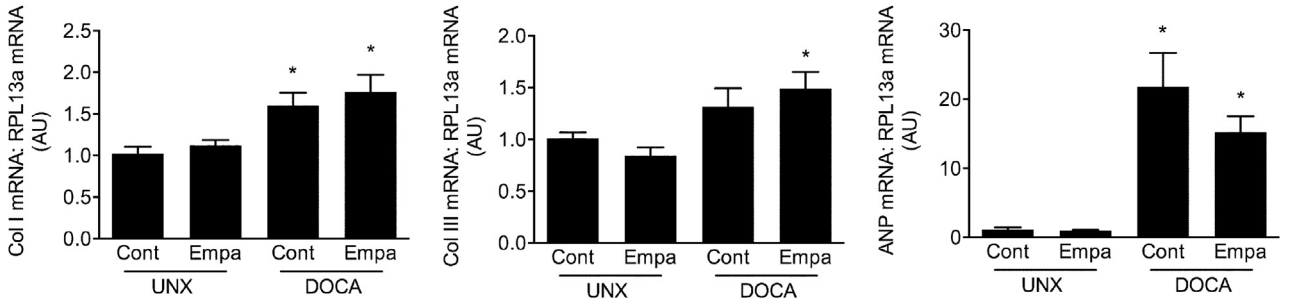

Hearts of DOCA salt rats showed evidence of atrial natriuretic peptide (ANP) activation, together with increased collagen I (Col I) and III mRNA. Empa had no effect on either ANP, or Col I or III mRNA. n = 8 for control (Cont) UNX; n = 7 for UNX empa; n = 14 for control DOCA; n = 13 for empa DOCA. *p < 0.05 compared to UNX animals treated with UNX + control. RPL13a = ribosomal protein L13A housekeeping gene; other abbreviations as in Figure 1.

increase in wall stress, there is an increase in wall thickness (i.e., hypertrophy) that allows the workload to be shared among a greater number of sarcomeric units. Although initially beneficial, the resultant changes in the pressure–volume relationship lead not only to cardiomyocyte hypertrophy but also to interstitial fibrosis, impaired relaxation, and ultimately HFpEF.

In contrast to vehicle-treated rats, the present study found that the administration of empagliflozin reduced LV mass and attenuated cardiomyocyte hypertrophy in conjunction with diminished wall stress and improved diastolic function. The attenuation in diastolic dysfunction was confined to the early, energy-dependent active phase of diastole as reflected by the shortening of the isovolumic relaxation constant (Tau) and a reduction in the minimum rate of ventricular pressure change (dP/dt_{min}). In contrast, dysfunction in the later energy-independent passive phase of diastole, as indicated by the end-diastolic pressure–volume relationship, was unaffected either by DOCA salt or by empagliflozin.

The previously noted changes in cardiac structure and function with empagliflozin provided a number of novel insights into the potential mode of action of the SGLT2 drug class in the HFpEF setting. As in humans with an excess of mineralocorticoid, the administration of DOCA in conjunction with a high salt diet leads to intravascular volume expansion, as indicated by reduced hematocrit. LV chamber volume, although not increased in this model, was nevertheless reduced by empagliflozin commensurate with an increase in hematocrit. Among animals on a normal diet that had not received DOCA, and in which intravascular volume was presumably normal, empagliflozin did not affect either hematocrit or chamber volume. These findings suggested that the beneficial effects of SGLT2 inhibition on the prevention of HF might be most marked when intravascular volume is increased.

The histopathological response to increased afterload included both cardiomyocyte hypertrophy and fibrosis with impairments in both the metabolically active, early component of diastole, together with the passive, later compliance-based phase. Unlike many other ostensibly cardioprotective agents that were examined in the DOCA salt model, which included angiotensin-converting enzyme inhibitors, angiotensin receptor blockers, mineralocorticoid receptor antagonists (14), dual vasopeptidase inhibitors (15), and endothelin antagonists (16), empagliflozin reduced hypertrophy and not fibrosis. Although interventions that reduce cardiac fibrosis also attenuated the abnormalities in passive diastolic compliance (6,17,18), this component of diastolic function was not abnormal in DOCA salt rats in the present study.

To elucidate the molecular mechanisms behind the improved diastolic function and early active relaxation, we performed Western blot analyses of a range of proteins involved in cardiac calcium handling. We observed minimal changes in proteins involved in relaxation or the hypertrophic response (Supplemental Figure 1). The lack of change led us to investigate whether the improved cardiac diastolic

function was secondary to improved myocardial energetics induced by empagliflozin therapy. We used RTq polymerase chain reaction to assess a wide range of genes known to be involved in fatty acid transport, fat, and glucose oxidation, as well as mitochondrial biogenesis (Supplemental Figure 2) (19). Much to our surprise, these results demonstrated minimal change in gene expression. We observed downregulated expression of uncoupling protein 3, PGC1α, pyruvate kinase, and CD36/fatty acid protein only in DOCA salt UNX animals. Empagliflozin therapy improved PGC1α gene expression in DOCA UNX animals, but we observed no change in protein content. Although at first these findings appeared incongruous to the functional improvements seen, they were in keeping with data from a wide body of investigators who demonstrated that most of benefits in rodents occurred from the hemodynamic effects and hemoconcentration, and not from altered energetics as a result of ketone metabolism (20,21).

To date, a wide range of hypotheses have been put forward to explain the reduction in HF hospitalization seen in the cardiovascular trials with SGLT2s, EMPA-REG Outcome trial (Empagliflozin, Cardiovascular Outcomes, and Mortality in Type 2 Diabetes trial) and CANVAS (CANagliflozin cardioVascular Assessment Study) trial, using 2 different SGLTs, empagliflozin and canagliflozin, respectively, and a third trial that will report shortly (3,4). Among these theories, considerable interest has focused on the proposal by Ferranini and Mayoux (22) that these salutary cardiac effects of SGLT2 inhibitors may be dependent on augmented ketone body formation and increased hematocrit. As elaborated on in their seminal paper, the investigators speculated that the reduction in HF with empagliflozin reflected the improved cardiac energetics that follow augmented ß-hydroxy-butyrate production coupled with enhanced oxygen delivery to the myocardium as a consequence of hemoconcentration. In the present study, conducted in the nondiabetic setting, we did not observe any differences in ß-hydroxy-butyrate between rats that had received either empagliflozin or vehicle. We did find an increase in hematocrit and improved cardiac function in animals treated with empagliflozin, which was consistent with the results of the recently published mediation analysis (20). Whether the relationship between hematocrit and cardiovascular outcome as seen in the EMPA-REG Outcome study might be a consequence of volume contraction, improved oxygen delivery, or both, could not be discerned from the present experimental study.

STUDY LIMITATIONS. Our study was not without limitations. First, empagliflozin therapy was commenced soon after DOCA was first administered. As such, further studies would be required to assess whether late treatment might also reverse the structural and functional manifestations of established HFpEF. Second, although DOCA salt is a well-validated model of HFpEF (23-25), it is only 1 example of the disorder. However, work by other investigators in an alternate model of HEpEF (pressure overload) demonstrated similar findings with improvement in diastolic function in response to SGLT2 inhibition (26). Similar to our work, the exact molecular mechanism by which this occurred remains elusive and requires further investigation. Finally, although we did not find any statistical differences in systolic blood pressure, as shown in **Figure 1**, levels were numerically slightly lower in DOCA salt animals that received empagliflozin compared with those that did not throughout much of the study.

CONCLUSIONS

Empagliflozin therapy reduced lung weight, improved LV mass, and ameliorated diastolic dysfunction in a rodent model of HFpEF. Potential pathophysiological mechanisms that underlie these salutary changes are likely multifactorial. Such factors include diminished pre-load and possibly afterload that reduce myocardial oxygen demand, along with an elevated hematocrit that proves increased oxygen delivery.

ADDRESS FOR CORRESPONDENCE: Dr. Kim A. Connelly, Keenan Research Centre, Li Ka Shang Knowledge Institute, St. Michael's Hospital, 61 Queen Street East, Toronto, Ontario M5C 2T2, Canada. E-mail: Connellyk@smh.ca.

JACC: BASIC TO TRANSLATIONAL SCIENCE VOL. 4, NO. 1, 2019
FEBRUARY 2019:27–37

PERSPECTIVES

COMPETENCY IN MEDICAL KNOWLEDGE: Despite 3 large trials demonstrating that SGLT2is reduced HF hospitalizations in patients with type 2 diabetes, the mechanisms underlying the observed benefit remain unclear. Currently, changes in hematocrit, pre-load, and afterload, together with altered myocardial energetics and metabolism, remain likely factors. We assessed the impact of empagliflozin on cardiac function structure in the UNX DOCA salt-sensitive rat, which was a nondiabetic experimental model of HFpEF.

TRANSLATIONAL OUTLOOK: Our study demonstrated that UNX male Sprague-Dawley rats that received DOCA in conjunction with 1% sodium chloride in drinking water (DOCA salt) developed hypertension and HFpEF in the absence of diabetes. Without significantly lowering blood pressure, empagliflozin reduced LV mass and ameliorated myocyte hypertrophy, which normalized LV wall stress and improved diastolic function. Importantly, these changes occurred in the absence of alterations in key calcium handling and hypertrophy signalling pathways, as well as key molecular markers of metabolism. These finding suggested that the impact of empagliflozin occurred primarily through altered hemodynamic effects, which provides a strong rationale for clinical studies in both HFrEF and HFpEF, regardless of diabetes status.

REFERENCES

1. Yeung DF, Boom NK, Guo H, Lee DS, Schultz SE, Tu JV. Trends in the incidence and outcomes of heart failure in Ontario, Canada: 1997 to 2007. CMAJ 2012;184:E765–73.

2. Bhatia RS, Tu JV, Lee DS, et al. Outcome of heart failure with preserved ejection fraction in a population-based study. N Engl J Med 2006;355:260–9.

3. Zinman B, Wanner C, Lachin JM, et al. Empagliflozin, cardiovascular outcomes, and mortality in type 2 diabetes. N Engl J Med 2015;373:2117–28.

4. Neal B, Perkovic V, Mahaffey KW, et al. Canagliflozin and cardiovascular and renal events in type 2 diabetes. N Engl J Med 2017;377:644–57.

5. Viel EC, Benkirane K, Javeshghani D, Touyz RM, Schiffrin EL. Xanthine oxidase and mitochondria contribute to vascular superoxide anion generation in DOCA-salt hypertensive rats. Am J Physiol Heart Circ Physiol 2008;295:H281–8.

6. Connelly KA, Kelly DJ, Zhang Y, et al. Inhibition of protein kinase C-beta by ruboxistaurin preserves cardiac function and reduces extracellular matrix production in diabetic cardiomyopathy. Circ Heart Fail 2009;2:129–37.

7. Bugyei-Twum A, Abadeh A, Thai K, et al. Suppression of NLRP3 inflammasome activation ameliorates chronic kidney disease-induced cardiac fibrosis and diastolic dysfunction. Sci Rep 2016;6:39551.

8. Connelly KA, Advani A, Kim S, et al. The cardiac (pro)renin receptor is primarily expressed in myocyte transverse tubules and is increased in experimental diabetic cardiomyopathy. J Hypertens 2011;29:1175–84.

9. Dong H, Mosca H, Gao E, Akins RE, Gidding SS, Tsuda T. Integrated wall stress: a new methodological approach to assess ventricular workload and myocardial contractile reserve. J Transl Med 2013;11:183.

10. Connelly KA, Kelly DJ, Zhang Y, et al. Functional, structural and molecular aspects of diastolic heart failure in the diabetic (mRen-2)27 rat. Cardiovasc Res 2007;76:280–91.

11. Civitarese RA, Talior-Volodarsky I, Desjardins JF, et al. The alpha11 integrin mediates fibroblast-extracellular matrix-cardiomyocyte interactions in health and disease. Am J Physiol Heart Circ Physiol 2016;311:H96–106.

12. Batchu SN, Thieme K, Zadeh FH, et al. The dipeptidyl peptidase-4 substrate CXCL12 has opposing cardiac effects in young mice and aged diabetic mice mediated by Ca(2+) flux and phosphoinositide 3-kinase gamma. Diabetes 2018;67:2443–55.

13. Iyer A, Chan V, Brown L. The DOCA-salt hypertensive rat as a model of cardiovascular oxidative and inflammatory stress. Curr Cardiol Rev 2010;6:291–7.

14. Brown L, Duce B, Miric G, Sernia C. Reversal of cardiac fibrosis in deoxycorticosterone acetate-salt hypertensive rats by inhibition of the renin-angiotensin system. J Am Soc Nephrol 1999;10 Suppl 11:S143–8.

15. Pu Q, Amiri F, Gannon P, Schiffrin EL. Dual angiotensin-converting enzyme/neutral endopeptidase inhibition on cardiac and renal fibrosis and inflammation in DOCA-salt hypertensive rats. J Hypertens 2005;23:401–9.

16. Ammarguellat F, Larouche I, Schiffrin EL. Myocardial fibrosis in DOCA-salt hypertensive rats: effect of endothelin ET(A) receptor antagonism. Circulation 2001;103:319–24.

17. Yuen DA, Connelly KA, Advani A, et al. Culture-modified bone marrow cells attenuate cardiac and renal injury in a chronic kidney disease rat model via a novel antifibrotic mechanism. PLoS One 2010;5:e9543.

18. Zhang Y, Connelly KA, Thai K, et al. Sirtuin 1 activation reduces transforming growth factor-beta1-induced fibrogenesis and affords organ protection in a model of progressive, experimental kidney and associated cardiac disease. Am J Pathol 2017;187:80–90.

19. Kato T, Niizuma S, Inuzuka Y, et al. Analysis of metabolic remodeling in compensated left ventricular hypertrophy and heart failure. Circ Heart Fail 2010;3:420–30.

20. Inzucchi SE, Zinman B, Fitchett D, et al. How does empagliflozin reduce cardiovascular mortality? Insights from a mediation analysis of the EMPA-REG OUTCOME trial. Diabetes Care 2018;41:356–63.

21. Lopaschuk GD, Verma S. Empagliflozin's fuel hypothesis: not so soon. Cell Metab 2016;24:200–2.

22. Ferrannini E, Mark M, Mayoux E. CV Protection in the EMPA-REG OUTCOME trial: a "thrifty substrate" hypothesis. Diabetes Care 2016;39:1108–14.

23. Ogata T, Miyauchi T, Sakai S, Takanashi M, Irukayama-Tomobe Y, Yamaguchi I. Myocardial fibrosis and diastolic dysfunction in deoxycorticosterone acetate-salt hypertensive rats

is ameliorated by the peroxisome proliferator-activated receptor-alpha activator fenofibrate, partly by suppressing inflammatory responses associated with the nuclear factor-kappa-B pathway. J Am Coll Cardiol 2004;43:1481–8.

24. Schwarzl M, Hamdani N, Seiler S, et al. A porcine model of hypertensive cardiomyopathy: implications for heart failure with preserved ejection fraction. Am J Physiol Heart Circ Physiol 2015;309:H1407–18.

25. Allan A, Fenning A, Levick S, Hoey A, Brown L. Reversal of cardiac dysfunction by selective ET-A receptor antagonism. Br J Pharmacol 2005;146:846–53.

26. Byrne N, Parajuli N, Levasseu RJ, et al. Empagliflozin prevents worsening of cardiac function in an experimental model of pressure overload-induced heart failure. J Am Coll Cardiol Basic Trans Science 2017;2:347–54.

KEY WORDS diastole, heart failure with preserved ejection fraction, sodium-glucose–linked co-transporter-2 inhibitor, systole

APPENDIX For supplemental tables and figures, please see the online version of this paper.

JACC: BASIC TO TRANSLATIONAL SCIENCE VOL. 4, NO. 1, 2019

EDITORIAL COMMENT

The Growing Case for Use of SGLT2i in Heart Failure

Additional Benefits of Empagliflozin in a HFpEF Rodent Model*

Chae-Myeong Ha, PhD, Adam R. Wende, PhD

Heart disease associated with diabetes mellitus (DM) continues to be the leading cause of death worldwide. However, with the development of renal sodium glucose transport inhibitors (SGLTi) there appears to be new hope. Specifically, the use of SGLTi as a treatment for type 2 diabetes (T2D) leads to lower blood glucose levels by inhibiting SGLT2, which accounts for ~90% of glucose reabsorption in the kidney proximal convoluted tubule. At this point, a number of SGLT2i have been approved for treatment of T2D, namely: empagliflozin (1), canagliflozin (2), and dapagliflozin (3), which have each shown improvement in cardiovascular outcomes in clinical trials. These gliflozins have demonstrated cardiovascular beneficial effects including reduced mortality from cardiovascular causes (1-3), and decreased hospitalization from heart failure (1,3). The mechanisms of these successes in clinical trials have begun to be worked out by multiple groups that recently found improvements in cardiac function by administering empagliflozin to *db/db* diabetic mice (4,5). In these studies, Verma et al. (4) found that ATP production and cardiac function was improved following 4 weeks of empagliflozin administration to *db/db* mice compared with vehicle treatment. This effect is associated with preserved cardiac glucose and lipid metabolism (4). Additionally, in female *db/db* mice, Habibi et al. (5) showed that 5 weeks of empagliflozin treatment improved diastolic function, myocardial fibrosis, and mitochondrial expansion. On the other hand, the effect of empagliflozin on pressure overload-induced heart failure resulting from transverse aortic constriction (TAC), in the absence of diabetes, also had protective effects. In this study, Byrne et al. (6) found that 2 weeks of oral administration of empagliflozin after TAC improved cardiac systolic function as measured in vivo or ex vivo. However, there were no changes in remodeling of cardiac mass, left ventricle structure, cardiac fibrosis, and immune cell infiltration into the cardiac tissue (6). In either case, both the human trials and these mechanistic studies in rodent models that show encouraging results of SGLT2i therapy in either diabetes or pressure overload-induced heart failure suggests that these agents should be examined for treatment of additional heart failure etiologies.

SEE PAGE 27

One area of cardiovascular disease that has proven exceptionally resistant to current therapy options is that of heart failure with preserved ejection fraction (HFpEF). These patients have symptoms suggestive of heart failure, but with normal left ventricular ejection fraction. This disease is associated with age, female sex, hypertension, obesity, renal dysfunction, and atrial fibrillation (7). It has complex pathophysiology in addition to diastolic dysfunction. The current treatment options available have been able to relieve volume overload and alleviate other concurrent chronic diseases in patients to reduce or prevent hospitalizations (8). This limitation of therapeutic options for HFpEF appears to be coming to an end

*Editorials published in *JACC: Basic to Translational Science* reflect the views of the authors and do not necessarily represent the views of *JACC: Basic to Translational Science* or the American College of Cardiology.

From the Department of Pathology, Division of Molecular and Cellular Pathology, University of Alabama at Birmingham, Birmingham, Alabama. Both authors have reported that they have no relationships relevant to the contents of this paper to disclose.

All authors attest they are in compliance with human studies committees and animal welfare regulations of the authors' institutions and Food and Drug Administration guidelines, including patient consent where appropriate. For more information, visit the *JACC: Basic to Translational Science* author instructions page.

ISSN 2452-302X https://doi.org/10.1016/j.jacbts.2019.01.003

with the paper by Connelly et al. (9) in this issue of *JACC: Basic to Translational Science*.

Connelly et al. (9) examined the hypothesis that SGLT2i may have beneficial effects in nondiabetic HFpEF, extending what was previously observed in patients with diabetes (1,10) and experimental models of pressure overload-induced heart failure model (6). The complex nature of hypertension, which results from various factors including genetic, lifestyle, and autonomic nerve systems, can limit modeling of HFpEF. A growing number of researchers have used a deoxycorticosterone acetate (DOCA)-salt model to replicate an overactive sympathetic nervous and renin-angiotensin system. DOCA leads to a renal sodium imbalance, resulting in hypervolemia (11). The addition of 0.6% to 1% NaCl to drinking water or uninephrectomy intensifies the hypertension. The DOCA model more accurately replicates multiple physiological connections to neurological, cardiovascular, renal circulation, and immune system changes in addition to the cardiac blood pressure outcome. Connelly et al. (9) used a rat model of uninephrectomy with DOCA and 1% NaCl water to induce HFpEF. Then in these or control animals a subset were treated with empagliflozin-containing chow. The resulting 4 groups were followed and assessed systemically in metabolic cage, for biochemical endpoints, cardiac function by echocardiography and cardiac catherization, cardiac remodeling by histopathology, and molecularly. The authors found that empagliflozin attenuated cardiac hypertrophy, preserved lung weight, and ameliorated diastolic dysfunction. However, empagliflozin had no effect on systolic blood pressure, cardiac fibrosis, and fibrosis-related gene expression. This partially improved cardiac function, but had no effect on fibrosis similar to results previously reported for empagliflozin-treated experimental diabetic and pressure-overload rodent models (5,6). Although a specific mechanism is not fully elucidated, the authors point out, "potential pathophysiological mechanisms that underlie these salutary changes are likely multifactorial." Despite this limitation, the continued successes of multiple groups to show protection via empagliflozin treatment of heart failure resulting from diverse etiologies is promising. This strongly supports the need for continued mechanistic work to define the regulated pathways and help elucidate the possibility and efficacy of this drug class for future use. One important distinction of this study and the TAC study mentioned in the previous text is that the mechanism may be independent of other known beneficial effects of SGLT2i, such as lowering glucose in diabetes. However, because this may not be related to calcium-channel expression or fatty acid oxidation-related gene expression, as suggested by Connelly et al. (9), other interesting possibilities remain.

It is noteworthy that the effects of empagliflozin have similar patterns to the prior reports with a T2D model (4,5) and that of other heart disease models without diabetes, such as TAC (6) and now HFpEF (9) (**Figure 1**). However, a number of limitations concerning the specific mechanisms, such as changes in circulating metabolites, improved hemodynamics through natriuresis, osmotic diuresis, neurohormonal changes, or immune system adaptation, must be accounted for when considering SGLT2i as a therapeutic option for heart failure treatment. In addition to the specific physiological mechanisms, SGLT2i for heart failure should be fully defined in the current model by measuring energy production efficiency in heart muscle (12), gene regulation, and post-translational protein modifications, which are in

FIGURE 1 Schematic of Clinical Observations, Promises, and the Future of SGLT2i

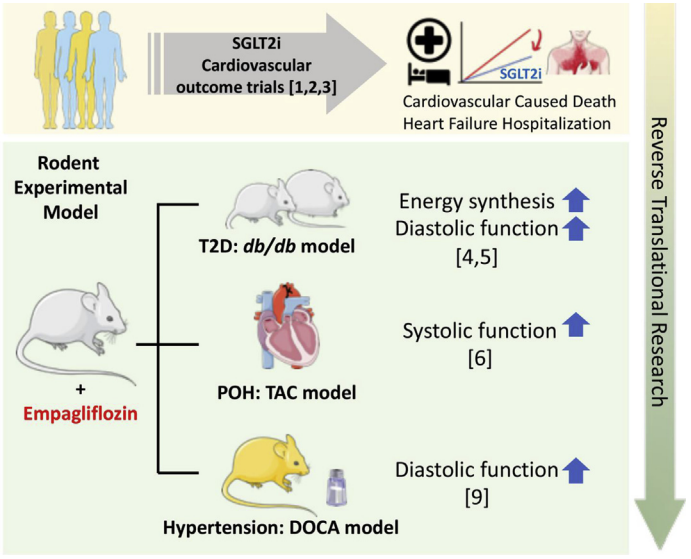

Patient trials of SGLT2i for the treatment of diabetes have revealed improved cardiovascular outcomes, reduced mortality, and better quality of life as it pertains to hospitalization **(top)** (1–3). Rodent studies have revealed cardiac benefits in either diabetes or pressure overload which is expanded to HFpEF in the study published by Connelly et al. (9) **(lower)** (4–6). The figure was produced using images modified from Servier Medical Art (smart.servier.com). DOCA = deoxycorticosterone acetate; POH = pressure overload-induced heart failure; SGLT2i = sodium/glucose cotransporter 2 inhibitor; T2D = type 2 diabetes; TAC = transverse aortic constriction.

JACC: BASIC TO TRANSLATIONAL SCIENCE VOL. 4, NO. 1, 2019
FEBRUARY 2019:38–40

part regulated by sensing of energy status, the difference in contractility caused by the effect of calcium flux control in the process of regulating sodium reabsorption, or changes in the mitochondrial environment around the cardiac sarcomeres. Many questions remain regarding SGLT2i's efficacy in the failing heart, but the study by Connelly et al. (9) extends our knowledge on the potential benefits of SGLT2i on myocardial function and applicable disease etiologies.

ADDRESS FOR CORRESPONDENCE: Dr. Adam R. Wende, University of Alabama at Birmingham, 901 19th Street South, BMR2 Room 506, Birmingham, Alabama 35294. E-mail: adamwende@uabmc.edu.

REFERENCES

1. Zinman B, Wanner C, Lachin JM, et al. Empagliflozin, cardiovascular outcomes, and mortality in type 2 diabetes. N Engl J Med 2015;373:2117–28.

2. Neal B, Perkovic V, Mahaffey KW, et al. Canagliflozin and cardiovascular and renal events in type 2 diabetes. N Engl J Med 2017;377:644–57.

3. Wiviott SD, Raz I, Bonaca MP, et al. Dapagliflozin and cardiovascular outcomes in type 2 diabetes. N Engl J Med 2019;380:347–57.

4. Verma S, Rawat S, Ho KL, et al. Empagliflozin increases cardiac energy production in diabetes: Novel translational insights into the heart failure benefits of SGLT2 inhibitors. J Am Coll Cardiol Basic Trans Science 2018;3:575–87.

5. Habibi J, Aroor AR, Sowers JR, et al. Sodium glucose transporter 2 (SGLT2) inhibition with empagliflozin improves cardiac diastolic function in a female rodent model of diabetes. Cardiovasc Diabetol 2017;16:9.

6. Byrne NJ, Parajuli N, Levasseur JL, et al. Empagliflozin prevents worsening of cardiac function in an experimental model of pressure overload-induced heart failure. J Am Coll Cardiol Basic Trans Science 2017;2:142.

7. Andersen MJ, Borlaug BA. Heart failure with preserved ejection fraction: current understandings and challenges. Curr Cardiol Rep 2014;16:501.

8. Redfield MM. Heart failure with preserved ejection fraction. N Engl J Med 2016;375:1868–77.

9. Connelly KA, Zhang Y, Visram A, et al. Empagliflozin improves diastolic function in a nondiabetic rodent model of heart failure with preserved ejection fraction. J Am Coll Cardiol Basic Trans Science 2019;4:27–37.

10. Tikkanen I, Narko K, Zeller C, et al. Empagliflozin reduces blood pressure in patients with type 2 diabetes and hypertension. Diabetes Care 2015;38:420–8.

11. Basting T, Lazartigues E. DOCA-salt hypertension: an update. Curr Hypertens Rep 2017;19:32.

12. Lopaschuk Gary D, Verma S. Empagliflozin's fuel hypothesis: not so soon. Cell Metabolism 2016;24:200–2.

KEY WORDS heart failure, HFpEF, SGLT2i

JACC: BASIC TO TRANSLATIONAL SCIENCE VOL. 4, NO. 1, 2019

PRECLINICAL RESEARCH

Cardiomyocyte SMAD4-Dependent TGF-β Signaling is Essential to Maintain Adult Heart Homeostasis

Prachi Umbarkar, PhD,[a] Anand P. Singh, PhD,[a] Manisha Gupte, PhD,[a] Vipin K. Verma, PhD,[a] Cristi L. Galindo, PhD,[a] Yuanjun Guo, MD,[a,b] Qinkun Zhang, MD,[a] James W. McNamara, PhD,[c] Thomas Force, MD,[a] Hind Lal, PhD[a]

VISUAL ABSTRACT

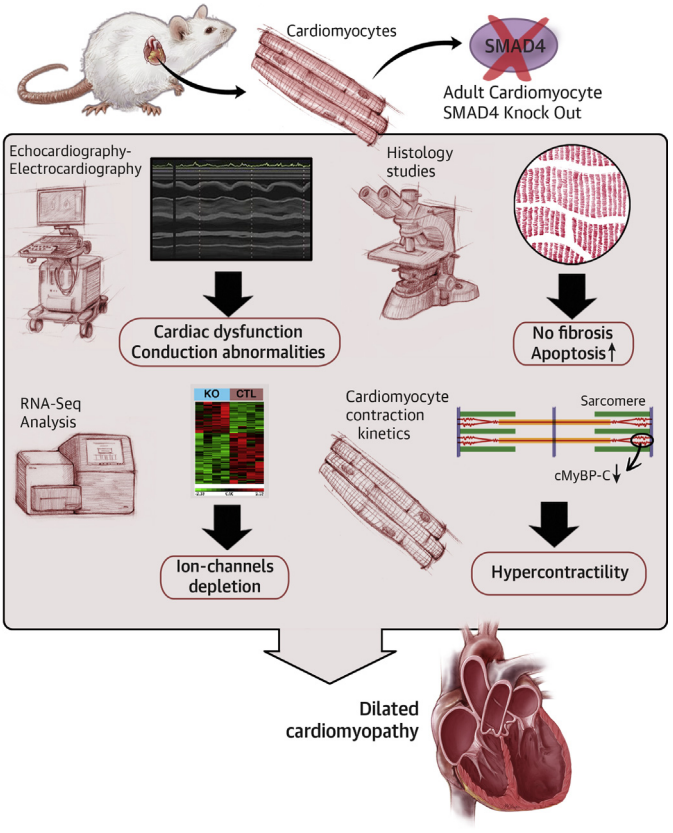

Umbarkar, P. et al. J Am Coll Cardiol Basic Trans Science. 2019;4(1):41-53.

HIGHLIGHTS

- **SMAD4 is the central intracellular mediator of TGF-β pathway.**
- **CM-specific loss of SMAD4 causes cardiac dysfunction independent of fibrotic remodeling.**
- **Deletion CM-SMAD4 affects CM survival.**
- **CM-SMAD4 loss leads to down-regulation of several ion channels' genes, resulting in cardiac conduction abnormalities.**
- **CM-SMAD4 deletion alters sarcomere shortening kinetics, in parallel with reduction in cardiac myosin-binding protein C levels.**
- **These results demonstrate a fundamental role for CM-SMAD4–dependent TGF-β signaling in adult heart homeostasis.**

From the [a]Division of Cardiovascular Medicine, Vanderbilt University Medical Center, Nashville, Tennessee; [b]Department of Pharmacology, Vanderbilt University, Nashville, Tennessee; and the [c]Division of Cardiovascular Health and Disease, Department of Internal Medicine, Heart, Lung and Vascular Institute, University of Cincinnati College of Medicine, Cincinnati, Ohio. This work was supported by research grants to Dr. Lal from the National Heart, Lung, and Blood Institute (R01HL133290, R01HL119234) and American Heart Association (13SDG16930103). Dr. Galindo was supported by research grant (K01HL121045). Dr. Gupte was supported by Training Grant in Cardiovascular Research (T32 HL007411) from the National Heart, Lung, and Blood Institute. All other authors have reported that they have no relationships relevant to the contents of this paper to disclose.

ISSN 2452-302X https://doi.org/10.1016/j.jacbts.2018.10.003

ABBREVIATIONS AND ACRONYMS

CM = cardiomyocyte

cMyBP-C = cardiac myosin-binding protein C

CSA = cross-sectional area

CTL = control

DCM = dilated cardiomyopathy

KO = knockout

LV = left ventricle/ventricular

MAPK = mitogen-activated protein kinase

MCM = MerCreMer

PI3K = phosphoinositide-3 kinase

RNA-Seq = RNA sequencing

TAK1 = transforming growth factor beta-activated kinase 1

TAM = tamoxifen

TGF = transforming growth factor

SUMMARY

The role of the transforming growth factor (TGF)-β pathway in myocardial fibrosis is well recognized. However, the precise role of this signaling axis in cardiomyocyte (CM) biology is not defined. In TGF-β signaling, SMAD4 acts as the central intracellular mediator. To investigate the role of TGF-β signaling in CM biology, the authors deleted SMAD4 in adult mouse CMs. We demonstrate that CM-SMAD4–dependent TGF-β signaling is critical for maintaining cardiac function, sarcomere kinetics, ion-channel gene expression, and cardiomyocyte survival. Thus, our findings raise a significant concern regarding the therapeutic approaches that rely on systemic inhibition of the TGF-β pathway for the management of myocardial fibrosis. (J Am Coll Cardiol Basic Trans Science 2019;4:41–53)

Heart failure is a major health problem worldwide. At present, approximately 6.5 million people in the United States experience heart failure, and this number is expected to grow to more than 8 million by 2030 (1,2). Heart failure has increased spending on health care services, resulting in an economic burden of about $31 billion/year (2). Although diagnosis and treatments have improved, a poor survival rate in heart failure patients suggests a critical need for research in cardiac pathophysiology.

SEE PAGE 54

Transforming growth factor (TGF)-β are cytokines that play pleiotropic roles in a wide range of cellular processes during embryonic development, tissue homeostasis, and disease (3,4). The TGF-β superfamily consists of more than 30 ligands that belong to subfamilies like the TGF-β, bone morphogenetic proteins, activins, inhibins, growth differentiation factors, and Nodal and anti-Müllerian hormones. In canonical TGF-β signaling, TGF-β ligands bind to specific Ser/Thr kinase receptors (type I and type II), which mediate activation of receptor-specific SMADs. Activated receptor-specific SMADs form heteromeric complexes with a common mediator-SMAD, SMAD4. This SMAD complex translocates into the nucleus, where it regulates transcription of various genes via other transcriptional cofactors (5,6). In addition to SMAD-dependent canonical signaling, TGF-β can regulate the activity of other signaling pathways, such as TGF-β-activated kinase 1 (TAK1), mitogen-activated protein kinases (MAPKs), phosphoinositide-3 kinase (PI3K), Ras homolog family member A, protein phosphatase 2A, and nuclear factor κB (7–13). Collectively, these are referred to as noncanonical or SMAD-independent pathways. The extent of interactions among these canonical and noncanonical signaling molecules varies considerably depending on the context, but are essential to deliver spatially and temporally specific TGF-β signaling outputs (14).

TGF-βs are often chronically overexpressed in diseased hearts and are instrumental in eliciting multiple, even opposing cellular responses (15–20). For instance, excessive TGF-β signaling contributes to cardiac dysfunction in muscular dystrophy, whereas blockade of TGF-β signaling using neutralizing Abs (N-Abs) increases left ventricular (LV) dilatation and mortality after myocardial infarction (21,22). Moreover, disruption of cardiomyocyte (CM) TGF-β signaling by deletion of the TGF-β receptor mitigates pressure overload-induced maladaptive remodeling via noncanonical TAK1 signaling (23). An elegant study by Kong et al. (24) demonstrated that TGF-β-SMAD3 signaling activation in cardiac fibroblasts is required for cardiac repair following myocardial infarction. Despite studies suggesting the importance of TGF-β signaling to cardiac pathophysiology, the exact role of CM canonical TGF-β signaling in cardiac homeostasis has remained enigmatic.

In the present study, we examined the role of CM canonical TGF-β signaling in maintaining adult heart homeostasis. As SMAD4 is a central intracellular mediator of canonical TGF-β signaling, we examined the effects of CM-specific SMAD4 deletion on cardiac function. A previous study has shown that CM-specific SMAD4 deletion results in developmental cardiac defects and embryonic lethality (25). Hence,

All authors attest they are in compliance with human studies committees and animal welfare regulations of the authors' institutions and Food and Drug Administration guidelines, including patient consent where appropriate. For more information, visit the *JACC: Basic to Translational Science* author instructions page.

Manuscript received August 10, 2018; revised manuscript received August 10, 2018, accepted August 10, 2018.

FIGURE 1 Generation and Characterization of CM-Specific SMAD4 KO Mice

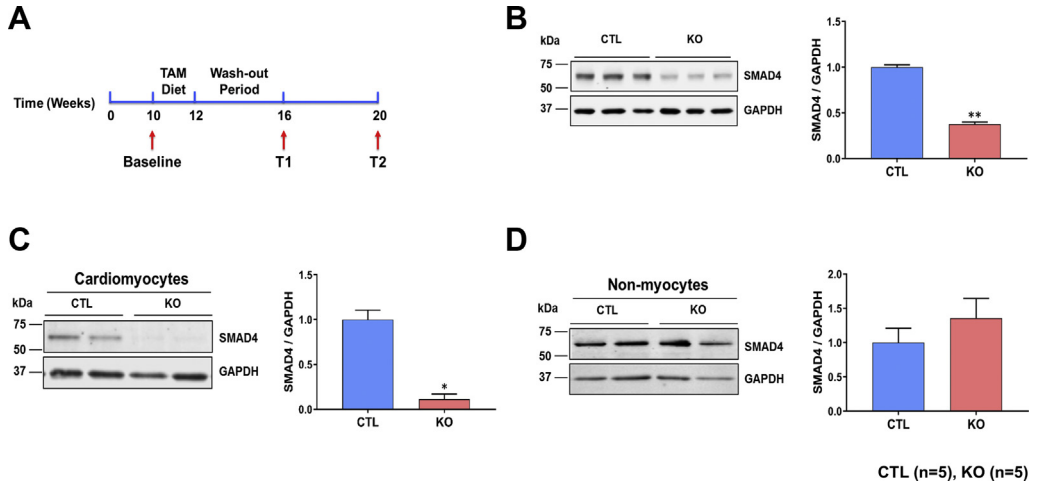

(A) Experimental design showing 10-week-old mice were fed a tamoxifen (TAM) diet for 2 weeks followed by a 4-week wash-out period. T1 and T2 represent time points selected for studies. **(B)** Representative Western blot and quantification of SMAD4 expression in control (CTL) and knockout (KO) hearts at 4 weeks after TAM treatment. **(C)** Representative Western blot quantification of SMAD4 expression in cardiomyocytes (CMs) isolated from CTL and KO hearts at 4 weeks after TAM treatment. **(D)** Representative Western blot quantification of SMAD4 expression in non-CMs isolated from CTL and KO hearts at 4 weeks after TAM treatment. *p = 0.0286, **p = 0.0079. All p values are versus CTL. GAPDH = glyceraldehyde 3-phosphate dehydrogenase.

we designed a model in which SMAD4 is conditionally deleted in adult mouse CMs using tamoxifen (TAM)-inducible alpha-myosin heavy chain promoter-driven Cre recombinase. We report that CM-specific knockdown of SMAD4 significantly alters the cardiac contractile function at cellular as well as organ level. Moreover CM-specific SMAD4 deficiency is associated with a reduction in gene expression of several ion channels and cardiac conduction abnormalities. These findings provide the first evidence that endogenous CM canonical TGF-β signaling is essential for maintaining adult heart homeostasis.

METHODS

A detailed description of the Methods is provided in the Supplemental Appendix.

MICE. To achieve conditional deletion of SMAD4 specifically in CM, $SMAD4^{fl/fl}$ mice (Stock No. 017462, The Jackson Laboratory, Bar Harbor, Maine) were crossed with mice carrying the MerCreMer (MCM) transgene driven by the alpha-myosin heavy chain promoter ($Myh6\text{-}Cre^{+/+}$) (Stock No. 005657, The Jackson Laboratory). Further details of generation and characterization of the CM-specific SMAD4 knockout (KO) mice are described in the Results section. The Institutional Animal Care and Use Committee of Vanderbilt University Medical Center approved all animal procedures and treatments used in this study (protocol #M1700133-00).

STATISTICAL ANALYSIS. Analyses were performed using GraphPad Prism (version 7.02, GraphPad Software, La Jolla, California). Differences between 2 data groups (SMAD4 protein expression, ion-channel gene expression, morphometric, and electrocardiography parameters) were evaluated for significance by the Mann-Whitney test. For comparisons of more than 2 groups (echocardiographic and CM-contractility parameters, protein expression studies), analysis of variance followed by Tukey's multiple comparison test was applied. All data are expressed as mean ± SEM. For all tests, a p value <0.05 was considered statistically significant.

RESULTS

GENERATION AND CHARACTERIZATION OF CM-SPECIFIC SMAD4 KO MICE. To investigate the role of CM TGF-β signaling in the adult heart, we generated a mouse model in which SMAD4 is conditionally deleted in CM-specific manner. $SMAD4^{fl/fl}$ mice were crossed with $Myh6\text{-}Cre^{+/+}$ mice to generate $SMAD4^{fl/fl}Cre^{+/-}$. Also, $Myh6\text{-}Cre^{+/+}$ transgenic mice were crossed with C57BL/6 mice (Stock No. 000664,

JACC: BASIC TO TRANSLATIONAL SCIENCE VOL. 4, NO. 1, 2019
FEBRUARY 2019:41–53

FIGURE 2 CM-Specific Deletion of SMAD4 Causes Cardiac Dysfunction

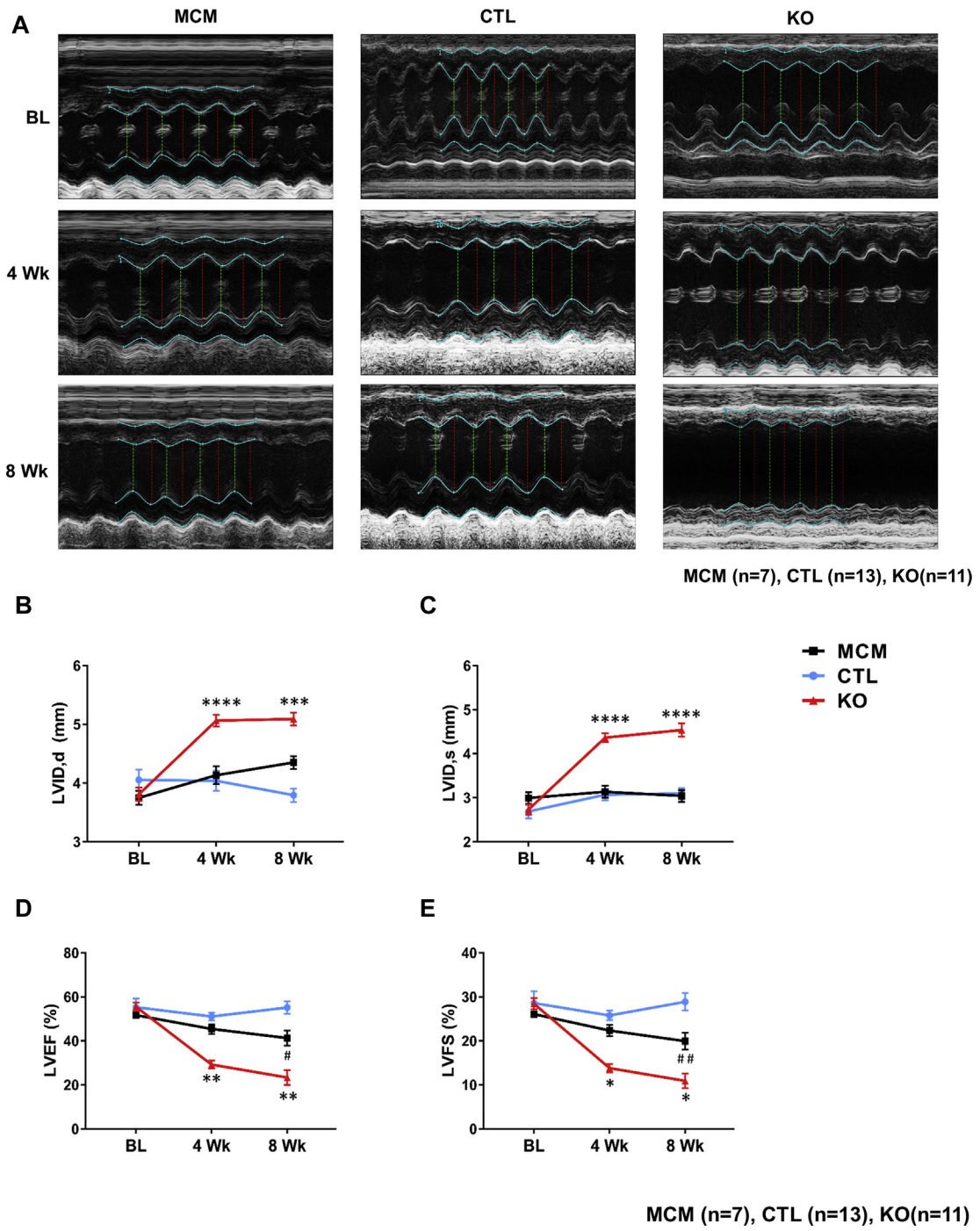

CTL and SMAD4 KO mice underwent baseline transthoracic echocardiographic examination and then were subjected to a TAM treatment for 2 weeks. After a 4-week wash-out period, mice were then followed with serial echocardiography assessment at the time points shown. **(A)** Representative images of serial echocardiographic measurements. (**B**) Left ventricular internal dimension in diastole (LVID,d). ****$p < 0.0001$ versus MerCreMer (MCM) group, ***$p = 0.0008$ versus MCM group. **(C)** LVID in systole (LVID,s). ****$p < 0.0001$ versus MCM. **(D)** LV ejection fraction (LVEF). **$p = 0.0035$ versus MCM group (time = 4 weeks), **$p = 0.0014$ versus MCM group, #$p = 0.0161$ versus CTL group (time = 8 weeks). **(E)** LV fractional shortening (LVFS). *$p = 0.0220$ versus MCM group (time = 4 weeks), *$p = 0.0184$ versus MCM group, ##$p = 0.0096$ versus CTL (time = 8 weeks). BL = baseline; Wk = weeks; other abbreviations as in Figure 1.

FIGURE 3 **CM-Specific SMAD4 Deletion Induces Cardiac Remodeling**

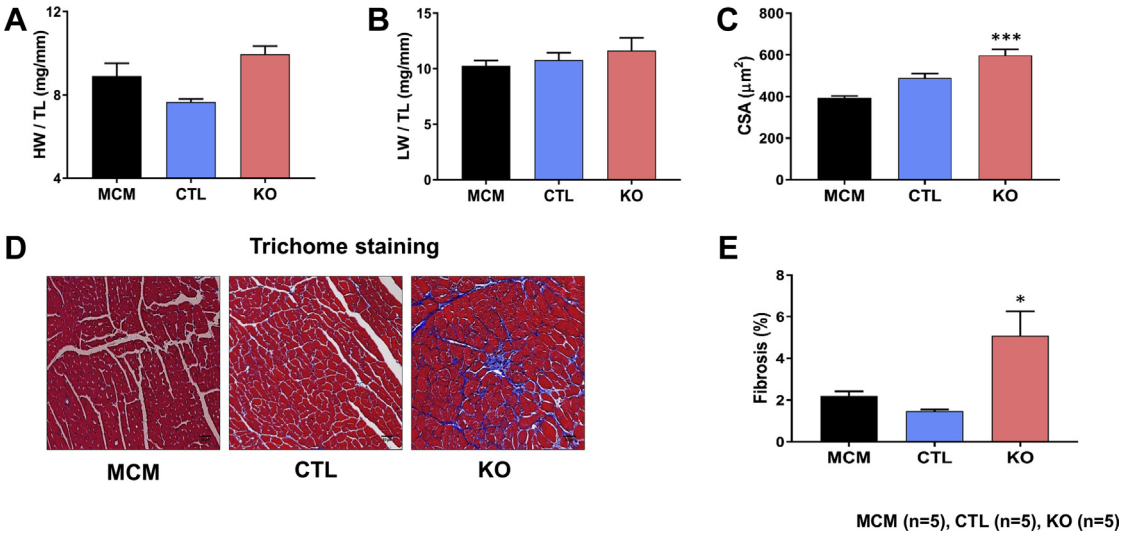

Morphometric studies were performed at the end of 8 weeks after TAM treatment. **(A)** Heart weight (HW) to tibia length (TL). **(B)** Lung weight (LW) to TL. **(C)** Quantification of cardiomyocyte cross-sectional area (CSA). ***p = 0.0002 versus MCM group. **(D)** Masson's trichome staining. Representative trichome-stained LV regions. **(E)** Quantification of LV fibrosis. *p = 0.0165 versus MCM group. Scale bar = 30 μm. Abbreviations as in Figures 1 and 2.

The Jackson Laboratory) to generate Myh6-Cre$^{+/-}$. A well-established TAM chow diet protocol was used to induce the CM-specific expression of Cre recombinase, as we previously reported (26,27). Briefly, at 10 weeks of age, when physiological development is largely complete, all male mice were placed on a TAM chow diet (400 mg/kg, TD.130859, Harlan Sprague-Dawley, Indianapolis, Indiana) for 2 weeks followed

FIGURE 4 **CM-Specific SMAD4 Deletion Induces Cardiac Remodeling**

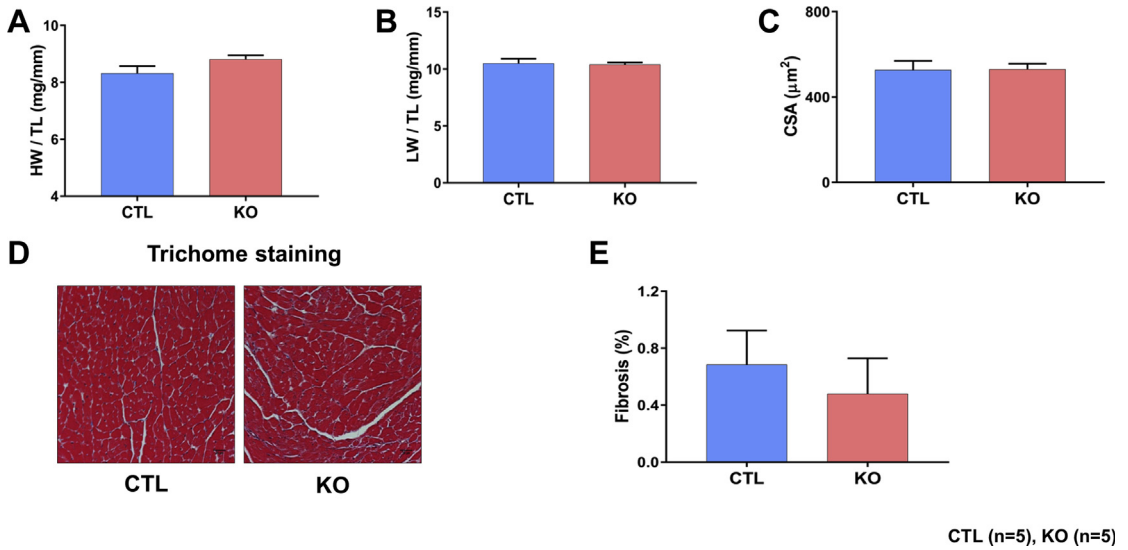

Morphometric studies were performed at the end of 4 weeks after TAM treatment. **(A)** HW to TL. **(B)** LW to TL. **(C)** Quantification of cardiomyocyte CSA. **(D)** Masson's trichome staining. Representative trichome-stained LV regions. **(E)** Quantification of LV fibrosis. Scale bar = 30 μm. Abbreviations as in Figures 1 to 3.

FIGURE 5 CM-Specific SMAD4 Deletion Leads to Cardiac Cell Death

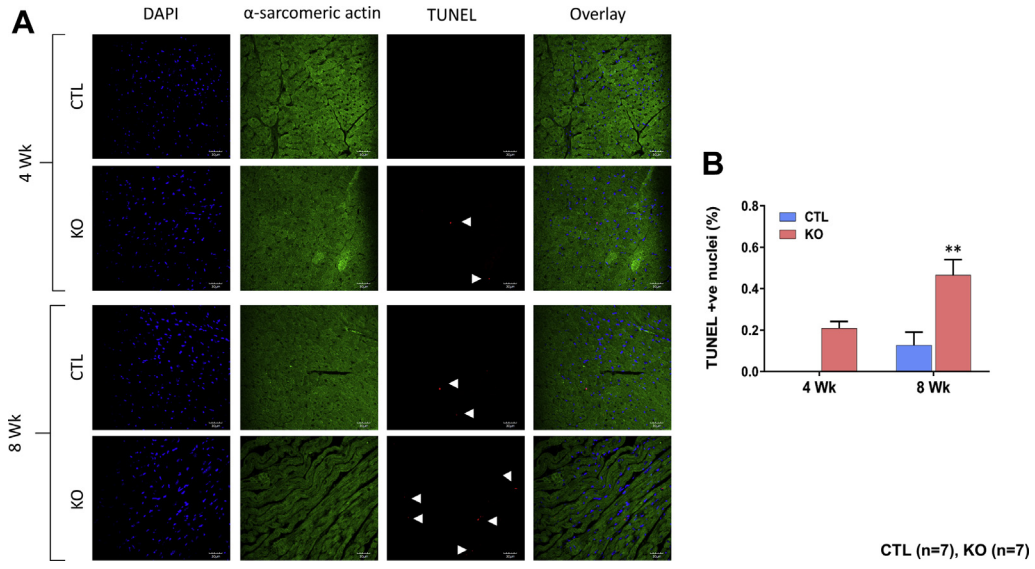

(A) Representative images show terminal deoxynucleotidyl transferase dUTP nick-end labeling (TUNEL)–positive cardiomyocytes from the CTL and KO hearts. **(B)** Quantification shows significantly increased number of TUNEL-positive myocytes in KO mice at 8 weeks after TAM treatment. **p = 0.0069 versus CTL group. Scale bar = 30 μm. Abbreviations as in Figures 1 to 3.

by regular chow for an additional 4 weeks (to allow the clearance of TAM from the mice) (Figure 1A). SMAD4$^{fl/fl}$/Cre$^{+/-}$/TAM mice were the conditional KO mice, whereas littermates SMAD4$^{fl/fl}$/Cre$^{-/-}$/TAM represented control (CTL) animals. Myh6-Cre$^{+/-}$/TAM mice were used as no-flox Cre CTL animals (MCM). There were no differences in mortality between CTL and SMAD4 KO mice up to the termination of the study (i.e., 8 weeks after TAM treatment). Western blot analysis of LV tissue lysates confirmed that TAM treatment led to a ~60% reduction in SMAD4 protein levels in KO (Figure 1B). To confirm CM-specific SMAD4 deletion, Western blotting was performed with protein extracted from isolated CMs and non-myocytes. SMAD4 protein levels were significantly low (~90% deletion) in CMs, as expected, non-myocytes displayed no change (Figures 1C and 1D).

CM-SPECIFIC DELETION OF SMAD4 CAUSES DILATED CARDIOMYOPATHY. We performed serial M-mode echocardiography to assess the effect of CM-SMAD4 deletion on cardiac function. Importantly, to account for any confounding effects of Cre overexpression or TAM on cardiac function, these critical controls were also included in the study (Figure 2A, Supplemental Table 1). At baseline, MCM, CTL, and SMAD4 KO hearts had comparable chamber dimensions and ventricular function. At 4 weeks after TAM treatment, SMAD4 KO animals had a substantial increase in LV internal dimension in diastole and systole in comparison with CTL animals, indicating dilative remodeling of the LV (Figures 2B and 2C). These changes were associated with marked LV dysfunction as reflected by a significant decline in LV ejection fraction and LV fractional shortening (Figures 2D and 2E). At 8 weeks after TAM treatment, MCM displayed a modest but significant reduction in LV ejection fraction and LV fractional shortening as compared with the CTL group. Considering the fact that SMAD4 KO mice had a significant decline in cardiac function parameters as compared with both the CTL and MCM groups, our findings strongly indicate that cardiac dysfunction developed in SMAD4 KO animals is the specific effect of deletion of CM-canonical TGF-β signaling.

At the end of each time point, heart weight to tibia length and lung weight to tibia length ratios were compared. These parameters were comparable between the SMAD4 KO and CTL groups at both time points (Figures 3A, 3B, 4A, and 4B). For the assessment of cardiac hypertrophy, CM cross-sectional area (CSA) was measured. We found no significant difference in CSA between the SMAD4 KO and CTL groups at 4 weeks after TAM treatment (Figure 4C). However, at 8 weeks, CSA was significantly higher in SMAD4 KO

FIGURE 6 Effect of CM-Specific SMAD4 Deletion on CM Contraction Kinetics and on Contractility-Regulating Proteins

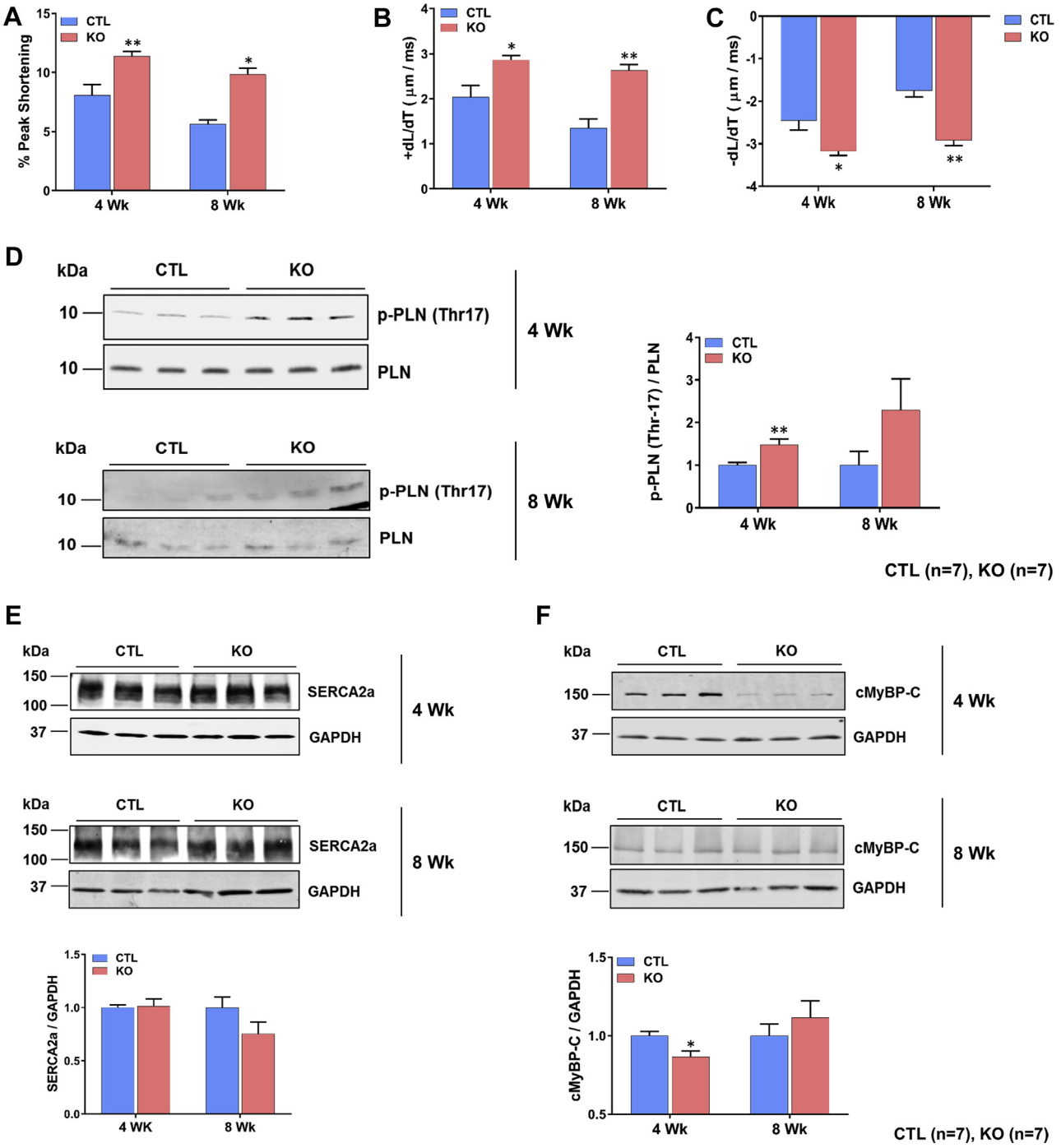

CMs were isolated from the hearts of experimental mice at the end of each time point and sarcomere shortening parameters assessed (n = 10 to 20 CMs/heart and 8 to 9 hearts/group). **(A)** Sarcomere peak shortening normalized to resting sarcomere length (% peak shortening). *p = 0.0104, **p = 0.0033 versus CTL group. **(B)** Maximal relengthening (+dL/dT) velocity. *p = 0.0101, **p = 0.0035. **(C)** Maximal shortening (-dL/dT) velocity. *p = 0.0102, **p = 0.0041. Western blot analysis of proteins that regulate calcium homeostasis and cardiomyocyte contractility. Representative Western blots and quantification. **(D)** Phospholamban (PLN). **p = 0.0099. **(E)** Sarco/endoplasmic reticulum Ca^{2+}-ATPase 2a (SERCA2a). **(F)** Cardiac myosin binding protein C (cMyBP-C). *p = 0.0317. All p values are versus the CTL group. Abbreviations as in Figures 1 to 3.

FIGURE 7 RNA-Seq Analysis Reveals Alteration in Ion Channel Genes in SMAD4 KO Mice

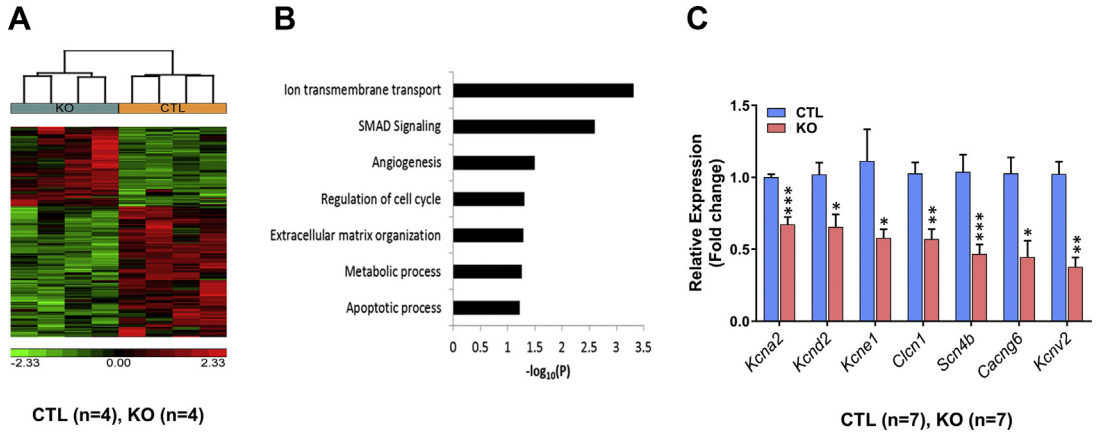

RNA sequencing (RNA-Seq) analysis was performed at 4 weeks after TAM treatment. **(A)** Hierarchical clustering of 161 genes detected as significantly differential (at least 1.5-fold, p value <0.05) between the CTL and SMAD4 KO groups. **(B)** Gene Ontology analysis. **(C)** Quantitative polymerase chain reaction analysis of ion-channel genes: kcna2 (***p = 0.0006), kcnd2 (*p = 0.0291), kcne1 (*p = 0.0111), clcn1 (**p = 0.0016), scn4b (***p = 0.0006), cacng6 (*p = 0.0130), and kcnv2 (**p = 0.0012). All p values are versus the CTL group. Abbreviations as in Figures 1 and 2.

mice than respective CTL animals (Figure 3C). Cardiac fibrosis was assessed by performing Masson's trichome staining. Examination of trichome-stained heart sections demonstrated that fibrosis was absent in SMAD4 KO mice at 4 weeks after TAM treatment (Figures 4D and 4E) and was prominently seen in these animals at 8 weeks (Figures 3D and 3E). To confirm the histology data, we analyzed expression levels of molecular markers for fibrotic remodeling by the quantitative polymerase chain reaction method. In agreement with the trichome staining results, we saw an increasing trend in the levels of col1a1, col1a2, and col3a1 in the KO group (Supplemental Figure 1). CM dropout due to cell death causes remodeling of the heart. Hence, we also examined cardiac sections for the presence of DNA fragmentation, a classical marker of cell death, by terminal deoxynucleotidyl transferase dUTP nick-end labeling staining. Cell death was significantly evident at 8 weeks after TAM treatment (Figures 5A and 5B). Considered together, these results demonstrate that CM-specific disruption of canonical TGF-β signaling via deletion of the critical intermediate regulator SMAD4 leads to dilated cardiomyopathy (DCM) development. Thus, CM-SMAD4 is indispensable for adult heart homeostasis.

CM-SPECIFIC SMAD4 DELETION DOES NOT AFFECT MAPK AND PI3K-AKT SIGNALING PATHWAYS. Previous studies showed that the TGF-β could activate MAPK and PI3K-AKT signaling pathway independently of SMADs (7,8,12). Thus, to verify whether any aberrant changes in the MAPK or PI3K-AKT pathway contributed to the observed cardiac phenotype in SMAD4 KO mice, we examined the protein levels of phosphorylated ERK1/2, p38, and AKT by Western blotting at both time points. The phosphorylation levels of ERK1/2, p38, and AKT were comparable in the LV lysates from SMAD4 KO and CTL mice (Supplemental Figures 2A to 2C). These results rule out the possible causal role of the MAPK and PI3K-AKT signaling pathways in the development of cardiac dysfunction in SMAD4 KO.

CM CONTRACTILITY IS AFFECTED BY CM-SPECIFIC SMAD4 DELETION. To determine whether the observed in vivo LV systolic dysfunction was attributable to defects in contractility of CMs, we assessed sarcomere contractility of CMs isolated from SMAD4 KO and CTL mice. Surprisingly, SMAD4 KO CMs displayed significantly higher sarcomere peak shortening, as well as sarcomere shortening and relengthening velocities compared with CMs isolated from CTL mice (Figures 6A to 6C).

Calcium homeostasis is a key factor in regulating CM contractility. Therefore, we next examined the effect of SMAD4 deletion on calcium handling proteins. Total protein levels of sarco- or endoplasmic reticulum Ca^{2+}-ATPase 2a (SERCA2a) and its inhibitor phospholamban were comparable in SMAD4 KO and CTL hearts. However, phospholamban was hyperphosphorylated in SMAD4 KO hearts, indicating a

FIGURE 8 **CM-Specific SMAD4 Deletion Causes Cardiac Conduction Abnormalities**

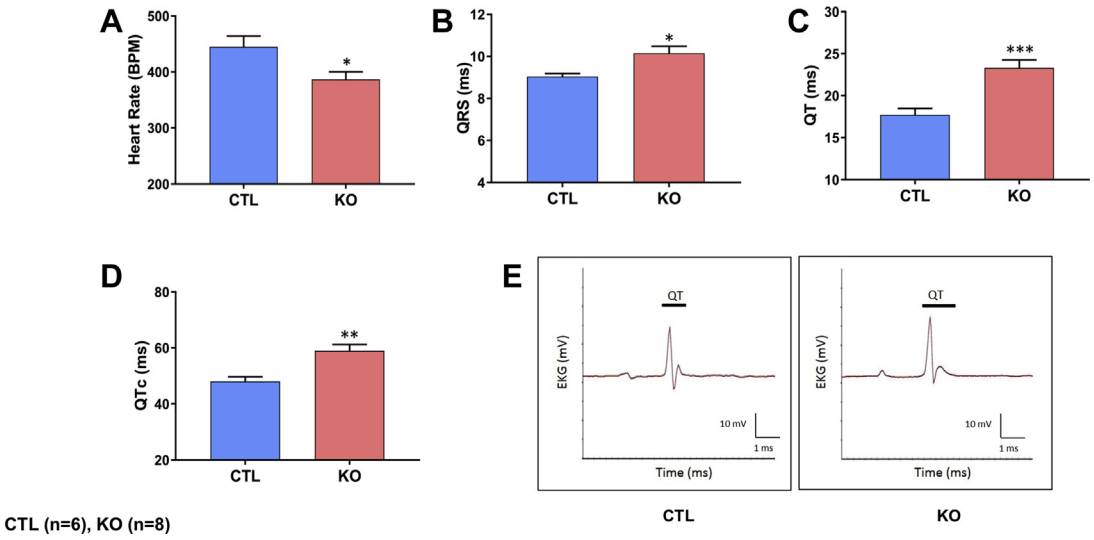

Electrocardiography (EKG) analysis was performed on mice at 4 weeks after TAM treatment and the following ECG parameters were examined: **(A)** heart rate (*p = 0.0426), **(B)** QRS interval (*p = 0.0127), **(C)** QT interval (***p = 0.0007), **(D)** QTc interval (**p = 0.0027), and **(E)** representative ECG traces. All p values are versus the CTL group. BPM = beats per minute; other abbreviations as in Figure 1.

reduction in its inhibitory effect on SERCA2a pump activity (Figures 6D and 6E).

The observed increase in CM contraction kinetics suggested that there might be alterations in myofilament calcium sensitivity and cross-bridge cycling rates. As cardiac myosin-binding protein C (cMyBP-C) is known to regulate these processes, we examined levels of these proteins by Western blotting. Indeed, cMyBP-C was significantly down-regulated in the SMAD4 KO hearts at 4 weeks after TAM treatment (Figure 6F). These results support our observation of improved CM contractility in SMAD4 KO mice.

RNA SEQUENCING RESULTS REVEAL DOWN REGULATION IN CARDIAC ION CHANNELS' GENES EXPRESSION IN SMAD4 KO MICE. To examine the primary consequences of CM-SMAD4 deletion on the cardiac transcriptome, RNA sequencing (RNA-Seq) analysis was performed at 4 weeks after TAM treatment. Comparison of SMAD4 KO versus littermate CTL animals resulted in the identification of 166 transcripts with significant differential expression (shown in Cluster), including 151 characterized gene products, and 15 uncharacterized transcripts (complementary DNAs, Expressed sequence tags, or long noncoding RNAs). Of the 151 altered genes, only 55 were up-regulated, with the majority (96 genes) down-regulated by at least 1.5-fold with $p < 0.05$ (Figure 7A).

Gene Ontology analysis identified ion transmembrane transport as the top over-represented biological process in SMAD4 KO hearts (Figure 7B). Based on this finding, we identified the ion-channel genes that were significantly down-regulated (*Clcn1, Kcnd2, Kcna2, Cacng6, Kcne1, Scn4b, Kcnv2*). We validated their gene expression by quantitative polymerase chain reaction and consistent with the RNA-Seq results, these genes showed significant down-regulation in the hearts of SMAD4 KO mice, compared with littermate CTL animals (Figure 7C).

SMAD4 KO MICE EXHIBIT ELECTROCARDIOGRAPHIC ABNORMALITIES. The identification of ion transmembrane transport as the top biological process in RNA-Seq analysis prompted us to examine whether CM-specific SMAD4 deletion causes any electrophysiological defects in SMAD4 KO mice. Thus, electrocardiography analysis was performed on SMAD4 KO and littermate CTL mice at 4 weeks after TAM. Indeed, slower heart rates were evident in SMAD4 KO than littermate CTL animals (Figure 8A). Furthermore, SMAD4 KO mice displayed prolongation of QRS, QT, and QTc intervals (Figures 8B to 8E).

DISCUSSION

Herein we examined the contribution of CM canonical TGF-β signaling to the heart function. We

FIGURE 9 CM Canonical TGF-β Signaling is Essential to Maintain Adult Heart Homeostasis

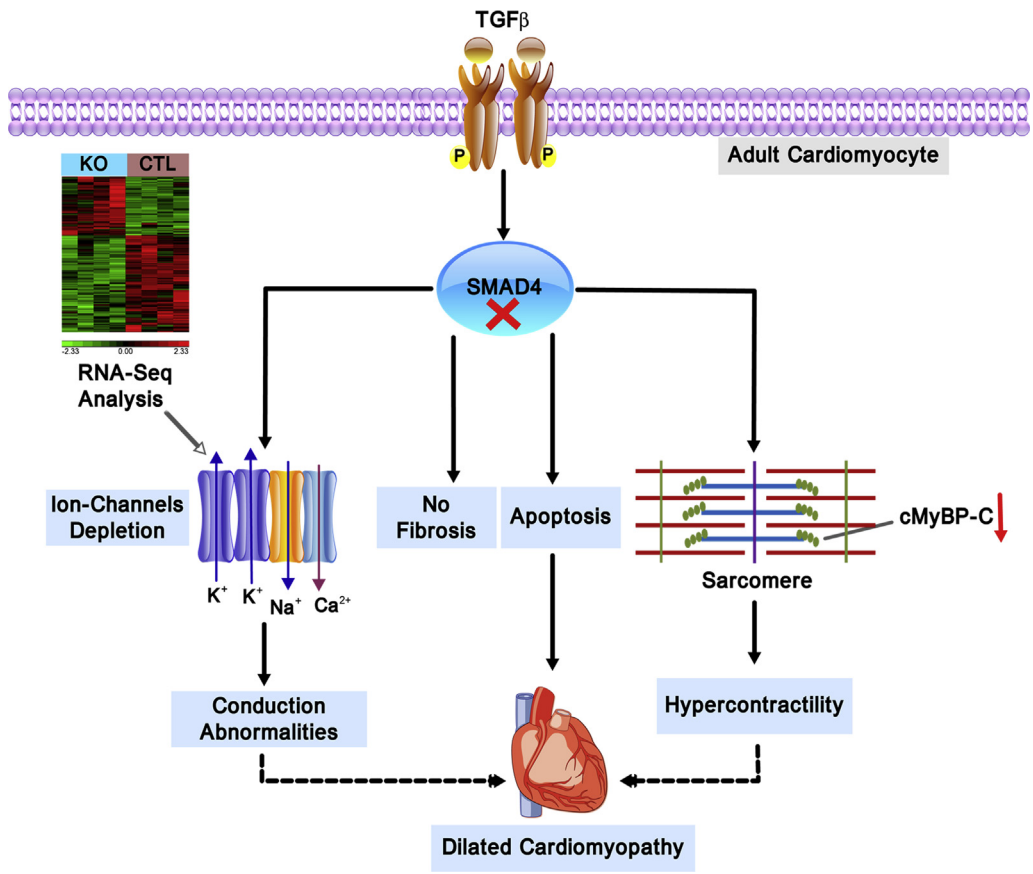

Deletion of canonical TGF-β signaling in adult CMs by targeting SMAD4 leads to down-regulation of several ion-channel genes and a key sarcomeric protein, cMyBP-C. These adverse effects of SMAD4 deletion results in cardiac conduction abnormalities and hyper contractile phenotype and are at least in part responsible for dilated cardiomyopathy development. Importantly, CM-specific canonical TGF-β signaling does not seem to be a significant contributor of fibrosis in adult hearts. Abbreviations as in **Figures 1, 6, and 7**.

demonstrated that CM-specific SMAD4 deletion in the fully mature heart causes DCM. Interestingly, cardiac dysfunction in SMAD4 KO mice was seen despite improved CM contractility and preceded by the development of pathological features of DCM such as hypertrophy and fibrosis. Furthermore, we also observed down-regulation of ion channels' gene expression and cardiac conduction abnormalities in SMAD4 KO mice. These results highlight a fundamental role for CM-specific canonical TGF-β signaling in the regulation of adult heart function (**Figure 9**).

In SMAD4 KO mice, development of marked cardiac dysfunction preceded the fibrotic remodeling indicating that fibrosis was not a cause of observed phenotype. It is well established that canonical TGF-β signaling is critical to fibroblast biology and fibrosis (24,28-31). Additionally, the previous study by the Kass lab (23) demonstrated that the activation of the noncanonical TGF-β pathway in CMs contributes to maladaptive fibrotic remodeling in pressure-overloaded hearts. Thus, it is possible that fibrosis observed at a later point could be a maladaptive response evoked by fibroblasts with intact TGF-β signaling or the effect of activation of noncanonical TGF-β signaling spared in CMs. Furthermore, a study pertaining to muscle-specific SMAD4 deletion in muscular dystrophy models revealed that functional enhancement of dystrophic muscle occurs without a significant reduction in fibrosis (21). In line with this report, our study also provides valuable evidence that CM-specific canonical TGF-β signaling is not a significant contributor to fibrotic remodeling and

highlights its ability to alter cardiac performance by targeting CM-specific pathways.

Wang et al. (32) demonstrated that targeted disruption of SMAD4 in CMs results in the early onset of cardiac hypertrophy and implicated the excessive activation of MEK1-ERK1/2 as the possible underlying mechanism. In stark contrast, herein we demonstrate that CM-SMAD4 does not regulate MEK1-ERK1/2 signaling or cardiac hypertrophy in the adult heart. This discrepancy might be due to differences in the timing of CM-specific SMAD4 deletion. Wang et al. (32) deleted SMAD4 in mouse embryos using alpha-myosin heavy chain promoter-driven Cre. Considering the essential role of SMAD4 in cardiogenesis (25), the phenotype of the animals used in the previous study might have been compromised by developmental defects. However, in our model, SMAD4 deletion was done when the physiological development of mice is complete, thus excluding the causal role of developmental defects in the observed cardiac phenotype. We believe that inducible loss-of-function approaches are likely of greater biological relevance in identifying the true targets of SMAD4 in the fully mature heart compared with transgenesis, embryonic knockout, or cell culture approaches.

To our complete surprise, SMAD4 KO mice displayed enhanced CM contractility. This finding contrasted with decreased cardiac function seen in these animals. However, further studies performed to ascertain these intriguing observations revealed that there was a remarkable reduction in cMyBP-C in SMAD4 KO hearts. MyBP-C is a crucial sarcomeric protein that has structural as well as regulatory functions in muscles. Genetic studies have identified MYBPC3 (cardiac isoform) as one of the major mutated genes that results in the development of hypertrophic and dilated cardiomyopathies (33,34). Several mouse models bearing such mutations showed haploinsufficiency and reduction in cMyBP-C levels (35–38). These models had increased myofilament calcium sensitivity and faster cross-bridge cycling rate, and developed a hypercontractile phenotype. Additionally, pathological features such as fibrosis, hypertrophy, and arrhythmogenesis were seen in these models. Thus, considering the phenotypic similarities in MYBPC3 mutants and SMAD4 KO mice, we speculate that reduction in cMyBP-C protein in SMAD4 KO heart may, at least in part, be responsible for development of cardiac abnormalities in these animals.

The disagreement between contractile function assessed in isolated myocytes and intact hearts of SMAD4 KO suggests that there might be impaired muscle force transduction, increased myocyte death, or compromised electrical activation of the myocardium. To examine whether CM-specific SMAD4 deletion has any effect on key proteins involved in muscle force transmission, we assessed levels of intercalated disc and costameric proteins by Western blotting. The expression of these proteins was not different in CTL and KO animals (Supplemental Figures 3A to 3D). However, analysis of terminal deoxynucleotidyl transferase dUTP nick-end labeling data suggested that in SMAD4 KO there is a progressive increase in cardiac cell death. Considering the prosurvival effect of TGF-β superfamily members on CM, it is not surprising that CM-specific SMAD4 deletion resulted in the CMs death in SMAD4 KO mice (39–41). Together, these evidences support our hypothesis that cardiac cell death might have contributed to the development of cardiac dysfunction in SMAD4 KO mice.

The most striking finding from RNA-Seq analysis was the significant down-regulation of several ion-channel genes in hearts from SMAD4 KO mice. Of these, the pivotal role of *Kcnd2* is demonstrated in encoding primary repolarizing current in rodents and when selectively eliminated in mice resulted in QT prolongation (42). Additionally, a mutation in gene SCN4B which codes for sodium channel β4 subunit has been implicated in congenital long-QT syndrome type 10 in humans (43). In keeping with these reports and RNA-Seq results, electrocardiography analysis revealed that SMAD4 KO mice exhibit QT prolongation. These observations suggest that down-regulation in the expression of ion-channel genes could possibly account for the alteration in the electrocardiography parameters of SMAD4 KO animals. However, given the possibility that QRS and QT prolongation may have resulted from the developing pathology, additional studies with more comprehensive electrophysiological assessments are necessary to explain whether SMAD4 KO mice exhibit causal relationship between conduction and contractility defects. To our knowledge, only a few reports have provided evidence for a direct role of TGF-β signaling in modulating ion channels essential for cardiac electrophysiology. For instance, Kaur et al. (44) showed that TGF-β-1 increases the transcription and activity of sodium channels in adult rat CMs. On the other hand, Ramos-Mondragon et al. (45) reported reduction in the expression and activity of sodium channel in TGF-β1-treated neonatal rat atrial myocytes. It is important to note that these studies are performed

in isolated CMs, which differ in biophysical and electrophysiological properties compared with the entire organ. With that said, our study is the first to provide evidence for the significant role of CM-specific SMAD4-dependent TGF-β signaling in regulating gene expression of ion channels that are essential for cardiac conduction.

CONCLUSIONS

In summary, we report that CM-specific deletion of canonical TGF-β signaling in fully mature CMs leads to cardiac dysfunction and dilated cardiomyopathy. Although canonical TGF-β signaling has been suggested as a critical target for the management of adverse fibrotic remodeling, our findings strongly suggest that cell-specific TGF-β responses should be considered when developing anti-TGF-β strategies for treating cardiac diseases to avoid interference with its beneficial actions.

ACKNOWLEDGMENTS The authors would like to thank Dr. Sakthivel Sadayappan, University of Cincinnati, for providing expert advice and antibodies to detect cardiac myosin binding protein C.

ADDRESS FOR CORRESPONDENCE: Dr. Hind Lal, Division of Cardiovascular Medicine, Vanderbilt University Medical Center, 2220 Pierce Avenue, PRB#348A, Nashville, Tennessee 37232. E-mail: hind.lal@vanderbilt.edu.

PERSPECTIVES

COMPETENCY IN MEDICAL KNOWLEDGE: Vast published data has established the central role of canonical TGF-β signaling in fibroblast activation, wound healing, and myocardial fibrosis. However, the role of canonical TGF-β signaling in fully mature functional CMs is not clear. Our studies establish that the CMs canonical TGF-β signaling is essential to preserve adult heart homeostasis. We also establish that this signaling axis in CMs is critical for maintaining cMyBP-C levels, sarcomere kinetics, and expression of key ion channels. Thus, the role of CM canonical TGF-β signaling in myocardial physiology appears to be substantial.

TRANSLATIONAL OUTLOOK: Pharmacological targeting of canonical TGF-β signaling is highly implicated for the management of multiple organ fibrosis including the myocardial fibrosis. In light of our finding presented herein, we suggest caution in going forward with the drugs that target canonical TGF-β signaling in the heart. Strategies for such drug development may include the cell-specific targeting or delineation of potential downstream targets. Thus, our finding identifies what we believe to be a new paradigm for pharmacological targeting of canonical TGF-β1 signaling and raises a significant concern regarding the approaches relies on systemic inhibition.

REFERENCES

1. Benjamin EJ, Blaha MJ, Chiuve SE, et al. Heart Disease and Stroke Statistics-2017 Update: a report From the American Heart Association. Circulation 2017;135:e146–603.

2. Heidenreich PA, Albert NM, Allen LA, et al. Forecasting the impact of heart failure in the United States: a policy statement from the American Heart Association. Circ Heart Fail 2013;6:606–19.

3. Wu MY, Hill CS. TGF-beta superfamily signaling in embryonic development and homeostasis. Dev Cell 2009;16:329–43.

4. Akhurst RJ, Hata A. Targeting the TGFbeta signalling pathway in disease. Nat Rev Drug Discov 2012;11:790–811.

5. Schmierer B, Hill CS. TGFbeta-SMAD signal transduction: molecular specificity and functional flexibility. Nat Rev Mol Cell Biol 2007;8:970–82.

6. Derynck R, Zhang YE. Smad-dependent and Smad-independent pathways in TGF-beta family signalling. Nature 2003;425:577–84.

7. Lee MK, Pardoux C, Hall MC, et al. TGF-beta activates Erk MAP kinase signalling through direct phosphorylation of ShcA. EMBO J 2007;26:3957–67.

8. Yamashita M, Fatyol K, Jin C, Wang X, Liu Z, Zhang YE. TRAF6 mediates Smad-independent activation of JNK and p38 by TGF-beta. Mol Cell 2008;31:918–24.

9. Yamaguchi K, Nagai S, Ninomiya-Tsuji J, et al. XIAP, a cellular member of the inhibitor of apoptosis protein family, links the receptors to TAB1-TAK1 in the BMP signaling pathway. EMBO J 1999;18:179–87.

10. Bhowmick NA, Ghiassi M, Bakin A, et al. Transforming growth factor-beta1 mediates epithelial to mesenchymal transdifferentiation through a RhoA-dependent mechanism. Mol Biol Cell 2001;12:27–36.

11. Petritsch C, Beug H, Balmain A, Oft M. TGF-beta inhibits p70 S6 kinase via protein phosphatase 2A to induce G(1) arrest. Genes Dev 2000;14:3093–101.

12. Bakin AV, Tomlinson AK, Bhowmick NA, Moses HL, Arteaga CL. Phosphatidylinositol 3-kinase function is required for transforming growth factor beta-mediated epithelial to mesenchymal transition and cell migration. J Biol Chem 2000;275:36803–10.

13. Freudlsperger C, Bian Y, Contag Wise S, et al. TGF-beta and NF-kappaB signal pathway cross-talk is mediated through TAK1 and SMAD7 in a subset of head and neck cancers. Oncogene 2013;32:1549–59.

14. Massague J. TGFβ signalling in context. Nat Rev Mol Cell Biol 2012;13:616–30.

15. Li RK, Li G, Mickle DA, et al. Overexpression of transforming growth factor-beta1 and insulin-like growth factor-I in patients with idiopathic hypertrophic cardiomyopathy. Circulation 1997;96:874–81.

16. Hein S, Arnon E, Kostin S, et al. Progression from compensated hypertrophy to failure in the pressure-overloaded human heart: structural deterioration and compensatory mechanisms. Circulation 2003;107:984–91.

17. Gramley F, Lorenzen J, Koellensperger E, Kettering K, Weiss C, Munzel T. Atrial fibrosis and atrial fibrillation: the role of the TGF-beta1 signaling pathway. Int J Cardiol 2010;143:405–13.

18. Deten A, Holzl A, Leicht M, Barth W, Zimmer HG. Changes in extracellular matrix and in

transforming growth factor beta isoforms after coronary artery ligation in rats. J Mol Cell Cardiol 2001;33:1191–207.

19. Li JM, Brooks G. Differential protein expression and subcellular distribution of TGFbeta1, beta2 and beta3 in cardiomyocytes during pressure overload-induced hypertrophy. J Mol Cell Cardiol 1997;29:2213–24.

20. Bujak M, Frangogiannis NG. The role of TGF-beta signaling in myocardial infarction and cardiac remodeling. Cardiovasc Res 2007;74:184–95.

21. Goldstein JA, Bogdanovich S, Beiriger A, et al. Excess SMAD signaling contributes to heart and muscle dysfunction in muscular dystrophy. Hum Mol Genet 2014;23:6722–31.

22. Frantz S, Hu K, Adamek A, et al. Transforming growth factor beta inhibition increases mortality and left ventricular dilatation after myocardial infarction. Basic Res Cardiol 2008;103:485–92.

23. Koitabashi N, Danner T, Zaiman AL, et al. Pivotal role of cardiomyocyte TGF-beta signaling in the murine pathological response to sustained pressure overload. J Clin Invest 2011;121:2301–12.

24. Kong P, Shinde AV, Su Y, et al. Opposing actions of fibroblast and cardiomyocyte smad3 signaling in the infarcted myocardium. Circulation 2018;137:707–24.

25. Song L, Yan W, Chen X, Deng CX, Wang Q, Jiao K. Myocardial smad4 is essential for cardiogenesis in mouse embryos. Circ Res 2007;101:277–85.

26. Ahmad F, Lal H, Zhou J, et al. Cardiomyocyte-specific deletion of Gsk3alpha mitigates post-myocardial infarction remodeling, contractile dysfunction, and heart failure. J Am Coll Caridol 2014;64:696–706.

27. Gupte M, Tumuluru S, Sui JY, et al. Cardiomyocyte-specific deletion of GSK-3beta leads to cardiac dysfunction in a diet induced obesity model. Int J Cardiol 2018;259:145–52.

28. Khalil H, Kanisicak O, Prasad V, et al. Fibroblast-specific TGF-beta-Smad2/3 signaling underlies cardiac fibrosis. J Clin Invest 2017;127:3770–83.

29. Guo Y, Gupte M, Umbarkar P, et al. Entanglement of GSK-3beta, beta-catenin and TGF-beta1 signaling network to regulate myocardial fibrosis. J Mol Cell Cardiol 2017;110:109–20.

30. Lal H, Ahmad F, Zhou J, et al. Cardiac fibroblast glycogen synthase kinase-3beta regulates ventricular remodeling and dysfunction in ischemic heart. Circulation 2014;130:419–30.

31. Biernacka A, Cavalera M, Wang J, et al. Smad3 signaling promotes fibrosis while preserving cardiac and aortic geometry in obese diabetic mice. Circ Heart Fail 2015;8:788–98.

32. Wang J, Xu N, Feng X, et al. Targeted disruption of Smad4 in cardiomyocytes results in cardiac hypertrophy and heart failure. Circ Res 2005;97:821–8.

33. Daehmlow S, Erdmann J, Knueppel T, et al. Novel mutations in sarcomeric protein genes in dilated cardiomyopathy. Biochem Biophys Res Commun 2002;298:116–20.

34. Richard P, Charron P, Carrier L, et al. Hypertrophic cardiomyopathy: distribution of disease genes, spectrum of mutations, and implications for a molecular diagnosis strategy. Circulation 2003;107:2227–32.

35. van Dijk SJ, Dooijes D, dos Remedios C, et al. Cardiac myosin-binding protein C mutations and hypertrophic cardiomyopathy: haploinsufficiency, deranged phosphorylation, and cardiomyocyte dysfunction. Circulation 2009;119:1473–83.

36. Cheng Y, Wan X, McElfresh TA, et al. Impaired contractile function due to decreased cardiac myosin binding protein C content in the sarcomere. Am J Physiol Heart Circ Physiol 2013;305:H52–65.

37. Fraysse B, Weinberger F, Bardswell SC, et al. Increased myofilament Ca2+ sensitivity and diastolic dysfunction as early consequences of Mybpc3 mutation in heterozygous knock-in mice. J Mol Cell Cardiol 2012;52:1299–307.

38. Carrier L, Knoll R, Vignier N, et al. Asymmetric septal hypertrophy in heterozygous cMyBP-C null mice. Cardiovasc Res 2004;63:293–304.

39. Kempf T, Eden M, Strelau J, et al. The transforming growth factor-beta superfamily member growth-differentiation factor-15 protects the heart from ischemia/reperfusion injury. Circ Res 2006;98:351–60.

40. Zaidi SH, Huang Q, Momen A, Riazi A, Husain M. Growth differentiation factor 5 regulates cardiac repair after myocardial infarction. J Am Coll Cardiol 2010;55:135–43.

41. Zhang Y, Alexander PB, Wang XF. TGF-beta family signaling in the control of cell proliferation and survival. Cold Spring Harbor Perspect Biol 2017;9:a022145.

42. Oudit GY, Kassiri Z, Sah R, Ramirez RJ, Zobel C, Backx PH. The molecular physiology of the cardiac transient outward potassium current (I(to)) in normal and diseased myocardium. J Mol Cell Cardiol 2001;33:851–72.

43. Medeiros-Domingo A, Kaku T, Tester DJ, et al. SCN4B-encoded sodium channel beta4 subunit in congenital long-QT syndrome. Circulation 2007;116:134–42.

44. Kaur K, Zarzoso M, Ponce-Balbuena D, et al. TGF-beta1, released by myofibroblasts, differentially regulates transcription and function of sodium and potassium channels in adult rat ventricular myocytes. PLoS One 2013;8:e55391.

45. Ramos-Mondragon R, Vega AV, Avila G. Long-term modulation of Na+ and K+ channels by TGF-beta1 in neonatal rat cardiac myocytes. Pflugers Archiv 2011;461:235–47.

KEY WORDS cardiomyocyte, cardiomyopathy, fibrosis, heart failure, SMAD4, TGF-β

APPENDIX For expanded Methods and References sections as well as supplemental figures and tables, please see the online version of this paper.

JACC: BASIC TO TRANSLATIONAL SCIENCE VOL. 4, NO. 1, 2019

EDITORIAL COMMENT

It's a SMAD, SMAD World

Cell Type–Specific SMAD Signaling in the Heart*

Amy D. Bradshaw, PhD

In the report by Umbarkar et al. (1) in this issue of *JACC: Basic to Translational Science,* the outcome of targeted reductions in SMAD4, a downstream mediator in the transforming growth factor (TGF)-β signaling pathway, in cardiac myocytes is evaluated. As SMAD4 global deletion results in embryonic lethality (2), the authors set out to address the functional significance of SMAD4 expression in myocytes in the adult heart using an inducible transgenic approach. The resulting cardiac phenotype is characterized by significant differences in cardiac contractile function as measured both in individual cells and in whole hearts. Deletion of SMAD4 in cardiac myocytes leads to alterations in expression of cardiac myosin binding protein-C and in mRNA encoding a number of ion channels. Changes in protein expression are reflected in a slower heart beat in SMAD4 mutant mice versus wild-type counterparts. The authors conclude that SMAD4 functions in adult cardiac myocytes to maintain homeostatic activity and myocyte viability and performance.

SEE PAGE 41

As Umbarkar et al. (1) point out, TGF-β is a well-characterized mediator of fibrotic collagen deposition in the heart. For example, inhibition of TGF-β signaling through administration of an anti-TGF-β antibody following induction of pressure overload, a murine model of cardiac fibrosis, is shown to reduce myocardial collagen content (3). Recently, targeted disruption of SMAD3, another downstream factor in the TGF-β signaling pathway, in activated fibroblasts is shown to reduce fibrotic deposition of collagen in response to pressure overload (4). In addition, signaling via TGF-β receptor II is demonstrated to be central to collagen accumulation resulting from cardiac myosin binding protein-C-induced cardiomyopathy, another model of cardiac fibrosis (5). Accordingly, TGF-β is an attractive target for therapies to treat fibrosis and has merited well-deserved attention in this regard. However, the pluripotent nature of TGF-β signaling, which is highly cell-type dependent, has led many to caution against global inhibition of TGF-β as a viable path to treat fibrosis. Umbarkar et al. (1) offer their recent findings as further proof that nontargeted inhibition of TGF-β activity is predicted to have adverse effects on other cell types in the heart, including cardiac myocytes.

Interestingly, in contrast to SMAD4, targeted deletion of SMAD3 in cardiac myocytes does not result in phenotypic alterations in cardiac function in the homeostatic adult heart (6). Whereas SMAD3 is implicated in the canonical TGF-β signaling pathway, SMAD4 is also known to act in bone morphogenic protein (BMP) signaling. TGF-β is member of the BMP super family, which contains at least 20 different members. Accordingly, BMP signaling in myocytes is predicted to also be influenced by diminished SMAD4 activity. Whereas relatively less is known concerning the role(s) of BMP signaling in the healthy adult heart, this area merits further investigation. The significant difference in cardiac myocyte physiology brought about by cell-specific SMAD4 deletion, not seen in the SMAD3-deleted myocyte-specific mice, suggests that signaling pathways associated with other BMP family members, in addition to TGF-β, might be significant

*Editorials published in *JACC: Basic to Translational Science* reflect the views of the authors and do not necessarily represent the views of *JACC: Basic to Translational Science* or the American College of Cardiology.

From the Division of Cardiology, Department of Medicine, Medical University of South Carolina, Charleston, South Carolina; and the Ralph H. Johnson Veterans Affairs Medical Center, Charleston, South Carolina. Dr. Bradshaw has reported that she has no relationships relevant to the contents of this paper to disclose.

The author attests she is in compliance with human studies committees and animal welfare regulations of the authors' institutions and Food and Drug Administration guidelines, including patient consent where appropriate. For more information, visit the *JACC: Basic to Translational Science* author instructions page.

ISSN 2452-302X https://doi.org/10.1016/j.jacbts.2019.01.006

for maintaining healthy cardiac myocyte activity in adult heart.

Two genetic pathologies associated with mutations in SMAD4 protein are Myhre's syndrome and juvenile polyposis—hereditary hemorrhagic telangiectasia (JP-HHT). Gain of function in SMAD4 gives rise to Myhre's syndrome characterized by short stature, dysmorphic facial features, and hearing loss among other pathologies (7). Recently, cardiovascular disruptions including pericardial disease and restrictive cardiomyopathy have been described in patients with Myhre's syndrome. To date, specific differences in myocyte function have not been reported in this syndrome; however, given the results presented by Umbarkar et al. (1), one might predict SMAD4-dependent phenotypic abnormalities in this cell type as well. Global loss of function of SMAD4 in people results in JP-HHT, characterized by arteriovenous malformations and early-onset colorectal cancer (8). Whether cardiac myocytes are affected in people with JP-HHT also remains to be determined, but might also provide interesting insight into the role of SMAD4 in cardiac myocytes.

TGF-β signaling is well accepted as a central determinant of cardiac fibroblast activity, particularly in regard to fibroblast activation and extracellular matrix (ECM) deposition and accumulation in fibrosis. However, receptors for TGF-β are expressed in multiple cell types in the heart, including smooth muscle cells, myocytes, endothelial cells, and inflammatory cells. As each cell type activates a distinct functional outcome in response to TGF-β stimulation, global inhibition of TGF-β is predicted to have consequences beyond fibroblast activation and ECM accumulation, as Umbarkar et al. (1) point out. In the heart, the concept that the regulation of TGF-β signaling, even if directed solely to activated fibroblasts to control collagen production, might also be problematic. As with many tissues, having optimal levels of cardiac collagen is critical for function. Illustrated by fibroblast deletion of SMAD3, loss of SMAD3 in activated fibroblasts gives rise to increased rupture and accentuates adverse remodeling following infarction, whereas, in response to pressure overload, less pathological fibrosis is observed with deletion of SMAD3 in activated fibroblasts (4,6). Simplistically, overdeposition of collagen can lead to increases in stiffness associated with diastolic dysfunction, whereas decreases in collagen content can lead to cardiac rupture after infarction (9). However, a growing appreciation that alterations in collagen assembly and cross-linking, fiber alignment, and ECM composition each influence progression of cardiac remodeling in disease is emerging. Each of these processes is likely to be influenced by TGF-β signaling in fibroblasts and in inflammatory cells. Likewise, insight into the role of TGF-β in controlling myocyte activity also deserves further analysis, as these pathways might also be exploited to improve cardiac function in disease. Fine-tuning distinct pathways and outcomes in cardiac cell types to TGF-β (and other TGF-β family members) is necessary to design innovative approaches for treating cardiac dysfunction in adult heart failure.

ADDRESS FOR CORRESPONDENCE: Dr. Amy D. Bradshaw, 30 Courtenay Drive, Room 325/ MSC 773, Medical University of South Carolina, Charleston, South Carolina 29425. E-mail: bradshad@musc.edu.

REFERENCES

1. Umbarkar P, Singh AP, Gupte M, et al. Cardiomyocyte SMAD4-dependent TGF-β signaling is essential to maintain adult heart homeostasis. J Am Coll Cardiol Basic Trans Sci 2019;4:41–53.

2. Nie X, Deng CX, Wang Q, Jiao K. Disruption of Smad4 in neural crest cells leads to mid-gestation death with pharyngeal arch, craniofacial and cardiac defects. Dev Biol 2008;316:417–30.

3. Kuwahara F, Kai H, Tokuda K, et al. Transforming growth factor-beta function blocking prevents myocardial fibrosis and diastolic dysfunction in pressure-overloaded rats. Circulation 2002;106:130–5.

4. Khalil H, Kanisicak O, Prasad V, et al. Fibroblast-specific TGF-beta-Smad2/3 signaling underlies cardiac fibrosis. J Clin Invest 2017;127:3770–83.

5. Meng Q, Bhandary B, Bhuiyan MS, et al. Myofibroblast-specific TGFbeta receptor II signaling in the fibrotic response to cardiac myosin binding protein C-induced cardiomyopathy. Circ Res 2018;123:1285–97.

6. Kong P, Shinde AV, Su Y, et al. Opposing actions of fibroblast and cardiomyocyte Smad3 signaling in the infarcted myocardium. Circulation 2018;137:707–24.

7. Lin AE, Michot C, Cormier-Daire V, et al. Gain-of-function mutations in SMAD4 cause a distinctive repertoire of cardiovascular phenotypes in patients with Myhre syndrome. Am J Med Genet A 2016;170:2617–31.

8. Gallione C, Aylsworth AS, Beis J, et al. Overlapping spectra of SMAD4 mutations in juvenile polyposis (JP) and JP-HHT syndrome. Am J Med Genet A 2010;152a:333–9.

9. Frangogiannis NG. Cardiac fibrosis: cell biological mechanisms, molecular pathways and therapeutic opportunities. Mol Aspects Med 2018 Aug 2 [E-pub ahead of print].

KEY WORDS collagen, Smad signaling, TGF-β

JACC: BASIC TO TRANSLATIONAL SCIENCE VOL. 4, NO. 1, 2019

PRECLINICAL RESEARCH

Bioactive Materials Facilitating Targeted Local Modulation of Inflammation

Richard P. Tan, MSc,[a,b,*] Alex H.P. Chan, BSc,[a,b,*] Simon Wei, PhD,[c] Miguel Santos, PhD,[a,d] Bob S.L. Lee, MSc,[a,b] Elysse C. Filipe, PhD,[b,e] Behnam Akhavan, PhD,[a,d,f] Marcela M. Bilek, PhD, MBA,[d,f,g,h] Martin K.C. Ng, MBBS, PhD,[b,i] Yin Xiao, PhD,[c] Steven G. Wise, PhD[a,b]

VISUAL ABSTRACT

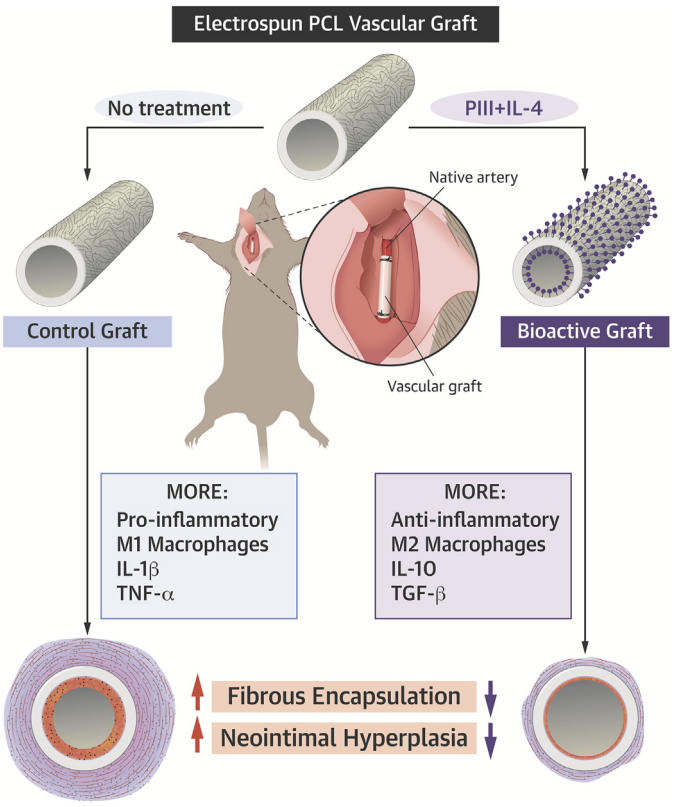

Tan, R.P. et al. J Am Coll Cardiol Basic Trans Science. 2019;4(1):56–71.

HIGHLIGHTS

- **Electrospun polycaprolactone surfaces were immobilized with a monolayer of the cytokine interleukin-4 to create a "bioactive" immunomodulatory surface capable of influencing the phenotype of macrophages responding to the material surface in vivo.**
- **Bioactive surfaces, evaluated in vitro by using macrophage culture, exhibited upregulation of anti-inflammatory M2 genes and facilitated morphological changes consistent with macrophage activation.**
- **As a subcutaneous implant in a 14-day model of acute inflammation, bioactive surfaces polarized macrophages from their M1 pro-inflammatory to M2 anti-inflammatory phenotypes, leading to a significant reduction in the local immune-driven foreign body response.**
- **As vascular grafts in a 28-day mouse carotid interposition model, bioactive grafts maintained their macrophage polarization and immunomodulatory effects, significantly reducing adventitial encapsulation and neointimal hyperplasia development.**

From the [a]Heart Research Institute, Sydney, New South Wales, Australia; [b]Sydney Medical School, University of Sydney, Sydney, New South Wales, Australia; [c]Science and Engineering Faculty, Queensland University of Technology, Brisbane, Queensland, Australia; [d]School of Physics, University of Sydney, Sydney, New South Wales, Australia; [e]Garvan Institute of Medical Research, Cancer Division, Sydney, New South Wales, Australia; [f]School of Aerospace, Mechanical and Mechatronic Engineering, University of Sydney, Sydney, New South Wales, Australia; [g]Charles Perkins Centre, University of Sydney, Sydney, New South Wales, Australia; [h]Sydney Nano Institute, University of Sydney, Sydney, New South Wales, Australia; and the [i]Royal Prince Alfred Hospital, Sydney, New South Wales, Australia. *Mr. Tan and Dr. Chan contributed equally to the manuscript and are joint first authors. This work was supported by the Australian Research Council (Dr. Bilek) and the National Health and Medical Research Council (APP1066174; Dr. Ng). Mr. Tan, Mr. Lee, and Dr. Filipe are recipients of an Australian Postgraduate Scholarship, and

ISSN 2452-302X https://doi.org/10.1016/j.jacbts.2018.10.004

SUMMARY

Cardiovascular disease is an inflammatory disorder that may benefit from appropriate modulation of inflammation. Systemic treatments lower cardiac events but have serious adverse effects. Localized modulation of inflammation in current standard treatments such as bypass grafting may more effectively treat CAD. The present study investigated a bioactive vascular graft coated with the macrophage polarizing cytokine interleukin-4. These grafts repolarize macrophages to anti-inflammatory phenotypes, leading to modulation of the pro-inflammatory microenvironment and ultimately to a reduction of foreign body encapsulation and inhibition of neointimal hyperplasia development. These resulting functional improvements have significant implications for the next generation of synthetic vascular grafts.

ABBREVIATIONS AND ACRONYMS

CAD = coronary artery disease

ELISA = enzyme-linked immunoadsorbent assay

IL = interleukin

PCL = polycaprolactone

PIII = plasma immersion ion implantation

qPCR = quantitative polymerase chain reaction

TGF = transforming growth factor

TNF = tumor necrosis factor

The role of inflammation in the genesis and progression of coronary artery disease (CAD) and other manifestations of atherosclerosis has long been established (1). Inflammatory cells drive the initial stages of plaque formation, express growth factors and cytokines that progress disease, and can worsen patient outcomes after an acute coronary syndrome (2). The recent CANTOS (Canakinumab Anti-inflammatory Thrombosis Outcome Study) trial showed that systemic administration of canakinumab, a selective antibody against the inflammatory cytokine interleukin (IL)-1β, significantly lowered the incidence of recurrent cardiovascular events (3). By systemically reducing inflammation while having no effect on lipid levels, CANTOS was a large-scale clinical trial showing that pharmaceutical anti-inflammatory therapy was effective in reducing cardiovascular events. Although these results will have a significant impact on the immediate direction of therapeutic interventions, systemic canakinumab treatment was associated with a higher risk of fatal infection and sepsis, most likely resulting from sustained global immune suppression. Accordingly, future translation of therapies for the treatment of CAD based on anti-inflammatory approaches will benefit from local, targeted modulation of inflammation.

The severity and extent of host foreign body immune responses toward cardiovascular interventional devices significantly affect their long-term performance. The modification of implantable medical devices using anti-inflammatory surface coatings has been previously explored (4). The most effective strategies rely on the controlled release of anti-inflammatory agents to halt local inflammatory responses in the surrounding tissue. Dexamethasone is a commonly used synthetic glucocorticoid hormone shown to reduce the levels of tumor necrosis factor (TNF)-α, IL-1β, IL-6, and interferon gamma. α-Melanocyte-stimulating hormone is a linear peptide shown to reduce TNF-α levels while increasing anti-inflammatory IL-10 levels. Previous controlled-release strategies using anti-inflammatory agents typically involved nonspecific, passive diffusion through polyelectrolyte layers, biodegradable coatings, or swelling coatings. Although these approaches have led to a reduction in some aspects of the foreign body response, including protein adsorption and cell adhesion in vitro, complications such as recurrent inflammatory responses and subsequent device replacement may potentially arise when drug elution is complete. Furthermore, nonspecific blockade of immune cell recruitment after elution of anti-proliferative drugs, as is the case for drug-eluting stents, can impair the resolution of chronic inflammation and hinder long-term device integration and function (5). Improved application of these strategies would therefore aim to better retain the bioactivity, stability, and residence time of locally delivered agents while more selectively modulating the

Mr. Chan and Dr. Santos have received funding support from the Heart Research Institute. The authors acknowledge the financial support of E. Brackenreg. The authors have reported that they have no relationships relevant to the contents of this paper to disclose.

All authors attest they are in compliance with human studies committees and animal welfare regulations of the authors' institutions and Food and Drug Administration guidelines, including patient consent where appropriate. For more information, visit the *JACC: Basic to Translational Science* author instructions page.

Manuscript received August 10, 2018; revised manuscript received October 10, 2018, accepted October 12, 2018.

immune response to facilitate prolonged functional benefits.

We have identified macrophages and their broad spectrum of phenotypes as master effectors of the foreign body response toward implanted materials. At the 2 ends of the spectrum are the M1 (pro-inflammatory) and M2 (anti-inflammatory) phenotypes, which regulate a host of inflammatory cytokines to either propagate or halt innate inflammation, respectively. Modification of the material surface to induce the M2 phenotype of responding macrophages may potentially represent an effective means of mitigating foreign body responses to implanted materials.

In the present study, we developed a novel off-the-shelf bioactive device coating for local and lasting modulation of the inflammatory response to implants. A plasma immersion ion implantation (PIII) surface treatment was used that facilitates the rapid covalent attachment of biomolecules while preserving their bioactivity (6). One of the most well-established and highly documented biomolecules responsible for M2 macrophage phenotype polarization is the cytokine IL-4 (7). Bioactive signaling chemokines such as IL-4 have not previously been immobilized on material surfaces without chemical linkers, representing a fundamentally new off-the-shelf approach to local regulation of inflammation. Herein we examined the in vitro behavior of macrophages in response to bioactive IL-4 surfaces before assessing the in vivo inflammatory responses in 2 distinct mouse models. Comprehensive immunohistochemical analysis of both subcutaneous and carotid arterial graft implants was used to quantitatively assess macrophage phenotype, local cytokine expression, and measures of functional outcome (including fibrous encapsulation and neointimal hyperplasia).

METHODS

PIII SURFACE TREATMENT. Surface modification of electrospun polycaprolactone (PCL) scaffolds was conducted by using PIII as previously described (8). Briefly, nitrogen was admitted into a custom-built vacuum chamber to a working pressure of 2×10^{-3} Torr, and plasma discharges were generated by inductively coupled radiofrequency power at a frequency of 13.56 MHz. Scaffolds were placed on an electrically biased stainless-steel holder. Ion acceleration was achieved through application of -20 kV pulses with a temporal width of 20 μs at a frequency of 50 Hz, drawing a current of 1.3 mA. PIII treatment was run for 800 s, providing ion fluences of 1×10^{16} ions/cm^2. Characterization methods of PIII-treated surfaces can be found in the Supplemental Methods.

BIOACTIVE IL-4 SURFACE CREATION. For in vitro experiments, scaffolds were biopsy punched into 5-mm diameter circular discs and placed into Eppendorf tubes. Recombinant mouse IL-4 (2 μg/ml in sterile phosphate-buffered saline) was added to each scaffold for 1 h at room temperature. To test IL-4 attachment, scaffolds were washed in sodium dodecyl sulfate (5% in phosphate-buffered saline) for 4 h at room temperature before enzyme-linked immunoadsorbent assay (ELISA) using an anti-IL-4 monoclonal antibody (Thermo Fisher Scientific, Waltham, Massachusetts) and horseradish peroxidase-conjugated secondary antibody (Abcam, Cambridge, Massachusetts). For in vivo experiments, both flat scaffolds and PCL conduits (0.5 mm diameter) were incubated in recombinant mouse IL-4 (2 μg/ml in sterile phosphate-buffered saline) for 1 h at room temperature and rinsed in sterile phosphate-buffered saline before implantation.

In vivo performance of bioactive IL-4 subcutaneous implants. Study approval was obtained from the Sydney Local Heath District Animal Welfare Committee (protocol number 2013/050). Experiments were conducted in accordance with the Australian Code of Practice for the Care and Use of Animals for Scientific Purpose. Mice were given four 1.5-cm incisions (two rows side-by-side) on their dorsal surfaces to create subcutaneous pockets, as previously described (9). Scaffolds were then inserted into each pocket (5 mice per time point equaling 5 scaffolds per group per time point) and sutured closed by using 6-0 silk sutures. Explants were taken at 3, 7, and 14 days' post-implantation; analysis is detailed in the Supplemental Methods.

In vivo performance of bioactive IL-4 vascular grafts. Study approval was obtained from the Sydney Local Heath District Animal Welfare Committee (protocol number 2015/016). Experiments were conducted in accordance with the Australian Code of Practice for the Care and Use of Animals for Scientific Purpose. C57/BL6 mice (male, 9 to 10 weeks old, 25 ± 2 g) were purchased from Australian BioResources (Moss Vale, NSW, Australia). Vascular grafts (5 per group) were implanted into the carotid artery by using a previously described technique (10). Briefly, the right common carotid artery was double ligated, and polyimide cuffs (Cole-Parmer North America, Vernon Hills, Illinois) were placed around each end. Overhanging arteries were everted on the plastic cuff, and grafts were then sleeved over each end and secured with 8-0 sutures. Clamps were removed, and blood flow was confirmed with pulsation. After 28 days, mice were perfused with heparinized saline (50 U/ml), and the grafted carotid artery

was isolated and dissected proximal and distal to the graft. Analysis of the vascular cross-sections is detailed in the Supplemental Methods.

RESULTS

CREATION OF A NOVEL IL-4–IMMOBILIZED BIOMATERIAL SURFACE. Control surfaces were PIII treated in nitrogen plasma for a duration of 800 s. Energetic ions accelerated by the 20-kV negative bias penetrate through the scaffold surface, breaking chemical bonds along their path and displacing atoms in the polymer structure. This results in a highly crosslinked, dense, carbonized structure at the surface of the scaffold (**Figure 1A**). The high density of broken bonds and displaced atoms allow for creation of new bonds (**Figure 1B**). The unpaired electrons that remain manifest as reactive radical groups (**Figure 1C**) embedded in the treated layer that gradually diffuse to the surface via thermally activated, local restructuring (Supplemental Results). Radical diffusion leads to surface oxidation, allowing direct covalent immobilization of IL-4 upon contact with the scaffold surface (6). Mechanical testing of scaffolds (n = 6 each group) exhibited no significant differences in Young's modulus or strain after PIII treatment (Supplemental Figure 1).

Bioactive IL-4 surfaces were created by incubating the PIII-treated surfaces in an IL-4 solution (2 μg/ml) for 1 h at room temperature (**Figure 1D**). Robust, covalent immobilization was shown by washing surfaces in sodium dodecyl sulfate (5%) for 4 h at room temperature to remove any passively adsorbed molecules (11,12), followed by IL-4 quantification using ELISA (n = 3 each group) (**Figure 1E**). Although the PIII-treated scaffolds retained IL-4 (bioactive IL-4), IL-4 was completely removed from the untreated PCL surfaces (passive IL-4).

BIOACTIVE IL-4 SURFACES MODULATE MACROPHAGE PHENOTYPE IN VITRO. RAW264.7 murine macrophages were seeded onto bioactive IL-4 surfaces to evaluate macrophage polarization (**Figure 2A**), as commonly reported (13–15). Macrophage morphology and material interaction were first characterized by using scanning electron microscopy. At 8 h post-seeding, cells cultured on bioactive IL-4 surfaces appeared more spread, with a notably rougher cell surface (**Figure 2B**). Cytoskeletal morphologies, observed by using confocal microscopy, further showed strikingly different morphology. Expression of M2 phenotype genes, arginase-1, CD163, CD206, and IL-10 revealed that passive IL-4 surfaces enhanced the expression of only arginase-1 and IL-10 but had no significant effect on CD163 or CD206. Similarly, PIII-only surfaces significantly increased arginase-1 expression but not the other markers. Only bioactive IL-4 surfaces significantly increased all marker expression at 8 h post-seeding compared with control (**Figure 2C**). These results show that IL-4 covalently immobilized on PIII-treated surfaces robustly polarizes macrophages toward an M2 phenotype and demonstrates that this immobilization approach is necessary for sustained bioactivity.

BIOACTIVE IL-4 SUBCUTANEOUS IMPLANTS REDUCE INFLAMMATORY CYTOKINES AND FIBROUS ENCAPSULATION. A 14-day subcutaneous mouse back model of acute inflammation was initially used to evaluate the in vivo functionality of bioactive IL-4 surfaces (16) (5 scaffolds per group) (**Figure 3A**), before further evaluation in a vascular context. Immunostaining markers for total macrophages ($CD68^+$), M1 (major histocompatibility complex Class II), and M2 (CD206) phenotypes were used to assess macrophage responses (**Figure 3B**). Increasing macrophage recruitment, observed on control surfaces, was reduced by 79 ± 6% and 86 ± 7% on bioactive IL-4 surfaces at days 7 and 14, respectively (**Figure 3B**, top). Bioactive IL-4 surfaces also increased M2 macrophage polarization by 159 ± 11% at day 3, suggesting earlier M2 polarization compared with control (**Figure 3B**, middle). Bioactive IL-4 surfaces also exhibited a 360 ± 15% higher M2/M1 macrophage ratio at day 14 compared with control, indicating a predominantly M2 phenotype residing at the implant surface in the late phases post-implantation (**Figure 3B**, bottom). These results were observed in representative images illustrating a large accumulation of macrophages on control surfaces with a predominantly M1 phenotype. In contrast, bioactive IL-4 surfaces exhibited a significant reduction in total macrophage accumulation and an enhancement of the M2 phenotype (**Figure 3C**).

To corroborate these findings, quantitative polymerase chain reaction (qPCR) and ELISA analysis for classic M1 and M2 markers were conducted at days 3 and 7 post-implantation to assess gene and protein expression changes, respectively. qPCR results revealed that bioactive implants had significantly less TNF-α and inducible nitric oxide synthase at day 3 (Supplemental Figure 2A) and the ELISA results showed significantly reduced IL-1β and IL-6 in bioactive implants at days 3 and 7 (Supplemental Figure 2B). These results were consistent with our immunohistochemistry and validated the presence of a robust anti-inflammatory microenvironment surrounding bioactive subcutaneous implants by independently demonstrating an upregulation of M2 markers and a downregulation of M1 markers.

FIGURE 1 **Characterization of PIII Treatment on PCL Control Surfaces**

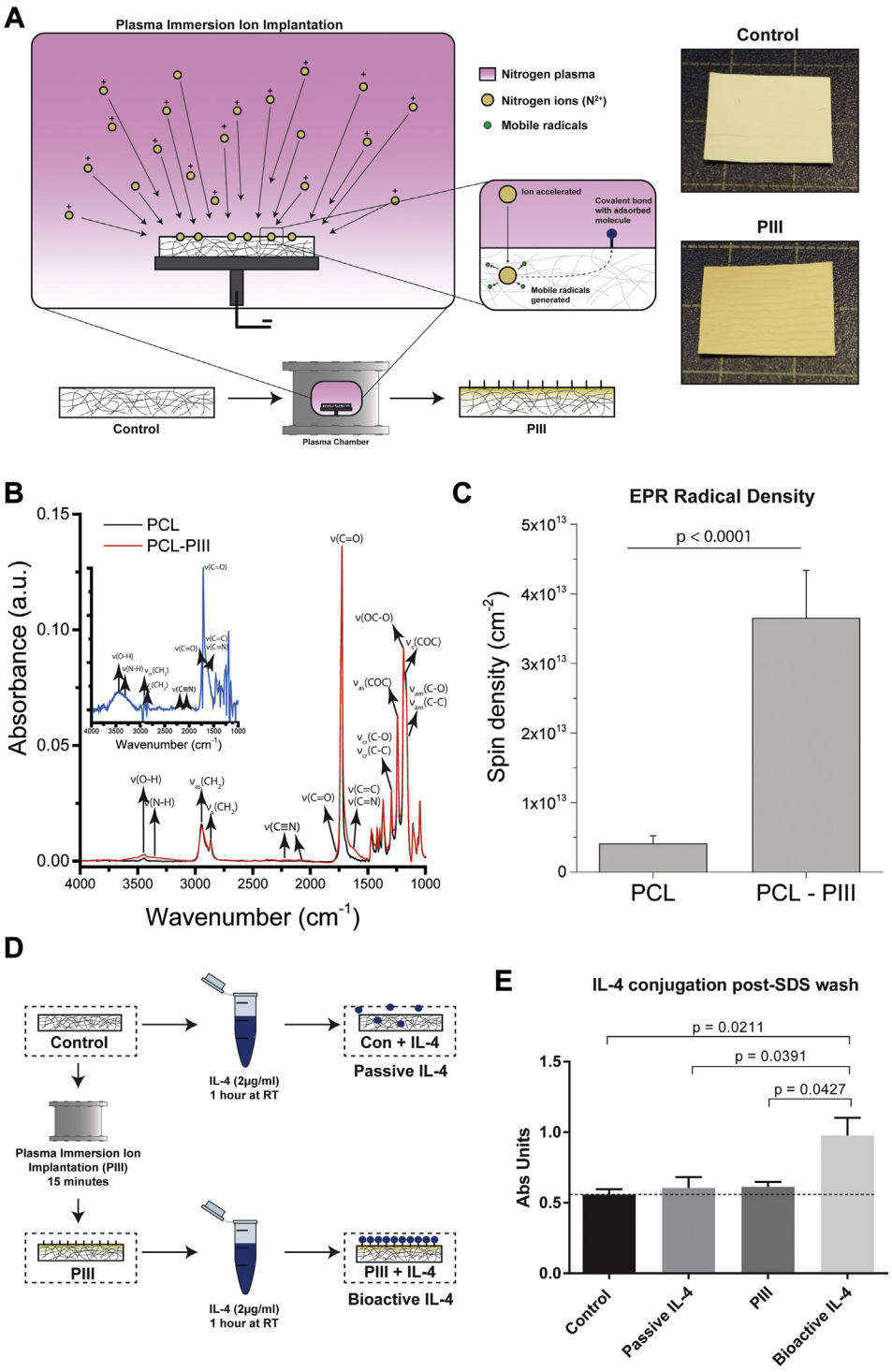

(A) Plasma immersion ion implantation (PIII) schematic with representative images of control surfaces before **(top)** and after **(bottom)** treatment. **(B)** Attenuated total reflectance Fourier-transform infrared spectroscopy (ATR FT-IR) surface characterization. **(C)** Electron paramagnetic resonance (EPR) characterization. **(D)** Diagram of experimental groups. **(E)** Interleukin-4 (IL-4) retention enzyme-linked immunoadsorbent assay (n = 3 per group). PCL = polycaprolactone; RT = room temperature; SDS = sodium dodecyl sulfate.

FIGURE 2 **In Vitro Biofunctionality of IL-4 Bioactive Surfaces**

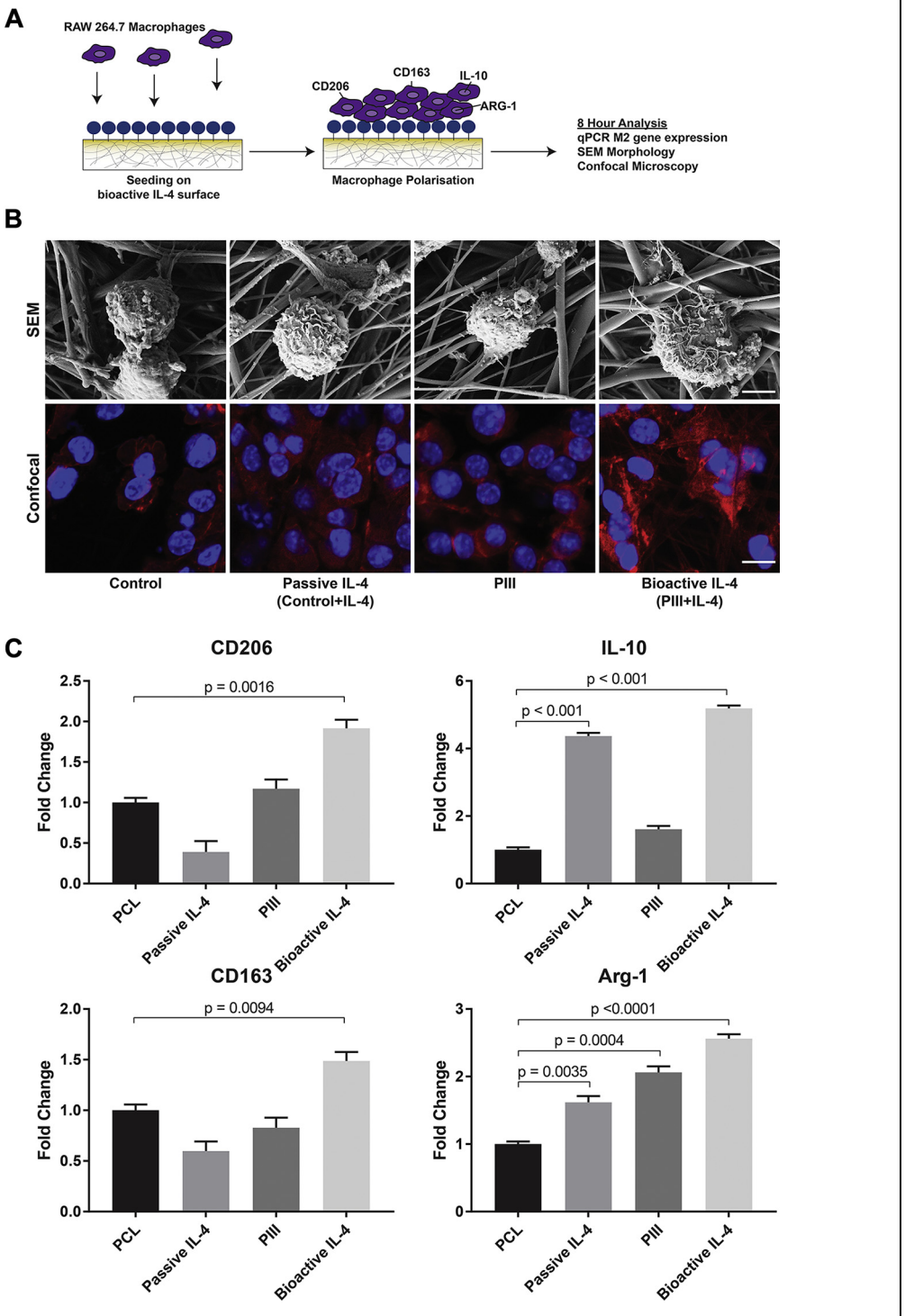

(A) Schematic of experimental design. **(B)** Scanning electron microscopy (SEM) (top row; scale bar represents 50 μm) and confocal microscopy (bottom row; scale bar represents 5 μm) of cultured macrophages. **(C)** Quantitative polymerase chain reaction (qPCR) of M2 Phenotype genes (n = 5 per group). Abbreviations as in Figure 1.

FIGURE 3 Implantation of Bioactive IL-4 Surfaces in Subcutaneous Mouse Model

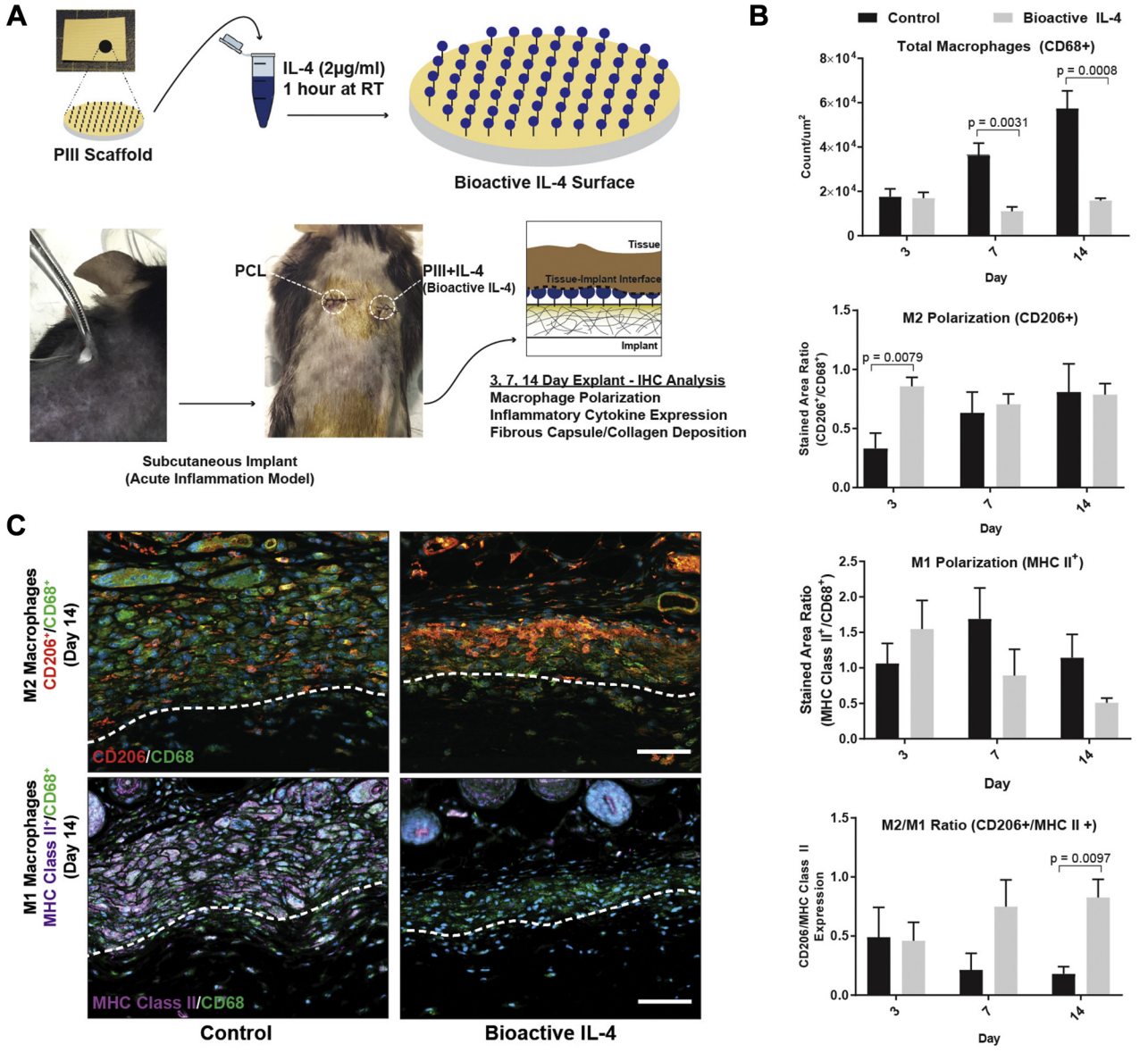

(A) Experimental design schematic. **(B)** Immunohistological quantification of macrophages at the implant surface: total $CD68^+$ macrophages **(top)**, $CD206^+$ M2 polarization **(middle)**, and M2/M1 ($CD206^+$/ major histocompatibility complex (MHC) Class II^+) ratio **(bottom)**. **(C)** Representative images of M2 **(top row)** and M1 **(bottom row)** macrophages. CD68 stained in **green**, CD206 stained in **orange**, and MHC Class II stained in **purple**. **Dotted lines** represent the interface between tissue **(above)** and implant **(below)**. Scale bar represents 60μm; n = 5 per group. IHC = immunohistochemical; other abbreviations as in Figure 1.

Further immunohistochemical analysis was conducted to confirm the expression of inflammatory cytokines (5 scaffolds per group). IL-10 and transforming growth factor (TGF)-β were chosen as classic anti-inflammatory cytokines, whereas IL-1β and TNF-α are well-characterized pro-inflammatory cytokines (17). Bioactive IL-4 surfaces increased IL-10 expression by 432 ± 26% at day 7 compared with controls (Figure 4A). TGF-β expression was also increased 1025 ± 11% at day 7 on bioactive IL-4 surfaces. Representative images show this increased IL-10 and TGF-β present at the scaffold/tissue interface in bioactive surfaces (Figure 4B). Corresponding changes to classically pro-inflammatory cytokines occurred at later time points, with significant differences at day 14. IL-1β and TNF-α

FIGURE 4 **Inflammatory Cytokine Quantification at the Implant Surface In Vivo**

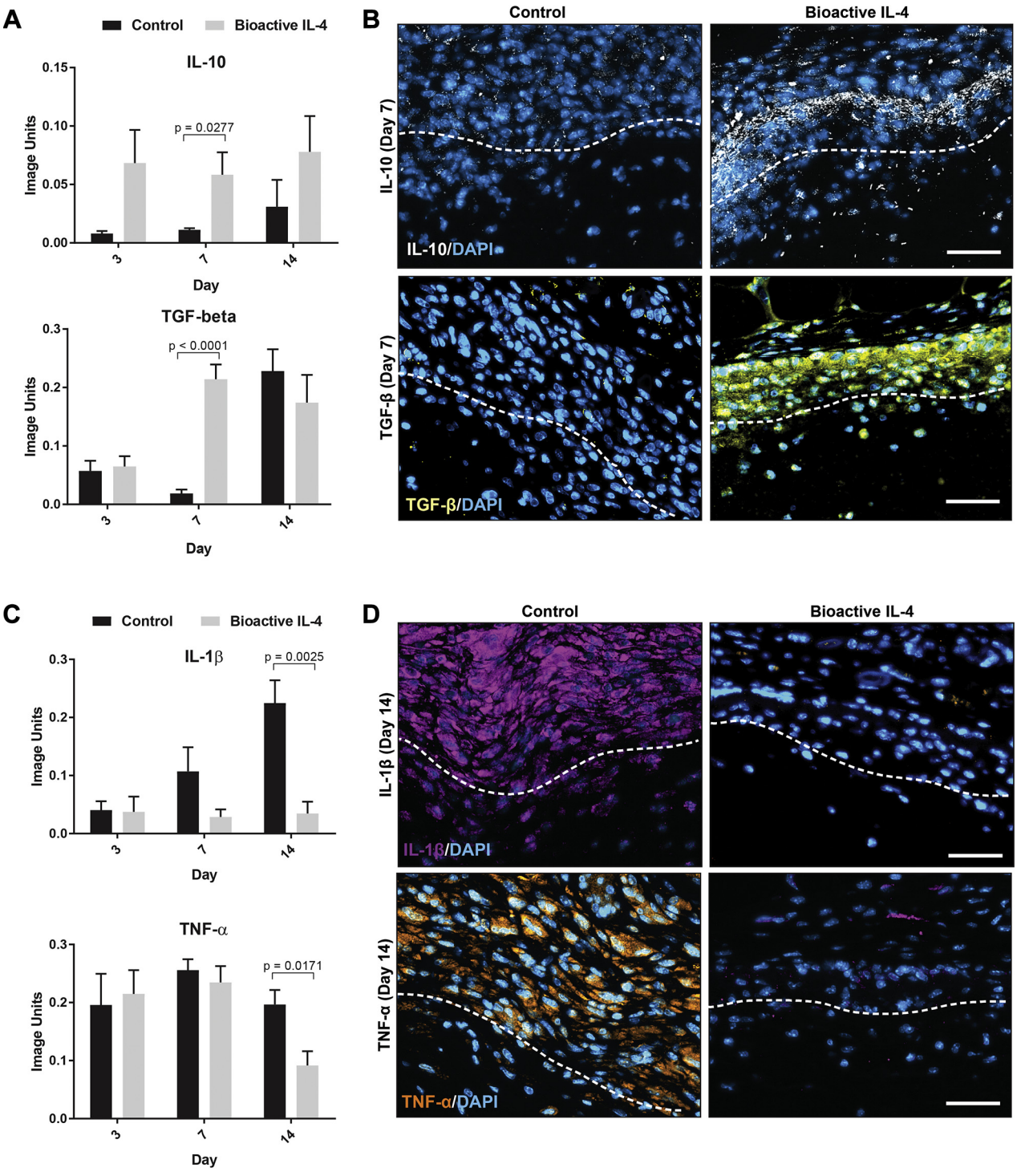

(A) Immunohistological quantification of anti-inflammatory cytokines IL-10 **(top)** and transforming growth factor (TGF)-β **(bottom)**. **(B)** Representative images of IL-10 **(top)** and TGF-β **(bottom)** expression at the implant surface stained in **white** and **yellow** respectively. **(C)** Immunohistological quantification of pro-inflammatory cytokines IL-1β **(top)** and tumor necrosis factor (TNF)-α **(bottom)**. **(D)** Representative images of IL-1β **(top)** and TNF-α **(bottom)** expression at the implant surface stained in **purple** and **orange** respectively. **Dotted lines** represent the interface between tissue **(above)** and implant **(below)**. Scale bar represents 40 μm; n = 5 per group. Abbreviations as in Figure 1.

FIGURE 5 Functional Outcomes of Bioactive IL-4 Surfaces In Vivo

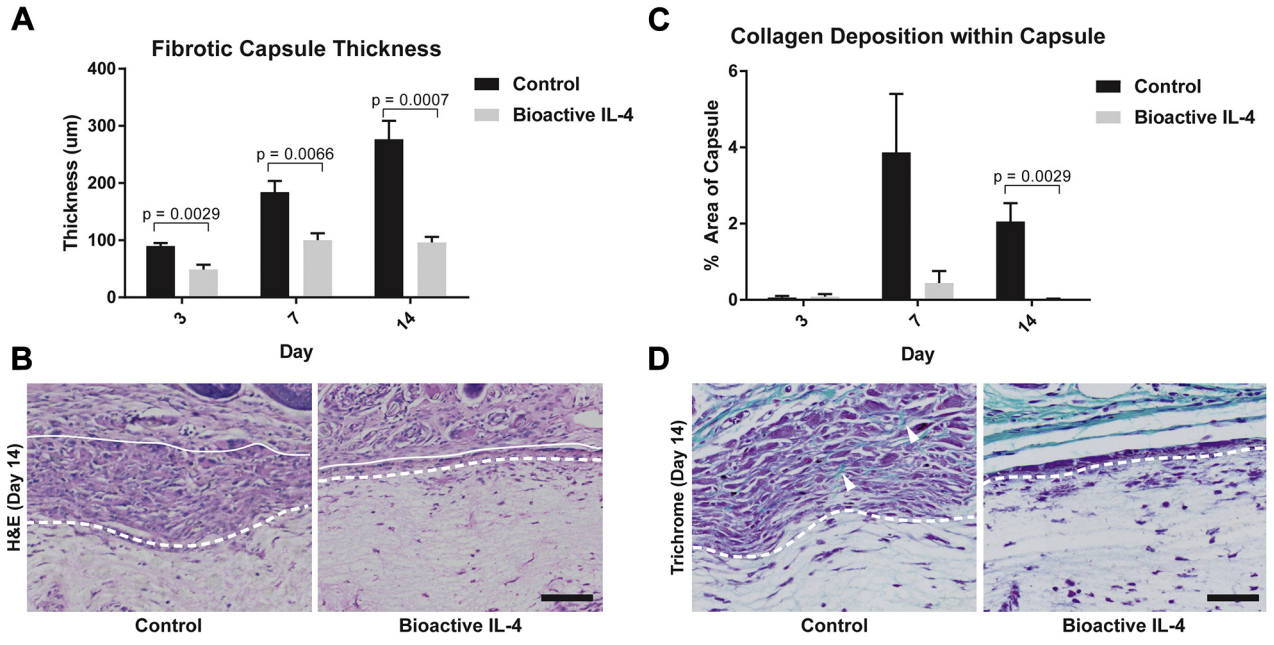

(A) Measurement of fibrotic capsule formation/thickness at the implant surface **(top)**. **(B)** Representative hematoxylin and eosin (H&E) stains of fibrotic capsules. **(C)** Quantification of collagen deposition at the implant surface. **(D)** Representative trichrome stains of collagen **(green)** within the fibrotic capsule, highlighted by **arrows**. **Dotted lines** represent the interface between tissue **(above)** and implant **(below)**. Scale bar represents 50 μm, n = 5 per group. IL-4 = interleukin 4.

expression was 84 ± 7% and 53 ± 5% less, respectively, on bioactive IL-4 surfaces compared with control (Figure 4C). Again, representative images clearly show these striking changes at the material interface where bioactive IL-4 implants seem to all drastically reduce IL-1β and TNF-α (Figure 4D).

We next sought to characterize functional changes arising from an increased proportion of M2 macrophages and positive regulation of local cytokine production. The fibrotic capsule thickness for the control implants increased steadily over time, as expected, from 90 ± 5.1 μm at day 3 to 276.6 ± 132.1 μm by day 14 (Figure 5A). In contrast, the capsule thickness on bioactive IL-4 surfaces was reduced at all time points with a final reduction of 65 ± 4% at day 14, compared with control, evident in representative images (Figure 5B). Furthermore, peak collagen deposition in PCL controls occurred at day 7 comprising 3.8 ± 2% of the capsule area, with less (2.0 ± 0.7%) by day 14 (Figure 5C). In bioactive IL-4 surfaces, collagen was reduced at day 7 with a significant reduction at day 14, as seen in representative images (Figure 5D). Reductions in collagen deposition over time further suggest significant modulation of the host foreign body response.

BIOACTIVE IL-4 SYNTHETIC ARTERIAL GRAFTS REDUCE LOCAL INFLAMMATION AND NEOINTIMAL HYPERPLASIA. Small diameter vascular grafts were manufactured with bioactive IL-4 surfaces on both the luminal and adventitial surfaces, implanted into an established mouse carotid interposition grafting model, and explanted at 28 days (Figure 6A). Consistent with results from the subcutaneous implant study, IL-4 grafts significantly reduced total macrophages present by 54 ± 6% compared with control (Figure 6B). These macrophages also showed a 47 ± 12% increase in the M2 phenotype and a corresponding decrease in the M1 phenotype by 52 ± 9%, demonstrating similar macrophage polarization effects. This outcome was further supported by a 93 ± 11% increase in the M2/M1 ratio of bioactive IL-4 grafts compared with control. These changes are highlighted in representative images, showing fewer total macrophages and enhanced expression of CD206 with less major histocompatibility complex class II (Figure 6C).

Further examination revealed that anti-inflammatory IL-10 and TGF-β levels were significantly increased by 122 ± 11% and 539 ± 35%, respectively, in bioactive IL-4 grafts compared with controls (Figures 7A and 7B). In addition,

FIGURE 6 **Investigation of IL-4 Bioactive Surfaces for Synthetic Vascular Grafts**

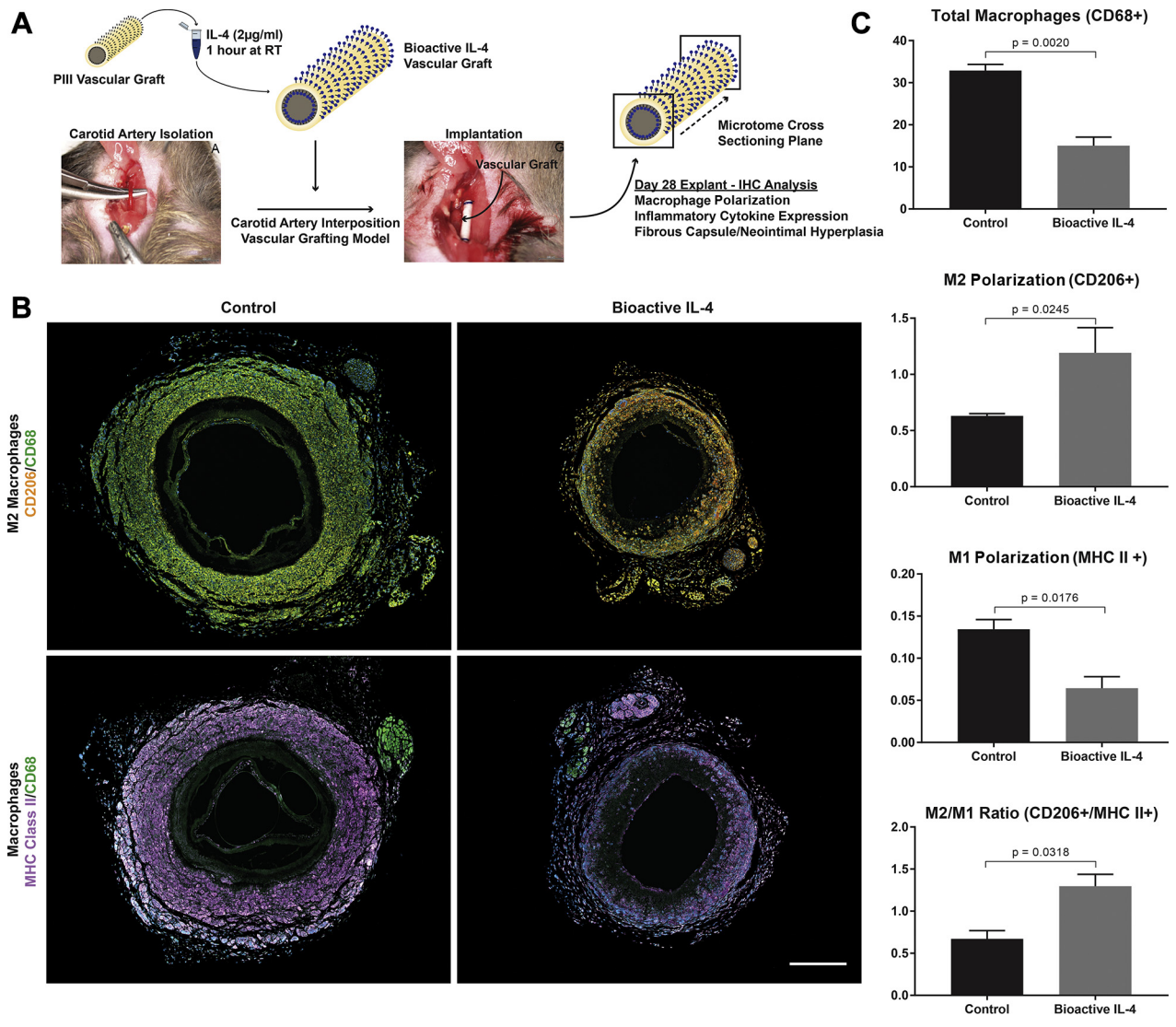

(A) Experimental design schematic; vascular graft dimensions 0.5 mm (inner diameter) × 6 mm length. **(B)** Representative immunostained images of macrophage responses; M2 **(top row)** and M1 **(bottom row)** macrophages. CD68 stained in **green**, CD206 stained in **orange**, and MHC Class II stained in **purple**. Scale bar represents 500 μm. **(C)** Quantification of$CD68^+$ total macrophages **(top)**, $CD206^+$ M2 polarization **(middle)**, MHC Class II^+ M1 polarization, and M2/M1 ($CD206^+$/MHC Class II^+) ratio **(bottom)**. n = 3 slides (each region of the graft) per animal, with a total of 5 animals per group. Abbreviations as in **Figures 1 and 3**.

pro-inflammatory IL-1β and TNF-α expression was 43 ± 9% and 50 ± 3% less in bioactive IL-4 grafts (**Figures 7C and 7D**). Representative images of graft cross-sections demonstrate clear increases in levels of IL-10 and TGF-β, as well as corresponding reductions in IL-1β and TNF-α (**Figure 7E**).

To confirm these findings, qPCR and ELISA analyses were conducted on vascular grafts at days 3 and 7 post-implantation. qPCR results showed that the bioactive grafts had significantly less TNF-α and inducible nitric oxide synthase at days 3 and 7, in addition to reduced CD86 at day 7 (Supplemental Figure 3A). ELISA results supported that bioactive grafts had less IL-1β, IL-6, and TNF-α at day 7 (Supplemental Figure 3B). Consistent with the immunohistochemistry data, these additional results further support our proposed immunomodulatory effects of bioactive surfaces.

In a vascular graft context, inflammatory processes drive both fibrous encapsulation and neointimal

FIGURE 7 Immunohistochemical Analysis of Inflammatory Cytokines in Vascular Grafts

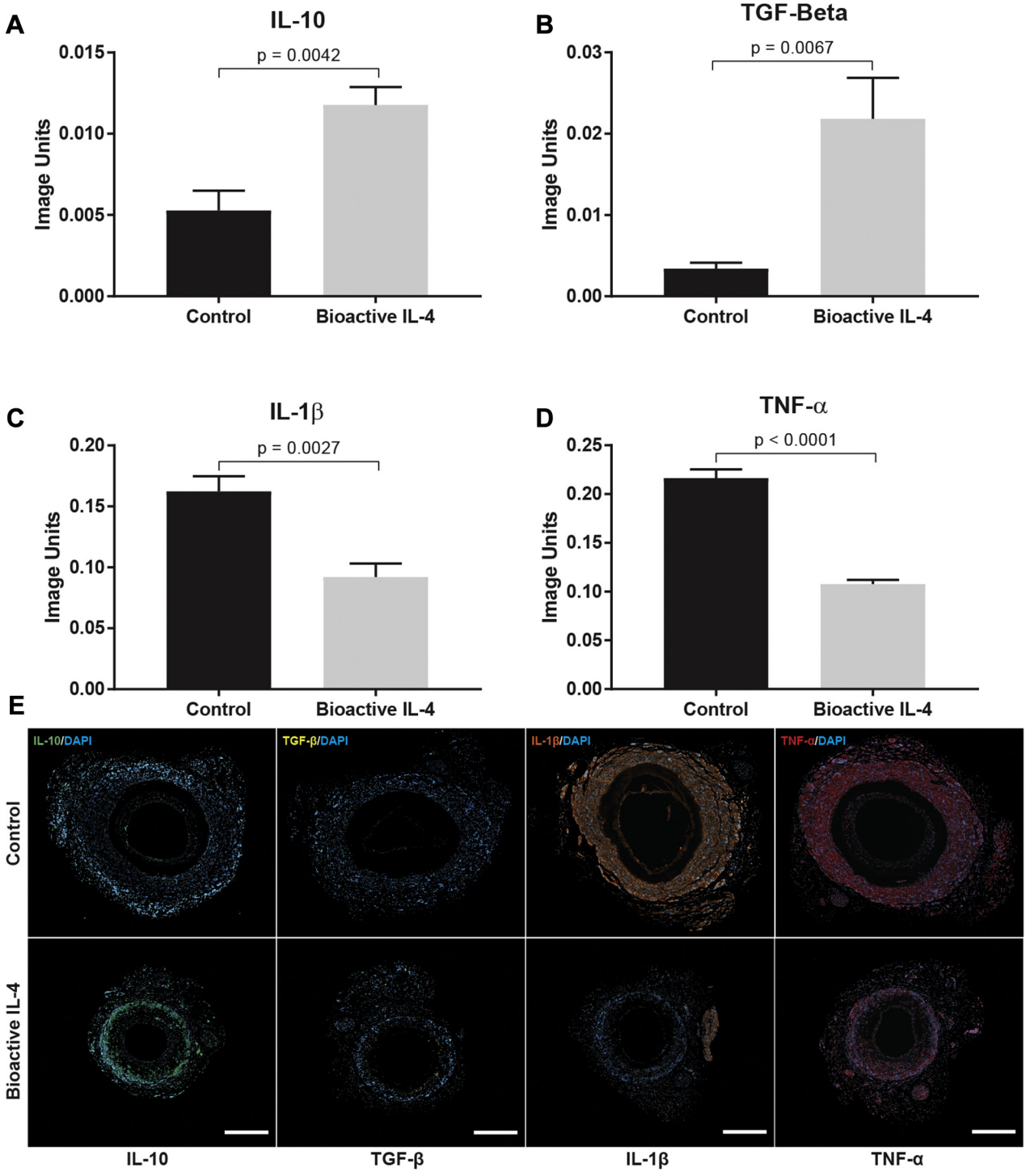

(A) IL-10. **(B)** TGF-β. **(C)** IL-1β. **(D)** TNF-α. **(E)** Representative images of cytokine expression within vascular graft cross sections: control **(top row)** versus bioactive **(bottom row)**. IL-10 stained in **green**, TGF-β stained in **white**, IL-1β stained in **orange**, and TNF-α stained in **red**. Scale bar represents 1 mm; n = 3 slides (each region of the graft) per animal, with a total of 5 animals per group. Abbreviations as in Figures 1 and 4.

FIGURE 8 **Functional Outcomes of Bioactive IL-4 Surfaces for Synthetic Vascular Grafts**

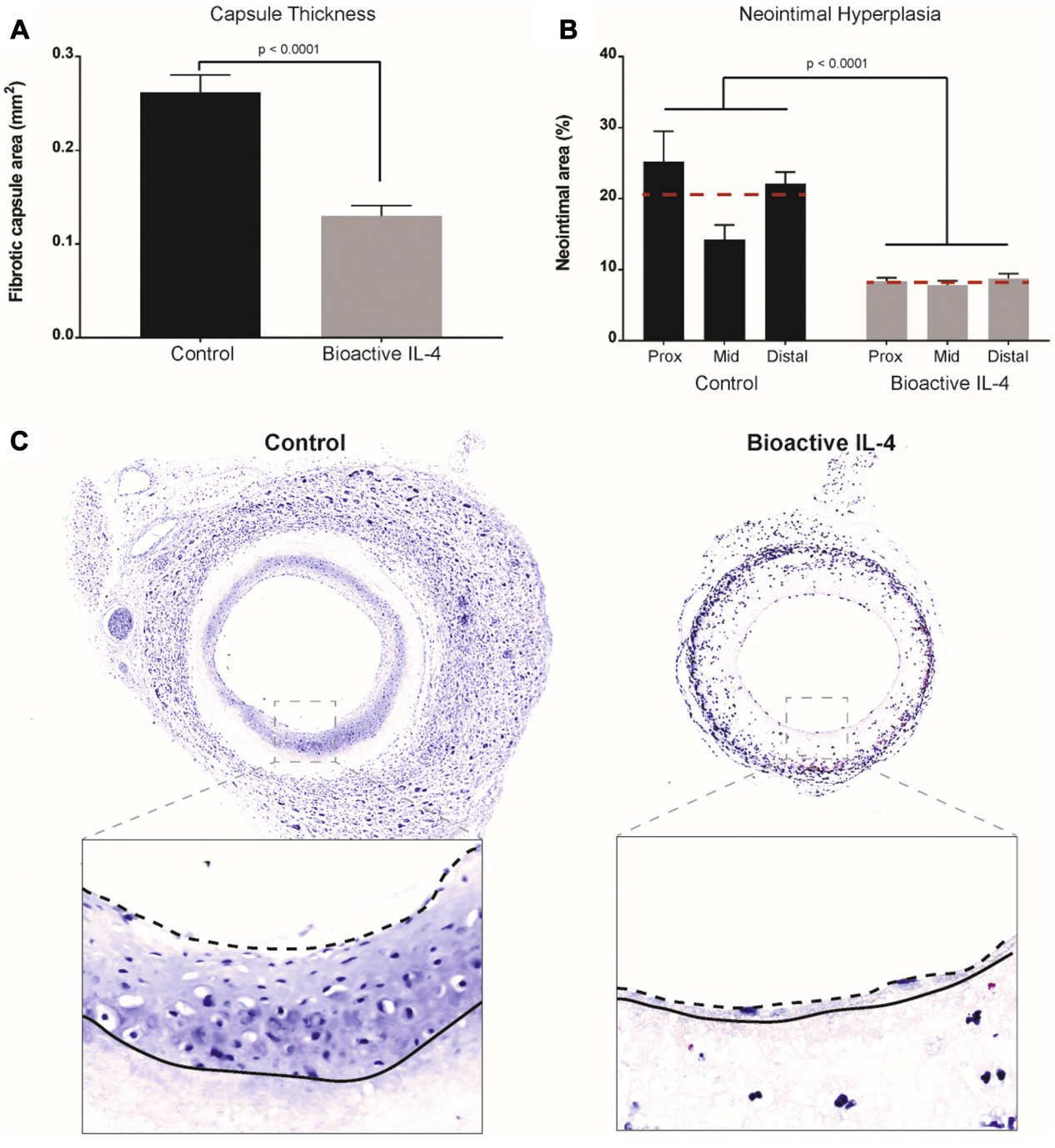

(A) Quantification of adventitia capsule thickness. **(B)** Quantification of neointimal hyperplasia development along 3 segments of vascular graft lumen. **(C)** Representative images of capsule thickness on the adventitia of vascular grafts, scale bar represents 150 μm; representative magnified images of vascular graft lumens **(inset)**. Scale bar represents 40 μm. **Dotted lines** represent the luminal edge of hyperplasia, and **solid lines** represent the luminal graft surface. n = 3 slides (each region of the graft) per animal with the average represented as the **red dotted line**; total of n = 5 animal averages per group. IL-4 = interleukin 4.

hyperplasia leading to graft failure. Adventitial capsule thickness on bioactive IL-4 grafts was 50 ± 1% less than control (**Figure 8A**). In addition, neointimal hyperplasia in bioactive IL-4 grafts was significantly less throughout the length of the graft (**Figure 8B**). The greatest decreases were observed at the proximal and distal anastomoses, with a reduction of 69 ± 6.7% and 61 ± 6.1%, respectively, relative to control. The midsection of the graft also saw significantly less hyperplasia (51 ± 9.6%) compared with control (**Figure 8C**). No significant changes to re-endothelialization were observed between the grafts (Supplemental Figure 4). Further characterization of the neointima observed increases in smooth muscle cells and proliferating cells compared to control while the elastin in the neointima was not significantly different (Supplemental Figure 5). Collectively, these results suggest that local modulation of macrophage phenotypes and cytokine profiles were responsible for significant reductions in neointimal hyperplasia.

DISCUSSION

CAD has become increasingly characterized as a chronic inflammatory disorder, prompting consideration of new anti-inflammatory therapeutic interventions. An overabundance of immune cells is common to atherosclerosis progression and neointimal hyperplasia development. The underlying immune cell presence arises from a complex interplay of inflammatory cytokines, which act to coordinate, propagate, and sustain inflammatory responses. Clinical evidence highlights the therapeutic potential of inhibiting cytokine expression to reduce inflammation and improve outcomes. Although the deployment of cardiovascular materials and devices in high-risk areas is an established treatment for CAD, accelerated inflammatory responses are a major cause of failure (18). In search of the next generation of CAD therapies, there remains an unmet need for cardiovascular devices fabricated from materials capable of modulating local inflammatory responses.

The present study describes rapid resolution of the inflammatory response to implanted materials in 2 separate mouse models, leading to durable functional improvements. Previous studies have shown the feasibility of local modulation of inflammation, using drug release or direct injection approaches to influence cell populations and chemokine profiles (19). Together, these studies have highlighted the limitation of using nonspecific suppressive drugs and the transient effects of these approaches, with most studies showing changes only in the first few days after implantation. Our results show that electrospun PCL scaffolds and conduits can be robustly functionalized with bioactive IL-4 to drive rapid polarization of macrophages to an anti-inflammatory M2 phenotype.

Multiple studies have now reported that implanted materials that promote an early shift to more M2-like macrophages at the material interface have an improved host response. The "alternatively activated" M2 phenotype is driven by signaling from M2-polarizing cytokines, including IL-4 (20). Previous research on IL-4-mediated regulation of the local response to materials has been limited to short-term elution from flat scaffolds. Examples include release from silk scaffolds over 24 h successfully polarizing macrophages in vitro (21) and microsphere-mediated release from poly(lactic-co-glycolic acid) scaffolds that increased the proportion of $CD206^{+}$ macrophages after 1 day in vivo, but local gene expression changes beyond this time were inconsistent (20). Similarly, release of IL-4 from polypropylene meshes showed no change to the number of local macrophages but a shift toward M2 phenotype at 14 days in a mouse subcutaneous implant model (22). Together, these studies illustrate the promise of early-stage macrophage polarization at the tissue implant interface toward an M2 phenotype. However, the applicability of this approach to any functional application, such as in a high-blood flow environment, has yet to be performed.

Robust immobilization of IL-4 onto the surface of PCL substrates was consistent with previous use of PIII surface activation of polymers to immobilize other biomolecules, including fibrillin-1 to polytetrafluoroethylene (PTFE) (23) and tropoelastin to expanded polytetrafluoroethylene (ePTFE) (24) and polyurethane conduits (6). In vitro macrophage interactions with bioactive IL-4 surfaces provided evidence of retained IL-4 bioactivity. The effects of IL-4 immobilization through PIII are consistent with the transient and variable effects on gene expression previously described for eluted IL-4 (20,21). PIII treatment is also well suited to the modification of implanted materials due to the established benefits of a long shelf-life post-treatment and the rapid covalent binding of a range of biomolecules during solution incubation (6). At the bedside, these off-the-shelf features would allow for the preparation of bioactive surfaces by simply taking pre-treated PIII materials/devices off the shelf and immersing them in IL-4

solutions, ready for transplant into patients with minimal time and cost expenditures.

The findings of the present study suggest that simultaneous changes to the local expression of both pro- and anti-inflammatory cytokines may be a more suitable approach to achieve rapid and comprehensive resolution of inflammation. Modulating macrophage phenotype and behavior is potentially an effective way of accomplishing this goal, demonstrating a preferable immunomodulatory strategy in the context of materials for vascular repair. Furthermore, these changes led to functional reductions in fibrous encapsulation sustained for at least 14 days. In contrast, studies using passive release of IL-4 commonly report upregulation of M2 macrophages surrounding implants but typically no significant differences in total cell accumulation (20) or macrophages (22) at the implant interface. In fact, M2 macrophage polarization is greatest at distances farthest from the surface of drug elution, accentuating the disadvantage of passive release strategies in which IL-4 diffuses away from the implant site. Significant reductions in cell accumulation and fibrous encapsulation seen on bioactive IL-4 surfaces demonstrate improved functional outcomes compared with passive release strategies. More broadly, our findings suggest the potential utility for a diverse range of tissue repair applications. Previous studies have highlighted benefits for regulating the inflammatory response to scaffolds in the context of soft tissue and wound repair, as well as potentially in cardiac patches to treat myocardial infarction in which the role of macrophage polarization has recently been highlighted (25). Studies thus far share the limitation of being restricted to analysis in tissue, with none to date modulating inflammation in flowing blood.

The present study reports sustained effectiveness in a vascular graft context with direct implications for vascular materials and devices deployed in contact with circulation. Regulating fibrotic encapsulation is important for limiting compliance mismatch between the graft and adjacent native vasculature, which has long been correlated with poor patency in small-diameter applications (26). Restenosis, the main source of long-term graft occlusion, is caused by neointimal hyperplasia and widely accepted to be inflammation driven. Previous studies have clearly reported this link observing reduced neointima formation after inhibition of leukocyte trafficking (27), release of dexamethasone (28), the cytotoxic drugs paclitaxel and sirolimus (29), and specific anti-inflammatory CX_3CR1 antagonists (30). Although these strategies have collectively shown promising in vitro results, beneficial long-term outcomes in vivo have not been reported, with efficacy often limited to the period of drug elution. In addition to the benefit of immobilization to address these issues, bioactive IL-4 surfaces drive a rapid shift of the native immune response that would be expected to have lasting effects long after the IL-4 biomolecules are removed from the surface. By elevating M2 macrophage populations, yielding favorable modulation of the inflammatory response through regulation of both pro- and anti-inflammatory cytokines, the foreign body response is more quickly resolved. Our research has significant implications for improving the inflammatory response to all implants, with potential applications for cardiovascular devices in contact with flowing blood such as the prevention of foreign body encapsulation and neointimal hyperplasia in small diameter conduits.

STUDY LIMITATIONS. Limitations to this study include the use of a small animal model of grafting, with a nondiseased phenotype, and a short-time frame of neointimal hyperplasia assessment. While the mouse grafting model used in this study facilitates quantification of clinically relevant endpoints such as neointimal hyperplasia and re-endothelialization, the established pre-clinical pathway includes larger animals including sheep. The sheep model more closely resembles human pathology and incorporates additional considerations of graft efficacy including thrombogenicity and longer-term graft performance. The wild-type mice used in this study have a healthy vasculature, lacking the persistent inflammatory environment commonly present in atherosclerosis and CAD. Use of fat-fed or transgenic animals may potentially benefit future studies investigating bioactive vascular grafts in cardiovascular disease phenotypes. The findings of this study justify the further assessment of bioactive IL-4 surfaces in the context of atherosclerosis and in larger animal models with implications for improving the efficacy of all implants, including small diameter vascular grafts.

CONCLUSIONS

The present study evaluated a novel bioactive device coating that modulates macrophage phenotype and extensively suppresses local inflammatory responses. The bioactivity of our surfaces relies on a covalently immobilized layer of IL-4, a key regulator of macrophage recruitment and anti-inflammatory polarization, to provide comprehensive suppression of

inflammation. As a subcutaneous implant, bioactive IL-4 surfaces exhibited increased polarization of macrophages to their anti-inflammatory M2 phenotype, reducing the overall recruitment of macrophages. This finding also correlates with the favorable regulation of inflammatory cytokine production that led to striking reductions in the formation of the foreign body fibrotic capsule at 2 weeks after implantation. Using these materials as vascular grafts, we observed the same striking effects on macrophage reduction, M2 polarization, and positive regulation of the local cytokine environment, which translate to important functional outcomes, most notably a significant reduction in foreign body encapsulation and neointimal hyperplasia development after 1 month in vivo. The collective findings of our 2 models have significant implications for improving the inflammatory response and the long-term performance of medical implants, with demonstrated potential for cardiovascular devices in contact with flowing blood.

ACKNOWLEDGMENTS The authors acknowledge the facilities as well as scientific and technical assistance at the Australian Center for Microscopy and Microanalysis, The University of Sydney.

ADDRESS FOR CORRESPONDENCE: Mr. Richard P. Tan, Applied Materials Group, The Heart Research Institute, 7 Eliza Street, Newtown NSW 2042, Australia. E-mail: richard.tan@hri.org.au.

PERSPECTIVES

COMPETENCY IN MEDICAL KNOWLEDGE: CAD and other manifestations of atherosclerosis have become increasingly characterized as inflammatory disorders. The success of future interventional therapies for CAD requires effective delivery of anti-inflammatory agents that can provide localized and sustained suppression of inflammation while avoiding the adverse effects of systemic administration, including infection. Representing an alternative approach to systemic treatment, this study investigates the targeted delivery of the anti-inflammatory cytokine IL-4 through bioactive coatings on materials capable of being implanted into the vasculature.

TRANSLATIONAL OUTLOOK: Given their roles as major effectors of innate immunity, targeting macrophage phenotype and behavior may represent a more focused and comprehensive approach to immunomodulation, with potentially greater impact on improved cardiac outcomes for implanted vascular materials. Bioactive surfaces with immobilized IL-4 can modulate local inflammation in a sustained and robust manner. These have numerous applications for implants and devices being implanted into high-risk cardiovascular areas, with the immediate benefits of improving device performance as well as the long-term advantages of mitigating chronic inflammation that drive CAD pathology.

REFERENCES

1. Hansson GK. Inflammation, atherosclerosis, and coronary artery disease. N Engl J Med 2005;352:1685–95.

2. Mulvihill NT, Foley JB. Inflammation in acute coronary syndromes. Heart 2002;87:201–4.

3. Ridker PM, Everett BM, Thuren T, et al. Antiinflammatory therapy with canakinumab for atherosclerotic disease. N Engl J Med 2017;377:1119–31.

4. Bridges AW, García AJ. Anti-Inflammatory polymeric coatings for implantable biomaterials and devices. J Diabetes Sci Technol 2008;2:984–94.

5. Hiroyuki O, Tsutomu T, Kiyoshi Y. Therapies targeting inflammation after stent implantation. Curr Vasc Pharmacol 2013;11:399–406.

6. Bilek MM. Biofunctionalization of surfaces by energetic ion implantation: review of progress on applications in implantable biomedical devices and antibody microarrays. Appl Surf Sci 2014;310:3–10.

7. Pajarinen J, Tamaki Y, Antonios JK, et al. Modulation of mouse macrophage polarization in vitro using IL-4 delivery by osmotic pumps. J Biomed Mater Res A 2015;103:1339–45.

8. Kondyurin A, Bilek M. 10—Protection in an aggressive environment. Ion Beam Treatment of Polymers. Amsterdam, the Netherlands: Elsevier, 2008:243–60.

9. Liu H, Wise SG, Rnjak-Kovacina J, et al. Biocompatibility of silk-tropoelastin protein polymers. Biomaterials 2014;35:5138–47.

10. Chan AH, Tan RP, Michael PL, et al. Evaluation of synthetic vascular grafts in a mouse carotid grafting model. PLoS One 2017;12:e0174773.

11. Bilek MM, McKenzie DR. Plasma modified surfaces for covalent immobilization of functional biomolecules in the absence of chemical linkers: towards better biosensors and a new generation of medical implants. Biophysical Reviews 2010;2:55–65.

12. Bilek MM, Bax DV, Kondyurin A, et al. Free radical functionalization of surfaces to prevent adverse responses to biomedical devices. Proc Natl Acad Sci U S A 2011;108:14405–10.

13. Liu CP, Zhang X, Tan QL, et al. NF-κB pathways are involved in M1 polarization of RAW 264.7 macrophage by polyporus polysaccharide in the tumor microenvironment. PLoS One 2017;12:e0188317.

14. Liu CY, Xu JY, Shi XY, et al. M2-polarized tumor-associated macrophages promoted epithelial-mesenchymal transition in pancreatic cancer cells, partially through TLR4/IL-10 signaling pathway. Lab Invest 2013;93:844–54.

15. Li B, Cao H, Zhao Y, et al. In vitro and in vivo responses of macrophages to magnesium-doped titanium. Sci Rep 2017;7:42707.

16. Tan RP, Lee BSL, Chan AH, et al. Non-invasive tracking of injected bone marrow mononuclear cells to injury and implanted biomaterials. Acta Biomater 2017;53:378–88.

17. Anderson JM, Rodriguez A, Chang DT. Foreign body reaction to biomaterials. Semin Immunol 2008;20:86–100.

18. Inoue T, Croce K, Morooka T, Sakuma M, Node K, Simon DI. Vascular inflammation and repair: implications for reendothelialization,

restenosis, and stent thrombosis. J Am Coll Cardiol Intv 2011;4:1057–66.

19. Browne S, Pandit A. Biomaterial-mediated modification of the local inflammatory environment. Front Bioeng Biotechnol 2015;3:67.

20. Minardi S, Corradetti B, Taraballi F, et al. IL-4 release from a biomimetic scaffold for the temporally controlled modulation of macrophage response. Ann Biomed Eng 2016;44:2008–19.

21. Reeves AR, Spiller KL, Freytes DO, Vunjak-Novakovic G, Kaplan DL. Controlled release of cytokines using silk-biomaterials for macrophage polarization. Biomaterials 2015;73:272–83.

22. Hachim D, LoPresti ST, Yates CC, Brown BN. Shifts in macrophage phenotype at the biomaterial interface via IL-4 eluting coatings are associated with improved implant integration. Biomaterials 2017;112:95–107.

23. Hajian H, Wise SG, Bax DV, et al. Immobilisation of a fibrillin-1 fragment enhances the biocompatibility of PTFE. Colloids Surf B Biointerfaces 2014;116:544–52.

24. Wise SG, Liu H, Kondyurin A, et al. Plasma ion activated expanded polytetrafluoroethylene vascular grafts with a covalently immobilized recombinant human tropoelastin coating reducing neointimal hyperplasia. ACS Biomaterials Sci Eng 2016;2:1286–97.

25. Mongue-Din H, Patel AS, Looi YH, et al. NADPH oxidase-4 driven cardiac macrophage polarization protects against myocardial infarction-induced remodeling. J Am Coll Cardiol Basic Trans Science 2017;2:688.

26. Baird RN, Abbott WM. Pulsatile blood-flow in arterial grafts. Lancet 1976;308:948–50.

27. Lavin B, Gomez M, Pello OM, et al. Nitric oxide prevents aortic neointimal hyperplasia by controlling macrophage polarization. Arterioscler Thromb Vasc Biol 2014;34:1739–46.

28. Liu X, De Scheerder I, Desmet W. Dexamethasone-eluting stent: an anti-inflammatory approach to inhibit coronary restenosis. Expert Rev Cardiovasc Ther 2004;2:653–60.

29. Wessely R, Schömig A, Kastrati A. Sirolimus and paclitaxel on polymer-based drug-eluting stents: similar but different. J Am Coll Cardiol 2006;47:708–14.

30. Ali MT, Martin K, Kumar AH, et al. A novel CX3CR1 antagonist eluting stent reduces stenosis by targeting inflammation. Biomaterials 2015;69:22–9.

KEY WORDS covalent biomolecule immobilization, inflammation, interleukin-4, neointimal hyperplasia, plasma-based ion implantation, radical functionalized surface, vascular graft

APPENDIX For supplemental figures, results, and methods, please see the online version of this paper.

JACC: BASIC TO TRANSLATIONAL SCIENCE VOL. 4, NO. 1, 2019

PRECLINICAL RESEARCH

miR-29b Mediates the Chronic Inflammatory Response in Radiotherapy-Induced Vascular Disease

Suzanne M. Eken, MD, PhD,[a] Tinna Christersdottir, MD,[b] Greg Winski, MD,[a] Traimate Sangsuwan, MSc,[c] Hong Jin, MD, PhD,[a] Ekaterina Chernogubova, PhD,[a] John Pirault, PhD,[d] Changyan Sun, MSc,[a] Nancy Simon, MSc,[a] Hanna Winter, MSc,[e,f] Alexandra Backlund, PhD,[a] Siamak Haghdoost, PhD,[c,g] Göran K. Hansson, MD, PhD,[a] Martin Halle, MD, PhD,[b,h,*] Lars Maegdefessel, MD, PhD[a,e,f,*]

VISUAL ABSTRACT

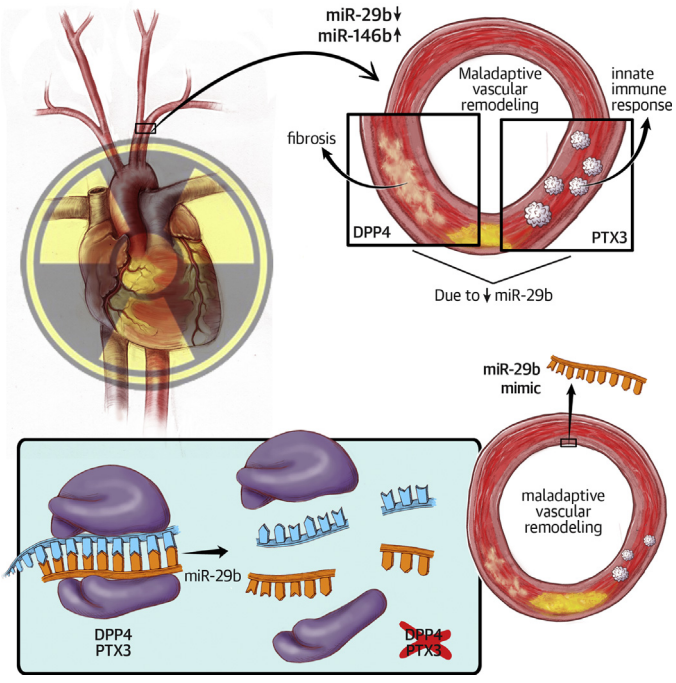

Eken, S.M. et al. J Am Coll Cardiol Basic Trans Science. 2019;4(1):72–82.

HIGHLIGHTS

- **Radiotherapy is a powerful treatment strategy in patients with oncological diseases.**
- **Radiation-induced vasculopathy can dose dependently increase the risk of ischemic cardiovascular diseases (e.g., myocardial infarction, heart failure, stroke).**
- **The microRNA miR-29b is repressed in radiation-induced vasculopathy (human irradiated vs. nonirradiated tissue specimen, as well as in murine and cell culture models of irradiation).**
- **Pentraxin-3 and dipeptidyl-peptidase 4 are the main downstream effectors of miR-29b in radiation-induced vasculopathy.**
- **miR-29b mimics were able to limit pentraxin-3 and dipeptidyl-peptidase 4 levels in the irradiated vasculature (murine model) and to constrain the burden of vascular inflammation.**

From the [a]Cardiovascular Medicine Unit, Department of Medicine, Solna, Karolinska Institute, Stockholm, Sweden; [b]Department of Molecular Medicine and Surgery, Karolinska Institute, Stockholm, Sweden; [c]Department of Molecular Biosciences, Wenner-Gren Institute, Stockholm University, Stockholm, Sweden; [d]INSERM UMR_S1116, Université de Lorraine, Vandoeuvre-lès-Nancy, France; [e]Technical University Munich, Department of Vascular and Endovascular Surgery, Munich, Germany; [f]German Center for Cardiovascular Research (DZHK) partner site Munich, Munich, Germany; [g]University of Caen Normandie, LARIA-CIMAP, Caen, France; and the [h]Department of Reconstructive Plastic Surgery, Karolinska University Hospital, Stockholm, Sweden. *Drs. Halle and Maegdefessel contributed equally to this work and are joint senior authors. The study was supported through funding from Radiumhemmet (161072), the Swedish Society of Medicine (SLS-595621, both to Dr. Halle) and the Stockholm County Council (SLL20170080 to Drs. Halle and Hansson) and funding from the Swedish Heart-Lung-Foundation (20120615, 20130664, 20140186),

ISSN 2452-302X https://doi.org/10.1016/j.jacbts.2018.10.006

SUMMARY

As a consequence of the success of present-day cancer treatment, radiotherapy-induced vascular disease is emerging. This disease is caused by chronic inflammatory activation and is likely orchestrated in part by microRNAs. In irradiated versus nonirradiated conduit arteries from patients receiving microvascular free tissue transfer reconstructions, irradiation resulted in down-regulation of miR-29b and up-regulation of miR-146b. miR-29b affected inflammation and adverse wound healing through its targets pentraxin-3 and dipeptidyl-peptidase 4. In vitro and in vivo, we showed that miR-29b overexpression therapy, through inhibition of pentraxin-3 and dipeptidyl-peptidase 4, could dampen the vascular inflammatory response.

ABBREVIATIONS AND ACRONYMS

$Apoe^{-/-}$ = apolipoprotein E knockout

DIG = digoxigenin

DPP4 = *Dpp4*, dipeptidyl-peptidase 4

FFT = free flap tissue transfer

HCtAEC = human carotid artery endothelial cell

HCtASMC = human carotid artery smooth muscle cell

mRNA = messenger ribonucleic acid

miRNA = microRNA

NR = nonirradiated

PTX3 = *Ptx3*, pentraxin-3

RNA = ribonucleic acid

SMC = smooth muscle cell

TGF = tumor growth factor

vRTx = radiation vasculopathy

Extraordinary efforts and great successes in cancer therapy have led to a growing cohort of cancer survivors (1). Despite being cancer-free, these patients have an increased risk of developing disease, ranging from cognitive impairment to heart failure, which can be attributed to previous cancer treatment (2). In this context, radiation-induced vascular disease or radiation vasculopathy (vRTx) is an under-recognized problem with high-impact long-term sequelae, such as stroke and myocardial infarction (3–5). In a manner proportional to radiation dosage and location, radiation therapy for breast cancer and Hodgkin lymphoma increases the risk for ischemic heart disease (6,7). In patients with head and neck cancer, carotid artery irradiation is a significant risk factor for carotid occlusive disease (5,8,9). In free flap tissue transfer (FFT) surgery, a procedure involving transplantation of a vascularized tissue by using microvascular anastomosis to repair large defects after tumor resection, irradiation is reported to be a risk factor for vascular complications (10–12).

The underlying pathophysiological mechanism of vRTx is a chronic inflammatory reaction initiated by the cellular response to ionizing radiation (13). In the vessel wall, this action induces various maladaptive events, including unbridled vascular cell proliferation, remodeling, and oxidative stress as well as tumor growth factor (TGF)-β-regulated nuclear factor kappa B activation. This type of chronic inflammatory reaction is known to cause intimal hyperplasia and accelerated atherosclerotic plaque development (14), leading to cardiovascular morbidity and mortality as well as reconstruction complications with FFT (15) in these patients.

Different cellular processes initiating the pathological vascular response are difficult to influence separately. MicroRNAs (miRNAs) have generated a great deal of attention because of their ability to critically regulate biological pathways (16). miRNAs can inhibit gene expression at different levels by acting as master regulators of protein output (17). miRNA modulation can influence and reverse disease processes and is used in preclinical as well as clinical studies (18,19). The vasculature, a sensitive and tightly regulated system, is especially under miRNA control, with it being implicated and applied in various vascular diseases (20,21). Moreover, miRNAs play a crucial role in the DNA damage response (22).

The current study investigated mechanisms through which down-regulation of miRNAs is involved in the adverse vascular response to irradiation and explored application of miRNA modulators as a therapeutic modality to reduce vRTx through dampening of the innate immune response and inhibition of an adverse healing response.

METHODS

HUMAN TISSUE SPECIMENS. Samples from Karolinska University Hospital's Biobank of Irradiated Tissues at Karolinska (Stockholm, Sweden) were

the Ragnar Söderberg Foundation (M-14/55), a DZHK Junior Research Group grant, a European Research Council Starting Grant (*NORVAS*), the Karolinska Institute Cardiovascular Program Career Development Grant, and the Swedish Research Council (2015-03140_4) (all to Dr. Maegdefessel). The authors have reported that they have no relationships relevant to the contents of this paper to disclose.

All authors attest they are in compliance with human studies committees and animal welfare regulations of the authors' institutions and Food and Drug Administration guidelines, including patient consent where appropriate. For more information, visit the *JACC: Basic to Translational Science* author instructions page.

Manuscript received August 15, 2018; revised manuscript received October 18, 2018, accepted October 18, 2018.

TABLE 1 Patient Characteristics

Age (yrs)/ Sex	RT Dose (Gy)	Time After Radiotherapy (weeks)	Donor Artery Origin	Current Smoking	CVD	NSAID Use
77/F	50	200	Forearm	No	No	No
64/M	68	44	Forearm	Yes	Yes	Yes
53/F	64	176	Fibula	Yes	No	Yes
45/F	64	119	Fibula	No	No	Yes
61/F	68	126	Fibula	No	No	Yes
79/M	64	620	Fibula	No	Yes	Yes
66/M	46	350	Fibula	No	No	Yes
52/M	68	100	Fibula	No	No	Yes
60/F	68	217	Fibula	No	No	No
60/M	46	50	Forearm	No	No	No
65/F	68	79	Forearm	No	No	Yes
70/M	66	128	Fibula	No	No	Yes
66/M	68	126	Thigh	No	No	No
39/F	68	83	Forearm	No	No	Yes
62/M	64	406	Fibula	No	No	No

CVD = cardiovascular disease; NSAID = nonsteroidal anti-inflammatory drug.

analyzed. Fifteen pairs of arterial biopsy samples were harvested during head and neck cancer reconstruction with microvascular free tissue transfer in 15 pre-operatively irradiated patients. Before performing microvascular anastomosis, biopsy samples were harvested from radiated branches of the external carotid artery (recipient site) and from the nonradiated (donor) artery of the transferred autologous tissue (Table 1). Biopsy samples were freed from surrounding tissue and surgical material under a dissection microscope, where care was taken not to damage the endothelium. Vascular tissue was placed in RNAlater (Thermo Fisher Scientific, Waltham, Massachusetts) or Allprotect Tissue Reagent (Qiagen, Hilden, Germany), frozen and stored at -80°C until ribonucleic acid (RNA) extraction. For immunohistochemical analysis, tissue from a paired subset of 3 patients was fixed in 10% formalin and paraffin embedded.

The study was approved by the Ethical Committee of Stockholm and was performed in agreement with institutional guidelines and the principles of the Declaration of Helsinki. All enrolled patients gave written, informed consent.

IN VITRO EXPERIMENTS. Cell culturing. Primary, proliferating human carotid artery smooth muscle cells (HCtASMCs) and human carotid artery endothelial cells (HCtAECs) (Cell Applications, San Diego, California) were cultured up to passages 5 through 8 in subtype-specific growth medium (Cell Applications). Cells were seeded on 6-, 12-, or 24-well plates and treated or radiated at a density of 70% to 80%. Endothelial cells were cultured and seeded in gelatin-coated (Attachment Factor Protein 1X, Thermo Fisher Scientific) flasks and plates.

Luciferase reporter assay. Luciferase reporter assay was performed as previously described (23). In brief, HEK293 cells (Public Health England Culture Collections, Salisbury, United Kingdom) were seeded on 96-well (PTX3, 1×10^4 cells/well) and 24-well (1×10^5 cells/well) plates. At 50% to 60% confluence, cells were transfected with luciferase reporter plasmid pLS, pLS-*DPP4*-3′UTR, or its mutant (100 ng/well, Active Motif), together with control or pre-miR-29b (10 nmol/l final concentration) by using DharmaFECT DUO Transfection Reagent (Thermo Fisher Scientific) according to the manufacturer's protocol. After a 24-h transfection period, luciferase activity was quantified by using the LightSwitch Luciferase Assay Kit (Thermo Fisher Scientific) according to the manufacturer's instructions.

Irradiation. Cells were placed inside a biological irradiator and were treated with 2 doses of 2 Gy (0.4 Gy/min; total irradiation time, 2 × 5 min) with 24 h between radiation dosages. Control cells were taken out of the incubator for a similar amount of time but did not receive irradiation.

KINETIC LIVE CELL IMAGING FOR PROLIFERATION AND APOPTOSIS. Cells in 6-well (for protein analysis) or 24-well (for RNA analysis) plates were used for these experiments. Directly after irradiation, medium was removed and replaced with fresh medium (Cell Applications). Cells were placed in a live-cell imaging incubator (IncuCyte, Essen Bioscience, Hertfordshire, United Kingdom) and images taken every 2 h for the course of 5 days. Proliferation was defined as an increase in cell confluence as the average of 9 pictures per well in a 24-well plate or 16 pictures per well in a 6-well plate. For apoptosis measurements, cell medium was supplied with caspase-3/7 reagent (Essen Bioscience) at a concentration of 5 μmol/l, as recommended by the manufacturer. Apoptosis was measured as the number of positive cells per photographed area. Experiments were run in triplicate.

IN VIVO IRRADIATION. In vivo experiments were approved by the Swedish Board for Agriculture (ethical permit no. N89/13). For in vivo irradiation, we used 10-week-old C57BL6/N apolipoprotein E knockout (*Apoe*$^{-/-}$) mice (Taconic Biosciences, Rensselaer, New York) weighing 20 to 30 g. Anesthesia consisted of intraperitoneal injection of 750 μg ketamine (Ketalar, Pfizer, Sollentuna, Sweden), 10 μl (1 mg/ml) of medetomidine (Domitor, Orion Pharma

Animal Heath, Sollentuna, Sweden), and 75 μl of phosphate-buffered saline. Depth of anesthesia was verified with a pedal reflex test. Animals (n = 9 to 11 per group) were fixated onto a heating pad and covered by a 7-mm-thick lead chamber with an open area (1.5 × 2.2 cm) also restricted by a collimator (2.5 × 2 cm) exposing the upper chest and neck region to radiation beams. Mice were placed in a biological irradiator (X-RAD 320, Precision X-Ray Inc., North Branford, Connecticut), and the uncovered area was irradiated at 0.7 Gy/min to a total dose of 14 Gy at 320 kV, 12.5 mA, 8 FOS, with an F2 filter consisting of aluminum, copper, and tin. Control mice received sham irradiation.

After irradiation, mice received atipamezole (Antisedan, Orion Pharma Animal Heath) 20 μl (5 mg/ml) for anesthesia reversal. Harvesting and organ handling are described in the Supplemental Methods section.

IN VIVO miR-29B MODULATION. For miR-29b overexpression, radiated mice (n = 6) received 2 dosages of 2 mg/kg miR-29b mimics (Ambion, Thermo Fisher Scientific) using the vector reagent Jet-PEI (Polyplus-transfection SA, Illkirch-Graffenstaden, France) for transfection. Control mice (n = 6) received 0.5 mg/kg (dosage according to the manufacturer's instructions) Jet-PEI–carried mimics with random (scrambled) sequences (Thermo Fisher Scientific). Mimics and controls were injected intraperitoneally 1 day before and 1 day after irradiation. Tissues were harvested 14 days after irradiation.

PREPARATION OF CELLS AND TISSUE SAMPLES FOR QUANTITATIVE REVERSE TRANSCRIPTION-POLYMERASE CHAIN REACTION. RNA isolation was performed according to standardized procedures described in the Supplemental Methods section. miRNA and messenger ribonucleic acid (mRNA) expression was quantified according to quantitative polymerase chain reaction using TaqMan (Thermo Fisher Scientific) FAM- or VIC-labeled mRNA and miRNA assays (Supplemental Tables 1 to 3).

TISSUE HISTOLOGY. Human tissue was fixed for 48 h in 10% formalin at room temperature, paraffin embedded, and cut into 5-μm-thick slides. Hematoxylin and eosin, Oil Red O, Sirius Red, and immunohistochemical stainings were performed according to standardized protocols. All primary antibodies were purchased from Abcam, Cambridge, United Kingdom (Supplemental Table 4). Dipeptidyl-peptidase 4 (DPP4)- and pentraxin-3 (PTX3)-positive cells were measured by counting the cells in 4 high-power fields of 2 to 4 different (human or mouse) vessels per group (nonradiated vs. irradiated in human; miR-29b modulated in mice upon radiation or sham irradiation). Counting was performed by a blinded investigator using ImageJ software (National Institutes of Health, Bethesda, Maryland). All histological analyses were obtained at room temperature by using a Hamamatsu NanoZoomer Slide Scanner with NDP.view2 software (Hamamatsu Photonics, Hamamatsu, Japan). More details are provided in the Supplemental Methods section.

IN SITU HYBRIDIZATION. For in situ hybridization, we used Exiqon miRCURY locked nucleic acid double digoxigenin (DIG)-labeled probes (50-30 probe sequence for miR-29b, AACACTGATTTCAAATGGT GCT; miR-146b, AGCCTATGGAATTCAGTTCTCA) with the accompanying kit and protocol (Qiagen, Hilden, Germany). In brief, tissue sections were deparaffinized. Nucleases were inactivated with proteinase K followed by a 2-h hybridization at hybridization temperature (53°C). Slides were washed in saline sodium citrate buffers. DIG-labeled probes were detected by using standard DIG detection methods.

STATISTICAL METHODS. SPSS version 22 (IBM Corporation, Armonk, New York) was used to analyze patient data. To compare 2 groups, Student's *t*-test was used. Paired data were analyzed by using paired-sample *t*-tests. Differences between ≥2 groups versus a control group were analyzed with 1-way analysis of variance plus a Bonferroni correction for multiple comparisons. Statistical analysis for the murine experimental data was conducted by using GraphPad Prism software version 7.0 (GraphPad Software, La Jolla, California). Differences in RNA expression were calculated as fold change versus control by using the mean delta Ct ($^{\Delta}$Ct, defined as $Ct^{\text{target RNA}}$ minus $Ct^{\text{endogenous control}}$) within groups. To correct for multiple *t*-tests in the live cell imaging experiments, the Holm-Šidák method with an alpha of 0.05 was used.

RESULTS

miR-29B IS DECREASED AND miR-146B INCREASED IN RADIATED VERSUS NONRADIATED VASCULAR TISSUE. In 15 pairs of arterial tissue samples from 15 patients undergoing microvascular free tissue transfer reconstructions (FFT), we compared the expression of 11 well-known miRNAs in cardiovascular disease, cancer, or both (Supplemental Table 1, **Figure 1A**). For some tissue pairs, miRNA expression could not be measured because of insufficient total RNA quantity (**Figure 1B**). Patient age ranged from 39 to 79 years (median, 62 years). Total radiation dosage

FIGURE 1 miRNA and Target Profiling in Radiated Versus Nonradiated Human Arteries

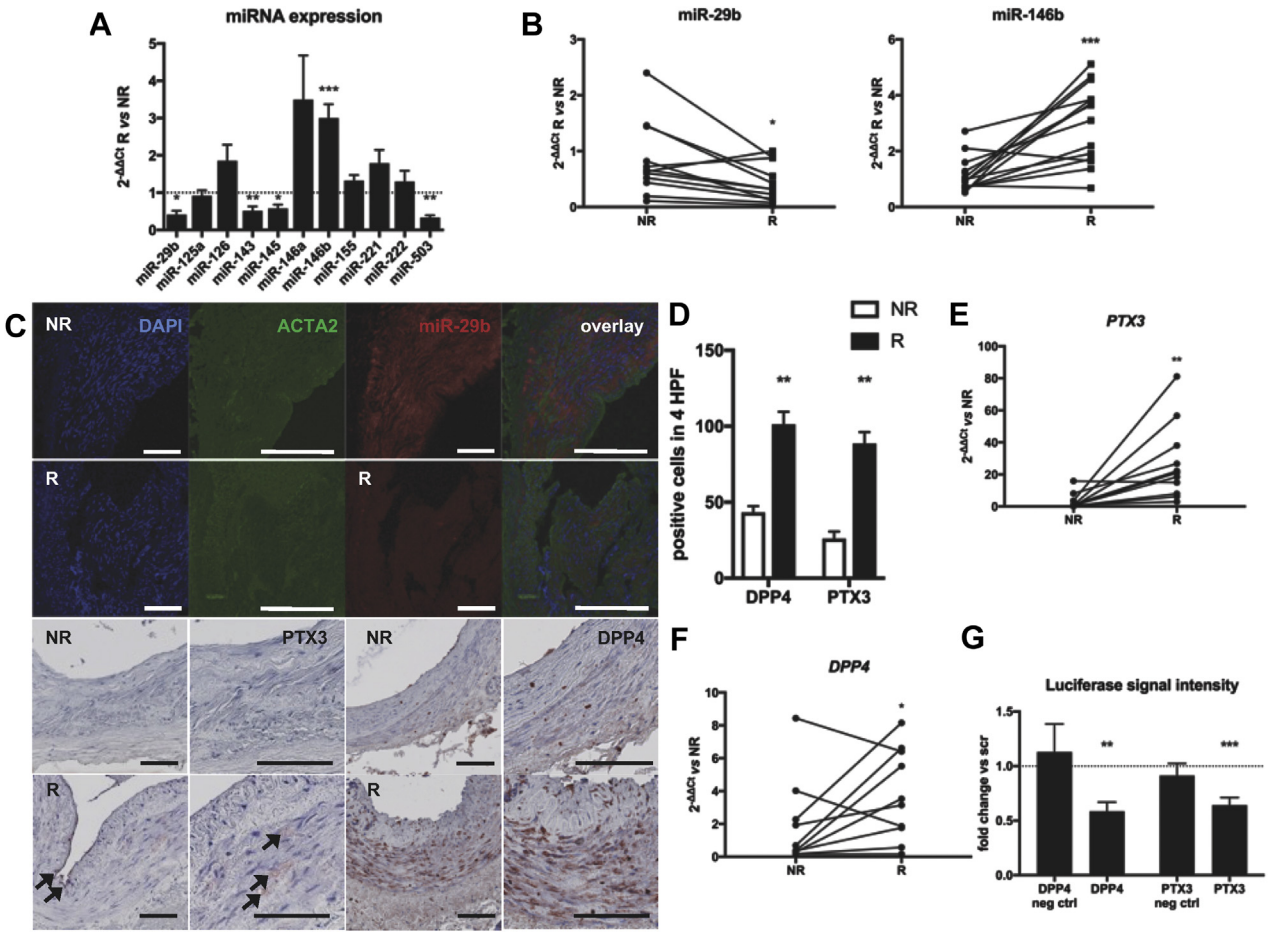

(A) Expression of 11 vascular disease-related microRNAs (miRNAs) in radiated (R) versus nonradiated (NR) arteries. n = 12 per group. Mean ± SEM. *p < 0.05; **p < 0.01; ***p < 0.001. **(B)** miR-29b was down-regulated and miR-146b upregulated in radiated versus nonradiated arteries harvested at microvascular tissue transfers. n = 15. *p < 0.05; ***p < 0.001. **(C)** Fluorescent in situ hybridization of miR-29b showing its expression in the tunica media of nonradiated vessels. Pentraxin-3 (PTX3) and dipeptidyl-peptidase 4 (DPP4) protein expression is increased throughout the vessel wall after radiation. ACTA2 = smooth muscle actin; DAPI = 4′,6-diamidino-2-phenylindole. Bars, 100 μm. **(D)** Quantification of staining for miR-29b target protein markers. n = 3 in each group. HPF = high-power field. **p < 0.01 in 1-way analysis of variance. **(E)** miR-29b target *PTX3* was up-regulated after irradiation. n = 10. **p < 0.01. **(F)** miR-29b target *DPP4* was upregulated after irradiation. n = 10. *p < 0.05, **p < 0.01, ***p < 0.001 in paired-sample *t*-tests. **(G)** miR-29b mimics significantly inhibited *DPP4* and *PTX3* luciferase activity compared with scrambled control (scr) oligonucleotides. Mean ± SEM. **p < 0.01, ***p < 0.001 in Student's *t*-test of scrambled versus miR-29b mimic. *EV* = empty vector; *mut* = mutated seed sequence; Neg ctrl = negative control.

was between 46 and 68 Gy (median, 66 Gy). Tissue was harvested during FFT, which occurred between 44 and 620 weeks after radiotherapy (median, 126 weeks). Other patient characteristics are listed in Table 1.

Among other miRNAs, miR-29b and miR-146b were significantly deregulated in radiated tissue, miR-29b being decreased and miR-146b increased (Figure 1B). Fluorescent in situ hybridization of miR-29b in these arteries was concordant with quantitative reverse transcription-polymerase chain reaction results, both miRNAs having a clear predilection for the intimal-medial layer, where smooth muscle cells (SMCs) reside (Figures 1C and 1D, top 2 rows). miR-143-145 and miR-503 were down-regulated along with miR-29b (Figure 1A). These 2 miRNAs were not further investigated because they could not be detected in human SMCs or endothelial cells in vitro (miR-503) or because of their mRNA target profile was more associated with SMC development and phenotype than with innate immunity (miR-143-145 cluster).

FIGURE 2 Murine Vascular miR-29b, miR-146b, *Ptx3*, and *Dpp4* Expression After Irradiation

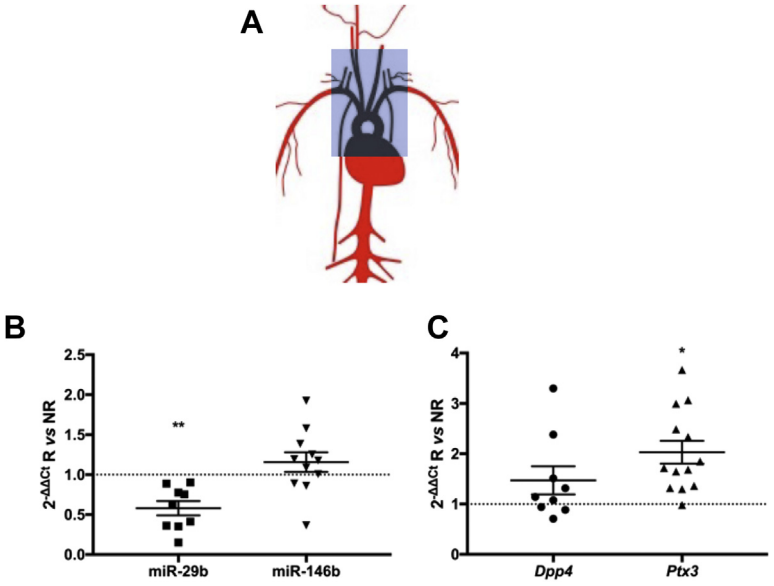

(A) Descriptive figure of the irradiated area in our in vivo radiation model. **(B)** Expression of miR-29b, but not of miR-146b, was altered in irradiated arterial tissue. n = 9 to 11 in each group. **(C)** Irradiation caused up-regulation of *Ptx3* gene expression but not *Dpp4* gene expression. Mean ± SEM. *$p < 0.05$; **$p < 0.01$ in Student's *t*-test. Abbreviations as in Figure 1.

EXPRESSION OF miR-29B TARGETS PTX3 AND DPP4 IS INCREASED UPON IRRADIATION. In previously published RNA analyses with the same method used in different samples, with a more recent harvest after irradiation (13,24), we searched for experimentally validated (25) miR-29b and miR-146b gene targets regulated in a direction inverse to that of the miRNA. In radiated versus nonradiated tissue, PTX3 was the most profoundly upregulated miR-29b target (Figure 1E). DPP4 levels were also significantly higher in radiated tissue (Figure 1F). The predicted miR-29b gene target DPP4 (or CD26) is related to radiation injury and impaired wound healing (26). With luciferase reporter assay, PTX3 and DPP4 were validated as miR-29b targets in HEK293 cells (Figure 1G).

In formalin-fixed, paraffin-embedded arterial tissue from a subset of patients, we could localize PTX3 and DPP4 protein expression in the intimal and medial layer of radiated arteries, whereas expression in their nonradiated counterparts was markedly lower (Figures 1C [bottom two rows] and 1D).

IRRADIATION AFFECTS VASCULAR miR-29B AND *PTX3* EXPRESSION IN A MURINE MODEL. Male *Apoe*$^{-/-}$ mice were subjected to irradiation using a model based on the method described by Stewart et al. (27). In mice receiving a single irradiation dose of 14 Gy in a designated mediastinal and neck area, including the heart and large vessels (Figure 2A), irradiated arteries exhibited a significant down-regulation of miR-29b and no significant up-regulation of miR-146b at 14 days compared with those given sham irradiation (Figure 2B). There was significant concordant up-regulation of Ptx3 after irradiation. *Dpp4* gene expression showed a trend toward up-regulation but was not significantly affected (Figure 2C). Histological analysis of the carotid artery 10 weeks after irradiation revealed no striking fibrotic or atherosclerotic differences between the radiated and sham radiated mice (Supplemental Figure 1).

miR-29B AND miR-146B EXPRESSION LEVELS, AND THEIR TARGETS, REACT TO IRRADIATION IN VITRO. Using a biological irradiator, we exposed human carotid artery SMCs and endothelial cells (HCtASMCs and HCtAECs) to 2 consecutive irradiation (radiotherapy) doses of 2 Gy, with 24 h between radiotherapy fractions, which was determined by the common clinical radiotherapy regimen for head and neck tumors (28). Radiotherapy significantly inhibited HCtASMC proliferation, which was statistically significant from 4 days after the last exposure (Supplemental Figures 2A and 2B). HCtAEC proliferation was not significantly affected (Supplemental Figure 2C). We measured miRNA and target gene expression 24 h after radiotherapy. In radiated

FIGURE 3 Irradiation Affects miR-29b, miR-146b, and Target Gene Expression In Vitro; Pathological Changes Are Partly Corrigible With miRNA Mimics

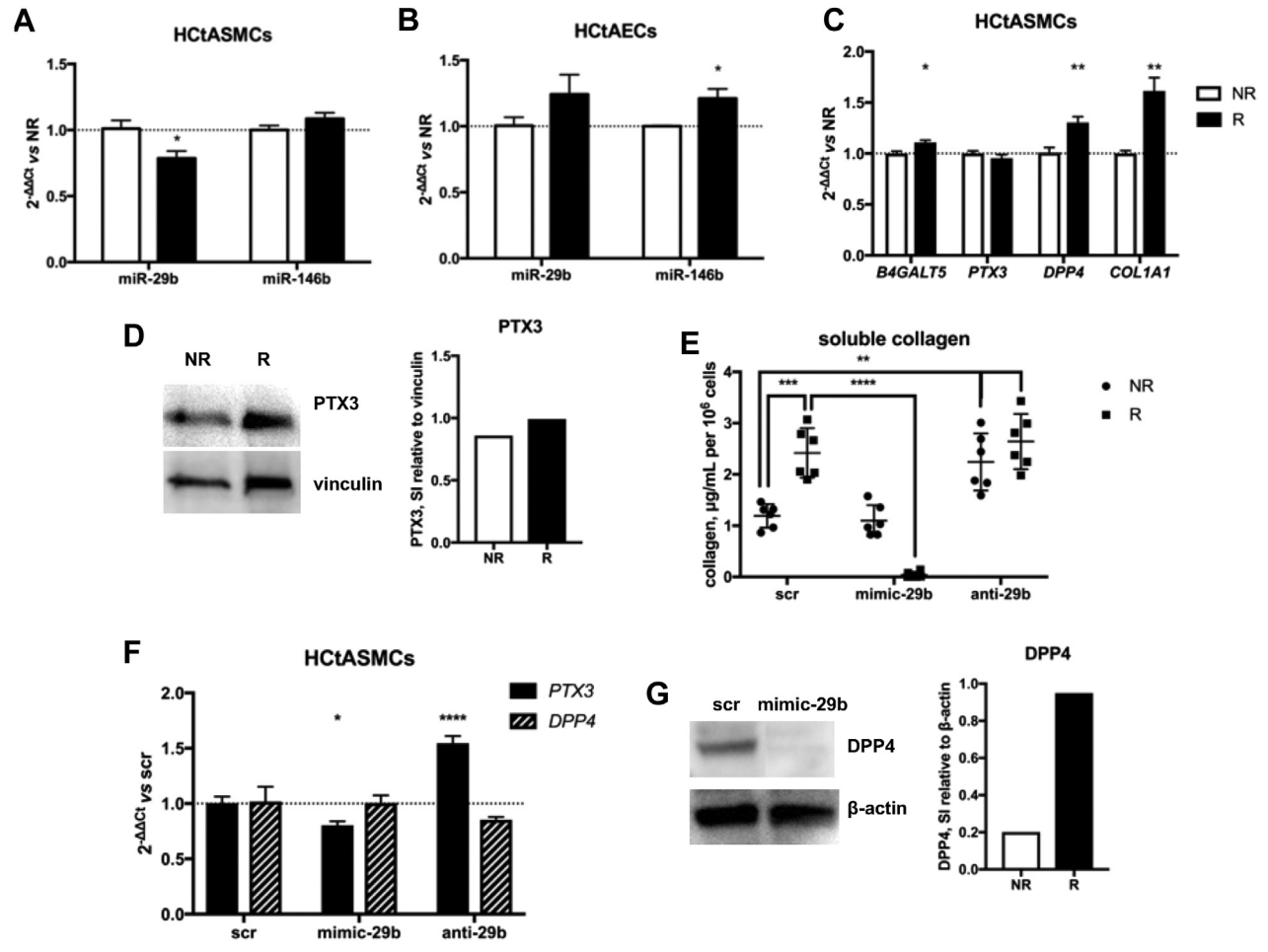

(A) In human carotid artery smooth muscle cells (HCtASMCs), 2 × 2 Gy of irradiation resulted in significantly reduced miR-29b expression; miR-146b expression was not affected. *p < 0.05. **(B)** The opposite was observed with human carotid artery endothelial cells (HCtAECs). *p < 0.05. **(C)** miR-29b target gene expression in HCtASMCs after irradiation. n = 6 in each group. Mean ± SEM. *p < 0.05, **p < 0.01 in Student's *t*-test. **(D)** Western blot analysis showed an increase in PTX3 protein expression after irradiation. **(E)** Treatment with miR-29b mimics resulted in undetectable soluble collagen in supernatant from radiated HCtASMCs but not from control HCtASMCs. **p < 0.01; ***p < 0.001; ****p < 0.0001. **(F)** miR-29b mimic treatment reduced *PTX3* expression in HCtASMCs. n = 6 in each group. Mean ± SEM. *p < 0.05, ****p < 0.0001 in 1-way analysis of variance. *DPP4* gene expression remained unchanged but was reduced on the protein level as shown with **(G)** Western blotting of HCtASMCs. Other abbreviations as in Figure 1.

HCtASMCs, but not in HCtAECs, miR-29b was down-regulated (Figure 3A). Radiated HCtAECs, but not HCtASMCs, exhibited up-regulation of miR-146b (Figure 3B). In HCtASMCs, expression of the miR-29b targets B4GALT5, DPP4, and COL1A1 was increased (Figure 3C). Although *PTX3* gene expression was not increased, Western blotting showed elevated levels of PTX3 protein in these cells (Figure 3D).

miR-29b is known to regulate extracellular matrix function by targeting collagen genes (29). Gamma radiation is well known to cause a TGF-β–mediated fibrotic response induced by fibroblasts (30) and SMCs (31). In radiated cells, a nonsignificant upward trend was observed in soluble collagen secretion, as measured in supernatant sampled 24 h after radiotherapy (Supplemental Figure 2D).

MODULATION OF miR-29B ALTERS EXPRESSION OF INFLAMMATION- AND FIBROSIS-RELATED TARGETS IN VITRO. Transfection of HCtASMCs with miR-29b mimics before radiotherapy completely abrogated soluble collagen secretion (Figure 3E) and decreased post-radiotherapy *PTX3* expression, whereas anti-miR-29b greatly stimulated *PTX3* expression

FIGURE 4 miR-29b Mimics Dampen Acute vRTx

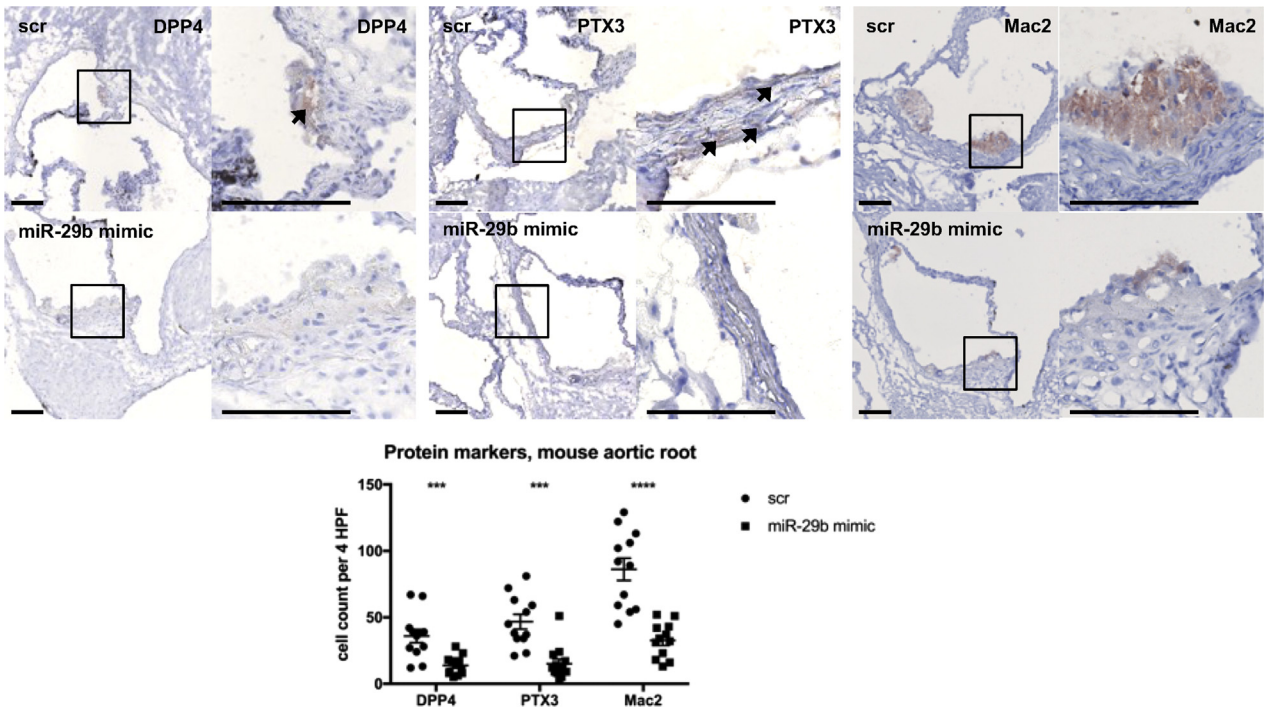

Jet-PEI–delivered miR-29b mimics caused decreased DPP4 protein expression in aortic root plaque, as well as a reduction in PTX3 protein in the vessel wall. Staining for the macrophage surface glycoprotein galectin-3 (Mac-2) revealed significantly increased macrophage influx in scrambled- compared with mimic-treated mice. Bars, 200 μm. n = 12 in each group. Mean ± SEM. ***p < 0.001, ****p < 0.0001 in 1-way analysis of variance. vRTx = radiation vasculopathy; other abbreviations as in Figure 1.

(Figure 3F). Interestingly, anti-miR-29b had no marked profibrotic effect in radiated cells, possibly because further suppression of already low miR-29b levels does not add to the fibrotic stimulus. In nonradiated cells, however, it induced a significant increase in soluble collagen production. Profibrotic DPP4 was not affected by miR-29b on the gene expression level, but Western blotting in HCtASMC lysates showed that expression of DPP4 protein was negatively affected by transfection with miR-29b mimics (Figure 3G). Because DPP4 has a soluble form, detectable in blood plasma and associated with a profibrotic phenotype, we assessed DPP4 expression in the supernatant of ECs or SMCs but could not detect the protein, independent of irradiation (data not shown).

MODULATION OF miR-29B AFFECTS TARGET PROTEIN EXPRESSION AND INFLAMMATION IN VIVO. We subjected 12 *Apoe*$^{-/-}$ male mice to the 1 × 14 Gy irradiation protocol, of which 6 received miR-29b mimics 1 day before and 1 day after irradiation. Target genes *Ptx3* and *Dpp4* were not significantly affected (Supplemental Figure 3A), but on the protein level, PTX3 and DPP4 expression showed marked differences in the medial layer of aortic ring tissue in scrambled- versus mimic-treated mice (Figure 4, left 2 panels). Staining for the macrophage surface glycoprotein galectin 3 (Mac-2) revealed marked macrophage influx in aortic ring atherosclerotic plaques of scrambled- compared with miR-29b mimic-treated mice (Figure 4, right panel). Smooth muscle actin staining revealed no differences in SMC quantity between miR-29b mimic-treated and control mice (Supplemental Figure 3B). Collectively, miR-29b mimics dampened the direct inflammatory reaction to irradiation, without affecting SMC content.

DISCUSSION

Irradiation is an important risk factor for atherosclerosis and subsequent cardiovascular disease (32,33). As master regulators in many cellular processes initiated by vascular injury, miRNAs can be crucial actors in vRTx. miRNAs play a crucial role in the DNA damage

response (22), and miRNA inhibition or stimulation can blunt irradiation effects on cell survival and proliferation (34). We have identified 2 miRNAs known to play a crucial role in vascular cell biology and pathology in relation to atherosclerosis, miR-29b and miR-146b, to be down- respectively up-regulated in irradiated vascular tissue. The expression of 2 well-known vascular miRNAs, miR-143 and miR-145, was also altered, but they were not further investigated; we consider that down-regulation of the atheroprotective miR-143-145 cluster as confirmation that irradiation induces an atheroprone phenotype.

miR-146a and miR-146b arise from 2 evolutionarily conserved miRNA genes located on chromosomes 5 and 10, respectively. In their mature form, they differ only by 2 nucleotides in the 3′ end. miR-146b, unlike miR-146a, is responsive to interleukin-10 and therefore might be involved in inflammation resolution (35). Enforced miR-146b expression in monocytes reduces production of a multitude of inflammatory cytokines (35,36), suggesting that this miRNA is part of a negative feedback loop limiting inflammation (37). We observed up-regulation of miR-146b in irradiated human arterial tissue. It is likely that this up-regulation is symptomatic of the chronic inflammatory response in vRTx and can be seen as an attempt to resolve inflammation. Inhibition of miR-146b would likely aggravate the inflammatory reaction and therefore be counterproductive; potentially beneficial effects of miR-146b mimics could be a direction for further investigation.

The miR-29 family of miRNAs consists of miR-29a and miR-29b-1, of which the encoding gene is located on chromosome 7, and miR-29b-2 and miR-29c, originating from chromosome 1. miR-29b-1 and miR-29b-2 have identical mature sequences, are therefore indistinguishable on polymerase chain reaction, and share the name miR-29b. In a vascular biological context, miR-29b is best known as regulator of the collagen- and extracellular matrix–associated mRNAs critically involved in cardiovascular fibrosis (38). miR-29b limits collagen gene expression and thus can weaken the vascular wall in abdominal aortic aneurysms (39), as well as the matrix of fibrous caps in atherosclerosis (40). Strategies of inhibiting miR-29b are thus an attractive option for increasing vessel wall and lesion stability. In vRTx, conversely, excess collagen production and turnover is pathognomonic for the maladaptive healing response. Inhibition of collagen production through miR-29b stimulation might therefore put an end to the downward spiral of inflammation and fibrosis in vRTx.

DPP4 (also known as CD26) is a transmembrane glycoprotein with an extracellular domain binding to adenosine deaminase and matrix proteins such as fibronectin and collagen (41). The function of DPP4 in vascular disease is under intensive investigation because its inhibitor, alogliptin (a novel glucose-lowering agent in the treatment of type 2 diabetes mellitus), displays antiatherogenic effects in low-density lipoprotein receptor knockout (42) and *Apoe*$^{-/-}$ mice (43). In addition, DPP4/CD26 indicates a type of fibroblasts with an increased profibrotic potential responsible for wounding- and irradiation-induced skin fibrosis and scarring, as well as tumor growth, through activation of the serine protease fibroblast activation protein-α (26). DPP4 has previously been proposed as a target of miR-29b (44), an interaction we were able to confirm in the vRTx context.

PTX3 is a secreted pattern recognition molecule providing resistance against fungal, bacterial, and viral pathogens. Together with its family members C-reactive protein and serum amyloid P component, it initiates complement activation and phagocytosis. In contrast to C-reactive protein, PTX3 is evolutionarily well conserved (45) and expressed within the vasculature, making it a good target to study in humans as well as animal models within this context. Interestingly, PTX3 has inflammatory as well as regulatory capacities, as its release induces both proinflammatory and anti-inflammatory signaling (46,47). PTX3 is a validated target of miR-29b (48) and a key regulatory protein in pathophysiological processes in which innate immunity, inflammation, and extracellular matrix remodeling intersect (45).

In vRTx, we have previously described sustained high expression of *PTX3* mRNA at earlier time points after radiotherapy (24). The current study is the first to describe gene expression patterns in irradiated human arteries at a median of >2 years after radiotherapy. Tissue damage caused by radiation injury is commonly divided into early and late adverse effects, according to the time elapsed from treatment to symptoms. Early adverse effects typically affect rapidly proliferating cells, such as epithelial cells of the skin and mucosa, whereas late adverse effects often are an effect of a progressive, systemic disease in which symptoms may not be evident until decades after radiotherapy (49,50).

STUDY LIMITATIONS. vRTx is the result of a pathologic stimulus (irradiation), creating a cascade of inflammatory reactions. Depending on timing after irradiation, various maladaptive vascular changes can

be observed, and timing of (preventive) therapy appears crucial. This study proposes miR-29b overexpression as a potential preventive therapy, but could not identify an optimal administration time-point, which in part relates to the experimental murine model not completely being able to reflect all moieties of human radiotherapy-induced disease. The lack of an ideal in vivo model that is able to mimic the various features of human disease remains problematic for most cardiovascular diseases. Furthermore, other miRNAs and targets that were not assessed by us, might likely also play important roles in vRTx and could be modulated to prevent the disease. Their effects remain to be elucidated in further studies.

CONCLUSIONS

In vivo and in vitro, we showed that PTX3 and DPP4 expression are hallmarks of radiation injury to vascular tissues and can be suppressed with miR-29b mimics. These findings not only suggest that stimulation of miR-29b can be a candidate therapy to prevent vRTx but also stress the importance of a cautious approach when considering miR-29b inhibition as therapy against various atherosclerotic disease manifestations. In patients with vRTx associated with perivascular fibrosis (51), miR-29b stimulation, rather than inhibition, might be the most effective treatment.

ACKNOWLEDGMENTS The Swedish Radiation Safety Authority provides advice and information in the event of a nuclear energy accident as well as any other incident or accident involving radiation.

ADDRESS FOR CORRESPONDENCE: Dr. Lars Maegdefessel, Karolinska Institute, Department of Medicine, Solna, 171 76 Stockholm, Sweden. E-mail: lars.maegdefessel@ki.se.

PERSPECTIVES

COMPENTENCY IN MEDICAL KNOWLEDGE: Radiotherapy is an established and powerful therapeutic strategy for the treatment of patients with cancer. The downside for this form of curative approach is a substantial increase in cardiovascular complications. Thus, supportive treatment schemes need to be developed to limit the risk and burden of radiotherapy-induced vasculopathies. The targeting of miRNAs via antisense oligonucleotides could serve as a sufficient and effective approach to limit the multiple features (inflammation, fibrosis, and proliferation) associated with radiotherapy-induced vasculopathies.

TRANSLATIONAL OUTLOOK: Safety and efficiency of miRNA mimics are currently under investigation, and interestingly a Phase II clinical trial utilizing miR-29 mimics (promiR-29, Remlarsen) is ongoing in cutaneous fibrotic disorders. Here, mimics are being applied topically to the skin, which limits undesired off-target effects in organ systems in which systemically administered miRNA modulators assimilate to a much higher degree (e.g., liver, kidney). For the treatment of vascular diseases, cell type–specific or local ways of delivery (using stents and balloons) could limit off-target effects, while triggering local uptake and efficiency of these potent therapies.

REFERENCES

1. DeSantis CE, Lin CC, Mariotto AB, et al. Cancer treatment and survivorship statistics, 2014. CA Cancer J Clin 2014;64:252–71.

2. Shahrokni A, Wu AJ, Carter J, Lichtman SM. Long-term toxicity of cancer treatment in older patients. Clin Geriatr Med 2016;32:63–80.

3. Groarke JD, Nguyen PL, Nohria A, Ferrari R, Cheng S, Moslehi J. Cardiovascular complications of radiation therapy for thoracic malignancies: the role for non-invasive imaging for detection of cardiovascular disease. Eur Heart J 2014;35:612–23.

4. Jaworski C, Mariani JA, Wheeler G, Kaye DM. Cardiac complications of thoracic irradiation. J Am Coll Cardiol 2013;61:2319–28.

5. Plummer C, Henderson RD, O'Sullivan JD, Read SJ. Ischemic stroke and transient ischemic attack after head and neck radiotherapy: a review. Stroke 2011;42:2410–8.

6. Darby SC, Ewertz M, McGale P, et al. Risk of ischemic heart disease in women after radiotherapy for breast cancer. N Engl J Med 2013;368:987–98.

7. Nilsson G, Holmberg L, Garmo H, et al. Distribution of coronary artery stenosis after radiation for breast cancer. J Clin Oncol 2012;30:380–6.

8. Gujral DM, Chahal N, Senior R, Harrington KJ, Nutting CM. Radiation-induced carotid artery atherosclerosis. Radiother Oncol 2014;110:31–8.

9. Abayomi OK. Neck irradiation, carotid injury and its consequences. Oral Oncol 2004;40:872–8.

10. Fosnot J, Fischer JP, Smartt JM Jr., et al. Does previous chest wall irradiation increase vascular complications in free autologous breast reconstruction? Plast Reconstr Surg 2011;127:496–504.

11. Herle P, Shukla L, Morrison WA, Shayan R. Preoperative radiation and free flap outcomes for head and neck reconstruction: a systematic review and meta-analysis. ANZ J Surg 2015;85:121–7.

12. Halle M, Bodin I, Tornvall P, Wickman M, Farnebo F, Arnander C. Timing of radiotherapy in head and neck free flap reconstruction—a study of postoperative complications. J Plast Reconstr Aesthet Surg 2009;62:889–95.

13. Halle M, Gabrielsen A, Paulsson-Berne G, et al. Sustained inflammation due to nuclear factor-kappa B activation in irradiated human arteries. J Am Coll Cardiol 2010;55:1227–36.

14. Libby P, Ridker PM, Hansson GK. Progress and challenges in translating the biology of atherosclerosis. Nature 2011;473:317–25.

15. Tall J, Bjorklund TC, Skogh AC, Arnander C, Halle M. Vascular complications after radiotherapy in head and neck free flap reconstruction: clinical outcome related to vascular biology. Ann Plast Surg 2015;75:309–15.

16. Bartel DP. MicroRNAs: target recognition and regulatory functions. Cell 2009;136:215–33.

17. Ebert MS, Sharp PA. Roles for microRNAs in conferring robustness to biological processes. Cell 2012;149:515–24.

18. Gomez IG, MacKenna DA, Johnson BG, et al. Anti-microRNA-21 oligonucleotides prevent Alport nephropathy progression by stimulating metabolic pathways. J Clin Invest 2015;125:141–56.

19. Janssen HL, Reesink HW, Lawitz EJ, et al. Treatment of HCV infection by targeting microRNA. N Engl J Med 2013;368:1685–94.

20. Schober A, Nazari-Jahantigh M, Weber C. MicroRNA-mediated mechanisms of the cellular stress response in atherosclerosis. Nat Rev Cardiol 2015;12:361–74.

21. van Rooij E, Olson EN. MicroRNA therapeutics for cardiovascular disease: opportunities and obstacles. Nat Rev Drug Discov 2012;11:860–72.

22. Wan G, Mathur R, Hu X, Zhang X, Lu X. miRNA response to DNA damage. Trends Biochem Sci 2011;36:478–84.

23. Li Y, Challagundla KB, Sun XX, Zhang Q, Dai MS. MicroRNA-130a associates with ribosomal protein L11 to suppress c-Myc expression in response to UV irradiation. Oncotarget 2015;6:1101–14.

24. Christersdottir Bjorklund T, Reilly SJ, Gahm C, et al. Increased long-term expression of pentraxin 3 in irradiated human arteries and veins compared to internal controls from free tissue transfers. J Translat Med 2013;11:223.

25. Hsu SD, Lin FM, Wu WY, et al. miRTarBase: a database curates experimentally validated microRNA-target interactions. Nucleic Acids Res 2011;39:D163–9.

26. Rinkevich Y, Walmsley GG, Hu MS, et al. Skin fibrosis. Identification and isolation of a dermal lineage with intrinsic fibrogenic potential. Science 2015;348:aaa2151.

27. Stewart FA, Heeneman S, Te Poele J, et al. Ionizing radiation accelerates the development of atherosclerotic lesions in ApoE-/- mice and predisposes to an inflammatory plaque phenotype prone to hemorrhage. Am J Pathol 2006;168:649–58.

28. Bartelink H, Van den Bogaert W, Horiot JC, Jager J, van Glabbeke M. Concomitant cisplatin and radiotherapy in a conventional and modified fractionation schedule in locally advanced head and neck cancer: a randomised phase II EORTC trial. Eur J Cancer 2002;38:667–73.

29. Kriegel AJ, Liu Y, Fang Y, Ding X, Liang M. The miR-29 family: genomics, cell biology, and relevance to renal and cardiovascular injury. Physiol Genomics 2012;44:237–44.

30. Burger A, Loffler H, Bamberg M, Rodemann HP. Molecular and cellular basis of radiation fibrosis. Int J Radiat Biol 1998;73:401–8.

31. Alexakis C, Guettoufi A, Mestries P, et al. Heparan mimetic regulates collagen expression and TGF-beta1 distribution in gamma-irradiated human intestinal smooth muscle cells. FASEB J 2001;15:1546–54.

32. Gray K, Kumar S, Figg N, et al. Effects of DNA damage in smooth muscle cells in atherosclerosis. Circ Res 2015;116:816–26.

33. Bashar K, Healy D, Clarke-Moloney M, Burke P, Kavanagh E, Walsh SR. Effects of neck radiation therapy on extra-cranial carotid arteries atherosclerosis disease prevalence: systematic review and a meta-analysis. PLoS One 2014;9:e110389.

34. Wagner-Ecker M, Schwager C, Wirkner U, Abdollahi A, Huber PE. MicroRNA expression after ionizing radiation in human endothelial cells. Radiat Oncol 2010;5:25.

35. Curtale G, Mirolo M, Renzi TA, Rossato M, Bazzoni F, Locati M. Negative regulation of Toll-like receptor 4 signaling by IL-10-dependent microRNA-146b. Proc Natl Acad Sci U S A 2013;110:11499–504.

36. Hulsmans M, Van Dooren E, Mathieu C, Holvoet P. Decrease of miR-146b-5p in monocytes during obesity is associated with loss of the anti-inflammatory but not insulin signaling action of adiponectin. PLoS One 2012;7:e32794.

37. Cheng HS, Sivachandran N, Lau A, et al. MicroRNA-146 represses endothelial activation by inhibiting pro-inflammatory pathways. EMBO Mol Med 2013;5:949–66.

38. van Rooij E, Sutherland LB, Thatcher JE, et al. Dysregulation of microRNAs after myocardial infarction reveals a role of miR-29 in cardiac fibrosis. Proc Natl Acad Sci U S A 2008;105:13027–32.

39. Maegdefessel L, Azuma J, Toh R, et al. Inhibition of microRNA-29b reduces murine abdominal aortic aneurysm development. J Clin Invest 2012;122:497–506.

40. Ulrich V, Rotllan N, Araldi E, et al. Chronic miR-29 antagonism promotes favorable plaque remodeling in atherosclerotic mice. EMBO Mol Med 2016;8:643–53.

41. Zhong J, Maiseyeu A, Davis SN, Rajagopalan S. DPP4 in cardiometabolic disease: recent insights from the laboratory and clinical trials of DPP4 inhibition. Circ Res 2015;116:1491–504.

42. Akita K, Isoda K, Shimada K, Daida H. Dipeptidyl-peptidase-4 inhibitor, alogliptin, attenuates arterial inflammation and neointimal formation after injury in low-density lipoprotein (LDL) receptor-deficient mice. J Am Heart Assoc 2015;4:e001469.

43. Ta NN, Schuyler CA, Li Y, Lopes-Virella MF, Huang Y. DPP-4 (CD26) inhibitor alogliptin inhibits atherosclerosis in diabetic apolipoprotein E-deficient mice. J Cardiovasc Pharmacol 2011;58:157–66.

44. Shi S, Koya D, Kanasaki K. Dipeptidyl peptidase-4 and kidney fibrosis in diabetes. Fibrogenesis Tissue Repair 2016;9:1.

45. Mantovani A, Garlanda C, Doni A, Bottazzi B. Pentraxins in innate immunity: from C-reactive protein to the long pentraxin PTX3. J Clin Immunol 2008;28:1–13.

46. Bottazzi B, Doni A, Garlanda C, Mantovani A. An integrated view of humoral innate immunity: pentraxins as a paradigm. Annu Rev Immunol 2010;28:157–83.

47. Garlanda C, Jaillon S, Doni A, Bottazzi B, Mantovani A. PTX3, a humoral pattern recognition molecule at the interface between microbe and matrix recognition. Curr Opin Immunol 2016;38:39–44.

48. Abonnenc M, Nabeebaccus AA, Mayr U, et al. Extracellular matrix secretion by cardiac fibroblasts: role of microRNA-29b and microRNA-30c. Circ Res 2013;113:1138–47.

49. Stone HB, Coleman CN, Anscher MS, McBride WH. Effects of radiation on normal tissue: consequences and mechanisms. Lancet Oncol 2003;4:529–36.

50. Darby S, McGale P, Peto R, Granath F, Hall P, Ekbom A. Mortality from cardiovascular disease more than 10 years after radiotherapy for breast cancer: nationwide cohort study of 90 000 Swedish women. BMJ 2003;326:256–7.

51. Khan AA, Paget JT, McLaughlin M, Kyula JN, et al. Genetically modified lentiviruses that preserve microvascular function protect against late radiation damage in normal tissues. Sci Transl Med 2018;10(425).

KEY WORDS arteriosclerosis, inflammation, microRNA, radiotherapy

APPENDIX For an expanded Methods section as well as supplemental tables and figures, please see the online version of this paper.

JACC: BASIC TO TRANSLATIONAL SCIENCE VOL. 4, NO. 1, 2019

PRECLINICAL RESEARCH

Connective Tissue Growth Factor Inhibition Enhances Cardiac Repair and Limits Fibrosis After Myocardial Infarction

Laura E. Vainio, MD,[a,b] Zoltán Szabó, MSc,[a,b] Ruizhu Lin, MSc,[a] Johanna Ulvila, PhD,[a] Raisa Yrjölä, MSc,[a] Tarja Alakoski, MSc,[a,b] Jarkko Piuhola, MD, PhD,[c] Walter J. Koch, PhD,[d] Heikki Ruskoaho, MD, PhD,[e] Shaun D. Fouse, PhD,[f] Todd W. Seeley, PhD,[f] Erhe Gao, MD, PhD,[d] Pierre Signore, PhD,[f] Kenneth E. Lipson, PhD,[f] Johanna Magga, PhD,[a,b] Risto Kerkelä, MD, PhD[a,g]

VISUAL ABSTRACT

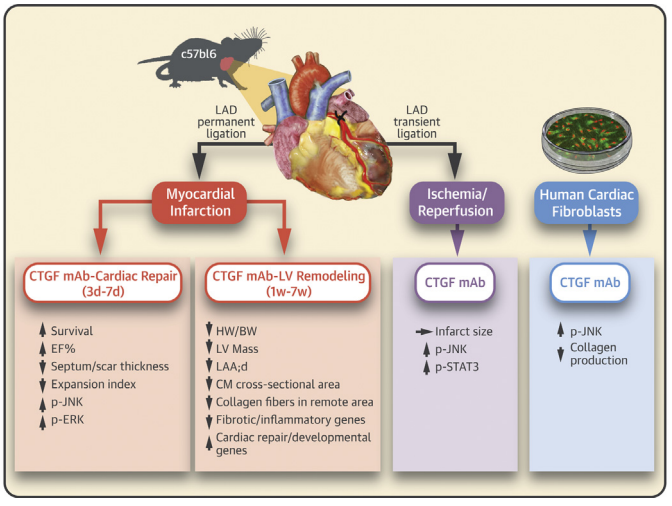

Vainio, L.E. et al. J Am Coll Cardiol Basic Trans Science. 2019;4(1):83–94.

HIGHLIGHTS

- To study the role of CTGF in post-MI cardiac repair and LV remodeling, we antagonized the function of CTGF with a mAb.
- Treatment of mice with CTGF mAb during post-MI cardiac repair improved survival and resulted in better preserved LV systolic function.
- Treatment with CTGF mAb during post-MI LV remodeling reduced the heart weight to body weight ratio, LV mass, cardiomyocyte hypertrophy, and fibrosis in the remote nonischemic myocardium.
- CTGF mAb treatment induced c-Jun N-terminal kinase phosphorylation in ischemic hearts in vivo and in cultured human cardiac fibroblasts.
- In conclusion, treatment of mice with CTGF mAb in a model of MI enhances cardiac repair and reduces adverse post-MI LV remodeling.

From the [a]Research Unit of Biomedicine, Department of Pharmacology and Toxicology, University of Oulu, Oulu, Finland; [b]Biocenter Oulu, University of Oulu, Oulu, Finland; [c]Division of Cardiology, Department of Internal Medicine, Oulu University Hospital and University of Oulu, Oulu, Finland; [d]Center for Translational Medicine, Lewis Katz School of Medicine, Temple University, Philadelphia, Pennsylvania; [e]Division of Pharmacology and Pharmacotherapy, Faculty of Pharmacy, University of Helsinki, Helsinki, Finland; [f]FibroGen, Inc., San Francisco, California; and the [g]Medical Research Center Oulu, Oulu University Hospital and University of Oulu, Oulu, Finland. Drs. Vainio, Magga, and Kerkelä were supported by the Finnish Foundation for Cardiovascular Research. Dr. Vainio was supported by the Finnish Medical Foundation. Dr. Magga was supported by grant 268505 from the Academy of Finland. Dr. Kerkelä was supported by grants 131020 and 297094 from the Academy of Finland, by the Sigrid Juselius Foundation, and by the Jane and Aatos Erkko Foundation. Drs. Fouse, Seeley, Signore, and Lipson hold stock in FibroGen. All other authors have reported that they have no relationships relevant to the contents of this paper to disclose.
All authors attest they are in compliance with human studies committees and animal welfare regulations of the authors' institutions and Food and Drug Administration guidelines, including patient consent where appropriate. For more information, visit the *JACC: Basic to Translational Science* author instructions page.

Manuscript received August 24, 2018; revised manuscript received October 22, 2018, accepted October 23, 2018.

ISSN 2452-302X https://doi.org/10.1016/j.jacbts.2018.10.007

ABBREVIATIONS AND ACRONYMS

CTGF = connective tissue growth factor

ECM = extracellular matrix

ERK = extracellular signal-regulated kinase

FB = fibroblast

I/R = ischemia–reperfusion

HF = heart failure

Ig = immunoglobulin

JNK = c-Jun N-terminal kinase

LV = left ventricular

mAb = monoclonal antibody

MI = myocardial infarction

TGF = transforming growth factor

SUMMARY

Myocardial infarction (MI)–induced cardiac fibrosis attenuates cardiac contractile function, and predisposes to arrhythmias and sudden cardiac death. Expression of connective tissue growth factor (CTGF) is elevated in affected organs in virtually every fibrotic disorder and in the diseased human myocardium. Mice were subjected to treatment with a CTGF monoclonal antibody (mAb) during infarct repair, post-MI left ventricular (LV) remodeling, or acute ischemia–reperfusion injury. CTGF mAb therapy during infarct repair improved survival and reduced LV dysfunction, and reduced post-MI LV hypertrophy and fibrosis. Mechanistically, CTGF mAb therapy induced expression of cardiac developmental and/or repair genes and attenuated expression of inflammatory and/or fibrotic genes. (J Am Coll Cardiol Basic Trans Science 2019;4:83–94)

Heart disease is the leading cause of death in the western world with almost one-half of those deaths attributable to coronary heart disease (1). In response to cardiac stresses, such as myocardial infarction (MI), the heart undergoes structural and functional remodeling, with cardiomyocyte hypertrophy and excessive production of the extracellular matrix (ECM) as typical features (2). Molecular mechanisms that underlie cardiac fibrotic disorders are still mostly unclear, and no specific therapies exist for treatment of myocardial fibrosis.

SEE PAGE 95

Connective tissue growth factor (CTGF/CCN2) belongs to the CCN family (Connective tissue growth factor [CTGF], Cystein rich protein [CYR61], and Nephroblastoma overexpressed [NOV]) of matricellular proteins that consists of 6 homologous cysteine-rich proteins (3). Dysregulation of CCN protein expression or activities takes place in chronic inflammation or tissue injury, such as fibrosis, atherosclerosis, restenosis after vascular injury, arthritis, cancer, diabetic nephropathy, and retinopathy (3,4). CTGF expression is elevated in human fibrotic diseases of virtually every organ or tissue (4). Patients with heart failure (HF) show elevated levels of plasma CTGF, which correlates with the severity of the disease (5). Plasma levels of CTGF are also useful in differentiating acute HF patients from patients with other causes of dyspnea and peripheral edema (6). CTGF expression in the myocardium is also induced in various animal models of myocardial fibrosis (for review, see Daniels et al. [7] and Leask [8]). Cardiomyocyte-specific overexpression of CTGF in transgenic mice alone did not induce fibrosis but did enhance pressure overload–induced cardiac fibrosis (9). On the other hand, pressure overload induced fibrosis was not attenuated in mice where CTGF was deleted in cardiomyocytes and cardiac fibroblasts (10), but not from other cell types in which CTGF may have been produced (11). However, no data are available from studies in which the function of CTGF was antagonized in the ischemic heart or during post-MI fibrotic remodeling.

FG-3019 (pamrevlumab) is a human monoclonal antibody (mAb) against CTGF that has shown efficacy in a randomized, placebo-controlled phase 2 clinical trial in subjects with idiopathic pulmonary fibrosis (12), as well as in phase 2 clinical trials for treatment of pancreatic cancer and Duchenne muscular dystrophy (NCT02210559 and NCT02606136, respectively). A chimeric antibody, designated FG-3149, has the binding motif of FG-3019 and a mouse IgG2a constant region. FG-3149 binds CTGF with similar affinity as FG-3019 but is less immunogenic in rodents than the human antibody. FG-3149 has shown activity in animal models of bronchopulmonary dysplasia (13), pressure overload–induced HF (14), and genetic cardiomyopathy (15,16). In the present study, we aimed to investigate the role of CTGF in cardiac repair following MI, in post-MI cardiac fibrosis, and in acute ischemia–reperfusion (I/R) injury.

METHODS

STUDY DESIGN. The experimental design was approved by Animal Experiment Committee in State Provincial Office of Southern Finland, and the methods were carried out in accordance with the national regulations of the usage and welfare of laboratory animals. Mice were subjected to MI by permanent ligation of the left anterior descending coronary artery or to I/R injury by transient ligation of the left anterior descending coronary artery, and treated with either CTGF mAb or control mouse immunoglobulin-G (IgG). The protocols are shown in **Figure 1**. A more detailed description of Methods is available in the Supplemental Material.

RNA SEQUENCING ANALYSIS. RNAseq analysis was performed via single-end sequencing chemistry at a 75 base-pair read length (Illumina NextSeq, Illumina, Inc., San Diego, California). Sequences were de-multiplexed, and FASTQ generation was performed (Basespace, Illumina). Sequences were aligned to 10 mm, annotated using the RefSeq Gene 2013.04.01 build, and gene expression levels were quantitated using reads per kilobase of transcript, per million mapped reads (RPKM, Strand NGS, Strand Life Sciences, Bengaluru, India). Genes with a raw read count of >20 in at least 1 sample were used for further analysis. Altered transcripts were defined as having a >1.5-fold difference in expression at $p < 0.05$ (*t*-test). Gene ontology analysis was performed using gene ontology consortium software (17,18). To identify common upstream regulators, gene sets were loaded into Pathway Studio MammalPlus 12.0.1.9 (Elsevier, Amsterdam, the Netherlands), and links to common regulators were identified.

STATISTICAL ANALYSIS. Statistical analysis was performed with SPSS software (IBM, Armonk, New York). When 2 groups were compared, Student's *t*-test or Mann-Whitney U test was performed. To compare multiple groups, 1-way analysis of variance was used, followed by Tukeys's post hoc test to compare all the groups or Dunnett's post hoc test to compare other groups with the control IgG-treated MI or I/R group. The Kruskall-Wallis test was performed when data did not represent normal distribution. Survival analysis was calculated by the Kaplan-Meier method, and groups were compared by the log-rank (Mantel-Cox) test. Data are shown as mean ± SD. Differences were considered statistically significant at $p < 0.05$.

RESULTS

THERAPY WITH CTGF mAb DURING POST-MI CARDIAC REPAIR IMPROVES SURVIVAL (STUDY I). To investigate for the effect of CTGF mAb during cardiac repair after MI, mice were subjected to experimental MI, and 3 days after ligation, treatment began with either IgG or CTGF mAb for 4 days (Study I) (Figure 1). CTGF mAb significantly improved post-MI survival ($p < 0.05$) (Figure 2A). Echocardiography analysis at 7 days post-MI showed better preserved LV systolic function in mice treated with CTGF mAb compared with mice treated with control IgG (ejection fraction: 27.1 ± 5.2% vs. 16.3 ± 3.4%; $p < 0.05$) (Figure 2B, Table 1). No difference was observed in LV diameter or LV posterior wall thickness (Figure 2B, Table 1). Analysis for inflammation in the infarcted area by CD45 staining showed no difference between MI groups, and no difference was observed in expression of inflammatory genes in the remote LV between the MI groups (Supplemental Figure 1). Histological analysis of LV sections showed a decrease in septum thickness versus the scar thickness ratio in CTGF mAb–treated mice compared with control IgG-treated mice, which resulted in an observed decrease in the infarct expansion index (Figure 2C). Analysis for collagen content in the remote zone showed no difference between the experimental groups (Figure 2D). Analysis for central signaling pathways from the infarct scar showed induction of extracellular signal-regulated kinase (ERK) and c-Jun N-terminal kinase 2 (JNK2) phosphorylation in MI hearts treated with CTGF mAb (Figure 2E). No difference was observed in p38 or SMAD2 signaling between the MI groups (Figure 2E).

FIGURE 1 Summary of Experimental Protocols

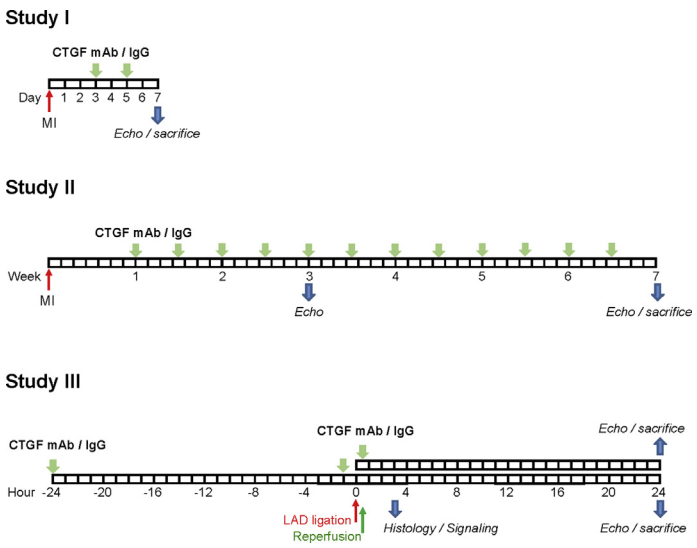

Study I, protocol for inhibition of connective tissue growth factor (CTGF) during post–myocardial infarction (MI) cardiac repair (treatment initiation on day 3, treatment completion on day 7). Study II, protocol for CTGF inhibition during post-MI cardiac remodeling (treatment initiation on day 7, treatment completion at the end of week 7). Study III, protocol for CTGF inhibition during and/or after acute ischemia (treatment 24 and 1 h before ischemia or only at reperfusion). IgG = immunoglobulin-G; LAD = left anterior descending; mAb = monoclonal antibody.

CTGF mAb REDUCES POST-MI LV HYPERTROPHY AND FIBROSIS (STUDY II). To investigate for the potential of CTGF mAb in post-MI remodeling, mice were subjected to experimental MI, and 1 week later treatment began with either control IgG or CTGF mAb for 6 weeks (Study II) (Figure 1). There was no difference in overall survival in MI groups because only 1 mouse was lost in the IgG group and none were lost in CTGF mAb group during the treatments. Two weeks

FIGURE 2 CTGF mAb Enhances LV Function (Study I)

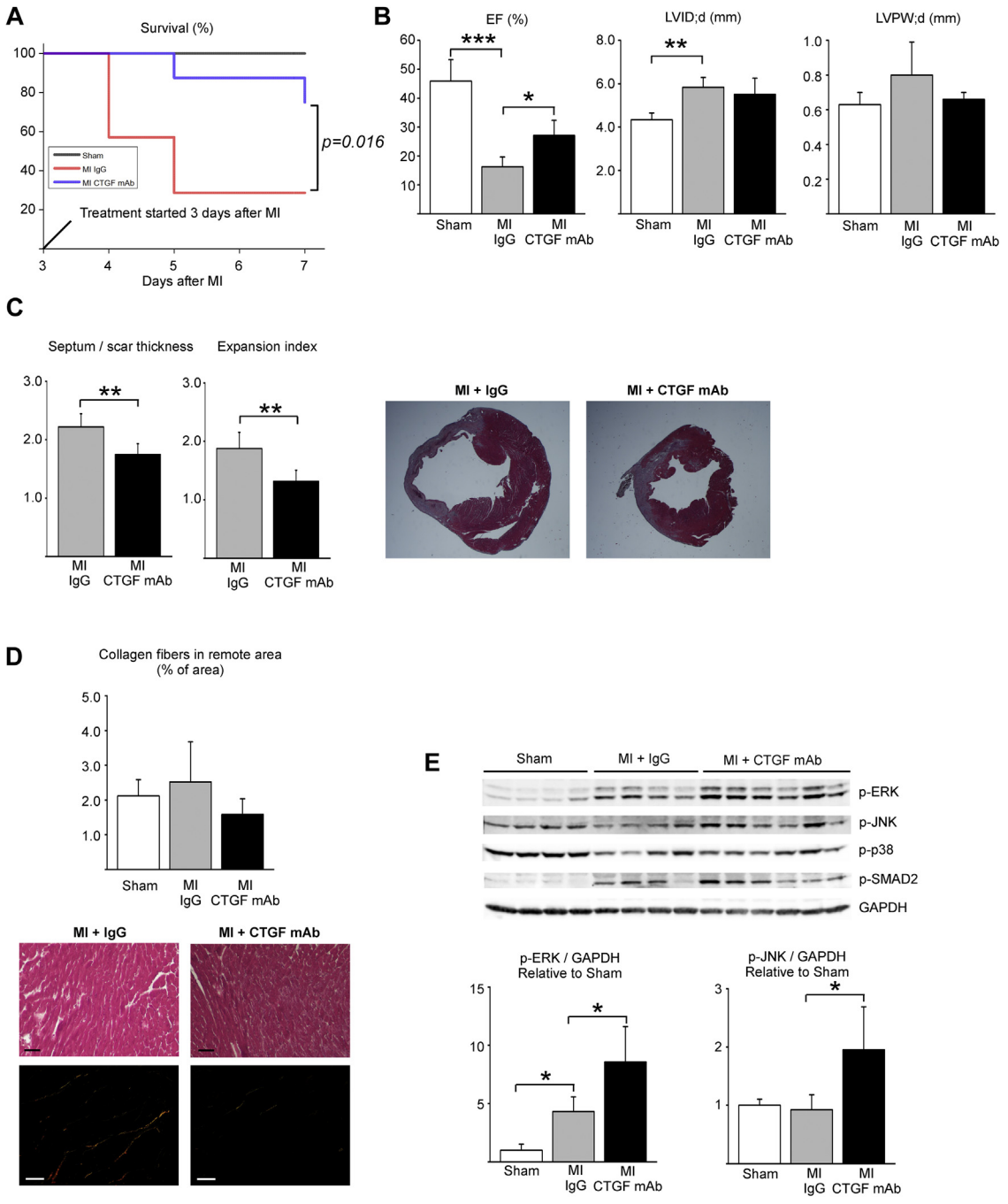

Mice were subjected to MI, and 3 days after surgery randomly divided to receive either IgG vehicle or CTGF mAb for 4 days. **(A)** Survival of animals during the experiment. **(B)** Left ventricular (LV) ejection fraction (EF), end-diastolic dimension (LVID;d), and posterior wall thickness (LVPW;d) were analyzed by echocardiography at 7 days after MI injury. **(C)** Ratio of thickness of septum versus thickness of infarct and the infarct expansion index. **(D)** Analysis of interstitial fibrosis from picrosirius red–stained LV sections under polarized light. Masson's trichrome-stained sections from the same tissue block are also shown. Scale bar: 50 μm. **(E)** Western blot analysis of LV samples from infarct areas for phosphorylated extracellular signal-regulated kinase (p-ERK), c-Jun N-terminal kinase (p-JNK), p38, and SMAD2. Glyceraldehyde 3-phosphate dehydrogenase (GAPDH) was used as loading control. Data are presented as mean ± SD; number of animals was sham (n = 4), IgG (n = 5), and CTGF mAb (n = 8). *p < 0.05; **p < 0.01; ***p < 0.001. Abbreviations as in Figure 1.

after initiating treatment, echocardiography analysis showed no difference in LV structure or function between the MI groups (Supplemental Table 1). Analysis of harvested hearts after 6 weeks showed that CTGF mAb treatment resulted in a reduced heart weight to body weight ratio compared with the IgG-treated mice ($p < 0.01$) (**Figure 3A**). Echocardiography analysis at 6 weeks showed that mice treated with CTGF mAb had significantly lower LV mass and left atrial size ($p < 0.01$ and $p < 0.05$, respectively) (**Figure 3A**). No difference was observed in LV systolic function. Full echocardiography data are listed in Supplemental Table 2.

Cardiomyocyte size was increased in both MI groups compared with sham-operated mice, but treatment with CTGF mAb significantly reduced the MI-induced increase in cardiomyocyte hypertrophy (**Figure 3B**). Histological analysis of hearts subjected to experimental MI showed that CTGF mAb treatment significantly attenuated the increase in capillary size in the LV ($p < 0.05$) without changing the capillary density (**Figure 3C**). Picrosirius red staining showed reduction in MI-induced fibrosis in the remote, non-ischemic myocardium in mice treated with CTGF mAb compared with MI mice treated with IgG (**Figure 3D**) ($p < 0.01$). Determination of length of infarction showed no difference between the MI groups (Supplemental Figure 2).

TABLE 1 CTGF mAb Therapy During Post-MI Cardiac Repair Enhances LV Function (Study I)

	Sham (n = 4)	MI + IgG (n = 5)	MI + CTGF mAb (n = 8)
LVEDD (mm)	4.34 ± 0.31	5.84 ± 0.45*	5.51 ± 0.75*
LVESD (mm)	3.43 ± 0.31	5.41 ± 0.50†	4.81 ± 0.74*
LVEDPW (mm)	0.63 ± 0.07	0.80 ± 0.19	0.66 ± 0.04
LVESPW (mm)	0.91 ± 0.12	0.98 ± 0.13	0.97 ± 0.11
LVED Vol (μl)	85.5 ± 14.0	170 ± 30.0*	151 ± 47.7*
LVES Vol (μl)	49.1 ± 12.1	143 ± 30.1†	111 ± 40.0*
EF (%)	45.9 ± 7.46	16.3 ± 3.36‡	27.1 ± 5.22†·§
FS (%)	22.8 ± 4.27	7.46 ± 1.57‡	12.8 ± 2.61†·§
HR (beats/min)	465 ± 45	488 ± 49	453 ± 43
SV (μl)	36.0 ± 8.08	28.0 ± 3.42	39.4 ± 9.57
CO (ml/min)	17.0 ± 5.47	13.8 ± 2.82	17.9 ± 5.30
E/E′	−44.0 ± 6.54	−40.9 ± 14.2	−31.7 ± 6.17
IVRT (ms)	14.6 ± 1.28	14.8 ± 3.68	15.6 ± 2.84
LV mass (mg)	84.5 ± 15.2	157 ± 48.8*	117 ± 27.5
HW/BW (mg/g)	5.34 ± 0.59	7.27 ± 1.75	6.07 ± 0.66

Values are mean ± SD. The mice were subjected to myocardial infarction (MI), and 3 days after surgery randomly divided to receive either immunoglobulin (IgG) vehicle or connective tissue growth factor (CTGF) monoclonal antibody (mAb) for 4 days, and subjected to echocardiography analysis. LV mass and heart weight versus body weight (HW/BW) were analyzed. *$p < 0.05$. †$p < 0.01$. ‡$p < 0.001$ versus sham. §$p < 0.05$ versus MI + IgG.

CO = cardiac output; E/E′ = mitral E/E′ ratio; EF = ejection fraction; FS = fractional shortening; HR = heart rate; IVRT = isovolumic relaxation time; LV = left ventricular; LVEDD = LV end-diastolic dimension; LVESD = end-systolic dimension; LVEDPW = LV end-diastolic posterior wall thickness; LVESPW = LV end-systolic posterior wall thickness; LVED Vol = LV end-diastolic volume; LVES Vol = LV end-systolic volume, SV = stroke volume.

CTGF mAb REGULATES GENES RELATED TO FIBROSIS AND/OR INFLAMMATION AND CARDIAC REPAIR (STUDY II). To explore potential mechanisms that mediated the cardioprotective effects of CTGF mAb, we performed RNA sequencing analysis of samples from mice subjected to chronic MI and treated with either control IgG (n = 5) or CTGF mAb (n = 5) for 6 weeks. We identified >1,000 genes with significantly altered expression after MI (fold change [FC] >1.5; $p < 0.05$) (Data Set 1 in the Supplemental Material). CTGF mAb treatment significantly affected expression of 72 transcripts in MI hearts (FC >1.5; $p < 0.05$) (Supplemental Table 3), 60 of which were also MI-altered. Gene ontology enrichment analysis indicated that 24 of 72 transcripts affected by CTGF mAb treatment were related to fibrosis and/or inflammation. An investigation of shared upstream regulators indicated that many transcripts are known to be co-regulated by multiple inflammatory factors, such as transforming growth factor (TGF)-β1, tumor necrosis factor-α, and interleukin-1β (**Figure 3E**). Normalized RNAseq data showed downregulation of selected MI-induced genes, and reduced expression of PAI-1 (Serpine1) was also confirmed by Western blotting (Supplemental Figure 3).

CTGF mAb treatment upregulated expression of 42 transcripts related to cardiac development and/or repair, including Nkx2-5 and Cited4 (Cbp/P300 interacting transactivator with Glu/Asp rich carboxy-terminal domain 4) in post-MI hearts (**Figure 3F**, Supplemental Figure 4). In addition, although it did not meet fold-change cutoffs, RNAseq analysis revealed significant induction of GATA binding protein 4 (GATA-4) expression in CTGF mAb–treated hearts compared with hearts treated with control IgG (Supplemental Figure 4).

CTGF mAb HAS NO EFFECT ON INFARCT SIZE FOLLOWING MYOCARDIAL I/R INJURY (STUDY III). To assess if antagonizing the function of CTGF affected acute cardiac I/R injury, wild-type mice were subjected to 30 min of ischemia followed by reperfusion (Study III) (**Figure 1**). Analysis for cardiac injury by determination of apoptosis at 3 h after reperfusion showed no difference between the control IgG and CTGF mAb treatments (**Figure 4A**). When assessed 24 h after reperfusion, CTGF mAb treatment had no effect on the size of the area at risk (**Figure 4B**). Analysis of infarct size revealed no difference between the groups, which suggested that CTGF mAb had no effect on cardiomyocyte viability following I/R injury (**Figure 4B**). Echocardiography analysis at 24 h after reperfusion showed no difference in LV structure or function between the groups (Supplemental Table 4).

FIGURE 3 CTGF mAb Protects Against Post-MI LV Hypertrophy and Fibrosis (Study II)

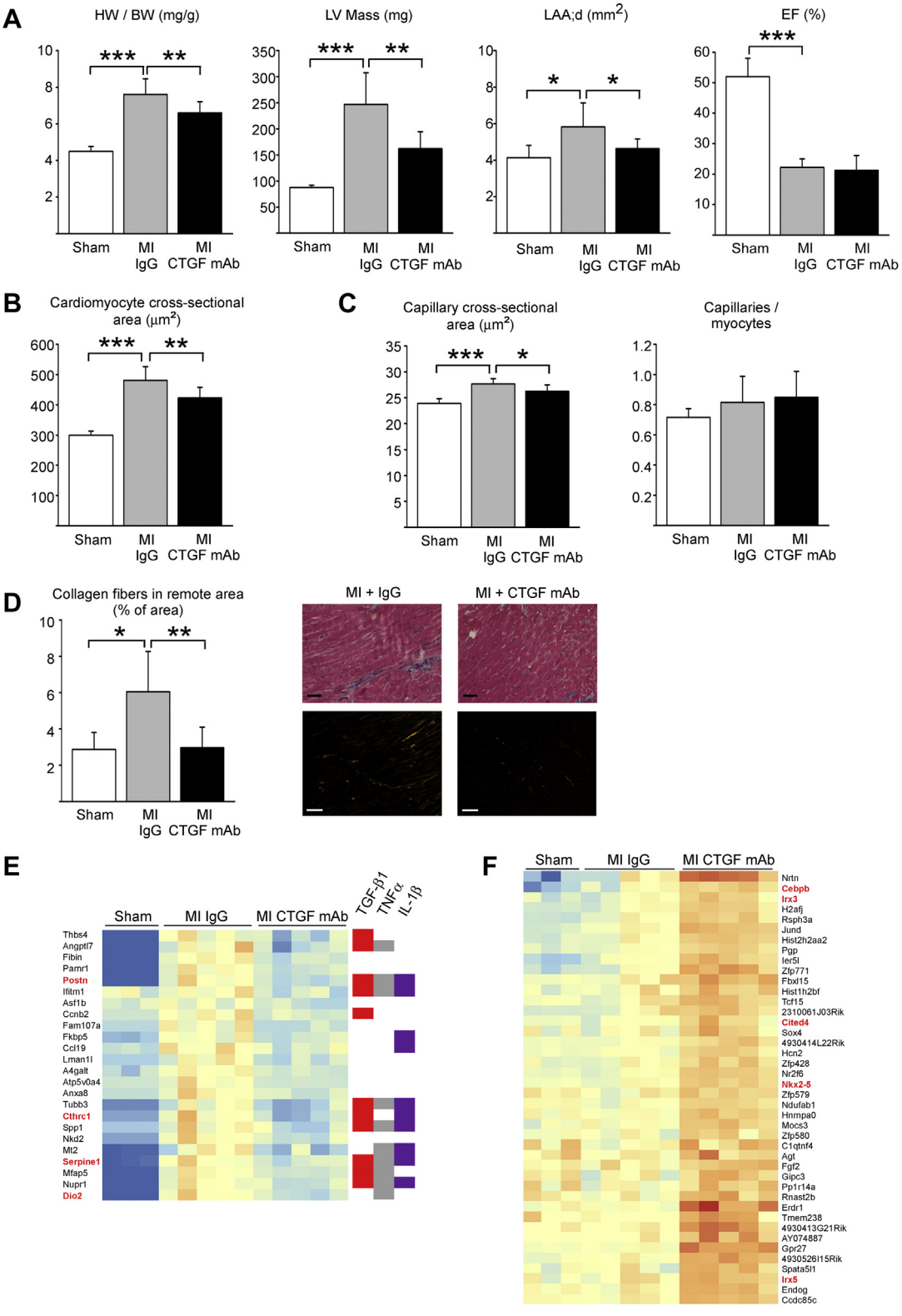

Continued on the next page

The effect of CTGF inhibition on central signaling mechanisms in the ischemic heart was assessed 3 h after reperfusion with Western blotting. Analysis for reperfusion injury salvage kinase pathways in the ischemic area showed no difference in phosphorylation of protein kinase B (Akt) or ERK between the mice treated with IgG or CTGF mAb (Figure 4C). In contrast, phosphorylation of JNK2 and the signal transducer and activator of transcription 3 were significantly increased in hearts of mice treated with CTGF mAb (Figure 4C). CTGF mAb had no effect on SMAD, p38, or protein kinase C (PKC)-α phosphorylation (Figure 4C).

JNK PATHWAY MEDIATES EFFECTS OF CTGF mAb. To more directly investigate the molecular function of CTGF mAb, we treated human cardiac FBs with CTGF mAb. Immunoblotting showed that treatment with CTGF mAb modestly reduced both basal and TGF-β1-induced αSMA and collagen-1 expression (Figure 5A). Examination of the affected signaling pathways showed that similar to findings in vivo, CTGF mAb induced JNK2 phosphorylation (Figure 5A). Antagonizing the function of CTGF also modestly reduced focal adhesion kinase (FAK) phosphorylation, but had no effect on ERK or SMAD2 phosphorylation (Figure 5A).

Quantitative analysis for the effect of CTGF mAb on collagen production showed that CTGF mAb significantly reduced both basal and TGF-β1-induced collagen production, but had no effect on basal or TGF-β1-induced FB proliferation (Figure 5B). We then investigated if JNK played a role in mediating the effects of CTGF mAb. Treatment of human cardiac FBs with JNK inhibitor I abrogated the reduced collagen production in CTGF mAb–treated cells, but had no effect on collagen production in control IgG-treated cells (Figure 5B). In contrast, FB proliferation was not affected by JNK inhibition (Figure 5B).

DISCUSSION

ECM forms the structural backbone of the heart, and provides efficient mechanical and electrical coupling during contraction. In HF, excessive accumulation of ECM not only increases ventricular stiffness, but also disrupts normal electrical coupling, which predisposes to conduction abnormalities, arrhythmias, and sudden cardiac death. However, fibrotic wound healing is necessary to form a stable infarct scar to prevent cardiac wall rupture. Therapy for HF patients with angiotensin-converting enzyme inhibitors, angiotensin II receptor antagonists, and mineralocorticoid receptor antagonists have been shown to attenuate the development of cardiac fibrosis (19,20). In addition, novel approaches, such as inhibition of fibronectin polymerization, may provide novel therapeutic approaches (21). In the present study, we investigated the potential of CTGF mAb therapy in protecting the heart from MI-induced injury and fibrosis.

TREATMENT WITH CTGF mAb DURING CARDIAC REPAIR. Repair of the infarcted heart can be divided into 3 overlapping phases: the inflammatory, proliferative, and maturation phases (22). The inflammatory phase in mouse hearts subjected to I/R injury lasts up to 72 hours after injury and is likely longer in hearts undergoing permanent MI. This is followed by a proliferative phase (days 3 to 7), which is characterized by FB proliferation, differentiation of FBs to myofibroblasts, and angiogenesis. Following repair of the infarct, activation of FBs occurs in both the peri-infarct area and the remote myocardium, which contribute to adverse remodeling of the LV. It is well documented that CTGF expression is elevated during wound healing in different tissues (23). In our study, treatment with CTGF mAb during the proliferative phase of cardiac repair (starting at day 3 after MI) resulted in better preserved ejection fraction at 1

FIGURE 3 Continued

Mice were subjected to MI and 1 week after surgery randomly divided to receive IgG vehicle or CTGF mAb for 6 weeks. **(A)** Analysis for heart weight to body weight (HW/BW) ratio, LV mass, left atrial end-diastolic area (LAA;d), and EF. **(B)** Analysis of cardiomyocyte cross-sectional area from Masson trichrome–stained LV sections. **(C)** Analysis of mean capillary cross-sectional size and the number of capillaries per cardiomyocyte in the nonischemic myocardium from CD31 staining, **(D)** Analysis of interstitial fibrosis from picrosirius red–stained LV sections under polarized light. Scale bar: 50 μm. **(A to D)** Data are presented as mean ± SD; number of animals was sham (n = 5), IgG (n = 7), and CTGF mAb (n = 8). *$p < 0.05$; **$p < 0.01$; ***$p < 0.001$. **(E)** Hierarchical clustering of RNAseq data for transcripts that were altered by MI and at least partially normalized by CTGF mAb, indicating that many of these genes are regulated by transforming growth factor-β1 (TGF-β1), tumor necrosis factor (TNF)-α, or interleukin (IL)-1β. **Red highlights** indicate genes associated with various fibrotic disorders. **(F)** Hierarchical clustering of RNAseq data showing transcripts whose expression was increased in hearts of mice treated with CTGF mAb. Known cardiac development and/or repair related genes are highlighted **(red)**. **(E and F)** Number of animals was sham (n = 3), IgG (n = 5), and CTGF mAb (n = 5). Abbreviations as in Figures 1 and 2.

FIGURE 4 **Antagonizing the Function of CTGF mAb During Cardiac I/R Injury (Study III)**

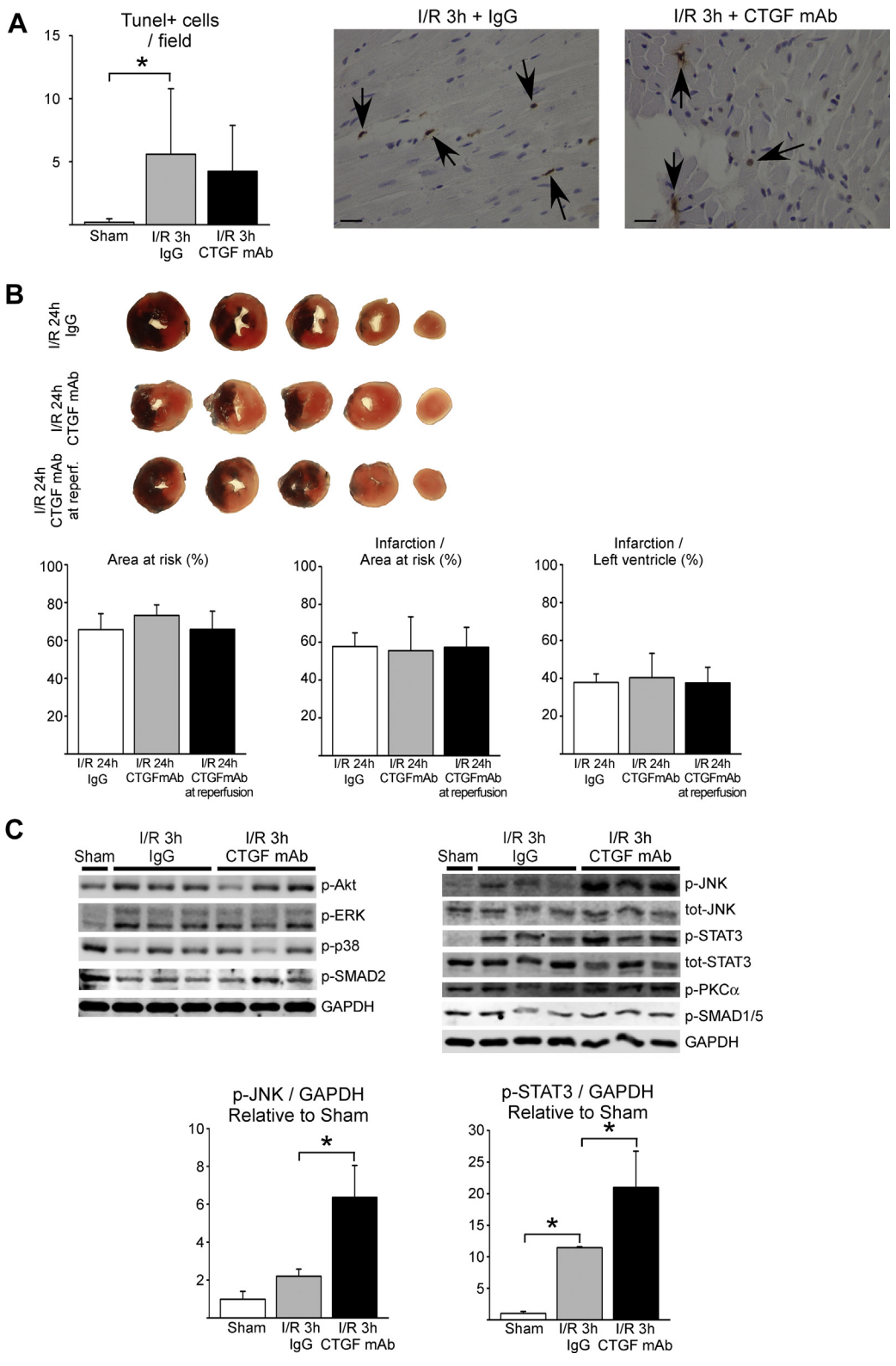

Continued on the next page

week after MI and also improved survival. We also found that CTGF mAb treatment started at day 3 after MI reduced infarct scar thinning and infarct expansion. Infarct expansion is associated with a decrease in LV systolic function and increased infarct rupture, which most often occurs at the infarct border zone during the first week after MI (24,25). In the present study, CTGF mAb–treated mice had less thinning of the infarct scar, which might have resulted in better preserved LV systolic function and provided protection from infarct rupture, and led to better post-MI survival. RNA sequencing data of samples from MI hearts treated with IgG or CTGF mAb showed that treatment with CTGF mAb induced expression of a number of genes involved in cardiac repair and/or development. Clear induction of Nkx2-5, a key nodal transcription factor in cardiogenesis, was noted, and further data mining revealed significant induction of GATA-4 expression in CTGF mAb–treated hearts. GATA-4 and Nkx2-5 physically interact and drive expression of a number of genes in cardiomyocytes (26), and are key mediators of cardiac repair and regeneration in the adult heart (27,28).

Cited4 encodes for the CREB-binding protein (CBP)/p300-interacting transactivator. Cardiomyocyte-specific overexpression of Cited4 in mice has also been shown to induce an increase in heart weight and cardiomyocyte size with normal systolic function, and to induce functional recovery and reduction in fibrosis long term after I/R injury (29). Induction of cardioprotective genes in hearts of CTGF mAb–treated mice might have contributed to better post-MI survival and better preserved LV systolic function after MI.

CTGF mAb IN DEVELOPMENT OF MYOCARDIAL FIBROSIS FOLLOWING MI. In the present study, we found that CTGF mAb treatment for 6 weeks post-MI resulted in reduced fibrosis in the remote, non-ischemic myocardium. In addition, CTGF mAb treatment during post-MI LV remodeling reduced the MI-induced increase in cardiomyocyte size and LV mass. RNA sequencing analysis of samples from surviving myocardium at 7 weeks after MI identified downregulation of MI-induced expression of inflammatory and fibrotic genes in hearts of CTGF mAb–treated mice. Previously, treatment with CTGF mAb in a genetic model of dilated cardiomyopathy showed that CTGF mainly regulated the genes related to ECM structural proteins and remodeling enzymes (15). These data, together with our present data, thus suggested that the antifibrotic effect of CTGF mAb in MI hearts arises from downregulation of inflammatory and fibrotic genes. The effect of CTGF mAb on cardiomyocyte hypertrophy in the present study probably also stemmed from altered FB function and altered release of local growth factors and cytokines from activated FBs.

Investigation of the mechanisms of CTGF action in cultured human FBs indicated that CTGF mAb reduced collagen production, but had no effect on FB proliferation. Recent studies indicated that the increase in LV fibrosis in the remote myocardium during post-MI LV remodeling was dependent on activation of existing FBs rather than FB proliferation, which mainly occurs 2 to 7 days post-MI in the infarct region (30). It is known that CTGF can modulate many signaling pathways independently of TGF-β (31). However, with respect to TGF-β signaling, it was previously reported that CTGF did not modulate canonical signaling (i.e., via SMAD 2/3), but instead modulated at least 2 non-canonical TGF-β signaling pathways, SMAD 1 and ERK (32). We found that CTGF mAb consistently activated the JNK2 isoform both in vivo and in vitro, but had no effect on SMAD signaling. Although there are previous data that showed that JNK2 is a negative regulator of FB proliferation (33), we found that inhibition of JNKs abrogated the antifibrotic effect of CTGF mAb in cultured human FBs.

EFFECT OF CTGF mAb ON ACUTE I/R INJURY. Previous data from studies that used transgenic mice with cardiac-restricted overexpression of rat CTGF suggested that CTGF protects the myocardium from

FIGURE 4 Continued

Mice were treated with IgG vehicle or CTGF mAb and subjected to ischemia–reperfusion injury (I/R). **(A)** Quantitative analysis of TUNEL-positive cells in hearts subjected to 30 min of ischemia and 3 h of reperfusion is shown. TUNEL-positive cells are marked with **arrows**; scale bar: 20 μm. **(B)** Mice were treated with IgG vehicle or CTGF mAb 24 h before ischemia and at reperfusion, or with CTGF mAb at reperfusion only. Infarct size and area at risk were analyzed from triphenyl tetrazolium chloride (TTC)–stained myocardial sections. **(C)** Western blot analysis of samples from infarct area 3 h after I/R injury. Analysis of phosphorylated protein kinase B (Akt), ERK, JNK, signal transducer and activator of transcription 3 (STAT3), p38, protein kinase C alpha (PKCα), SMAD2, and SMAD1/5 is shown. GAPDH was used as a loading control. Ratio of p-JNK to GAPDH and p-STAT3 to GAPDH data in the bar graphs are presented as mean ± SD. Number of animals in 3-h I/R experiment, including TUNEL labeling, was sham (n = 3), IgG (n = 6), and CTGF mAb (n = 6). Number of animals in 24-h I/R experiment including TTC staining was IgG (n = 11), CTGF mAb (n = 12), and CTGF in reperfusion (n = 12). TUNEL = terminal deoxynucleotidyl transferase dUTP nick end labeling; other abbreviations as in Figures 1 and 2.

FIGURE 5 CTGF mAb Activates JNK and Reduces Collagen Production in Cultured Human Cardiac Fibroblasts

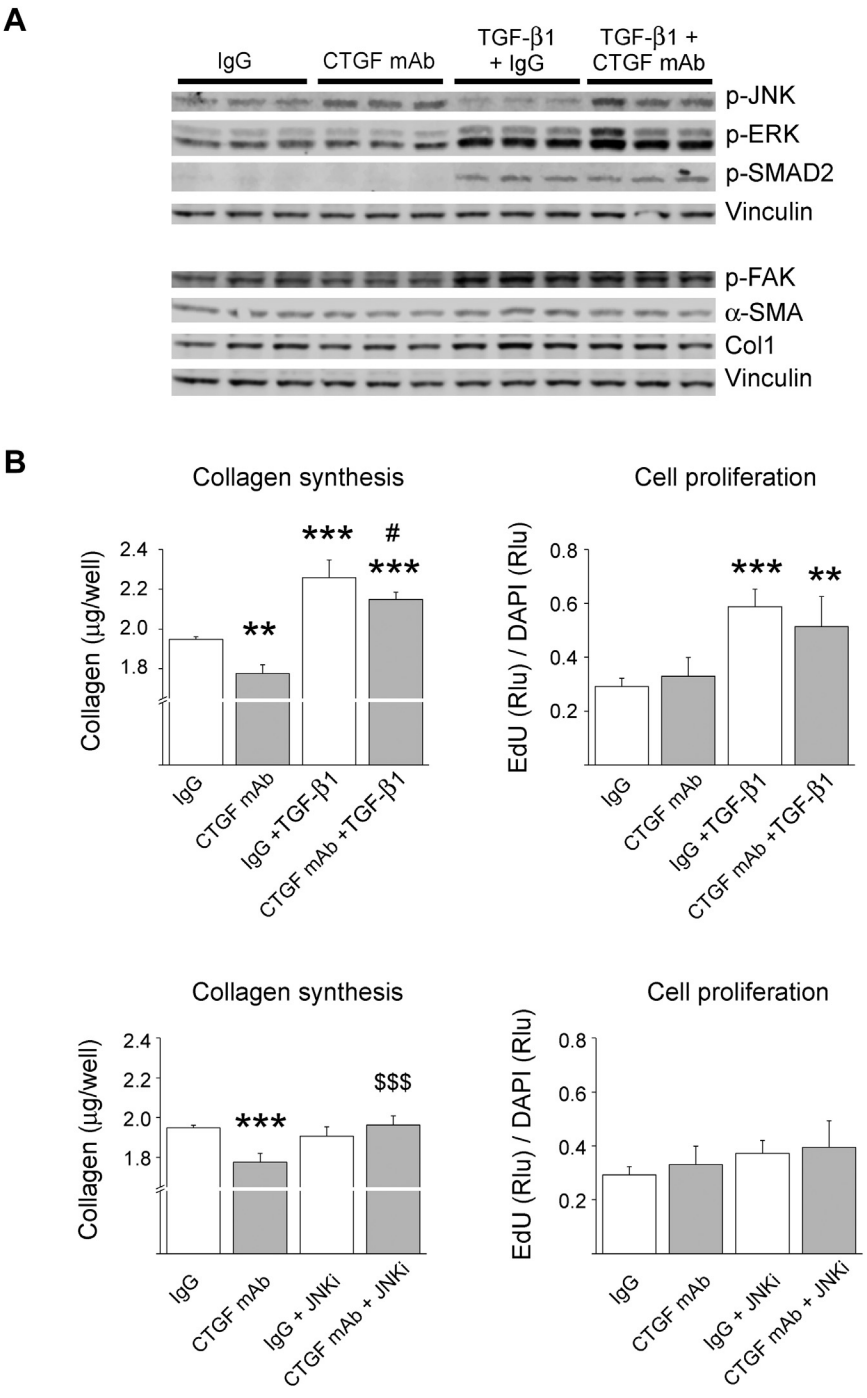

Cultured human fibroblasts were treated with 10 μg/ml CTGF mAb or control IgG, and co-treated with TGF-β1 (1 ng/ml) or inhibitor of JNK inhibitor (JNKi) [(L)-Form, 2 μM)], where indicated. **(A)** Western blot analysis for phosphorylated JNK2, p-ERK, phosphorylated SMAD2, phosphorylated focal adhesion kinase (p-FAK), smooth muscle alpha actin (α-SMA), and collagen 1 (Col1) is shown. Vinculin was used as loading control. **(B)** Quantitative analysis for collagen production and fibroblast proliferation. Data are presented as mean ± SD. **p < 0.01; ***p < 0.001 versus IgG; #p < 0.05 versus IgG + TGF-β1; $$$p < 0.001 versus CTGF mAb. N = 5 per group. Abbreviations as in Figures 1 to 3.

acute I/R injury (34). In the present study, we used strategies to administer CTGF mAb before I/R injury or immediately at reperfusion. Our data showed that treatment with CTGF mAb did not increase infarct size or compromise the recovery of LV systolic function at 24 h after I/R injury, as might be expected if CTGF were cardioprotective in acute I/R.

STUDY LIMITATIONS. There were some possible limitations to this study. Experimental MI surgery itself might have resulted in inflammatory effects (35) that could have affected the analysis of post-MI inflammation at 7 days after MI. However, our model for MI surgery, which included pericardial incision without open-chest surgery, resulted in shortened recovery and reduced inflammation compared with conventional open-chest models (36). Unfortunately, experimental MI in rodents and open-chest cardiac surgery in patients can damage the pericardium and may induce pericardial adhesions. CTGF mAb therapy during the proliferative phase of infarct repair might have had an effect on the development of the post-operative pericardial adhesions, which possibly contributed to increased survival and better preserved ejection fraction. Similar limitations should be considered when investigating any anti-fibrotic intervention during infarct repair in rodent MI models. In addition, analysis for infarct size at 24 h after I/R injury did not rule out the possibility that CTGF mAb could have had an effect on I/R injury analyzed at a later time point.

CONCLUSIONS

We found that therapy with CTGF mAb during the proliferative phase of post-MI cardiac repair attenuated infarct expansion, improved survival, and attenuated the decrease in LV systolic function. Intervention with CTGF mAb during post-MI LV remodeling reduced LV fibrosis and attenuated the MI-induced cardiomyocyte hypertrophy and increase in LV mass. Mechanistically, therapy with CTGF mAb attenuated the MI-induced increase in inflammatory and pro-fibrotic genes and enhanced expression of genes related to cardiac development and/or repair. In addition, studies with cultured human FBs indicated a role for JNK in reducing the collagen production by CTGF mAb. Further studies in large animal models are needed to establish if CTGF mAb provides a novel therapy for MI patients.

ACKNOWLEDGMENTS The authors thank Marja Arbelius, Kirsi Salo, Esa Kerttula, and Sirpa Rutanen for technical assistance.

ADDRESS FOR CORRESPONDENCE: Dr. Risto Kerkelä, Research Unit of Biomedicine, University of Oulu, P.O. Box 5000, FI-90014, Oulu, Finland. E-mail: Risto.Kerkela@oulu.fi.

PERSPECTIVES

COMPETENCY IN MEDICAL KNOWLEDGE: In a pre-clinical model of MI, therapy with CTGF mAb improved post-MI survival and attenuated development of LV fibrosis.

TRANSLATIONAL OUTLOOK: Further work is needed to assess whether CTGF mAb therapy provides benefit in large animal models of myocardial infarction.

REFERENCES

1. Writing Group M, Mozaffarian D, Benjamin EJ, et al. Heart Disease and Stroke Statistics-2016 Update: A Report From the American Heart Association. Circulation 2016; 133:e38–360.

2. Heusch G, Libby P, Gersh B, et al. Cardiovascular remodelling in coronary artery disease and heart failure. Lancet 2014;383:1933–43.

3. Leask A, Abraham DJ. All in the CCN family: essential matricellular signaling modulators emerge from the bunker. J Cell Sci 2006;119: 4803–10.

4. Jun JI, Lau LF. Taking aim at the extracellular matrix: CCN proteins as emerging therapeutic targets. Nat Rev Drug Discov 2011;10:945–63.

5. Koitabashi N, Arai M, Niwano K, et al. Plasma connective tissue growth factor is a novel potential biomarker of cardiac dysfunction in patients with chronic heart failure. Eur J Heart Fail 2008; 10:373–9.

6. Behnes M, Brueckmann M, Lang S, et al. Connective tissue growth factor (CTGF/CCN2): diagnostic and prognostic value in acute heart failure. Clin Res Cardiol 2014;103:107–16.

7. Daniels A, van Bilsen M, Goldschmeding R, van der Vusse GJ, van Nieuwenhoven FA. Connective tissue growth factor and cardiac fibrosis. Acta Physiol (Oxf) 2009;195:321–38.

8. Leask A. Getting to the heart of the matter: new insights into cardiac fibrosis. Circ Res 2015;116: 1269–76.

9. Yoon PO, Lee MA, Cha H, et al. The opposing effects of CCN2 and CCN5 on the development of cardiac hypertrophy and fibrosis. J Mol Cell Cardiol 2010;49:294–303.

10. Accornero F, van Berlo JH, Correll RN, et al. Genetic analysis of connective tissue growth factor as an effector of transforming growth factor beta signaling and cardiac remodeling. Mol Cell Biol 2015;35:2154–64.

11. Pi L, Fu C, Lu Y, et al. Vascular endothelial cell-specific connective tissue growth factor (CTGF) is necessary for development of chronic hypoxia-induced pulmonary hypertension. Front Physiol 2018;9:138.

12. Gorina E, Richeldi L, Raghu G, et al. PRAISE, a randomized, placebo-controlled, double-blind Phase 2 clinical trial of pamrevlumab (FG-3019) in IPF patients. Eur Respir J 2017;50:OA3400.

13. Alapati D, Rong M, Chen S, et al. Connective tissue growth factor antibody therapy attenuates hyperoxia-induced lung injury in neonatal rats. Am J Respir Cell Mol Biol 2011;45:1169–77.

14. Szabo Z, Magga J, Alakoski T, et al. Connective tissue growth factor inhibition attenuates left ventricular remodeling and dysfunction in pressure overload-induced heart failure. Hypertension 2014;63:1235–40.

15. Koshman YE, Sternlicht MD, Kim T, et al. Connective tissue growth factor regulates cardiac function and tissue remodeling in a mouse model of dilated cardiomyopathy. J Mol Cell Cardiol 2015;89:214–22.

16. Chatzifrangkeskou M, Le Dour C, Wu W, et al. ERK1/2 directly acts on CTGF/CCN2 expression to mediate myocardial fibrosis in cardiomyopathy caused by mutations in the lamin A/C gene. Hum Mol Genet 2016;25:2220–33.

17. Ashburner M, Ball CA, Blake JA, et al. Gene ontology: tool for the unification of biology. The Gene Ontology Consortium. Nat Genet 2000;25:25–9.

18. The Gene Ontology Consortium. Expansion of the Gene Ontology knowledge base and resources. Nucleic Acids Res 2017;45:D331–8.

19. Gourdie RG, Dimmeler S, Kohl P. Novel therapeutic strategies targeting fibroblasts and fibrosis in heart disease. Nat Rev Drug Discov 2016;15:620–38.

20. Talman V, Ruskoaho H. Cardiac fibrosis in myocardial infarction-from repair and remodeling to regeneration. Cell Tissue Res 2016;365:563–81.

21. Valiente-Alandi I, Potter SJ, Salvador AM, et al. Inhibiting fibronectin attenuates fibrosis and improves cardiac function in a model of heart failure. Circulation 2018;138:1236–52.

22. Shinde AV, Frangogiannis NG. Fibroblasts in myocardial infarction: a role in inflammation and repair. J Mol Cell Cardiol 2014;70:74–82.

23. Shi-wen X, Leask A, Abraham D. Regulation and function of connective tissue growth factor/CCN2 in tissue repair, scarring and fibrosis. Cytokine Growth Factor Rev 2008;19:133–44.

24. Gao XM, Xu Q, Kiriazis H, Dart AM, Du XJ. Mouse model of post-infarct ventricular rupture: time course, strain- and gender-dependency, tensile strength, and histopathology. Cardiovasc Res 2005;65:469–77.

25. Kelley ST, Malekan R, Gorman JH 3rd., et al. Restraining infarct expansion preserves left ventricular geometry and function after acute anteroapical infarction. Circulation 1999;99:135–42.

26. Durocher D, Charron F, Warren R, Schwartz RJ, Nemer M. The cardiac transcription factors Nkx2-5 and GATA-4 are mutual cofactors. EMBO J 1997;16:5687–96.

27. Pikkarainen S, Tokola H, Kerkela R, Ruskoaho H. GATA transcription factors in the developing and adult heart. Cardiovasc Res 2004;63:196–207.

28. Oka T, Maillet M, Watt AJ, et al. Cardiac-specific deletion of Gata4 reveals its requirement for hypertrophy, compensation, and myocyte viability. Circ Res 2006;98:837–45.

29. Bezzerides VJ, Platt C, Lerchenmuller C, et al. CITED4 induces physiologic hypertrophy and promotes functional recovery after ischemic injury. JCI Insight 2016;1.

30. Fu X, Khalil H, Kanisicak O, et al. Specialized fibroblast differentiated states underlie scar formation in the infarcted mouse heart. J Clin Invest 2018;128:2127–43.

31. Lipson KE, Wong C, Teng Y, Spong S. CTGF is a central mediator of tissue remodeling and fibrosis and its inhibition can reverse the process of fibrosis. Fibrogenesis Tissue Repair 2012;5:S24.

32. Nakerakanti SS, Bujor AM, Trojanowska M. CCN2 is required for the TGF-beta induced activation of Smad1-Erk1/2 signaling network. PLoS One 2011;6:e21911.

33. Sabapathy K, Hochedlinger K, Nam SY, Bauer A, Karin M, Wagner EF. Distinct roles for JNK1 and JNK2 in regulating JNK activity and c-Jun-dependent cell proliferation. Mol Cell 2004;15:713–25.

34. Ahmed MS, Gravning J, Martinov VN, et al. Mechanisms of novel cardioprotective functions of CCN2/CTGF in myocardial ischemia-reperfusion injury. Am J Physiol Heart Circ Physiol 2011;300:H1291–302.

35. Nossuli TO, Lakshminarayanan V, Baumgarten G, et al. A chronic mouse model of myocardial ischemia-reperfusion: essential in cytokine studies. Am J Physiol Heart Circ Physiol 2000;278:H1049–55.

36. Gao E, Lei YH, Shang X, et al. A novel and efficient model of coronary artery ligation and myocardial infarction in the mouse. Circ Res 2010;107:1445–53.

KEY WORDS connective tissue growth factor monoclonal antibody, fibrosis, heart failure, ischemia–reperfusion injury, left ventricle, myocardial infarction

APPENDIX For an expanded Methods section as well as supplemental tables and figures, please see the online version of this paper.

JACC: BASIC TO TRANSLATIONAL SCIENCE VOL. 4, NO. 1, 2019

EDITORIAL COMMENT

Connecting the Dots for Connective Tissue Growth Factor Roles in Cardiac Wound Healing After Myocardial Infarction*

Taben M. Hale, PhD,[a] Merry L. Lindsey, PhD[b]

In response to myocardial infarction (MI), the formation of scar comprised of extracellular matrix (ECM) is essential to maintain structure of the left ventricle (LV); however, too much or different ECM composition can generate an LV that is overly stiff and increases pre-load to the myocardium. Connective tissue growth factor (CTGF) (also known as CCN2) is a matricellular protein that influences fibroblast activation, cell migration, and cardiomyocyte hypertrophy (1). Cardiac fibroblast-mediated production of macrophage-recruiting chemokines are induced by CTGF (2,3). CTGF is low in the healthy adult heart and is markedly up-regulated in response to cardiac injury (4,5). CTGF gene expression is induced as early as 2 days after MI and remains elevated for up to 8 weeks (4,6). Therefore, understanding the mechanisms whereby CTGF regulates LV remodeling will provide insight into cardiac wound healing and help to elucidate additional targets that may be of therapeutic use.

SEE PAGE 83

In the study by Vainio et al. (7) in this issue of *JACC: Basic to Translational Science*, the potential of CTGF monoclonal antibody (mAb) therapy was tested in 3 different study protocols in mice: one inhibiting during the initial inflammation and scar formation period, a second evaluating chronic administration effects in a permanent occlusion MI model, and the third examining acute effects following ischemia and reperfusion (7). CTGF mAb during the early proliferative phase of MI limited infarct expansion, increased survival, and limited the development of LV systolic dysfunction. Starting administration later reduced remote fibrosis and myocyte hypertrophy. The mechanisms of action were to modulate development, inflammation, and ECM genes to promote repair. Jnk signaling in fibroblasts was identified as a major node of action.

This paper is interesting because CTGF is known for its role in activating fibroblast polarization to an ECM synthesizing cell phenotype (8), yet its inhibition enhanced rather than impaired repair. This report also highlights that timing is a crucial factor for consideration in drug administration, as different benefits were seen when the mAb was started at 3 days versus 7 days after MI and was evaluated at 1 week versus 7 weeks.

Protocol 1. The first protocol started mAb administration at 3 days after MI and evaluated at day 7 after MI. Under this administration, they observed less reduction in ejection fraction at 1 week, indicating that CTGF treatment slowed the progression of

*Editorials published in *JACC: Basic to Translational Science* reflect the views of the authors and do not necessarily represent the views of *JACC: Basic to Translational Science* or the American College of Cardiology.

From the [a]Department of Basic Medical Sciences, University of Arizona, College of Medicine-Phoenix, Phoenix, Arizona; and the [b]Department of Cellular and Integrative Physiology, University of Nebraska Medical Center and Research Service, Nebraska-Western Iowa Health Care System, Omaha, Nebraska. The authors have received funding from the American Heart Association under award number 19AIREA34460000; from the National Institutes of Health under award numbers HL075360, HL129823, HL137319, and HL141165; and from the Biomedical Laboratory Research and Development Service of the Veterans Affairs Office of Research and Development under award number 5I01BX000505. The content is solely the responsibility of the authors and does not necessarily represent the official views of the American Heart Association, National Institutes of Health, or the Veterans Administration.

All authors attest they are in compliance with human studies committees and animal welfare regulations of the authors' institutions and Food and Drug Administration guidelines, including patient consent where appropriate. For more information, visit the *JACC: Basic to Translational Science* author instructions page.

ISSN 2452-302X https://doi.org/10.1016/j.jacbts.2019.01.004

LV dilation. There was increased survival, although the cause was not given; rupture, acute heart failure indicated by lung congestion, and sudden cardiac death due to arrhythmias are the 3 causes typically observed. There was less infarct scar thinning and infarct expansion. From these findings, the authors conclude that enhanced ejection fraction and fractional shortening meant improved systolic physiology. Improved systolic physiology indicates myocyte actions versus diastolic physiology that indicates ECM differences. Because diastolic function also contributes to these equations and neither alone showed differences, the effect was likely due to the combination. The improvement in systolic properties is not likely due to preservation of myocytes in the infarct region, because initiation at 3 days after MI would not limit ischemic injury. The effect, therefore, was on surviving myocytes in the remote and border zones. Because treatment was started 3 days after MI surgery, it would have been good to see the day 3 echocardiography results to show that the 2 groups started out treatment looking the same. Day 7 was an appropriate time to evaluate, as most of inflammation and ECM responses occur by this time (9).

Protocol 2. The second protocol started mAb administration 1 week after MI and evaluated at week 7 MI. They observed reduced ECM accumulation (i.e., collagen) in the remote region. Myocyte size and LV mass were reduced, indicating a tempered hypertrophic response to MI. Infarct size was not different, as would be expected since treatment started 1 week after MI, a time when salvage would not be expected. RNA-seq showed repair (inflammation and ECM genes) and development genes increased with mAb treatment. The 2 most prominent development genes were Nkx2.5 and Gata4. This protocol revealed transforming growth factor (TGF) β-independent signaling stimulated by CTGF, which provides new targets for therapeutic exploration.

Protocol 3. The third protocol started mAb administration 24 h before MI (a prevention rather than inhibition strategy) and evaluated after 30 min ischemia and 3 or 24 h reperfusion. This protocol revealed findings that are in contrast to a previous report using cardiac myocyte-specific overexpression of rat CTGF, which showed protection from acute ischemia/reperfusion injury (10). Using the CTGF mAb strategy, the current study noted protection with inhibition, opposite the overexpression strategy used previously. These results highlight that translational protocols often do not recapitulate genetic models. We also have seen that matrix metalloproteinase-9 null and inhibition strategies show divergent effects on MI remodeling (11,12), highlighting the distinction between modifying gene expression under artificial conditions and using clinically relevant antibody or inhibitor strategies. Although therapeutic efficacy was not determined by measuring Ab concentrations in plasma or LV, it is likely that 100% inhibition was not achieved, providing another difference from gene deletion strategies. This protocol shows that the effects of the antibody are not acute and are not myocyte-centric, consistent with the other 2 study protocols showing that inflammation and ECM were the primary molecular targets.

Combined, the 3 study protocols reveal a lot about CTGF roles in MI wound healing. Standards have been set up for ischemia studies, and for the most part these are met in this study (9). At the same time, there were a few study limitations that should be noted. Because all 3 study protocols were distinct, results cannot be interwoven among them. Protocols 1 and 2 are translational, whereas protocol 3 is preventative.

The heart rate in the sham group (Table S1 in Vainio et al. [7]) was under 400 beats/min, and fractional shortening was an average of 25%, which is low for control mice (13). It is unusual for heart rate to increase with MI in the mouse permanent occlusion model, and a lack of wall thinning at day 7 after MI is not typical (9,13). It is likely there was wall thinning and infarction was achieved, based on the histological section shown in Figure 2C in Vainio et al. (7). The results combined indicate some technical issues with echocardiography acquisition that may be complicating data interpretation.

The 30-min ischemia period was the minimum time needed to induce infarction, and a lack of effect may indicate that minimal damage occurred. This protocol would not mimic the patient scenario, where 30 min to reperfusion is not the usual treatment window. The early increase in Jun kinase 2 and signal transducer and activator of transcription (STAT)3 to then signal fibroblast activation could indicate that CTGF treatment was stimulating a much earlier activation than typically seen.

Knockdown of CTGF in cardiac fibroblasts increases expression of CCN5 (3). Whereas CTGF promotes fibroblast activation, ECM accumulation, and cardiac hypertrophy, CCN5 has opposing effects (5). CCN5 was not measured in this study, and whether the improved cardiac outcomes in response to CTGF mAb are due to suppression of CTGF or up-regulation of CCN5 would be of interest to determine in future studies.

Regardless of the study limitations, the study by the Kerkela team reveals several mechanisms whereby CTGF is regulating negative components of

cardiac wound repair after MI through effects on propagating inflammation and ECM accumulation in the remote region. This study also highlights the benefits of using translational protocols to bridge between genetic mouse models and clinical application.

ADDRESS FOR CORRESPONDENCE: Dr. Merry L. Lindsey, Department of Cellular and Integrative Physiology, University of Nebraska Medical Center, 985850 Nebraska Medical Center, Omaha, Nebraska 68198-5850. E-mail: Merry.Lindsey@unmc.edu.

REFERENCES

1. Frangogiannis NG. Matricellular proteins in cardiac adaptation and disease. Physiol Rev 2012;92:635–88.

2. D'Souza KM, Biwer LA, Madhavpeddi L, Ramaiah P, Shahid W, Hale TM. Persistent change in cardiac fibroblast physiology after transient ACE inhibition. Am J Physiol Heart Circ Physiol 2015;309:H1346–53.

3. Tank J, Lindner D, Wang X, et al. Single-target RNA interference for the blockade of multiple interacting proinflammatory and profibrotic pathways in cardiac fibroblasts. J Mol Cell Cardiol 2014;66:141–56.

4. Ahmed MS, Oie E, Vinge LE, et al. Connective tissue growth factor-a novel mediator of angiotensin II-stimulated cardiac fibroblast activation in heart failure in rats. J Mol Cell Cardiol 2004;36:393–404.

5. Jeong D, Lee MA, Li Y, et al. Matricellular Protein CCN5 Reverses Established Cardiac Fibrosis. J Am Coll Cardiol 2016;67:1556–68.

6. Jumeau C, Rupin A, Chieng-Yane P, et al. Direct thrombin inhibitors prevent left atrial remodeling associated with heart failure in rats. J Am Coll Cardiol Basic Transl Sci 2016;1:328–39.

7. Vaini LE, Szabó Z, Lin R, et al. Connective tissue growth factor inhibition enhances cardiac repair and limits fibrosis after myocardial infarction. J Am Coll Cardiol Basic Trans Sci 2019;4:83–94.

8. Mouton AJ, Ma Y, Rivera Gonzalez OJ, et al. Fibroblast polarization over the myocardial infarction time continuum shifts roles from inflammation to angiogenesis. Basic Res Cardiol 2019;114:6.

9. Lindsey ML, Bolli R, Canty JM, et al. Guidelines for experimental models of myocardial ischemia and infarction. Am J Physiol Heart Circ Physiol 2018;314:H812–38.

10. Ahmed MS, Gravning J, Martinov VN, et al. Mechanisms of novel cardioprotective functions of CCN2/CTGF in myocardial ischemia-reperfusion injury. Am J Physiol Heart Circ Physiol 2011;300:H1291–302.

11. Iyer RP, Jung M, Lindsey ML. MMP-9 signaling in the left ventricle following myocardial infarction. Am J Physiol Heart Circ Physiol 2016;311:H190–8.

12. Iyer RP, de Castro Bras LE, Patterson NL, et al. Early matrix metalloproteinase-9 inhibition post-myocardial infarction worsens cardiac dysfunction by delaying inflammation resolution. J Mol Cell Cardiol 2016;100:109–17.

13. Lindsey ML, Kassiri Z, Virag JAI, de Castro Bras LE, Scherrer-Crosbie M. Guidelines for measuring cardiac physiology in mice. Am J Physiol Heart Circ Physiol 2018;314:H733–52.

KEY WORDS cardiac remodeling, collagen, editorial, extracellular matrix, RNA-seq

JACC: BASIC TO TRANSLATIONAL SCIENCE VOL. 4, NO. 1, 2019

PRECLINICAL RESEARCH

Circulating Pro-Vascular Progenitor Cell Depletion During Type 2 Diabetes

Translational Insights Into the Prevention of Ischemic Complications in Diabetes

Daniella C. Terenzi, BHSc,[a,b] Mohammed Al-Omran, MD, MSc,[b,c,d,e] Adrian Quan, MPHIL,[a] Hwee Teoh, PHD,[a,f] Subodh Verma, MD, PHD,[a,b,d,e] David A. Hess, PHD[c,e,g]

VISUAL ABSTRACT

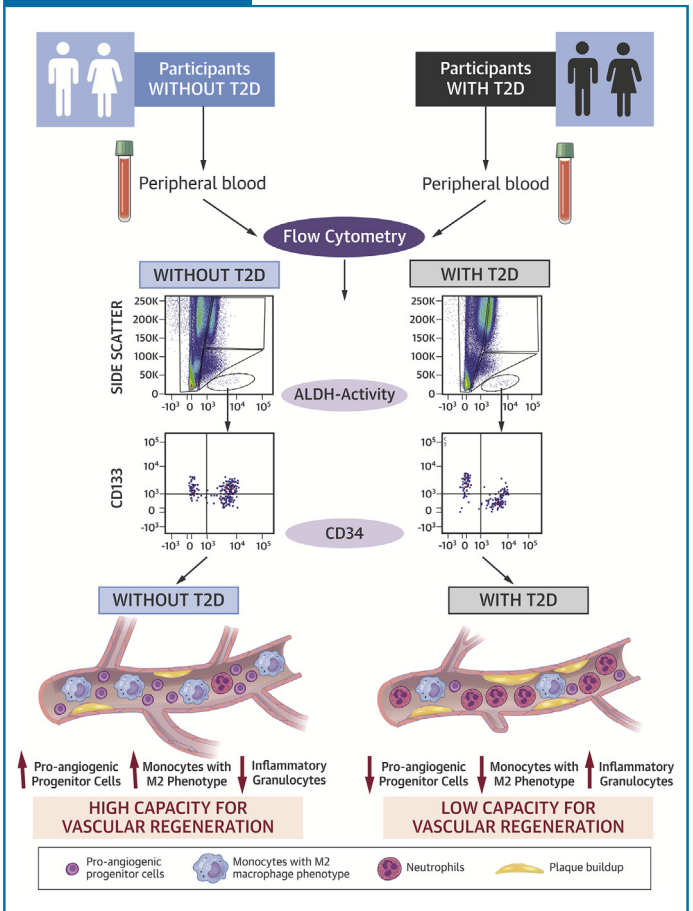

Terenzi, D.C. et al. J Am Coll Cardiol Basic Trans Science. 2019;4(1):98–112.

HIGHLIGHTS

- This study combined ALDH activity with cell surface marker expression to develop a multiparametric flow cytometry assay to assess proangiogenic progenitor and proinflammatory cell content in the peripheral blood of patients with T2D compared with age-matched control subjects.
- Patients with T2D exhibited an increased frequency of proinflammatory ALDH^{hi} cells with granulocyte side scatter properties and a decreased frequency of circulating monocytes with an M2 phenotype that is associated with proangiogenic and anti-inflammatory functions.
- Patients with T2D exhibited significant depletion of circulating provascular ALDH^{hi}CD34+ progenitor cells with primitive, migratory, endothelial, and pericyte phenotypes.
- Subgroup analyses that stratified patients with T2D according to age, duration of T2D, insulin requirement, and glycosylated hemoglobin levels revealed that only the duration of T2D correlated with vascular progenitor cell depletion.
- Flow cytometric assessment of circulating ALDH^{hi} cell subsets represents a promising translational approach for identifying patients with T2D at increased risk for cardiovascular comorbidities.

ISSN 2452-302X https://doi.org/10.1016/j.jacbts.2018.10.005

SUMMARY

Detection of vascular regenerative cell exhaustion is required to combat ischemic complications during type 2 diabetes mellitus (T2D). We used high aldehyde dehydrogenase (ALDH) activity and surface marker co-expression to develop a high-throughput flow cytometry–based assay to quantify circulating proangiogenic and proinflammatory cell content in the peripheral blood of individuals with T2D. Circulating proangiogenic monocytes expressing anti-inflammatory M2 markers were decreased in patients with T2D. Individuals with longer duration of T2D exhibited reduced frequencies of circulating proangiogenic ALDH^{hi}CD34+ progenitor cells with primitive (CD133) and migratory (CXCR4) phenotypes. This approach consistently detected increased inflammatory cell burden and decreased provascular progenitor content in individuals with T2D.

ABBREVIATIONS AND ACRONYMS

ALDH = aldehyde dehydrogenase

BM = bone marrow

HbA$_{1c}$ = glycosylated hemoglobin

ROS = reactive oxygen species

SSC = side scatter

T2D = type 2 diabetes mellitus

Wnt = wingless related integration site

Approximately 400 million individuals worldwide experience type 2 diabetes (T2D), and this number is expected to rise to >600 million by 2045 (1-3). Although various mechanisms have been suggested to mediate the vascular complications of diabetes, there is growing interest in the theory that diabetes may lead to chronic inflammation, which in turn increases oxidative stress on vascular regenerative cells, inciting a state of vasculopenia. This damaging microenvironment also contributes to the death and dysfunction of bone marrow (BM)-derived and circulating proangiogenic progenitor cells, leading to an inability to respond to vessel damage (4). Thus, ongoing endothelial damage combined with reduced blood vessel regenerative capacity in patients with T2D culminates in a 2- to 5-fold increased risk for the development of ischemic cardiovascular diseases, including critical limb ischemia, myocardial infarction, and stroke (1,3). Although newer antihyperglycemic agents reportedly improve cardiovascular outcomes in diabetes (5–15), the unmet need and residual risk remain prohibitively high in T2D (16).

To minimize the risks associated with reduced blood flow causing ischemia, multiple endogenous mechanisms can be activated to reverse vascular dysfunction (4). These multicellular processes include vasculogenesis, the creation of de novo vessels from endothelial progenitor cells; angiogenesis, the sprouting of new blood vessels from pre-existing vessels; and arteriogenesis, the beneficial remodeling of pre-existing collateral vessels to form a "natural bypass" toward the ischemic region (4,17). Although angiogenesis and postnatal vasculogenesis have been widely studied, both processes can be limited in adults by the scarcity of circulating provascular progenitor cells of hematopoietic and endothelial lineages (18,19). Although arteriogenesis is not as well understood, accessory immune cells (including monocytes and macrophages) are recruited to pre-existing collateral vessels and participate in vessel remodeling to activate blood flow (4,18,20,21). Thus, these processes rely on structural and secretory contributions from circulating hematopoietic and endothelial cells that originate from the BM (22,23). In the context of T2D, the impact of glucotoxicity and

From the [a]Division of Cardiac Surgery, Keenan Research Centre for Biomedical Science and Li Ka Shing Knowledge Institute of St. Michael's Hospital, Toronto, Ontario, Canada; [b]Institute of Medical Science, University of Toronto, Toronto, Ontario, Canada; [c]Division of Vascular Surgery, Keenan Research Centre for Biomedical Science and Li Ka Shing Knowledge Institute of St. Michael's Hospital, Toronto, Ontario, Canada; [d]Department of Surgery, University of Toronto, Toronto, Ontario, Canada; [e]Department of Pharmacology and Toxicology, University of Toronto, Toronto, Ontario, Canada; [f]Division of Endocrinology and Metabolism, Li Ka Shing Knowledge Institute of St. Michael's Hospital, Toronto, Ontario, Canada; and the [g]Robarts Research Institute, London, Ontario, Canada. This work was supported by operating grants from the Canadian Institutes for Health Research to Dr. Hess (no. 387189) and Dr. Verma (no. 153293). Dr. Hess holds the Sheldon H. Weinstein Chair in Diabetes Research at the Schulich School of Medicine, Western University, London, Ontario, Canada. Dr. Verma holds a Tier 1 Canada Research Chair in Cardiovascular Surgery at the University of Toronto, Toronto, Ontario, Canada. All other authors have reported that they have no relationships relevant to the contents of this paper to disclose.

All authors attest they are in compliance with human studies committees and animal welfare regulations of the authors' institutions and Food and Drug Administration guidelines, including patient consent where appropriate. For more information, visit the *JACC: Basic to Translational Science* author instructions page.

Manuscript received October 18, 2018; revised manuscript received October 27, 2018, accepted October 29, 2018.

increased oxidative stress on the frequency and function of these regenerative progenitor cells is not well understood.

Aldehyde dehydrogenase (ALDH) is an intracellular detoxification enzyme highly expressed in progenitor cells with documented proangiogenic secretory function (17). ALDH acts to protect long-lived cells from oxidative stress by metabolizing toxic alkylating aldehyde agents, which can lead to cellular damage. In addition, ALDH is the rate-limiting enzyme in the intracellular production of retinoic acid, a potent morphogen. Thus, as progenitor cells differentiate toward a mature phenotype, ALDH-activity is reduced. Our group and others have previously documented the proangiogenic signaling capacity of ALDH^{hi} progenitor cells from BM and umbilical cord blood (17,24,25).

BM cells of patients with T2D exhibit reduced expression of markers associated with proangiogenic progenitor cells (CD34 and CD133) due to premature differentiation accelerated by hyperglycemia and increased oxidative stress (18,23,26). The T2D BM microenvironment also exhibits increased cell turnover, lending to heightened inflammatory responses and inhibited distribution of provascular progenitor cells to ischemic tissues (23,27). The amplified inflammation leads to increased NADPH oxidase-1 function, which significantly elevates intracellular reactive oxygen species (ROS) formation (28). The examination of circulating progenitor cell content in the peripheral circulation may confirm the extent of this process (termed "regenerative cell exhaustion") and illuminate the therapeutic implications of BM dysfunction on vascular regeneration.

The goal of this study was to assess the balance between circulating vascular regenerative progenitor cells and inflammatory cells in patients with T2D. We used the detection of high ALDH-activity according to flow cytometry to quantify the prevalence of circulating progenitor cells in the peripheral blood of patients with T2D and age-matched control subjects. High ALDH-activity in conjunction with 6-color cell surface marker analyses allowed us to quantify the frequencies of proangiogenic and inflammatory cell types that affect the repair of ischemic injury in patients with T2D. Patients with T2D exhibited a significant decrease in circulating cells with hematopoietic and endothelial progenitor cell phenotype. In addition, circulating monocytes with an anti-inflammatory M2 phenotype were decreased in patients with T2D, and primitive granulocytes with proinflammatory function were significantly increased in patients with T2D, suggesting a shift toward a proinflammatory phenotype (29). These studies provide a foundation to assess vascular regenerative cell content during the progression of T2D and may be developed as a surrogate assay to estimate the capacity to mitigate ischemia via a provascular regenerative response.

METHODS

PATIENT CHARACTERISTICS. A total of 30 individuals >40 years of age with established T2D of >5 years were age- and sex-matched with 30 individuals without T2D. Written informed consent was provided, and all studies were approved prior to study initiation by the Advarra central institutional review board.

ISOLATION OF PERIPHERAL BLOOD MONONUCLEAR CELLS. Up to 50 ml of peripheral blood was drawn from each patient into ethylenediaminetetraacetic acid-lined blood collection tubes. Cells were layered on Hypaque-Ficoll solution placed in SepMate tubes (STEMCELL Technologies, Vancouver, British Columbia, Canada) to aid in the removal of red blood cells. Any red blood cells remaining were lysed with ammonium chloride and washed in phosphate-buffered saline to remove cellular debris.

ANALYSES OF PROGENITOR CELLS. Peripheral blood mononuclear cells were examined for ALDH-activity by using Aldefluor reagent (STEMCELL Technologies) following the manufacturer's instructions (17,24,25). Briefly, cells were incubated at 37°C for 30 min with Aldefluor reagent. Subsequently, cells were centrifuged, washed with phosphate-buffered saline, and resuspended in ALDH buffer to block the efflux of the fluorescent substrate via adenosine triphosphate-binding cassette transporters. Next, cells were labeled with fluorochrome-conjugated, anti-human antibodies to surface markers marking primitive (CD34 and CD133) and more mature (CD33 and CD45) hematopoietic cells, endothelial cells (CD31, CD146, and CD144), monocytes (CD14), M1/M2 phenotype (CD68, CD80, and CD163), and granulocyte (CD15, CD16b, and CD66b) phenotypes. Antibodies were from Becton Dickinson, Miltenyi, and BioLegend, as specified in Supplemental Table 1. Cells were incubated with the antibodies for 30 min at 2°C to 8°C and washed in phosphate-buffered saline to ensure that excess antibodies were removed from the sample. Circulating progenitor cell content was assessed via 6-color, multiparametric flow cytometry on a BD LSRFortessa X-20 cytometer (BD Biosciences (Franklin Lakes, New Jersey) and analyzed with the FlowJo version 10 software (FlowJo, LLC, Ashland, Oregon). Side scatter (SSC) property, a measure of light scatter due to

intracellular complexity or granularity, was used to further identify cells with low, intermediate, or high intracellular complexity. A minimum of 10^6 events was collected for every sample, assuring the analysis of >500 cells in the rare ALDH^{hi}SSC^{low} population.

STATISTICAL ANALYSIS. Statistical analyses were performed with the Student's *t*-test for comparison of results from the group with T2D versus the age-matched control individuals and for analyses of patients with T2D (n = 30) stratified into subgroups for assessment of correlations with sex (male, n = 12; female, n = 18), HbA_{1c} values (HbA_{1c} ≤7, HbA_{1c} >7, n = 15), insulin use (no insulin, n = 18; on insulin, n = 12), age (≤70 years, n = 16; >70 years, n = 14), and duration of T2D (≤13 years, n = 15; >13 years, n = 15) on relevant circulating cellular subpopulations. Data from all 30 patients with T2D were included in the subgroup analyses. The use of nonparametric tests or permutation tests was not required.

TABLE 1 Baseline Characteristics of the Study Population

	Control Subjects (n = 30)	Patients With T2D (n = 30)
Age, yrs	72.3 ± 1.6	71.4 ± 1.7
Male/female	12 (40)/18 (60)	12 (40)/18 (60)
Duration of T2D, yrs	NA	14.0 ± 0.9
HbA_{1c}, %	5.5 ± 0.1	7.2 ± 0.2*
LDL-C, mmol/L	2.5 ± 0.2	1.5 ± 0.1*
HDL-C, mmol/L	1.4 ± 0.1	1.3 ± 0.1
Total cholesterol, mmol/L	4.5 ± 0.2	3.5 ± 0.2*
Hypertensive therapy	24 (80)	26 (87)
Statin therapy	15 (50)	22 (73)
Metformin	0 (0)	23 (77)
Insulin	0 (0)	12 (40)

Values are mean ± SEM or n (%). *p < 0.001 with the Student's *t*-test.
HbA_{1c} = glycosylated hemoglobin; HDL-C = high-density lipoprotein cholesterol; LDL-C = low-density lipoprotein cholesterol; NA = not applicable; T2D = type 2 diabetes mellitus.

RESULTS

DEMOGRAPHIC AND BIOCHEMICAL CHARACTERISTICS. Baseline patient characteristics as well as their clinical histories are shown in **Table 1**. As expected, HbA_{1c} levels were higher in patients with T2D. The average duration of diabetes in this cohort was 14.0 ± 0.9 years, and the average age was 71.4 ± 1.7 years. The age and percent ratio of male to female patients (40:60) were balanced between the T2D cohort and matched control subjects. The frequency of patients taking an antihypertensive agent was equivalent in both populations. High-density lipoprotein cholesterol levels were similar between the groups, although total cholesterol and low-density lipoprotein cholesterol levels were significantly lower in patients with T2D. The lower total cholesterol and low-density lipoprotein cholesterol levels are likely due to greater use of statins within the T2D cohort (22 of 30) compared with the control group (15 of 30). The majority of the patients with T2D (77%) were taking metformin, and insulin was used by 12 (40%) of 30 patients with T2D.

CIRCULATING CELLS WITH PROANGIOGENIC MONOCYTE AND ANTI-INFLAMMATORY M2 PHENOTYPES WERE DECREASED IN PATIENTS WITH T2D. We first examined the relative expression of cell surface markers associated with hematopoietic, endothelial, monocyte, and granulocyte phenotypes. Importantly, previous studies have shown the functional relevance of these cell types in the coordination of proangiogenic responses after transplantation (30–33). When gated on total cellular events and analyzed for single-cell surface marker expression, the frequency of circulating cells expressing primitive hematopoietic and endothelial cell-associated surface markers was equivalent in patients with T2D and the matched control subjects (**Table 2**, Supplemental Figures 1A to 1H). In contrast, the frequencies of circulating cells expressing the monocyte marker CD14 or the M2 polarization marker CD163 were significantly decreased in patients with T2D (**Table 2**, Supplemental Figures 1I to 1L); the frequency of cells expressing CD80, a marker associated with the M1 phenotype, was increased in patients with T2D. Collectively, the diminished frequency of provascular CD14+ circulating monocytes combined with a shift from the M2 to M1 phenotype suggested increased inflammation in patients with T2D. In addition, more sensitive analyses using multiple markers combined with ALDH-activity was required to accurately detect differences in circulating proangiogenic progenitor cell frequencies.

ALDH^{hi}SSC^{hi} GRANULOCYTIC CELLS WERE INCREASED IN PATIENTS WITH T2D. To more definitively assess circulating proangiogenic progenitor cell frequencies in the peripheral blood of patients with T2D, the Aldefluor assay was used to detect circulating cells with high ALDH-activity, a conserved characteristic in multiple progenitor cell lineages. We have previously documented the robust proangiogenic secretory function of ALDH^{hi} cells from human umbilical cord blood and BM (17,24,25,34). We identified three distinct cell populations with high ALDH-activity segregated further according to SSC properties representing cells with increasing intracellular complexity. A reversible inhibitor of ALDH-activity, *N,N*-diethylaminobenzaldehyde, was used to discern cells with low versus high ALDH-activity (**Figure 1A**), alongside low (R1) versus intermediate (R2) versus

TABLE 2 Circulating Monocytes With Anti-inflammatory M2 Phenotypes Were Decreased in Patients With T2D

	Marker	Control	T2D	p Value	Description/Expression
Hematopoietic	CD45	91.1 ± 2.2	90.4 ± 2.2	0.82	Pan-leukocyte marker or leukocyte common antigen • Expressed on all hematopoietic cells except erythrocytes
	CXCR4/CD184	83.8 ± 1.3	82.4 ± 2.4	0.61	CXC chemokine receptor type 4 or fusin • Expressed on hematopoietic cells with migratory function
	CD33	49.4 ± 2.5	49.2 ± 2.4	0.95	Sialic acid binding IgG-like lectin 3 of Siglec-3 • Expressed on primitive cells of the myeloid lineage
	CD34	3.7 ± 0.7	2.9 ± 0.6	0.38	Sialomucin, adhesion to matrix and stromal cells in the bone marrow • Expressed on hematopoietic/endothelial progenitor cells
Endothelial	CD31	73.0 ± 1.9	72.3 ± 1.9	0.74	Platelet endothelial cell adhesion molecule (PECAM-1) • Expressed on monocytes, neutrophils, and endothelial cells
	CD144	44.0 ± 2.8	43.6 ± 2.5	0.91	Cadherin 5, type 2, or vascular endothelial–cadherin • Expressed on endothelial cells and some granulocytes
	CD146	1.4 ± 0.3	1.1 ± 0.2	0.40	Melanoma cell adhesion molecule (MCAM) or mucin 18 • Expressed on endothelial cells and pericytes
	CD133	1.5 ± 0.4	1.3 ± 0.3	0.57	Prominin-1, pentaspan transmembrane protein • Expressed on hematopoietic/endothelial progenitor cells
Monocyte	CD14	10.1 ± 1.7	5.9 ± 0.8	0.05	Co-receptor for bacterial lipopolysaccharide • Expressed on monocytes, macrophages, some granulocytes
	CD68	42.2 ± 3.0	43.6 ± 2.6	0.73	Macrosialin, scavenger receptor class D, member 1 • Expressed on monocytes and macrophages
M1 phenotype	CD80	3.6 ± 0.6	5.2 ± 0.5	0.04	B7-1, ligand for CD28 and CTLA-4 • Expressed on pro-inflammatory M1 macrophages
M2 phenotype	CD163	14.5 ± 1.0	10.8 ± 0.7	0.003	Low-affinity scavenger receptor for hemoglobin-haptoglobin • Expressed on anti-inflammatory M2 macrophages

The frequency of cells expressing mature and primitive hematopoietic and endothelial markers was equal in patients with type 2 diabetes mellitus (T2D) compared with age, gender, and sex-matched control subjects. The frequency of cells expressing the monocyte/macrophage marker CD14 was decreased in patients with T2D compared with control subjects. The frequency of cells expressing the M1 macrophage marker CD80 (pro-inflammatory phenotype) was increased whereas the frequency of cells expressing the M2 macrophage marker CD163 (anti-inflammatory phenotype) was decreased in patients with T2D compared with control subjects. Values are mean ± SEM. Statistical comparisons were conducted with the Student's *t*-test.

CTLA-4 = cytotoxic T-lymphocyte associated protein 4; IgG = immunoglobulin G.

high (R3) SSC as shown in Figure 1B. Importantly, the frequency of cells with ALDH^{hi}SSC^{low} (progenitor cells) and ALDH^{hi}SSC^{mid} (primarily monocytes) phenotypes were equal in patients with T2D compared with control subjects (Figures 1C and 1D). In contrast, cells with the ALDH^{hi}SSC^{hi} (granulocytes) phenotype were >2-fold increased in patients with T2D. These ALDH^{hi}SSC^{hi} cells expressed neutrophil markers, including CD15, CD16b, and CD66b; some were positive for the monocyte marker CD14, and all cells were negative for CD34 co-expression. These findings confirm that the ALDH^{hi}SSC^{hi} population primarily comprised granulocytes that can propagate inflammatory processes, again marking increased circulating inflammatory cell content in patients with T2D.

ALDH^{hi}SSC^{low} CELLS WITH PROGENITOR CELL SURFACE MARKER CO-EXPRESSION WERE DECREASED IN PATIENTS WITH T2D. ALDH^{hi}SSC^{low} cells can be described as a heterogeneous progenitor cell population comprising primarily hematopoietic (>90%) and endothelial (<10%) cell lineages (17), and they have both been shown to support angiogenic blood vessel formation in immunodeficient mice with femoral artery ligation. Although these cells are extremely rare in the peripheral circulation (<0.1%), they possess a robust proangiogenic signaling profile and also contain rare endothelial precursor cells with the capacity to integrate into sprouting vessels (35–38). Thus, detection of circulating ALDH^{hi}SSC^{low} cells is critical for the assessment of provascular regenerative capacity. Although we detected no significant differences in the overall frequency of ALDH^{hi}SSC^{low} or ALDH^{hi}SSC^{mid} cells between patients with T2D and matched control subjects, ALDH^{hi}SSC^{low} cells were further assessed for primitive hematopoietic and endothelial cell surface expression (CD34+/CD133+), early myeloid cell surface marker expression (CD34+/CD33+), and primitive migratory progenitor cells (CD34+/CXCR4+ cells). Both proangiogenic hematopoietic and vessel-integrating endothelial progenitor cells commonly express CD34 (36). The frequency of cells expressing CD34 alone was not different in the ALDH^{hi}SSC^{low} population (Supplemental Table 2) but patients with T2D exhibited significantly decreased frequencies of primitive progenitor (Figures 2A to 2C), early myeloid (Figures 2D to 2F), and migratory progenitor (Figures 2G to 2I) cells compared with control subjects; these findings indicate reduced vascular regenerative progenitor cell representation in patients with T2D (23,39).

FIGURE 1 **Circulating Progenitor Cell Subpopulations Are Discerned According to High ALDH-Activity and SSC Properties**

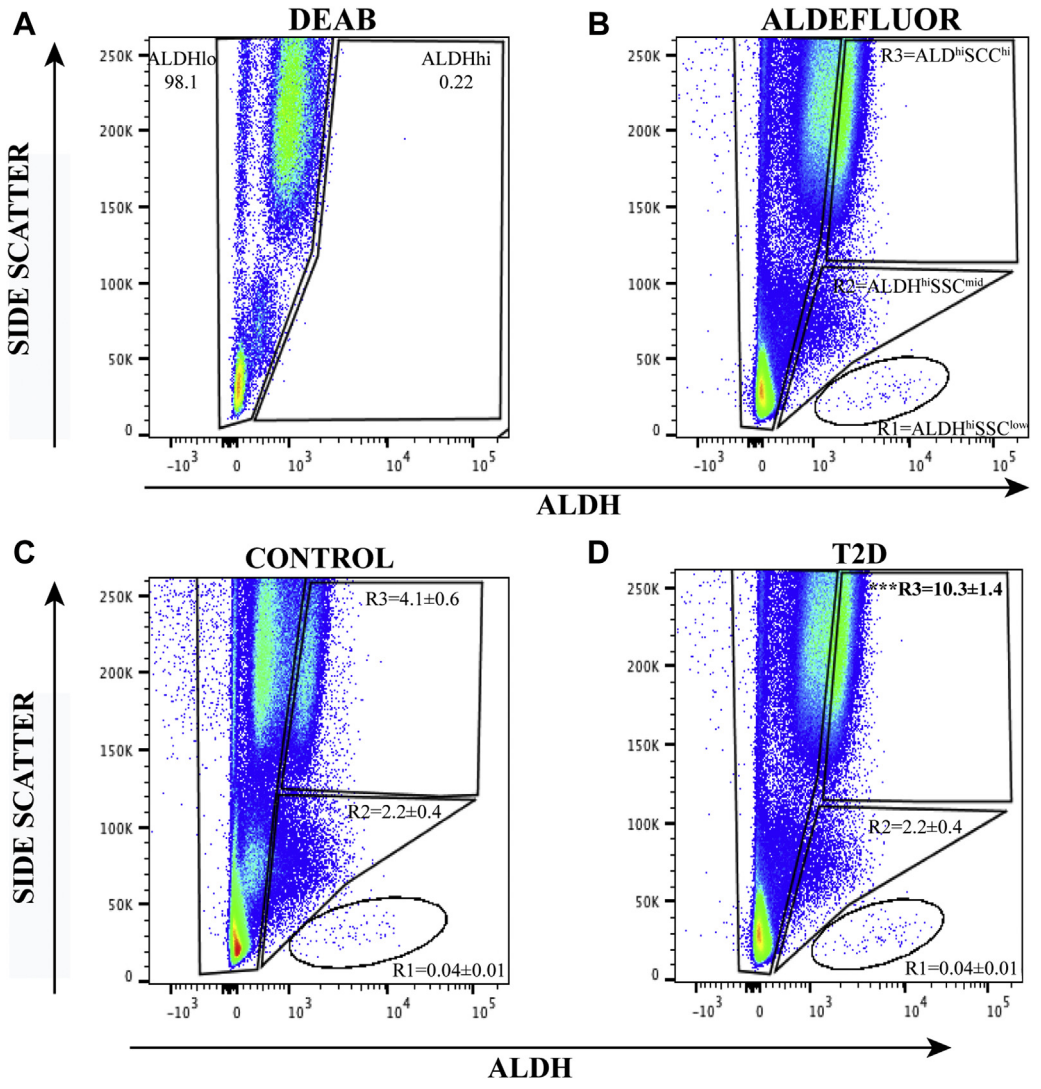

(A and B) Representative flow cytometry plots using *N,N*-diethylaminobenzaldehyde (DEAB) to inhibit aldehyde dehydrogenase (ALDH) activity establishing gates for low versus high ALDH-activity. Without inhibition, cells with high ALDH-activity exhibit increased fluorescence intensity (right shift) and detect primitive cells with a self-protective progenitor cell phenotype. High ALDH-activity combined with side scatter (SSC) properties selects for a progenitor cell subpopulation with low intracellular complexity (R1 = ALDH^{hi}SSC^{low} cells), a monocyte subpopulation with intermediate intracellular complexity (R2 = ALDH^{hi}SSC^{mid} cells), and a granulocytic subpopulation with high intracellular complexity (R3 = ALDH^{hi}SSC^{hi} cells). **(C and D)** Representative flow cytometry plots showing the frequencies of each population in control subjects and patients with type 2 diabetes mellitus (T2D). Compared with control subjects, patients with T2D exhibited an increased frequency of ALDH^{hi} cells within the granulocyte subpopulation (R3) and an equal frequency of circulating ALDH^{hi} cells with low (R1) and intermediate (R2) complexity. Values are mean ± SEM. ***p < 0.001 with the Student's *t*-test.

ALDH^{hi}SSC^{low} CELLS WITH ENDOTHELIAL-ASSOCIATED PHENOTYPES WERE DECREASED IN PATIENTS WITH T2D. We next compared the ALDH^{hi}SSC^{low} population for the expression of endothelial cell-associated and pericyte-associated adhesion molecules. Although the frequency of cells co-expressing CD34 and platelet endothelial cell adhesion molecule-1 (CD31) was equivalent between patients with T2D and control subjects (Figures 3A to 3C), primitive (CD34+) cells expressing vascular endothelial-cadherin and the pericyte marker CD146 were decreased in patients with T2D compared with control subjects

FIGURE 2 Circulating ALDH^{hi}SSC^{low} Cells With Primitive, Myeloid, and Migratory Phenotypes Are Decreased in Patients with T2D

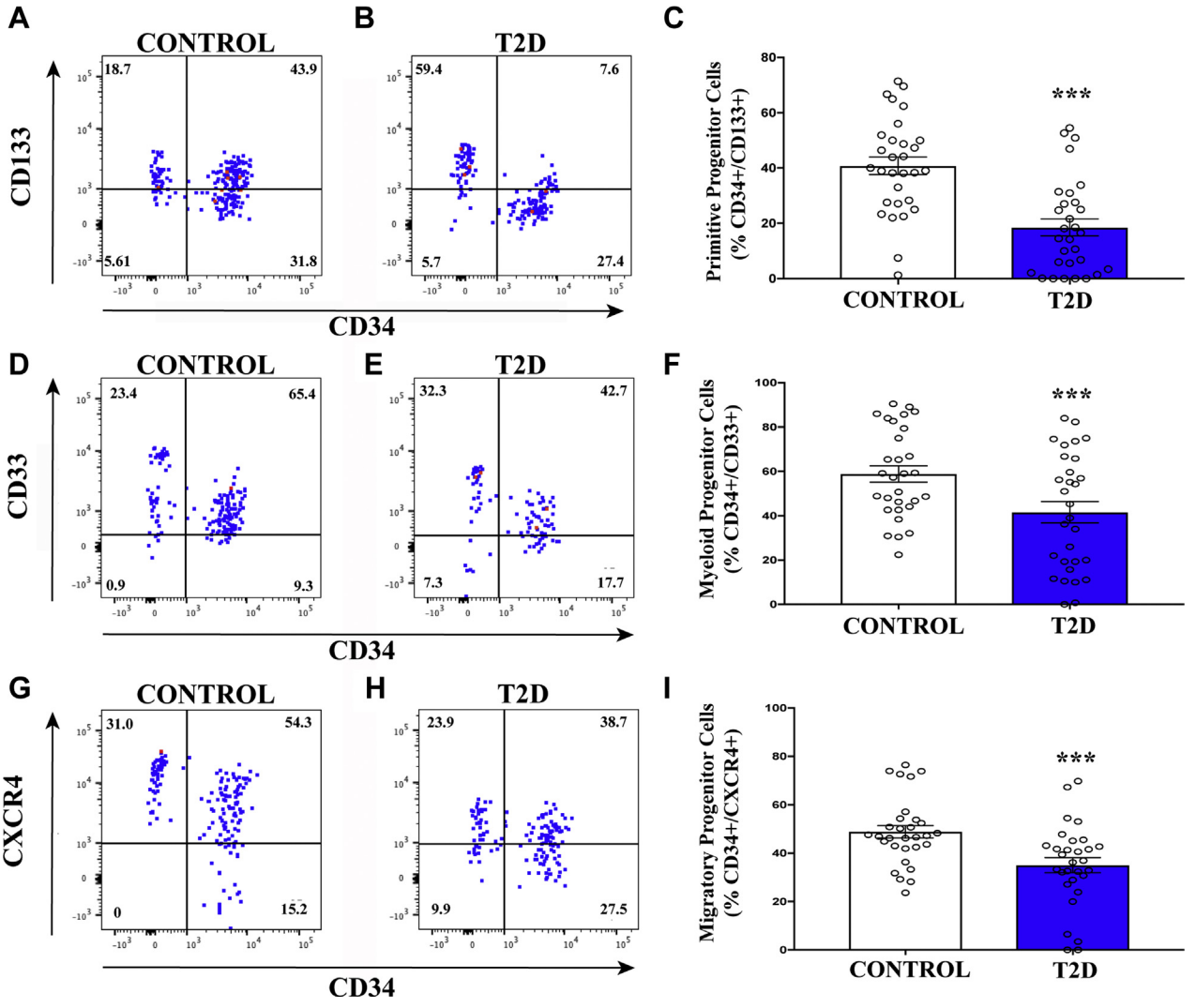

(A–C) The frequency of circulating ALDH^{hi}SSC^{low} progenitor cells with primitive cell phenotype (CD34+CD133+) was reduced in patients with T2D compared with control subjects. **(D–F)** The frequency of circulating ALDH^{hi}SSC^{low} progenitor cells with early myeloid cell phenotype (CD34+CD33+) was reduced in patients with T2D compared with control subjects. **(G–I)** The frequency of circulating ALDH^{hi}SSC^{low} progenitor cells with migratory phenotype (CD34+CXCR4+) was reduced in patients with T2D compared with control subjects. Values are mean ± SEM. ***$p < 0.01$ with the Student's *t*-test. Abbreviations as in Figure 1.

(Figures 3D to 3I). Cells expressing these markers are required for vasculogenic vessel formation (40). These findings were also consistent with the depletion of proangiogenic circulating cell content, potentially leading to a dysfunctional vascular regenerative response in patients with T2D.

ALDH^{hi}SSC^{mid} CELLS WITH PRIMITIVE AND M2 PHENOTYPES WERE DECREASED IN PATIENTS WITH T2D. Primitive circulating monocytes with proinflammatory and anti-inflammatory cytokine secretion patterns (33,41,42) were further assessed by analyses of CD68+ cells co-expressing CD34 or CD80 versus CD163 (M1/M2 marker) specifically within the ALDH^{hi}SSC^{mid} cell subset. These cells can best be described as monocytes that possess either anti-inflammatory or proinflammatory secretory activities characterized by co-expression of M1/M2 polarization markers, respectively (33,43). M2-polarized monocytes and tissue-resident M2 macrophages can contribute toward arteriogenic processes through secretion of cytokines and metalloproteinases that remodel pre-existing collateral vessels (44). In

FIGURE 3 Circulating ALDH^{hi}SSC^{low} Cells With Endothelial Cell and Pericyte-associated Adhesive Phenotypes Are Decreased in Patients With T2D

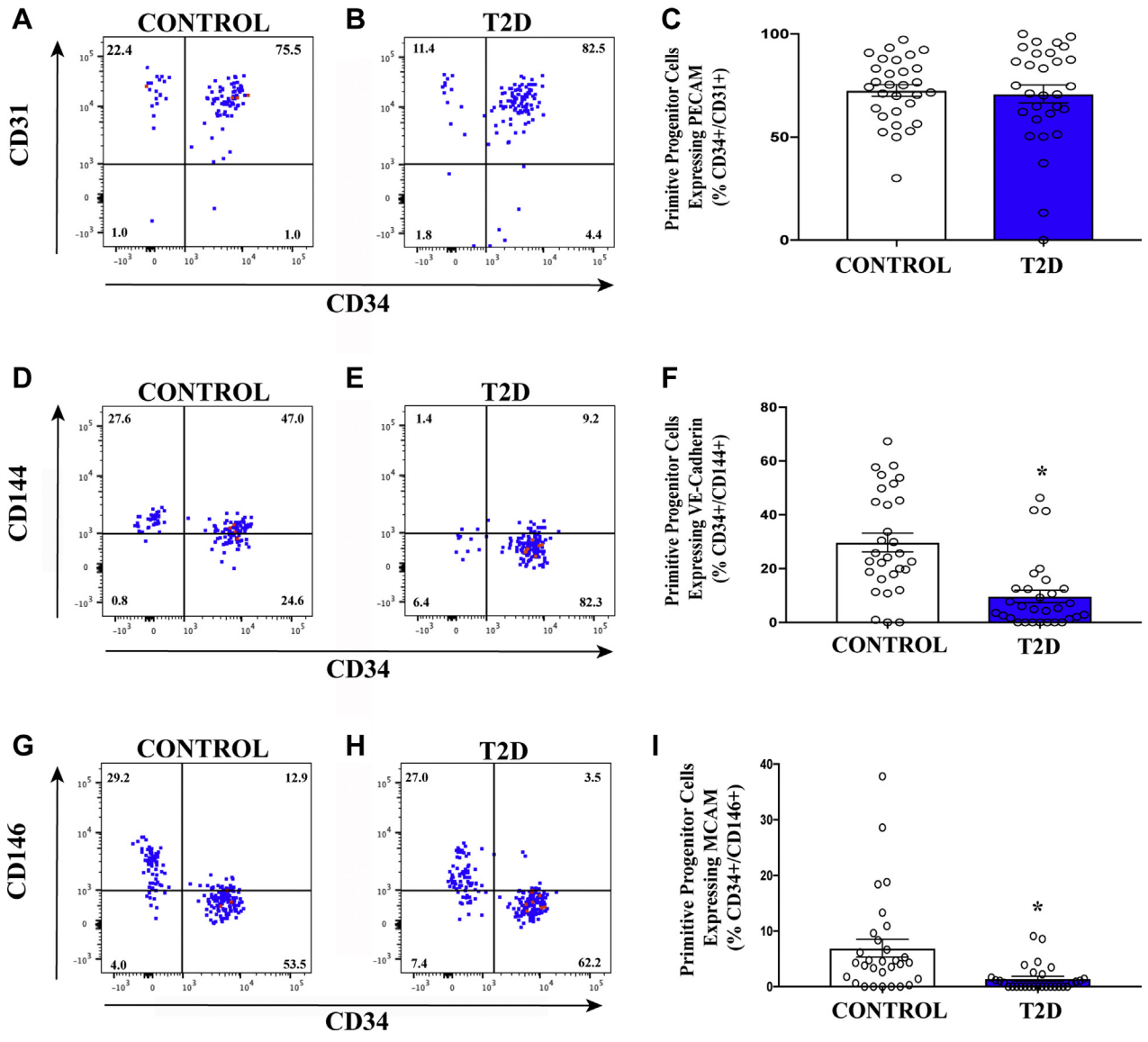

(A-C) The frequency of circulating ALDH^{hi}SSC^{low} progenitor cells co-expressing CD34 with hematopoietic/endothelial cell marker platelet endothelial cell adhesion molecule (PECAM) (CD31) was equivalent in patients with T2D compared with control subjects. **(D-F)** The frequency of circulating ALDH^{hi}SSC^{low} cells in progenitor cells co-expressing CD34 with the endothelial cell-associated marker vascular endothelial (VE)-cadherin (CD144) was decreased in patients with T2D compared with control subjects. **(G-I)** The frequency of circulating ALDH^{hi}SSC^{low} progenitor cells co-expressing CD34 with the endothelial/pericytes marker melanoma cell adhesion molecule (MCAM) (CD146) was decreased in patients with T2D compared with control subjects. Values are mean ± SEM. *$p < 0.001$ with the Student's *t*-test. Other abbreviations as in Figure 1.

contrast, M1 macrophages generally contribute toward inflammatory processes that may impede new vessel progression (18,43,45). Although we detected no significant differences in the frequency of ALDH^{hi}SSC^{mid} cells with M1 (CD68+/CD80+) phenotypes (Figures 4D to 4F), patients with T2D exhibited significantly reduced frequency of ALDH^{hi}SSC^{mid} cells with primitive (CD34+/CD68+) (Figure 4A to 4C) or M2 (CD34+/CD163+) (Figures 4G to 4I) phenotypes compared with control subjects. These findings validated the reduction in circulating monocytes with M2 polarization phenotype shown in Table 1 and suggest that patients with T2D may also exhibit reduced capacity to mediate arteriogenic vessel remodeling.

FIGURE 4 Circulating ALDH^{hi}SSC^{mid} Cells With M2 Phenotype Are Decreased in Patients With T2D

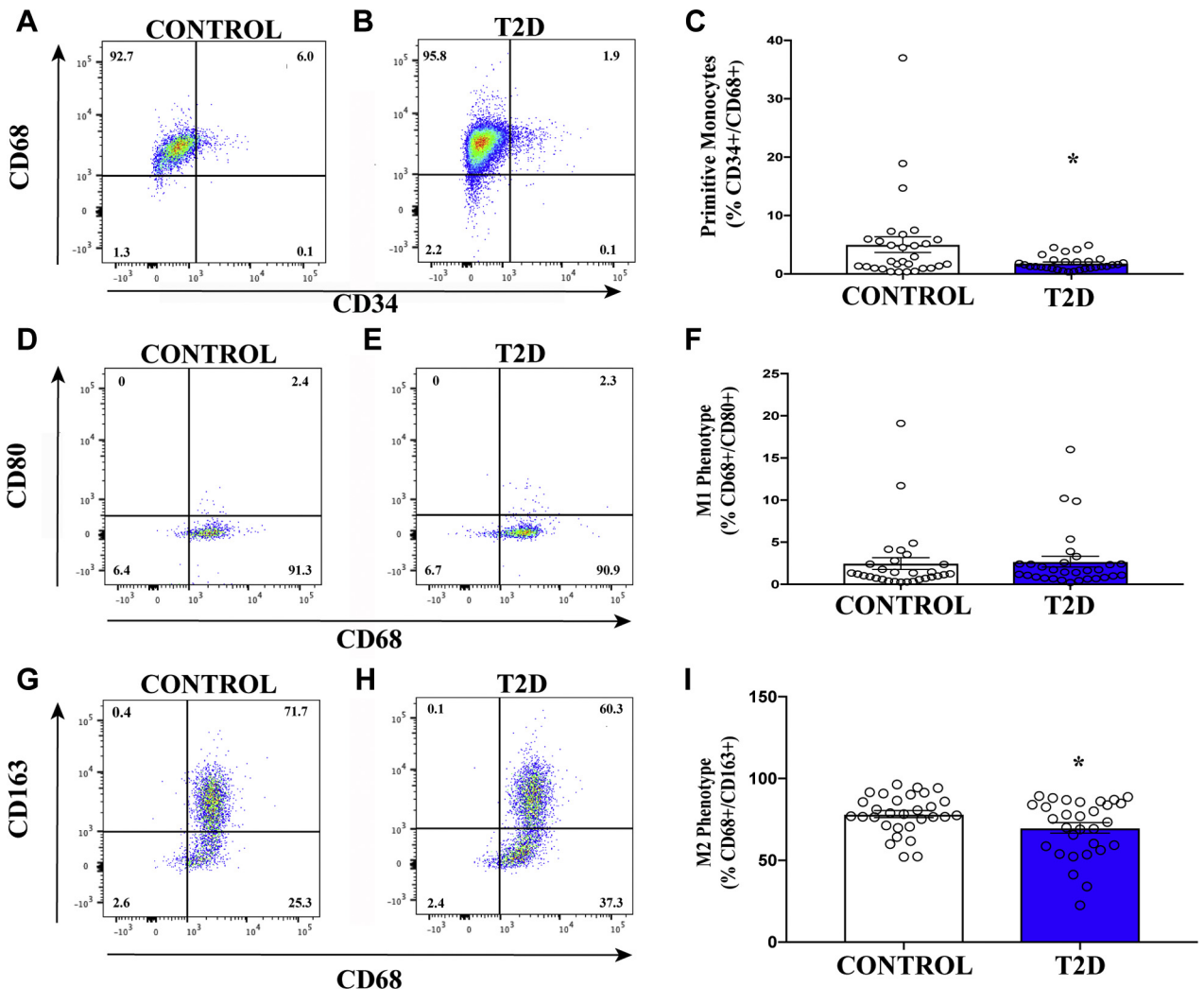

(A to C) The frequency of circulating ALDH^{hi}SSC^{mid} cells co-expressing CD34 with the macrophage scavenger receptor (CD68) was decreased in patients with T2D compared with control subjects. **(D to F)** The frequency of circulating ALDH^{hi}SSC^{mid} cells co-expressing CD68 with the M1 macrophage–associated marker CD80 was equal in patients with T2D compared with control subjects. **(G to I)** The frequency of circulating ALDH^{hi}SSC^{mid} progenitor cells co-expressing CD68 with the M2 macrophage–associated marker CD163 was decreased in patients with T2D compared with control subjects. Values are mean ± SEM. *$p < 0.05$ with the Student's *t*-test. Other abbreviations as in Figure 1.

INSULIN ADMINISTRATION CORRELATED WITH REDUCED CIRCULATING GRANULOCYTE FREQUENCY. To determine whether factors such as sex, insulin use, or HbA_{1c} status played a correlative role in the frequency of circulating provascular progenitor cells in patients with T2D, these patients were divided into 2 groups based on the median value for each category. The frequency of cell subsets with high ALDH-activity with primitive (CD34+/CD133+) and migratory (CD34+/CXCR4+) cell surface phenotype was equivalent in male (n = 12) and female (n = 18) patients with T2D (Supplemental Figure 2). Surprisingly, patients with HbA_{1c} values ≤7.0% (n = 15) or >7.0% (n = 15) also showed no significant difference in the frequencies of ALDH^{hi} cell subpopulations or in ALDH^{hi}SSC^{low} progenitor cells that expressed primitive or migratory phenotypes (Supplemental Figure 3). These data suggest that higher HbA_{1c} levels did not correlate with a reduction in circulating progenitor cell content during T2D.

We next segregated patients according to their use of daily insulin injections, a general indication of

FIGURE 5 Circulating ALDH^{hi}SSC^{hi} Inflammatory Cells Are Decreased in Patients Taking Insulin

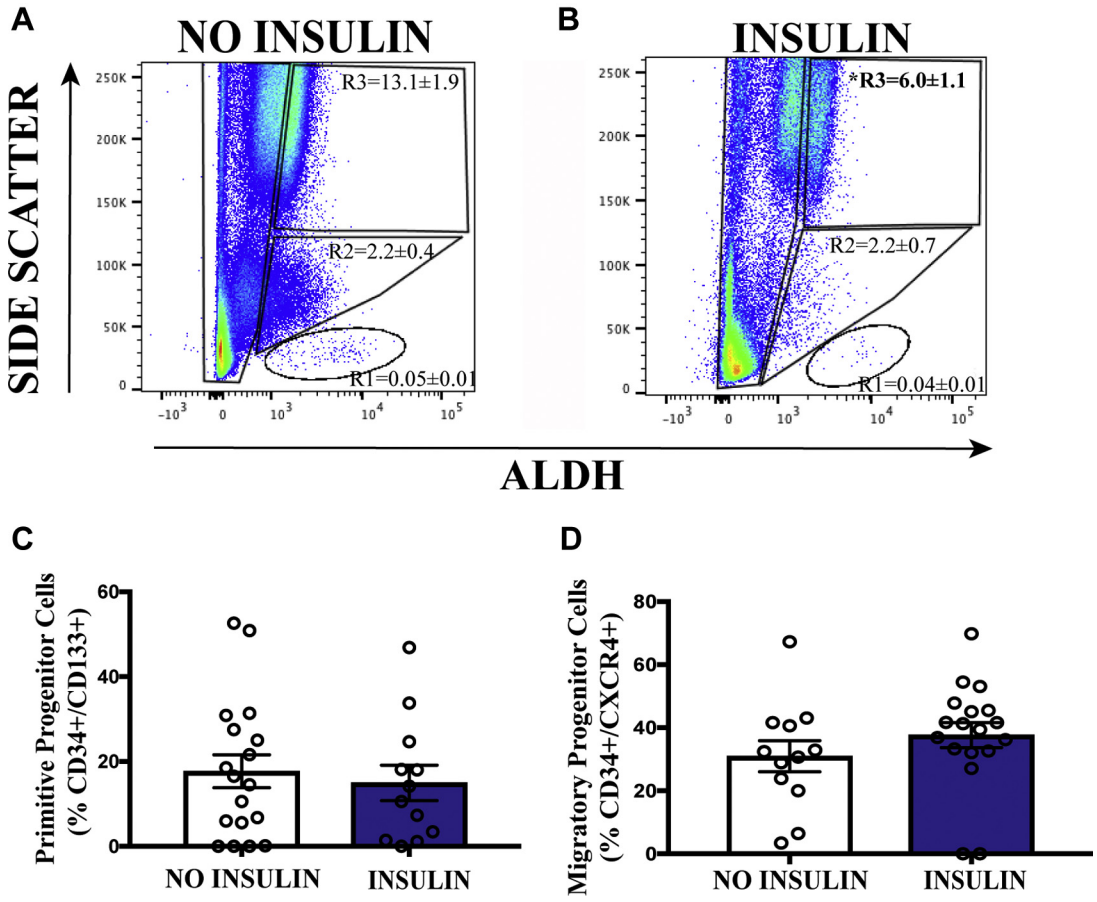

(A and B) The frequency of cells with high ALDH-activity and high SSC properties was decreased in patients with T2D taking insulin. **(C and D)** The frequency of primitive and migratory progenitor cells was equivalent in patients with T2D despite insulin therapy. Values are mean ± SEM. *p < 0.05 with the Student's *t*-test. Abbreviations as in Figure 1.

more advanced T2D whereby glycemia is not controlled by diet, exercise, and medication. There was a significant decrease in the frequency of circulating pro-inflammatory ALDH^{hi}SSC^{hi} granulocytes in patients receiving insulin therapy (Figures 5A and 5B). These data suggested reduced inflammation in patients who received insulin therapy; however, circulating primitive progenitor cell frequencies were not affected by insulin use (Figures 5C and 5D).

PROVASCULAR PROGENITOR CELL EXHAUSTION CORRELATED WITH INCREASED DURATION OF T2D. To further assess regenerative cell exhaustion during T2D, a process through which stem and progenitor cell frequency is reduced due to chronic disease, patients with T2D were subdivided based on chronological age or duration of T2D. Although increased age (≤70 years, n = 14; >70 years, n = 16) did not alter ALDH expression levels (Figures 6A and 6B) or primitive progenitor (CD34+/CD133+) or migratory (CD34+/CXCR4+) cell surface marker expression (Figures 6C and 6D), patients with increased duration of T2D (≤13 years, n = 15; >13 years, n = 15) demonstrated no difference in ALDH expression levels (Figure 6E and 6F), but did, however, exhibit significantly decreased frequency of primitive (CD34+/CD133+) and migratory (CD34+/CXCR4+) progenitor cells (Figures 6G and 6H). These data suggested that patients with prolonged T2D duration was the only analyzed subgroup that exhibited significantly reduced circulating proangiogenic progenitor cell content (23,46–48).

FIGURE 6 Circulating ALDH^{hi}SSC^{low} Cells With Primitive and Migratory Progenitor Cell Phenotypes Decreased With Longer Duration of Diabetes

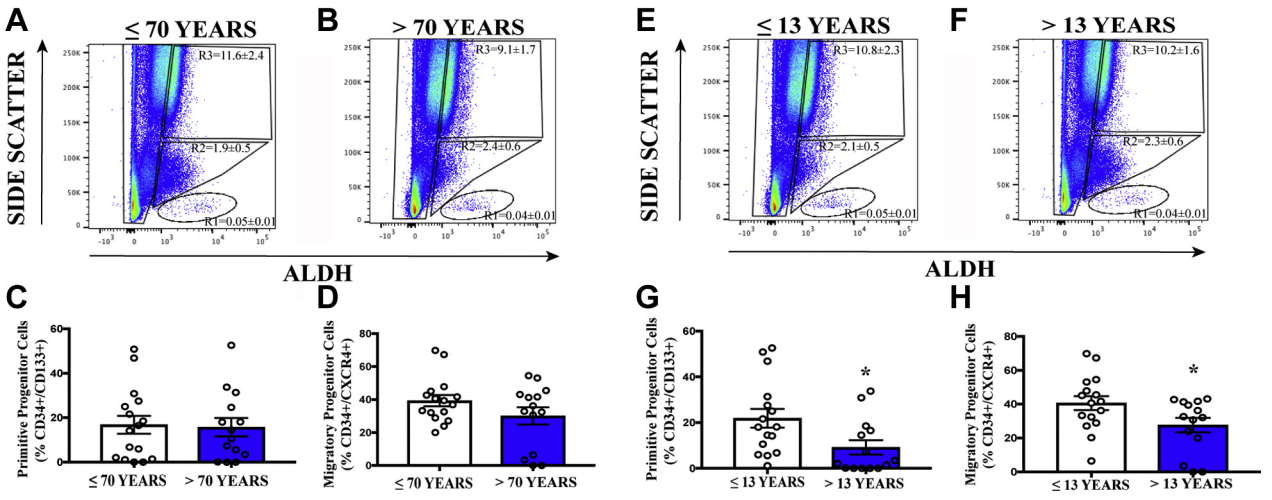

(A and B) In patients with T2D, the frequency of cells with high ALDH-activity was equivalent in patients ≤70 years of age compared with patients >70 years of age with T2D. **(C and D)** The frequency of circulating primitive progenitor cells (CD34+/CD133+) and migratory progenitor cells (CD34+/CXCR4+) was equivalent in patients ≤70 years of age compared with patients >70 years of age. **(E and F)** In patients with T2D, the frequency of cells with high ALDH-activity was equivalent in patients with diabetes duration ≤13 years compared with patients with diabetes duration >13 years. **(G and H)** However, the frequency of circulating primitive progenitor cells (CD34+/CD133+) and migratory progenitor cells was decreased in patients with diabetes duration ≤13 years compared with patients with diabetes duration >13 years. Values are mean ± SEM. *p < 0.05 with the Student's *t*-test. Abbreviations as in Figure 1.

DISCUSSION

The current study presents a novel diagnostic flow cytometry assay, using high ALDH-activity, a functional measure for a conserved progenitor cell function, combined with selected primitive and mature cell surface marker analyses, to characterize the frequency of cellular subsets with proangiogenic versus proinflammatory phenotypes from the peripheral blood of human patients with T2D compared with individuals without diabetes. The use of cell surface markers independently (e.g., CD34, CD133), as previously reported in several studies (35,39,49), revealed few differences in circulating cell frequencies between groups. However, by first detecting cells with high ALDH-activity, combined with SSC properties to discern granulocytic/neutrophil (SSC^{hi} cells), monocyte (SSC^{mid} cells), or primitive progenitor cell (SSC^{low} cells) subpopulations, allowed for additional comparison of primitive, progenitor cell markers (CD34, CD133) previously associated with proangiogenic secretory functions (37,38,50). By using this combined functional and phenotypic strategy, patients with T2D consistently exhibited the following unique characteristics: 1) an increased frequency of ALDH^{hi}SSC^{hi} granulocytes predicted to propagate inflammatory burden (51,52); 2) a reduced frequency of circulating ALDH^{hi}SSC^{mid} monocytes with CD14+ co-expression (33,43); 3) a shift in ALDH^{hi}SSC^{mid} cell M1/M2 balance toward the pro-inflammatory M1 phenotype (31,53); and 4) a decreased frequency of rare circulating ALDH^{hi}SSC^{low} progenitor cells that co-expressed CD34 and primitive (CD133), early myeloid (CD33), migratory (CXCR4), endothelial adhesion (CD144), or pericyte (CD146) cell surface markers. Collectively, these data suggest that a prolonged duration of T2D promotes a pro-inflammatory milieu, affecting both granulocytes and monocytes, in addition to depletion of rare progenitor cells shown previously to coordinate proangiogenic blood vessel repair in animal models (23,35,48,54,55).

The overall frequency of ALDH^{hi}SSC^{low} progenitor cells or CD34-expressing cells was surprisingly not decreased in patients with T2D compared with the control subjects. Selection for cells with high ALDH-activity (4,56) or CD34 expression (30,32,57,58) has been used in clinical trials as highly purified cell populations transplanted from autologous BM to combat ischemic disease. In contrast, a significant reduction in the frequency of circulating monocytes (33,42,43) with anti-inflammatory M2 phenotype (31,59,60) was easily detected in patients with T2D. These observations may be attributed to differences in the relative frequencies of circulating cells in the

peripheral blood of patients with T2D and nondiabetic control subjects. The frequency of ALDH^{hi}SSC^{low} cells in the peripheral blood of both cohorts was exceedingly low, comprising <0.1% of peripheral blood mononuclear cells, whereas CD14+ monocytes were >100-fold more abundant. Thus, careful analyses of the rare ALDH^{hi}SSC^{low} cell subset required multicolor assessment of CD34 co-expression in addition to multiple cell surface molecules with functional significance to quantify the depletion of circulating proangiogenic progenitor cells. The expression of primitive (CD133), early myeloid (CD33), chemokine (CXCR4), and cellular adhesion (CD144) molecules was consistently reduced in patients with T2D compared with nondiabetic control subjects. These findings suggest that ALDH^{hi} progenitor cells in the circulation of patients with T2D may exhibit deficits in cell adhesion and migration capacity toward ischemic endothelium. Therefore, direct comparison of ALDH^{hi}SSC^{low} cells for colony formation (24,25,34), cytokine secretion patterns (24), and migratory function in patients with T2D and control subjects are next required to assess potential functional deficits in circulating provascular cell populations.

Generalized inflammatory excess combined with circulating provascular progenitor cell depletion may contribute to an underlying issue affecting adult hematopoietic and endothelial progenitor cell maintenance in patients with T2D. This phenomenon, termed regenerative cell exhaustion, documents the loss of vascular regenerative capacity due to premature progenitor cell maturation and a reduction in the number of undifferentiated cells within the BM reservoir (27,28,46,61,62). Increased inflammation associated with chronic T2D is also known to induce increased expression of NADPH oxidase-1, which regulates the formation of ROS (28,63,64). Conceptually, although progenitor cells possess defense mechanisms such as elevated ALDH-activity to reduce oxidative stress and prevent premature apoptosis, excessive ROS may contribute to aberrant differentiation and maturation regulation within progenitor cells, resulting in the premature departure of vascular regenerative precursors from the endosteal niche in the BM (64–66). In the peripheral circulation, without the influence of developmental factors (e.g., Wnt [wingless related integration site], Notch) in the BM stem cell niche (67–70), cells are expected to demonstrate aberrant differentiation, generating dysfunctional cells with reduced contribution toward blood vessel repair and regeneration (71,72). Thus, further measurements of cell frequencies using this approach in the BM and other tissues may help correlate circulating cell deficiencies with compromised function in tissues.

To further show the utility of this assay, we stratified the T2D cohort based on patient sex, age, duration of diagnosed T2D, HbA_{1c} value, and the requirement for insulin. Notably, only the duration of T2D correlated with reduced proangiogenic progenitor cell frequency. Indeed, regenerative cell depletion became more prominent with extended duration of T2D.

To our knowledge, the current study is the first to clearly document the depletion of circulating provascular progenitor cell content by using ALDH-activity during established T2D in human subjects. Furthermore, patients with T2D exhibited a departure from an anti-inflammatory M2 phenotype toward a pro-inflammatory M1 phenotype compounded by an increase in circulating granulocytes. Throughout these analyses, we documented changes in the frequency of circulating cell phenotypes implicated in the restoration of vascular regenerative function in patients with T2D. In addition, this research provides a starting point for development of novel therapeutic approaches to combat ischemic vascular disease progression during T2D. It is evident that regenerative cell depletion and heightened inflammation during T2D generates a harsh microenvironment for functional revascularization (23,27,48,62,63). By reducing inflammation and limiting ROS, development of therapeutic strategies tailored to the restoration of the vascular regenerative cell generation and function may aid in the prevention of ischemic vascular comorbidities that are so devastating during the progression of T2D.

STUDY LIMITATIONS AND FUTURE DIRECTIONS. Care must be taken when extending the utility of these studies toward potential clinical application. First, the detection of very rare circulating cell populations by using flow cytometry provides a diagnostic tool to measure altered cell frequencies during T2D. Future long-term clinical studies should incorporate multiple assessments of circulating cell subpopulations as T2D progresses. With mindful trial design, this assay may reveal the sensitivity required to correlate changes in circulating cell frequencies with specific outcomes such as adverse cardiovascular events. Second, circulating cell subpopulations were not assayed for relevant proangiogenic function in this study. In future studies, we intend to assess colony formation as well as secretory and migratory functions of relevant cell populations as T2D

progresses. Third, analyses of tissue-resident progenitor cell or macrophage frequencies were not conducted in this study and are needed to determine how circulating cell content correlates with cell frequencies in the BM or other tissues affected by ischemia such as the heart or skeletal muscle. Finally, disease comorbidities such as obesity, atherosclerotic burden, previous ischemic events, and drug use need to be carefully controlled between groups when interpreting the relevance of these measurements on the potential alteration of T2D progression.

CONCLUSIONS

Circulating cells with pro-inflammatory phenotype were more abundant in patients with T2D, and rare ALDH-expressing progenitor cells previously associated with vascular regenerative function were markedly reduced. In addition, adhesive and migratory cell surface marker co-expression associated with homing to areas of ischemia and secretion of proangiogenic effectors was deficient on circulating ALDH^{hi} progenitor cells in patients with T2D. Collectively, alterations in these circulating cell phenotypes may presumably contribute to the gradual loss of the capacity for vascular repair. Although we can clearly detect differences in the frequencies of rare circulating progenitor cells by using high ALDH-activity, further studies are warranted to assess the vascular regenerative functions of these circulating cell populations. Functional analyses relevant to ischemic disease include the formation of myeloid hematopoietic and endothelial cell colonies, tubule formation, migration to areas of ischemia, and secretion of proangiogenic cytokines that coordinate vascular regenerative processes. Furthermore, functional testing of the capacity of these cell types to contribute to perfused neovessel formation in vivo is still required. Nonetheless, potential reversal of this "exhausted" vascular regenerative cell phenotype during T2D, through regenerative medicine strategies or by administration of therapeutic agents with documented cardiovascular protective effects, represents an exciting avenue to be tested in future studies.

ADDRESS FOR CORRESPONDENCE: Dr. David A. Hess, Robarts Research Institute, Western University, 1153 Richmond Street, London, Ontario N6A 5B7, Canada. E-mail: dhess@robarts.ca. OR Dr. Subodh Verma, Division of Cardiac Surgery, St. Michael's Hospital, Suite 8-003, 30 Bond Street, Toronto, Ontario M5B 1W8, Canada. E-mail: vermasu@smh.ca.

PERSPECTIVES

COMPETENCY IN MEDICAL KNOWLEDGE: Individuals with T2D are at a heightened risk of developing cardiovascular disorders and often endure poor outcomes after a cardiovascular event. This study shows, for the first time, that compared with individuals who are normoglycemic, those with established T2D exhibit depleted circulating vascular regenerative progenitor cell content measured in the circulation by using ALDH-activity, a conserved protective function demonstrated by proangiogenic endothelial and hematopoietic progenitor cells. In contrast, circulating monocytes exhibit a migration from a protective anti-inflammatory phenotype to one that is proinflammatory, collectively discouraging functional revascularization.

TRANSLATIONAL OUTLOOK: Using a combination of ALDH-activity measurement and cell surface marker expression, we have developed a novel diagnostic flow cytometry assay to evaluate the balance between circulating proangiogenic progenitor and proinflammatory cell content in peripheral blood. This study provides a critical translational perspective by the suggestion that the balance in these cells during the progression of T2D is critical to the development of and recovery from ischemic vascular comorbidities. The potential of developing this assay into a diagnostic tool to estimate the capacity to mitigate ischemia via a provascular regenerative response represents an exciting avenue for exploration and will need to be investigated.

REFERENCES

1. American Diabetes Association. 2. Classification and diagnosis of diabetes: standards of medical care in diabetes-2018. Diabetes Care 2018;41:S13–27.

2. Diabetes Canada Clinical Practice Guidelines Expert Committee, Punthakee Z, Goldenberg R, Katz P. Definition, classification and diagnosis of diabetes, prediabetes and metabolic syndrome. Can J Diabetes 2018;42 Suppl 1:S10–5.

3. International Diabetes Federation. IDF Diabetes Atlas—Eight Edition. Brussels, Belgium: International Diabetes Federation, 2017.

4. Qadura M, Terenzi DC, Verma S, Al-Omran M, Hess DA. Concise review: cell therapy for critical limb ischemia: an integrated review of preclinical and clinical studies. Stem Cells 2018;36:161–71.

5. Zinman B, Wanner C, Lachin JM, et al. Empagliflozin, cardiovascular outcomes, and mortality in type 2 diabetes. N Engl J Med 2015;373:2117–28.

6. Verma S, Mazer CD, Fitchett D, et al. Empagliflozin reduces cardiovascular events,

mortality and renal events in participants with type 2 diabetes after coronary artery bypass graft surgery: subanalysis of the EMPA-REG OUTCOME(R) randomised trial. Diabetologia 2018;61:1712–23.

7. Verma S, Mazer CD, Al-Omran M, et al. Cardiovascular outcomes and safety of empagliflozin in patients with type 2 diabetes mellitus and peripheral artery disease: a subanalysis of EMPA-REG OUTCOME. Circulation 2018;137:405–7.

8. Verma S, Bhatt DL, Bain SC, et al. Effect of liraglutide on cardiovascular events in patients with type 2 diabetes mellitus and polyvascular disease: results of the LEADER trial. Circulation 2018;137:2179–83.

9. Mann JF, Orsted DD, Brown-Frandsen K, et al. Liraglutide and renal outcomes in type 2 diabetes. N Engl J Med 2017;377:839–48.

10. Marso SP, Daniels GH, Brown-Frandsen K, et al. Liraglutide and cardiovascular outcomes in type 2 diabetes. N Engl J Med 2016;375:311–22.

11. Verma S, Leiter LA, Mazer CD, et al. Liraglutide reduces cardiovascular events and mortality in type 2 diabetes mellitus independently of baseline low-density lipoprotein cholesterol levels and statin use. Circulation 2018;138:1605–7.

12. Verma S, Poulter NR, Bhatt DL, et al. Effects of liraglutide on cardiovascular outcomes in patients with type 2 diabetes with or without history of myocardial infarction or stroke: a post hoc analysis from the LEADER trial. Circulation 2018;137:2179–83.

13. Sherman SE, Bell GI, Teoh H, et al. Canagliflozin improves the recovery of blood flow in an experimental model of severe limb ischemia. J Am Coll Cardiol Basic Trans Science 2018;3:327–9.

14. Verma S, Rawat S, Ho KL, et al. Empagliflozin increases cardiac energy production in diabetes. Novel translational insights into the heart failure benefits of SGLT2 inhibitors. J Am Coll Cardiol Basic Trans Science 2018;3:575–87.

15. Wanner C, Inzucchi SE, Lachin JM, et al. Empagliflozin and progression of kidney disease in type 2 diabetes. N Engl J Med 2016;375:323–34.

16. Prospective Studies Collaboration, Asia Pacific Cohort Studies Collaboration. Sex-specific relevance of diabetes to occlusive vascular and other mortality: a collaborative meta-analysis of individual data from 980 793 adults from 68 prospective studies. Lancet Diabetes Endocrinol 2018;6:538–46.

17. Hess DA, Meyerrose TE, Wirthlin L, et al. Functional characterization of highly purified human hematopoietic repopulating cells isolated according to aldehyde dehydrogenase activity. Blood 2004;104:1648–55.

18. Chambers SE, O'Neill CL, O'Doherty TM, Medina RJ, Stitt AW. The role of immune-related myeloid cells in angiogenesis. Immunobiology 2013;218:1370–5.

19. Norgren L, Hiatt WR, Dormandy JA, et al. Inter-society consensus for the management of peripheral arterial disease. Int Angiol 2007;26:81–157.

20. Bergers G, Song S. The role of pericytes in blood-vessel formation and maintenance. Neuro Oncol 2005;7:452–64.

21. Buschmann I, Heil M, Jost M, Schaper W. Influence of inflammatory cytokines on arteriogenesis. Microcirculation 2003;10:371–9.

22. King A, Balaji S, Keswani SG, Crombleholme TM. The role of stem cells in wound angiogenesis. Adv Wound Care (New Rochelle) 2014;3:614–25.

23. Fadini GP, Ferraro F, Quaini F, Asahara T, Madeddu P. Concise review: diabetes, the bone marrow niche, and impaired vascular regeneration. Stem Cells Transl Med 2014;3:949–57.

24. Putman DM, Liu KY, Broughton HC, Bell GI, Hess DA. Umbilical cord blood-derived aldehyde dehydrogenase-expressing progenitor cells promote recovery from acute ischemic injury. Stem Cells 2012;30:2248–60.

25. Putman DM, Cooper TT, Sherman SE, et al. Expansion of umbilical cord blood aldehyde dehydrogenase expressing cells generates myeloid progenitor cells that stimulate limb revascularization. Stem Cells Transl Med 2017;6:1607–19.

26. Patel RS, Li Q, Ghasemzadeh N, et al. Circulating CD34+ progenitor cells and risk of mortality in a population with coronary artery disease. Circ Res 2015;116:289–97.

27. Bigarella CL, Liang R, Ghaffari S. Stem cells and the impact of ROS signaling. Development 2014;141:4206–18.

28. Mangialardi G, Spinetti G, Reni C, Madeddu P. Reactive oxygen species adversely impacts bone marrow microenvironment in diabetes. Antioxid Redox Signal 2014;21:1620–33.

29. Loomans CJ, van Haperen R, Duijs JM, et al. Differentiation of bone marrow-derived endothelial progenitor cells is shifted into a proinflammatory phenotype by hyperglycemia. Mol Med 2009;15:152–9.

30. Mackie AR, Losordo DW. CD34-positive stem cells: in the treatment of heart and vascular disease in human beings. Tex Heart Inst J 2011;38:474–85.

31. Jetten N, Verbruggen S, Gijbels MJ, Post MJ, De Winther MP, Donners MM. Anti-inflammatory M2, but not pro-inflammatory M1 macrophages promote angiogenesis in vivo. Angiogenesis 2014;17:109–18.

32. Mathiyalagan P, Liang Y, Kim D, et al. Angiogenic mechanisms of human CD34(+) stem cell exosomes in the repair of ischemic hindlimb. Circ Res 2017;120:1466–76.

33. Urbich C, Heeschen C, Aicher A, Dernbach E, Zeiher AM, Dimmeler S. Relevance of monocytic features for neovascularization capacity of circulating endothelial progenitor cells. Circulation 2003;108:2511–6.

34. Capoccia BJ, Robson DL, Levac KD, et al. Revascularization of ischemic limbs after transplantation of human bone marrow cells with high aldehyde dehydrogenase activity. Blood 2009;113:5340–51.

35. Asahara T, Murohara T, Sullivan A, et al. Isolation of putative progenitor endothelial cells for angiogenesis. Science 1997;275:964–7.

36. Asahara T, Masuda H, Takahashi T, et al. Bone marrow origin of endothelial progenitor cells responsible for postnatal vasculogenesis in physiological and pathological neovascularization. Circ Res 1999;85:221–8.

37. Hess DA, Wirthlin L, Craft TP, et al. Selection based on CD133 and high aldehyde dehydrogenase activity isolates long-term reconstituting human hematopoietic stem cells. Blood 2006;107:2162–9.

38. Siemerink MJ, Klaassen I, Vogels IM, Griffioen AW, Van Noorden CJ, Schlingemann RO. CD34 marks angiogenic tip cells in human vascular endothelial cell cultures. Angiogenesis 2012;15:151–63.

39. Fadini GP, Miorin M, Facco M, et al. Circulating endothelial progenitor cells are reduced in peripheral vascular complications of type 2 diabetes mellitus. J Am Coll Cardiol 2005;45:1449–57.

40. Yoder MC, Mead LE, Prater D, et al. Redefining endothelial progenitor cells via clonal analysis and hematopoietic stem/progenitor cell principals. Blood 2007;109:1801–9.

41. Travnickova J, Tran Chau V, Julien E, et al. Primitive macrophages control HSPC mobilization and definitive haematopoiesis. Nat Commun 2015;6:6227.

42. Jaipersad AS, Lip GY, Silverman S, Shantsila E. The role of monocytes in angiogenesis and atherosclerosis. J Am Coll Cardiol 2014;63:1–11.

43. Dalton HJ, Armaiz-Pena GN, Gonzalez-Villasana V, Lopez-Berestein G, Bar-Eli M, Sood AK. Monocyte subpopulations in angiogenesis. Cancer Res 2014;74:1287–93.

44. Heil M, Schaper W. Influence of mechanical, cellular, and molecular factors on collateral artery growth (arteriogenesis). Circ Res 2004;95:449–58.

45. Peiser L, Gordon S. The function of scavenger receptors expressed by macrophages and their role in the regulation of inflammation. Microbes Infect 2001;3:149–59.

46. Kovacic JC, Moreno P, Hachinski V, Nabel EG, Fuster V. Cellular senescence, vascular disease, and aging: part 1 of a 2-part review. Circulation 2011;123:1650–60.

47. Dykstra B, de Haan G. Hematopoietic stem cell aging and self-renewal. Cell Tissue Res 2008;331:91–101.

48. Fadini GP, Ciciliot S, Albiero M. Concise review: perspectives and clinical implications of bone marrow and circulating stem cell defects in diabetes. Stem Cells 2017;35:106–16.

49. Werner N, Kosiol S, Scheigel T, et al. Circulating endothelial progenitor cells and cardiovascular outcomes. N Engl J Med 2005;355:999–1007.

50. Barcelos LS, Duplaa C, Krankel N, et al. Human CD133+ progenitor cells promote the healing of diabetic ischemic ulcers by paracrine stimulation

of angiogenesis and activation of Wnt signaling. Circ Res 2009;104:1095–102.

51. Rosales C. Neutrophil: a cell with many roles in inflammation or several cell types? Front Physiol 2018;9:113.

52. Wong SL, Demers M, Martinod K, et al. Diabetes primes neutrophils to undergo NETosis, which impairs wound healing. Nat Med 2015;21:815–9.

53. Martinez FO, Gordon S. The M1 and M2 paradigm of macrophage activation: time for reassessment. F1000Prime Rep 2014;6:13.

54. Sata M. Role of circulating vascular progenitors in angiogenesis, vascular healing, and pulmonary hypertension: lessons from animal models. Arterioscler Thromb Vasc Biol 2006;26:1008–14.

55. Xu H, Barnes GT, Yang Q, et al. Chronic inflammation in fat plays a crucial role in the development of obesity-related insulin resistance. J Clin Invest 2003;112:1821–30.

56. Perin EC, Murphy M, Cooke JP, et al. Rationale and design for PACE: patients with intermittent claudication injected with ALDH bright cells. Am Heart J 2014;168:667–73.

57. Gupta R, Losordo DW. Cell therapy for critical limb ischemia: moving forward one step at a time. Circ Cardiovasc Interv 2011;4:2–5.

58. Losordo DW, Henry TD, Davidson C, et al. Intramyocardial, autologous CD34+ cell therapy for refractory angina. Circ Res 2011;109:428–36.

59. Lee WJ, Tateya S, Cheng AM, et al. M2 macrophage polarization mediates anti-inflammatory effects of endothelial nitric oxide signaling. Diabetes 2015;64:2836–46.

60. Liu YC, Zou XB, Chai YF, Yao YM. Macrophage polarization in inflammatory diseases. Int J Biol Sci 2014;10:520–9.

61. Tchkonia T, Zhu Y, van Deursen J, Campisi J, Kirkland JL. Cellular senescence and the senescent secretory phenotype: therapeutic opportunities. J Clin Invest 2013;123:966–72.

62. Freund A, Orjalo AV, Desprez PY, Campisi J. Inflammatory networks during cellular senescence: causes and consequences. Trends Mol Med 2010;16:238–46.

63. Porto ML, Rodrigues BP, Menezes TN, et al. Reactive oxygen species contribute to dysfunction of bone marrow hematopoietic stem cells in aged C57BL/6 J mice. J Biomed Sci 2015;22:97.

64. Shao L, Li H, Pazhanisamy SK, Meng A, Wang Y, Zhou D. Reactive oxygen species and hematopoietic stem cell senescence. Int J Hematol 2011;94:24–32.

65. Shinohara A, Imai Y, Nakagawa M, Takahashi T, Ichikawa M, Kurokawa M. Intracellular reactive oxygen species mark and influence the megakaryocyte-erythrocyte progenitor fate of common myeloid progenitors. Stem Cells 2014;32:548–57.

66. Rauscher FM, Goldschmidt-Clermont PJ, Davis BH, et al. Aging, progenitor cell exhaustion, and atherosclerosis. Circulation 2003;108:457–63.

67. Williams AR, Hare JM. Mesenchymal stem cells: biology, pathophysiology, translational findings, and therapeutic implications for cardiac disease. Circ Res 2011;109:923–40.

68. Kfoury Y, Scadden DT. Mesenchymal cell contributions to the stem cell niche. Cell Stem Cell 2015;16:239–53.

69. Caplan AI, Correa D. The MSC: an injury drugstore. Cell Stem Cell 2011;9:11–5.

70. Colter DC, Sekiya I, Prockop DJ. Identification of a subpopulation of rapidly self-renewing and multipotential adult stem cells in colonies of human marrow stromal cells. Proc Natl Acad Sci U S A 2001;98:7841–5.

71. Zoungas S, Woodward M, Li Q, et al. Impact of age, age at diagnosis and duration of diabetes on the risk of macrovascular and microvascular complications and death in type 2 diabetes. Diabetologia 2014;57:2465–74.

72. Duncan AW, Rattis FM, DiMascio LN, et al. Integration of Notch and Wnt signaling in hematopoietic stem cell maintenance. Nat Immunol 2005;6:314–22.

KEY WORDS aldehyde dehydrogenase, angiogenesis, ischemia, progenitor cells, type 2 diabetes

APPENDIX For supplemental figures and tables, please see the online version of this paper.

JACC: BASIC TO TRANSLATIONAL SCIENCE
VOL. 4, NO. 1, 2019
ISSN 2452-302X

Letters

Dipeptidyl Peptidase-4 Inhibition Prevents Vascular Calcification by Potentiating the Insulin-Like Growth Factor-1 Signaling Pathway

Cardiovascular calcification is a growing burden and a leading contributor to acute cardiovascular events, but no therapeutics are currently available. Recently, Choi et al. (1) put forward dipeptidyl peptidase (DPP)-4 as a new pharmacological target to prevent aortic valve calcification. DPP-4 is an exopeptidase that cleaves many substrates, including insulin-like growth factor (IGF)-1 to a less bioactive molecule at the IGF-1 receptor, which is suggested to induce a potent anti-calcifying effect (2) However, as previously stressed (3), it remains to be carefully investigated whether DPP-4 inhibition represents a new strategy to prevent cardiovascular calcification and to ascertain if this anti-calcifying effect is related to the prevention of DPP-4–mediated IGF-1 inactivation.

For this objective, we compared the global gene expression profiles of human calcified carotid atherosclerotic plaques with those of adjacent sites, obtained from endarterectomy specimens (4) using Affymetrix GeneChip Human Gene 1.0 ST arrays (Affymetrix, Santa Clara, California). We assessed the mRNA expression level of DPP-4 and its relation with mRNA levels of the osteochondogenic and contractile markers, Runt-related transcription factor 2 (RUNX2) and myosin heavy chain 11 (MYH11), respectively. Furthermore, we assessed the impact of the DPP-4 inhibitor, sitagliptin, alone or combined with picropodophyllin, which inhibits both the activity of the IGF-1 receptor and its expression, on vascular calcification. We used an ex vivo mineralization assay of the aorta isolated from male wild-type Wistar rats and cut into 2- to 3-mm rings (3 to 5 rings per aorta). Calcium content of rat aortic rings was determined colorimetrically with o-cresolphthalein complexone.

Differences between the mRNA expression levels of DPP-4 and the IGF-1 receptor between human calcified carotid plaques and adjacent sites were assessed by paired *t* test corrected for multiple testing using the Benjamini-Hochberg false discovery rate (FDR) procedure. Pearson's correlation analyses were used to assess the relationships between DPP-4 and RUNX2 and MYH11 mRNA expression levels. To consider the variability in the degree of calcification between isolated rat aortas, differences between groups for the calcium content of rat aortic rings were analyzed using a generalized linear model with group as a factor and the aorta used as a co-factor, followed by Tukey-Kramer multiple comparison tests for post hoc analysis. A p value of <0.05 was considered statistically significant.

Similar to the results obtained for the human aortic valve (1), DPP-4 was among the most upregulated genes in calcified carotid plaques compared with adjacent sites (3.21-fold; FDR <0.001) (**Figure 1A**). Moreover, we observed a strong positive correlation between DPP-4 and RUNX2 gene expression levels and an inverse relation between DPP-4 and MYH11 expression levels (**Figure 1B**). Interestingly, calcified carotid plaques were also characterized by a marked decrease in IGF-1 receptor gene expression compared with adjacent sites (0.66-fold; FDR <0.001) (**Figure 1A**). These results supported a role for DPP-4 and IGF-1 in the vascular calcification process.

Culture of rat aortic rings in high-phosphate conditions (3.8-mM inorganic phosphate) during 7 days induced an increase in the aortic calcium content that was reduced by the addition of the DPP-4 inhibitor sitagliptin to the culture medium, as illustrated by calcium deposition with alizarin red staining (**Figure 1C**) and by increasing concentrations of IGF-1 (**Figure 1D**). The addition of the IGF-1 receptor inhibitor picropodophyllin prevented the inhibitory effect of sitagliptin (**Figure 1C**) and exogenous IGF-1 (**Figure 1D**) on aortic calcification, which supported the concept that the vascular anti-calcifying effect of DPP-4 inhibition was related to the potentiation of IGF-1 signaling. In a second set of experiments, we showed that the aortic calcification induced by high-phosphate conditions was significantly enhanced by the combination of sitagliptin and picropodophyllin (32.1 ± 7.1 μg/mg vs. 140.8 ± 7.1 μg/mg; $n = 4$ per condition; $p < 0.05$), but was unchanged in the

FIGURE 1 Role of the DPP-4/IGF-1 Signaling Pathway in Vascular Calcification

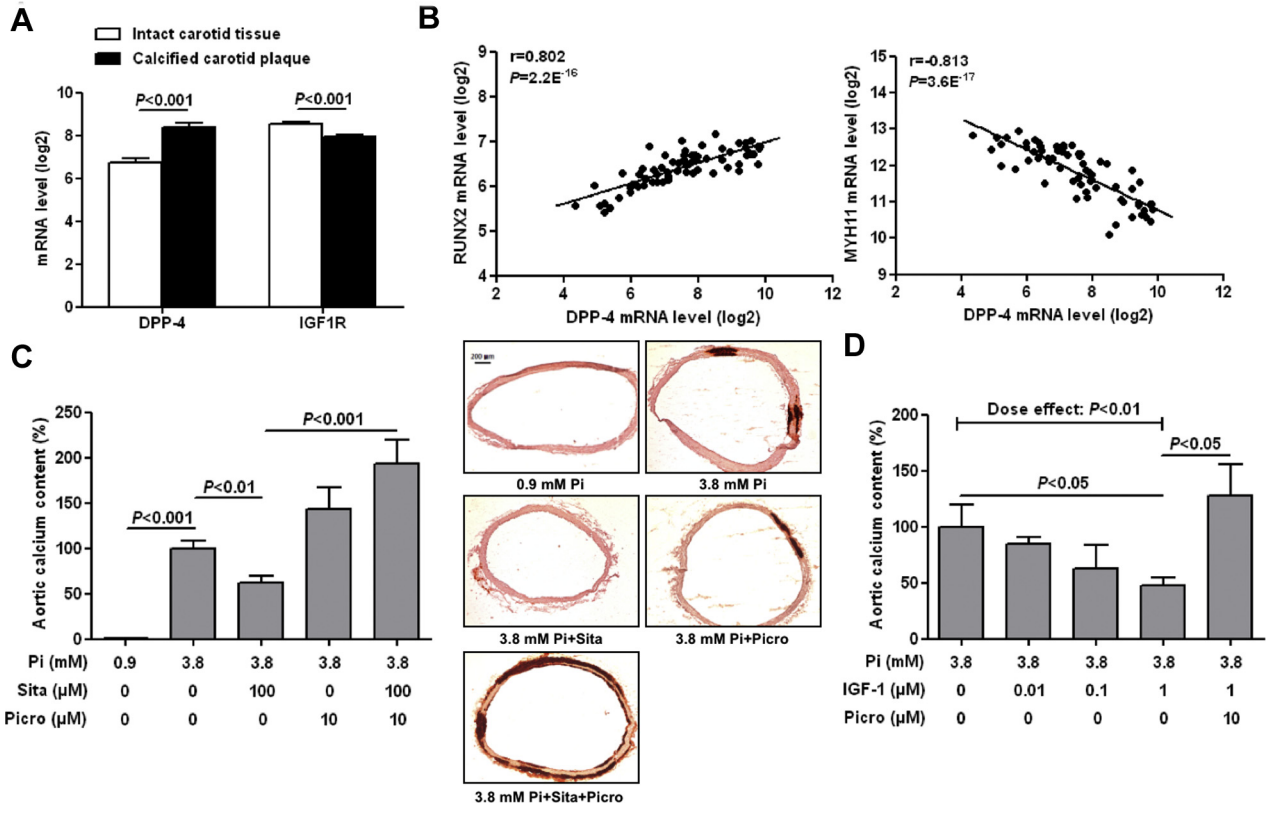

(A) mRNA expression levels of dipeptidyl peptidase-4 (DPP-4) and the insulin growth factor-1 (IGF-1) receptor between human calcified carotid plaques (n = 34) and distant intact tissues (n = 34). **(B)** Relationships between mRNA expression levels of DPP-4 with mRNA levels of runt-related transcription factor 2 (RUNX2) and myosin heavy chain 11 (MYH11). **(C)** Calcium content and representative images of calcium accumulation with Alizarin red staining in rat aortic rings cultured in normal (0.9-mM inorganic phosphate [Pi]) and high-phosphate (3.8-mM Pi) conditions during 7 days in the absence and in the presence of the DPP-4 inhibitor sitagliptin (Sita) and/or the inhibitor of IGF-1 receptor picropodophyllin (Picro) (n = 6 to 9 per condition). **(D)** Calcium content of rat aortic rings cultured in 3.8-mM Pi conditions during 7 days in the presence of increasing concentrations of IGF-1 and Picro (n = 4 per condition). Data are mean ± SEM.

presence of sitagliptin associated with the dual inhibitor of the IGF-1 and insulin receptors, BMS-754807 (40.5 ± 15.2 μg/mg; n = 4; $p < 0.05$ vs. sitagliptin and picropodophyllin). This suggested that the activation of the insulin receptor by IGF-1, which becomes prominent during blockade of the IGF-1 receptor, contributed to vascular calcification (5).

Ours results showed that alteration of DPP-4 and the IGF-1 axis represents a new mechanism of vascular calcification. Inhibitors of DPP-4 represent an exciting pharmacological avenue to slow vascular calcification by preventing IGF-1 inactivation and restoring IGF-1 receptor-dependent signaling. However, as previously stressed (2), IGF-1 was also shown to potentiate osteoblastic bone formation; inhibition of DPP-4 could be rather detrimental at an advanced stage of the calcific disease. In addition, DPP-4 metabolizes many other substrates that could exert unintended adverse effects in vivo, in particular, on cardiovascular calcification. Additional experiments are thus needed to assess the impact of DPP-4 inhibitors at this level in humans, but the cumulative experimental evidence strongly suggests that they may help to finally prevent cardiovascular calcification and its associated complications.

Olivier Varennes, PharmD
Aurélien Mary, PharmD, PhD
Giampiero Bricca, MD, PhD†
Saïd Kamel, PharmD, PhD
***Jeremy Bellien, PharmD, PhD**

*Service de Pharmacologie
Centre Hospitalier Universitaire de Rouen
1 rue de Germont
76031 Rouen Cedex
France
E-mail: jeremy.bellien@chu-rouen.fr

https://doi.org/10.1016/j.jacbts.2018.11.002

Please note: This work was supported by the French Government, managed by the National Research Agency (ANR) under the program Investissements d'Avenir, with the reference ANR-16-RHUS-0003_STOP-AS. The authors have reported that they have no relationships relevant to the contents of this paper to disclose. †Deceased October 14, 2015.

All authors attest they are in compliance with human studies committees and animal welfare regulations of the authors' institutions and US Food and Drug Administration guidelines, including patient consent where appropriate. For more information, visit the *JACC: Basic to Translational Science* author instructions page.

REFERENCES

1. Choi B, Lee S, Kim SM, et al. Dipeptidyl peptidase-4 induces aortic valve calcification by inhibiting insulin-like growth factor-1 signaling in valvular interstitial cells. Circulation 2017;135:1935–50.

2. Radcliff K, Tang TB, Lim J, et al. Insulin-like growth factor-I regulates proliferation and osteoblastic differentiation of calcifying vascular cells via extracellular signal-regulated protein kinase and phosphatidylinositol 3-kinase pathways. Circ Res 2005;96:398–400.

3. Bellien J, Kamel S. Letter by Bellien and Kamel regarding article, "Dipeptidyl peptidase-4 induces aortic valve calcification by inhibiting insulin-like growth factor-1 signaling in valvular interstitial cells." Circulation 2017;136:1670–1.

4. Ayari H, Bricca G. Microarray analysis reveals overexpression of IBSP in human carotid plaques. Adv Med Sci 2012;57:334–40.

5. Olesen P, Nguyen K, Wogensen L, Ledet T, Rasmussen LM. Calcification of human vascular smooth muscle cells: associations with osteoprotegerin expression and acceleration by high-dose insulin. Am J Physiol Heart Circ Physiol 2007;292:H1058–64.

JACC: BASIC TO TRANSLATIONAL SCIENCE VOL. 4, NO. 1, 2019

TRANSLATIONAL PERSPECTIVE

Chest Compressions During Sustained Inflation During Cardiopulmonary Resuscitation in Newborn Infants Translating Evidence From Animal Studies to the Bedside

Georg M. Schmölzer, MD, PhD

SUMMARY

Newborn infants receiving chest compressions in the delivery room have a high incidence of mortality (41%) and short-term neurological morbidity (e.g., 57% hypoxic-ischemic encephalopathy and seizures). Furthermore, infants who have no signs of life at 10 min despite chest compressions have 83% mortality, with 93% of survivors experiencing moderate-to-severe disability. The poor prognosis associated with receiving chest compressions in the delivery room raises questions as to whether improved cardiopulmonary resuscitation methods specifically tailored to the newborn could improve outcomes. Combining chest compressions during sustained inflation (CC+SI) has recently been shown to improve morbidity and mortality outcomes during cardiopulmonary resuscitation. Overall, CC+SI accomplishes the following: 1) significantly reduces time to return of spontaneous circulation, mortality, and epinephrine administration, and improves systemic and regional hemodynamic recovery; 2) significantly increases tidal volume and minute ventilation, and therefore alveolar oxygen delivery; 3) allows for passive ventilation during chest compression; and 4) does not increase lung or brain injury markers compared with the current standard of using 3:1 compression:ventilation ratio. A randomized trial comparing CC+SI versus a 3:1 compression:ventilation ratio during cardiopulmonary resuscitation in the delivery room is therefore warranted. (J Am Coll Cardiol Basic Trans Science 2019;4:116–21)

The neonatal resuscitation guidelines recommend initiating chest compressions (CCs) if an infant's heart rate remains <60 beats/min despite adequate ventilation for at least 30 s. CCs should be delivered at a rate of 90/min in sequences of 3 CCs followed by a pause to deliver 1 inflation at a rate of 30/min, which corresponds to a 3:1 compression:ventilation (C:V) ratio (**Figure 1**, Video 1) (Supplemental Appendix A). The 3:1 C:V ratio favors ventilation, as respiratory failure is the primary cause

From the Centre for the Studies of Asphyxia and Resuscitation, Royal Alexandra Hospital, Edmonton, Alberta, Canada; and the Department of Pediatrics, University of Alberta, Edmonton, Alberta, Canada. The SURV1VE trial is supported by the Early Career Investigator Award from the Canadian Institutes of Health Research Institute of Circulatory and Respiratory Health (AR1 155222) and by an E.W. AI Thrasher award from the THRASHER Research Fund. Dr. Schmölzer is a recipient of the Heart and Stroke Foundation/University of Alberta Professorship of Neonatal Resuscitation, a National New Investigator of the Heart and Stroke Foundation Canada, and an Alberta New Investigator of the Heart and Stroke Foundation Alberta.
The author attests he is in compliance with human studies committees and animal welfare regulations of the authors' institutions and U.S. Food and Drug Administration guidelines, including patient consent where appropriate. For more information, visit the *JACC: Basic to Translational Science* author instructions page.

Manuscript received September 7, 2018; revised manuscript received November 29, 2018, accepted December 20, 2018.

ISSN 2452-302X https://doi.org/10.1016/j.jacbts.2018.12.004

of asystole or bradycardia in newborn infants. In comparison, during adult cardiopulmonary resuscitation (CPR), a 30:2 C:V ratio is recommended, as the main cause of CPR is cardiovascular collapse.

Overall, ~0.1% of term infants and 5% of preterm infants receive CCs in the delivery room (DR). Infants who receive CCs have a high incidence of mortality (41%) and short-term neurological morbidity (e.g., 57% hypoxic-ischemic encephalopathy and seizures) (Supplemental Appendix A). Furthermore, newborns who received CCs and epinephrine but had no signs of life at 10 min following birth have 83% mortality, with 93% of survivors experiencing moderate-to-severe neurological disability. The poor prognosis associated with receiving CCs in the DR raises questions as to whether improved CPR methods specifically tailored to the newborn could improve outcomes. Therefore, continuing efforts should be made to improve CPR techniques, and alternative methods should be examined. However, the incidence of infants who need CPR at birth is rare and in general unexpected, and therefore randomized clinical trials of alternative CPR methods have not been performed.

CCs IN NEWBORN INFANTS

Newborn infants present with either severe bradycardia or asystole at birth because of severe asphyxia. If the heart rate remains <60 beats/min despite adequate ventilation for at least 30 s, CCs using the 3:1 C:V ratio should be started to achieve adequate oxygen delivery (Supplemental Appendix B). During 3:1 C:V, CCs are delivered at a rate of 90/min in sequences of 3 CCs followed by a pause to deliver 1 inflation at a rate of 30/min. However, this approach may not be optimizing cardiac output during neonatal CPR as every interruption in CC results in a drop in coronary perfusion pressure that needs to be regenerated during the next compression cycle. Schmölzer et al. (1) reported an alternative approach of performing CCs during continuous sustained inflation (SI) (i.e., constant high airway pressure providing CCs [CC+SI]), which resulted in passive ventilation during CCs in asphyxiated piglets. During CC+SI, CCs are delivered continuously, superimposed by a constant high airway pressure (**Figure 1**, Video 1). In addition, CC+SI significantly improved hemodynamic variables, minute ventilation, and time to return of spontaneous circulation (ROSC) compared with the 3:1 C:V CPR (1).

Schmölzer et al. (1) first reported improved recovery in asphyxiated newborn piglets with CC+SI, compared with 3:1 C:V CPR (mean arterial pressure: 51 vs. 31 mm Hg; pulmonary arterial pressure: 41 vs. 31 mm Hg; mean minute ventilation: 936 vs. 623 ml/kg; median time to ROSC: 38 vs. 143 s, respectively). However, CCs were performed at a rate of 120/min in the CC+SI group, which is higher than the currently recommended CC rate of 90/min, which could have added to the improved outcomes (1). Subsequently, the group reported that CC+SI 90/min compared with 3:1 C:V resulted in a reduction in the median (interquartile range) time to ROSC of 34 s (28 to 156 s) versus 210 s (72 to 300 s) ($p = 0.05$), less oxygen (3 of 8 vs. 8 of 8 required 100% oxygen during CPR; $p = 0.03$), and 3 of 8 piglets versus 6 of 8 piglets receiving epinephrine ($p = 0.32$) (2). Furthermore, a recent randomized piglet study compared CC rates of 90/min versus 120/min during CC+SI and reported similar time to ROSC, survival rates, and respiratory parameters (3). More importantly during CCs, carotid blood flow, mean arterial pressure, percent change in ejection fraction, and cardiac output were higher in the CC+SI 90/min group compared with the CC+SI 120/min group. In addition, Vali et al. reported that CC+SI is feasible in a transitional model of near-term lambs. These studies support the use of CC+SI during neonatal CPR and would warrant clinical trials. A small pilot trial in preterm infants <32 weeks' gestation reported a significantly shorter mean time to ROSC in the CC+SI group ($n = 5$; gestational age: 24.6 ± 1.3 weeks) than the 3:1 C:V group ($n = 4$; gestational age: 25.6 ± 2.3 weeks) (31 [9] s vs. 138 [72] s, respectively; $p = 0.011$) (4). Overall, there were no differences in short-term outcomes, including no differences in neonatal brain injury or chronic lung disease. However, there were 2/5 and 0/4 deaths between groups, which might have been due to the small sample size and warrants a larger randomized trial (Supplemental Appendix B).

The data presented suggest that CC+SI has the potential to improve the outcomes of asphyxiated newborn infants. Furthermore, the described novel technique of CC+SI might also be an alternative for pediatric or adult resuscitation. However, until now, no pediatric or adult studies have been performed. Several factors should be examined before a large clinical trial is conducted, however, including: 1) CC, ventilation, and synchrony; 2) adequate tidal volume (V_T) delivery and minute ventilation; 3) distending pressure; and 4) lung or brain injury (Supplemental Appendix B).

ABBREVIATIONS AND ACRONYMS

C:V ratio = compression to ventilation ratio

CC = chest compression

CC+SI = chest compression during sustained inflation

CCaV = continuous chest compression with asynchronous ventilations

CPR = cardiopulmonary resuscitation

DR = delivery room

ROSC = return of spontaneous circulation

SI = sustained inflation

V_T = tidal volume

FIGURE 1 Respiratory Waveforms During 3:1 Compression: Ventilation Ratio and Continuous Chest Compressions During Sustained Inflations and Their Pros and Cons

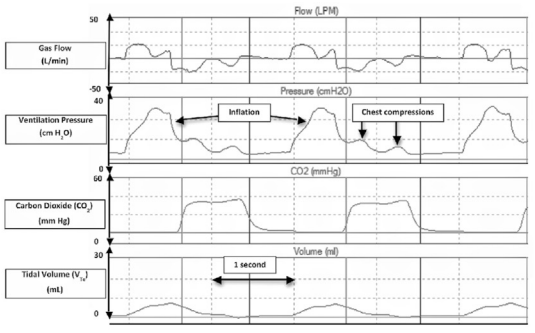

Pros:
- Synchronization between CC and ventilation

Cons:
- Interruptions of CC to deliver ventilation

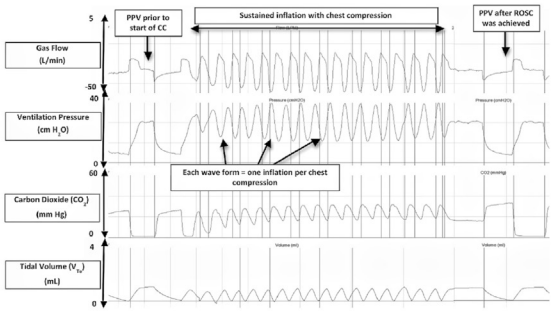

Pros:
- Faster time to ROSC
- Improved hemodynamic recovery
- Higher minute ventilation and alveolar oxygen delivery
- Passive ventilation during CC
- No synchronization between CC and ventilation

Cons:
- Hypothetical risk of lung and brain injury

Respiratory wave forms during cardiopulmonary resuscitation using 3:1 Compression:ventilation ratio (left image) and Chest Compression + Sustained Inflation (right image) (Gas flow, airway pressure, expired CO2, and tidal volume). See Video 1.

THE RATE OF CC, VENTILATION, AND SYNCHRONY

A mathematical model calculated that CC rates of 180/min for term infants and even higher rates in preterm infants could optimize systemic perfusion. Although these rates might be optimal in mathematical models, simulation studies reported faster rescuer fatigue with higher CC rates (e.g., 90/min vs. 120/min). Indeed, it is not practical and not infeasible to perform CCs at >120/min. When CC rates of 90/min versus 120/min during CC+SI were compared in asphyxiated newborn piglets, similar time to ROSC, survival rates, and respiratory parameters were reported (3). More importantly during CCs, carotid blood flow, mean arterial pressure, percent change in ejection fraction, and cardiac output were higher in the CC+SI 90/min group compared with the CC+SI 120/min group. This finding contradicts the mathematical model and supports the current recommendation of CCs at a rate of 90/min. Our observations are further supported by Idris et al., who reported that compression rates between 100/min and 120/min in adults experiencing out-of-hospital cardiac arrest were associated with greatest survival to hospital discharge, and higher rates do not improve outcomes (Supplemental Appendix C).

The current resuscitation guidelines recommend 3:1 C:V CPR with one inflation delivered after every third CC. Synchronized CC and ventilation may preclude the theoretical possibility of interfering V_T delivery and oxygenation by nonsynchronized CCs (Supplemental Appendix C). Manikin studies indicate that a 3:1 C:V ratio is favorable in terms of minute ventilation compared with higher C:V ratios (9:3 or 15:2 C:V). Similarly, animal trials comparing 3:1 C:V versus 9:3 or 15:2 C:V reported similar V_Ts but higher minute ventilation with 3:1 C:V. During simulated CPR, continuous CCs with asynchronous ventilations (CCaVs) with 90 CC and 30 nonsynchronized inflations resulted in lower V_T compared with 3:1 C:V. However, CCaV resulted in significantly higher minute ventilation compared with 3:1 C:V CPR (221 vs. 191 ml/kg/min, respectively) most likely due to the higher number of ventilations per minute. A study in asphyxiated piglets randomized to either CCaV or 3:1 C:V reported similar V_T delivery, minute ventilation (275 vs. 387 ml/kg), time to ROSC (114 vs. 143 s), and survival (6 of 8 and 3 of 8), respectively. Although there are concerns that CCaVs potentially interfere with V_T delivery, interference was only observed in ~30% of delivered inflations, which was similar to 3:1 C:V with interference in 25% of inflations. We believe that the observed interference also occurs during

neonatal resuscitation, which could attribute to an increased stress level during real-life resuscitations, and that this deviation from the guidelines is not exceptional.

ADEQUATE V_T DELIVERY

The primary purpose of inflations during CCs is to deliver an adequate V_T to facilitate gas exchange. However, delivery of an adequate V_T during CPR remains difficult. Several DR studies reported that mask ventilation is the most difficult task during neonatal CPR. Reduced V_T delivery leads to inadequate oxygenation, which often results from mask leak and/or airway obstruction (Supplemental Appendix D). Li et al. recently reported a case in which a large leak during mask ventilation in the DR resulted in severe bradycardia and the need for neonatal CCs. In addition, once CCs were started, the mask leak increased even more. This finding is further supported by manikin studies, which reported decreased expiratory V_T once CCs were started. A similar loss of expiratory V_T was reported by Li et al. (5) in asphyxiated piglets. During 3:1 C:V, a cumulated loss of V_T of 4.5 ml/kg occurred for each 3:1 C:V cycle and, during CCaV, a cumulated loss of V_T of 9.1 ml/kg for each cycle of 3 CCs and 1 inflation was observed. This outcome is concerning because a loss in V_T could cause lung de-recruitment, which might hamper oxygenation and therefore ROSC. In contrast, during CC+SI, a constant lung recruitment and establishment of functional residual capacity was observed (a gain of 2.3 ml/kg per CC+SI cycle) (5). This improvement in V_T may lead to better alveolar oxygen delivery and lung aeration. More importantly, the initial study by Schmölzer et al. (1) and the secondary analysis by Li et al. (5) is the first description of passive ventilation (and V_T delivery) during neonatal CPR. A similar observation was reported during chest recoil after a downward force is applied to the chest in infants undergoing surgery requiring general anesthesia and endotracheal intubation. Overall, the median (interquartile range) V_T generated was 2.4 ml/kg (0.8 to 4.0 ml/kg). Although Tsui et al. only applied gentle chest pressure, they could achieve ~33% of an infants' physiological V_T of 5 to 7 ml/kg. These data suggest that CC+SI would deliver an adequate V_T.

DISTENDING PRESSURE

The current neonatal resuscitation guideline recommends an initial distending pressure of 20 to 25 cm H_2O and a potentially higher distending pressure of 30 to 40 cm H_2O in term infants. Although there is ample evidence that a distending pressure of 20 to 25 cm H_2O causes high V_T delivery in preterm infants, no study, to the best of our knowledge, has ever measured V_T delivery during CC in the DR (Supplemental Appendix E). Solevåg et al. determined the distending pressure needed to achieve sufficient V_T during CC+SI using manikins and cadaver piglets. Distending pressure and V_T correlated in cadaver piglets ($r = 0.83$; $p < 0.001$), manikin ($r = 0.98$; $p < 0.001$), and combined data ($r = 0.49$; $p < 0.001$). V_T was delivered during chest recoil during CC in both models. In cadaver piglets, a distending pressure ~25 cm H_2O was needed to achieve an adequate V_T. This study suggests that chest recoil generates a distending pressure-dependent V_T, and that a distending pressure of ~25 cm H_2O is needed to achieve adequate V_T delivery. This is supported by the pilot trial comparing CC+SI and 3:1 C:V in preterm infants <32 weeks' gestation using a distending pressure of 24 cm H_2O (local hospital policy during neonatal resuscitation) (4). The study reported adequate V_T delivery and significantly higher minute ventilation in the CC+SI group compared with the 3:1 C:V group ($p < 0.001$), which suggests that CC+SI has the potential to improve ventilation and oxygenation during neonatal CPR.

LUNG AND BRAIN INJURY

There are concerns that sustained inflations could cause lung or brain injury. Lista et al. reported that premature infants between 25 and 28 weeks' gestation who received a sustained inflation had a higher rate of pneumothorax of 6% compared with 1% in the control group (Supplemental Appendix F). Similarly, meta-analyses suggested a trend toward higher pneumothorax rates when giving a sustained inflation. However, the mechanism for why sustained inflations might result in higher pneumothorax rates remains unknown. None of the animal studies examining CC+SI reported pneumothoraxes during autopsy or increased acute lung inflammation. Furthermore, pro-inflammatory cytokine concentrations in piglets given CC+SI compared with either a sham-operated or standard 3:1 C:V ratio were similar (2). Harling et al. reported similar cytokine levels in bronchoalveolar lavage fluid of preterm infant at 12 h of age, regardless of the 2 s or 5 s sustained inflation.

The main mechanism for brain injury is believed to be impaired venous return. Indeed, Sobotka et al. reported that a single SI causes a blood-brain barrier disruption indicated by increased numbers of blood vessel profiles with plasma protein extravasation in the cerebral cortex. In addition, after resuscitation

FIGURE 2 Study Flow Chart

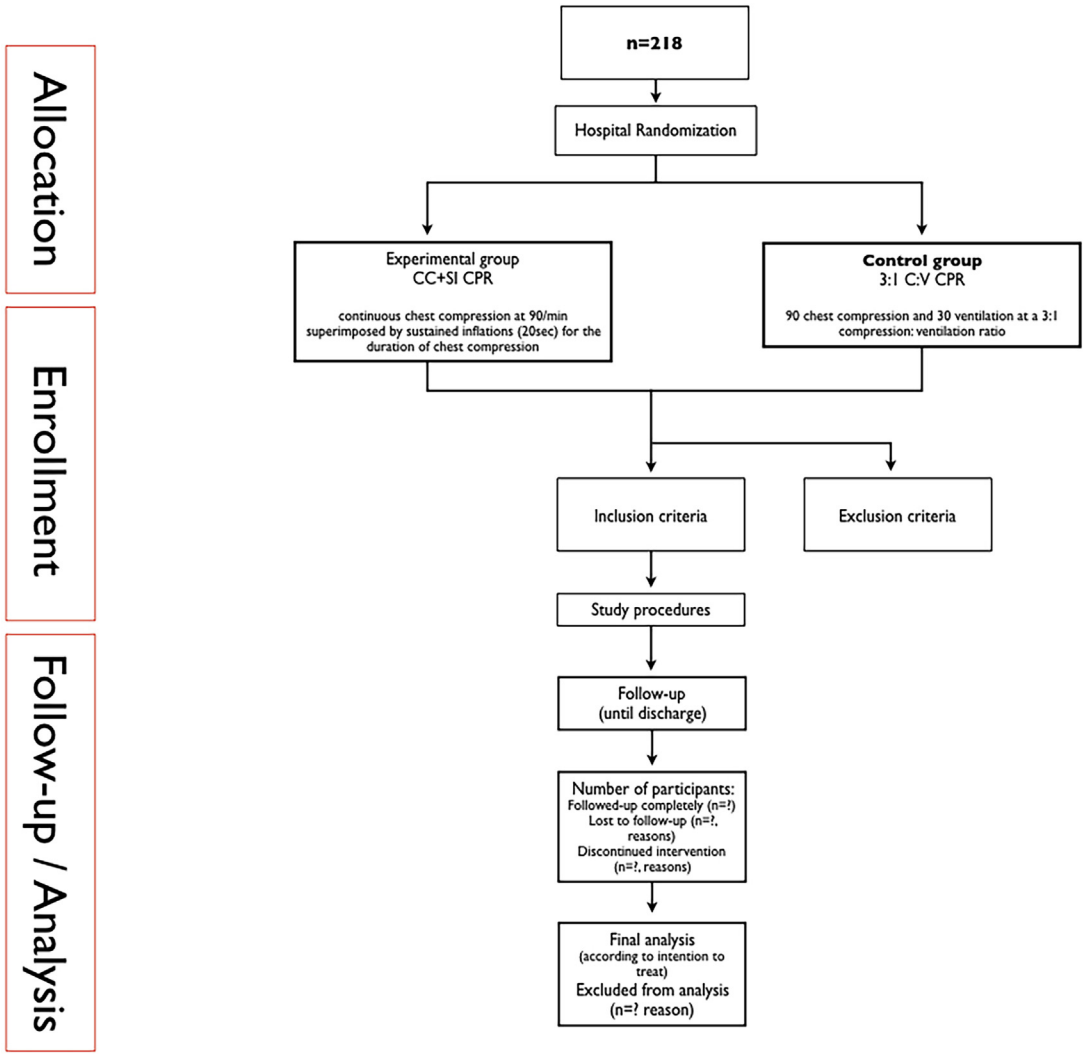

CC+SI = chest compression during sustained inflation; CPR = cardiopulmonary rescitation; C:V = compression to ventilation ratio.

with a single 30 s SI followed by ventilation in asphyxiated near-term lambs, increases in blood-brain barrier disruption and cerebral vascular leakage have been reported. This raises the possibility that SI may cause neurological injury. However, a recent study by Mustofa et al. reported similar concentrations of pro-inflammatory cytokines during CC+SI and 3:1 C:V CPR in both the thalamus and frontoparietal cortex (Supplemental Appendix G). Overall, these studies suggest that CC+SI during CPR does not increase acute brain and lung injuries more than the currently practiced technique of 3:1 C:V. However, a recent multicenter trial comparing sustained inflation versus positive pressure ventilation (SAIL [Sustained Aeration of Infant Lungs] trial) as initial respiratory support in the DR was terminated after 426 extreme premature infants between 23^{+0} and 26^{+6} were randomized, because of nonstatistically significant increase in mortality within 48 h after birth with an adjusted relative risk of SI versus positive pressure ventilation of 4.73 (95% CI: 1.4 to 16.2). Although this finding is concerning, the proposed SURV1VE trial (Sustained Inflation and Chest Compression Versus 3:1 Chest Compression to Ventilation Ratio During Cardiopulmonary Resuscitation of Asphyxiated Newborns: A Randomized Controlled Trial) will only

include infants >28 weeks' gestation, which are significantly older then the infants enrolled in the SAIL trial. Similarly, our recent pilot trial of CC+SI versus 3:1 in extreme premature infant did report similar mortality rates between CC+SI and 3:1 C:V, which is reassuring (4) (Supplemental Appendix F).

CONCLUSIONS

Morbidity and mortality rates are extremely high for newborns receiving CCs. The presented research describes a clear path from basic science to translation into DRs around the world. Based on the described clinical need, the animal data available, and preliminary human data, a randomized controlled trial is needed. Recruitment for the SURV1VE trial started in January 2018 (**Figure 2**).

ACKNOWLEDGMENT The study investigators thank the public for donating money to their funding agencies.

ADDRESS FOR CORRESPONDENCE: Dr. Georg M. Schmölzer, Centre for the Studies of Asphyxia and Resuscitation, Neonatal Research Unit, Royal Alexandra Hospital, 10240 Kingsway Avenue NW, Edmonton, Alberta T5H 3V9, Canada. E-mail: georg.schmoelzer@me.com.

REFERENCES

1. Schmölzer GM, O'Reilly M, LaBossiere J, et al. Cardiopulmonary resuscitation with chest compressions during sustained inflations: a new technique of neonatal resuscitation that improves recovery and survival in a neonatal porcine model. Circulation 2013;128:2495–503.

2. Li ES, Görens I, Cheung PY, et al. Chest compressions during sustained inflations improve recovery when compared to a 3:1 compression:ventilation ratio during cardiopulmonary resuscitation in a neonatal porcine model of asphyxia. Neonatology 2017;112:337–46.

3. Li ES, Cheung PY, Lee TF, Lu M, O'Reilly M, Schmölzer GM. Return of spontaneous circulation is not affected by different chest compression rates superimposed with sustained inflations during cardiopulmonary resuscitation in newborn piglets. PLoS ONE 2016;11.e0157249–14.

4. Schmölzer GM, O'Reilly M, Fray C, van Os S, Cheung PY. Chest compression during sustained inflation versus 3:1 chest compression:ventilation ratio during neonatal cardiopulmonary resuscitation: a randomised feasibility trial. Arch Dis Child Fetal Neonatal 2018;103:F455–60.

5. Li ES, Cheung PY, O'Reilly M, Schmölzer GM. Change in tidal volume during cardiopulmonary resuscitation in newborn piglets. Arch Dis Child Fetal Neonatal 2015;100:F530–3.

KEY WORDS asphyxia, cardiopulmonary resuscitation, delivery room, newborn/infant

APPENDIX For supplemental appendices (which include all of the studies referenced in the article [by name or dcription] throughout the text) and a video, please see the online version of this paper.

JACC: BASIC TO TRANSLATIONAL SCIENCE VOL. 4, NO. 1, 2019

STATE-OF-THE-ART REVIEW

Therapeutic Genome Editing in Cardiovascular Diseases

David M. German, MD, MPH,[a] Shoukhrat Mitalipov, PhD,[a,b] Anusha Mishra, PhD,[a] Sanjiv Kaul, MD[a]

SUMMARY

A variety of genetic cardiovascular diseases may one day be curable using gene editing technology. Germline genome editing and correction promises to permanently remove monogenic cardiovascular disorders from the offspring and subsequent generations of affected families. Although technically feasible and likely to be ready for implementation in humans in the near future, this approach remains ethically controversial. Although currently beset by several technical challenges, and not yet past small animal models, somatic genome editing may also be useful for a variety of cardiovascular disorders. It potentially avoids ethical concerns about permanent editing of the germline and allows treatment of already diseased individuals. If technical challenges of Cas9-gRNA delivery (viral vector immune response, nonviral vector delivery) can be worked out, then CRISPR-Cas9 may have a significant place in the treatment of a wide variety of disorders in which partial or complete gene knockout is desired. However, CRISPR may not work for gene correction in the human heart because of low rates of homology directed repair. Off-target effects also remain a concern, although, thus far, small animal studies have been reassuring. Some of the therapies mentioned in this review may be ready for small clinical trials in the near future. (J Am Coll Cardiol Basic Trans Science 2019;4:122–31) © 2019 The Authors. Published by Elsevier on behalf of the American College of Cardiology Foundation. This is an open access article under the CC BY-NC-ND license (http://creativecommons.org/licenses/by-nc-nd/4.0/).

Since the successful sequencing of the human genome more than 15 years ago, there has been an explosion of knowledge regarding the genetic contributions to common cardiovascular diseases, as well as advancement of the understanding of monogenic cardiovascular disorders. Although this knowledge has allowed for the development of potent pharmaceuticals and better risk stratification for cardiovascular diseases, the rapid development of CRISPR-Cas9 techniques in the past 5 years may dramatically change the outlook for novel therapies in cardiovascular disorders, including those previously thought untreatable.

CRISPR, which stands for "clustered regularly interspersed short palindromic repeats," refers to a mechanism that evolved in bacteria to identify and remove foreign DNA from their genomes, using an RNA guide and CRISPR-associated (Cas) nuclease (1). It was quickly recognized that such systems have the incredible ability to facilitate precise editing of genes in both mature and developing organisms. Although the introduction of CRISR-Cas9 has the potential to revolutionize the mechanistic understanding of cardiovascular diseases and aide in the development of novel pharmacological therapies, it is the prospect of genome modification in humans that would transform how cardiovascular diseases are treated.

Before the latest development of gene editing techniques, a few approaches that allowed gene targeting in animals existed (e.g., the generation of "knockout" mice). However, these techniques were time consuming, technically challenging, and

From the [a]Knight Cardiovascular Institute, Oregon Health and Science University, Portland, Oregon; and the [b]Center for Embryonic Cell and Gene Therapy, Oregon Health and Science University, Portland, Oregon. The authors have reported that they have no relationships relevant to the contents of this paper to disclose.

All authors attest they are in compliance with human studies committees and animal welfare regulations of the authors' institutions and US Food and Drug Administration guidelines, including patient consent where appropriate. For more information, visit the *JACC: Basic to Translational Science* author instructions page.

Manuscript received August 27, 2018; revised manuscript received October 25, 2018, accepted November 15, 2018.

ISSN 2452-302X https://doi.org/10.1016/j.jacbts.2018.11.004

inefficient. CRISPR has revolutionized gene targeting because it allows for production of double-stranded DNA breaks at precise, user-directed locations within the genome, thus facilitating editing of a chosen segment of DNA in an efficient manner (1).

Using the abilities of the CRISPR-Cas9 system requires introduction of a Cas9 nuclease and a segment of guide RNA (gRNA) into the cell(s) of interest, either through direct injection or via viral or nonviral vectors. In practice, the Cas9 nuclease most often comes from *Streptococcus pyogenes* (SpCas9), but *Staphylococcus aureus* Cas9 (SaCas9) is also frequently used because of its smaller size (thus, ease of entry into smaller vectors). The gRNA is approximately 100-nucleotides long and contains a 20-nucleotide protospacer sequence that hybridizes to complementary DNA, as well as a shorter 2 to 6 nucleotide protospacer-adjacent motif (PAM) that facilitates binding of host DNA to the Cas9 nuclease (**Central Illustration**). It is the customization of the protospacer that allows for Cas9 nuclease to create a specific double-stranded break (DSB) in host DNA at user-specified sites (1). However, the PAM sequence is necessary for host DNA recognition and binding by Cas9, as well as subsequent hybridization with the protospacer region of the gRNA and eventual DNA cleavage (2). Thus, it represents another key element required for target sequence specificity. For example, Cas9 from *S. pyogenes* recognizes a 5′-NGG-3′ PAM sequence, the requirement of which significantly limits target specificity while also increasing the probability of off-target activity. Theoretically, such a specific PAM requirement could limit the therapeutic potential of the technology. However, Cas9 enzymes from other bacterial species (e.g., *Streptococcus thermophilus*) (3,4), as well as those obtained via protein engineering (5), bind to a variety of PAMs with enhanced nucleotide specificity and fewer nonspecific bindings or cleavage. These new Cas9 versions are likely to render concerns over PAM specificity obsolete in the near future.

After cleavage by CRISPR-Cas9, DSBs can be repaired by 1 of 2 endogenous mechanisms. Nonhomologous end-joining (NHEJ) is the dominant mechanism in nonproliferating cells, including human myocardial cells, but it is error prone because the affected DNA segment is reconstructed without use of a DNA template (**Figure 1**). This method is highly vulnerable to production of insertion-deletion mutations (indels), and, in general, would not be an acceptable component of genome editing when the desired outcome is replacement of a dysfunctional gene with a functional one. However, if knockout is all that is desired, production of indel mutations via NHEJ may be a reasonable therapeutic approach, even in somatic cells.

Homology-directed repair (HDR) is the second but much less frequent means by which DSBs can be fixed in somatic cells. HDR machinery rebuilds the DSB site using either homologous chromosomal DNA or an exogenous template DNA strand (a single-stranded oligodeoxynucleotide [ssODN]) (**Figure 1**). The clinical applicability of CRISR-Cas9 in humans is hampered, in part, by the low rates of HDR compared with NHEJ in somatic gene editing.

In theory, genome editing techniques can be applied to both developing embryos and intact mature organisms to either produce loss-of-function in a gene with deleterious downstream effects (knockout) or to restore function to a mutated gene (knock in). In somatic genome editing, genetic modifications are created in differentiated cells in a developing or adult organism, which allows for treatment of established disease or for disease prophylaxis in those genetically at-risk. Cas9 and gRNA are typically delivered in vivo by a viral vector; adenovirus, adeno-associated virus (AAV), and lentivirus have been used most commonly in animals, and each has relative advantages and disadvantages.

Germline genome editing is the process of transforming embryonic or germ cell DNA and can be successfully accomplished ex vivo via direct co-injection of Cas9 and gRNA with sperm into human oocytes (6). It allows for complete and permanent transformation of the human genome, affecting all subsequent generations.

THERAPEUTIC APPLICATIONS

One of the promises of genome editing is that it will allow for treatment of monogenic diseases that currently have either ineffective or minimally effective therapies. In cardiovascular medicine, heritable cardiomyopathies, such as hypertrophic cardiomyopathy (HCM), dilated cardiomyopathy, and Duchenne muscular dystrophy (DMD), as well as heritable arrhythmic disorders, vasculopathies such as Marfan's syndrome, and infiltrative diseases such as transthyretin amyloidosis, are potential candidates for clinical applications of germline genome editing techniques (**Central Illustration**). Editing of the germline in these types of disorders, in which a single gene mutation is responsible for disease manifestation, is capable of permanent correction of the disorder in descendants of affected individuals or those carrying a deleterious mutation.

ABBREVIATIONS AND ACRONYMS

DMD = Duchenne muscular dystrophy

DSB = double-stranded break

HCM = hypertrophic cardiomyopathy

NHEJ = nonhomologous end-joining

CENTRAL ILLUSTRATION **The Different Genome Editing Approaches (Germline and Somatic) and the Potential Cardiovascular Conditions They Could Treat**

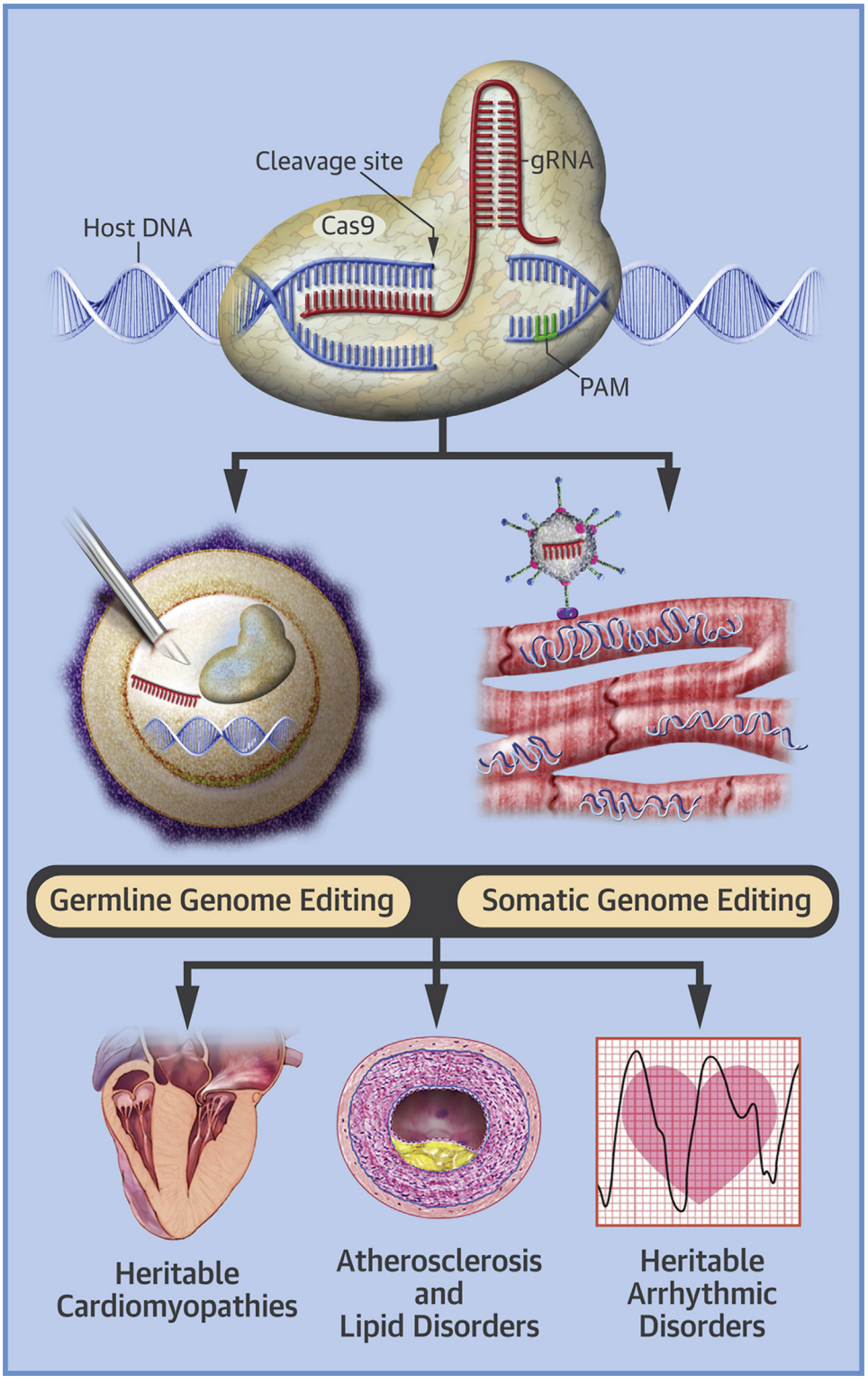

German, D.M. et al. J Am Coll Cardiol Basic Trans Science. 2019;4(1):122–31.

FIGURE 1 Types and Frequencies of DNA Repair in Somatic Cells After Gene Deletion by CRISPR

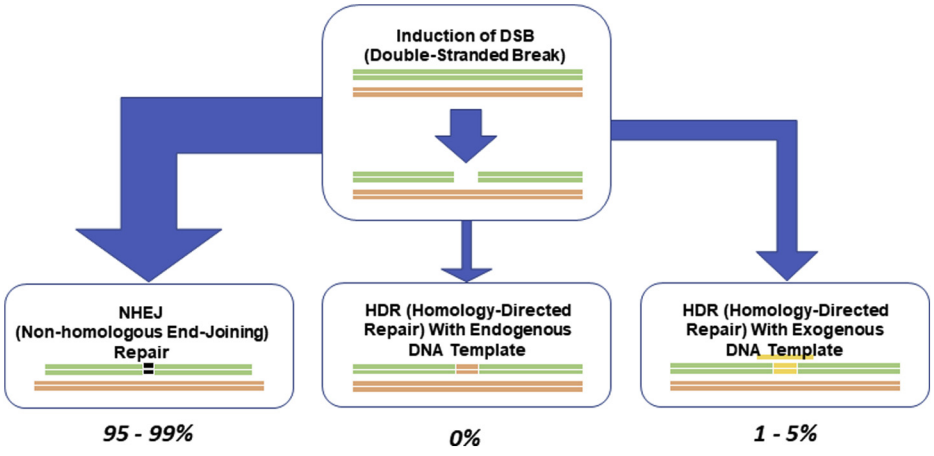

Homolog template is almost never used, and externally provided template is used infrequently. Almost all the repair is performed using NHEJ. CRISPR = clustered regularly interspersed short palindromic repeats; DSB = double-stranded break; HDR = homology-directed repair; NHEJ = nonhomologous end-joining.

For many disorders, germline genome editing is unlikely to find a major role in treatment and prevention because of the interplay of genetic and environmental factors in contributing to disease manifestation. For complex disorders such as coronary artery disease and atherosclerosis, somatic genome editing may eventually play a role in treatment. In addition, somatic genome editing may also be useful for post-natal treatment of monogenic disorders, especially because clinical application of germline genome editing is likely to remain ethically more controversial than somatic genome editing for some time. Nonetheless, with close to 7,500 monogenic disorders affecting approximately 780 million people, germline editing has the theoretical potential for permanently eliminating these diseases.

HYPERTROPHIC CARDIOMYOPATHY. HCM is a disease of cardiac muscle that results in ventricular hypertrophy and has a propensity for arrhythmias, syncope, and heart failure. Ventricular outflow tract obstruction and associated systolic anterior motion of the mitral leaflet and resulting mitral regurgitation, as well enhanced myocardial stiffness from fibrosis, are accompanying findings. A variety of sarcomeric gene mutations have been implicated in the disorder. Mutations in *MYBPC3* account for approximately one-third of all HCM in humans, as well as a significant number of cases of inherited dilated and noncompaction cardiomyopathy (7). Ma et al. (6) recently demonstrated the successful correction of a *MYBPC3* mutation in human germ cells using CRISPR-Cas9. They microinjected recombinant Cas9 protein with gRNA and ssODN DNA into human zygotes produced by fertilization of healthy donor oocytes with sperm from a male donor who was heterozygous for *MYBPC3* mutation. Most (66.7%) of the embryos injected in this way exhibited a homozygous wild-type genotype, as opposed to 47.4% of control embryos. However, 24% of the embryos exhibited mosaicism, and 9.3% had a persistent heterozygous mutant genotype. The mosaicism was attributed to the inability of CRISPR to correct all mutant genes after cell division occurred.

When the investigators co-injected Cas9 with sperm into M-phase oocytes, 72.4% of the 68 resulting embryos exhibited a homozygous wild-type genotype, and there were no mosaic or mutant embryos. The absence of mosaicism was attributed to gene correction before the fertilized egg started dividing. The remaining 27.6% of embryos were uniformly heterozygous for the wild-type allele and a NHEJ-mediated repair. In addition, genome sequencing of CRISPR-Cas9–targeted blastomeres failed to reveal significant off-target effects. The study demonstrated, for the first time, that CRISPR-Cas9 could be used to abolish disease-causing mutations in human embryos and that modifications to the timing of Cas9 injection during embryogenesis resulted in significant increases in HDR efficiency (**Figure 2**) (6). Furthermore, in mouse embryos, it was shown that adding RAD51 significantly increased the

FIGURE 2 Types and Frequencies of DNA Repair in Germline Cells After Gene Deletion by CRISPR

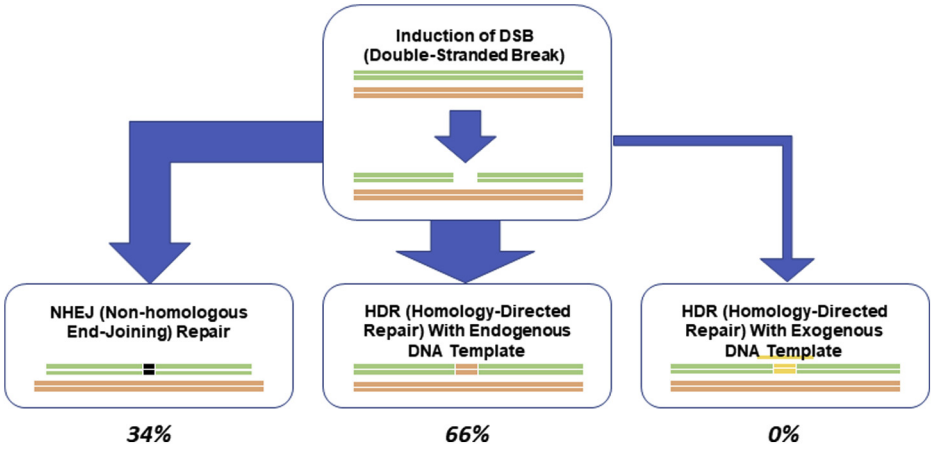

Unlike somatic cells, the externally provided template is not used, and NHEJ is used only one-third of the time. The homolog template (from the normal parent) is used for repair in two-thirds of cases. This form of repair is exclusive to the germline. Methods are being developed to increase homolog repair to 100% to obviate the need for pre-natal genetic diagnosis before in vitro implantation of the corrected embryo. Abbreviations as in Figure 1.

chances of HDR repair. This high incidence of HDR seems to be inherent in embryos and is probably meant to prevent spontaneous mutations from germline transmission. This method, in combination with pre-implantation genetic diagnosis, may be useful clinically in the prevention of transmission of HCM and other monogenic disorders.

Somatic genome editing might be feasible in HCM as well, because the development of cardiac hypertrophy, myocardial fibrosis, and symptomatic disease is generally a gradual process. Mearini et al. (8) administered nonmutant *Mybpc3* cDNA to *Mybpc3* knockout mice (without use of CRISPR-Cas9) via an AAV vector (specifically AAV9, the most cardiotropic AAV serotype) and found that this therapy successfully increased expression of functional cMyBP-C (to ~60% of wild-type levels). This prevented cardiac hypertrophy and cardiac functional impairment in young mice (8). Although AAV vectors are generally too small to package SpCas9, use of other Cas9 enzymes may allow for testing of somatic genome editing of this disease. Several other naturally occurring and engineered Cas9 enzymes are smaller in size, which may facilitate such viral delivery (5). However, it must be realized that HDR is uncommon in somatic cells (Figure 2, top panel); thus, gene correction in the human myocardium may not be possible.

DUCHENNE MUSCULAR DYSTROPHY. DMD is a relatively common X-linked disease that leads to progressive skeletal muscle weakness and fatal cardiomyopathy. It is caused by mutations in the *DMD* gene that codes for dystrophin. The gene is long, with 79 exons, and mutations anywhere along the length of the gene can cause the entire protein to be dysfunctional. Because of the heritability of the disorder and the lack of effective therapies, DMD is an appealing candidate for germline genome editing.

Investigators injected Cas9, gRNA targeting exon 23, and template ssODN DNA into zygotes of mice with a nonsense *Dmd* mutation and implanted the modified zygotes into female mice. Sequencing of *Dmd* exon 23 in these corrected mice revealed mosaicism in most animals, although a majority of them showed improvement in muscle function even when only a subset of cells had functional dystrophin that was restored through either NHEJ or HDR (9). Modifications of methods to include nuclease and gRNA injection into M-phase oocytes with sperm, as was done by Ma et al. (6), might further improve these results.

Achieving effective in vivo genome editing of cardiac muscle seems a more formidable task because of the difficulties of delivering Cas9 and gRNA to cardiac tissue. However, in a mouse model of DMD, El Refaey et al. (10) showed that systemic administration of *S. aureus* Cas9 and gRNA in an AAV vector led to restoration of the *DMD* reading frame, and thus, expression (in ~40% of cardiac muscle fibers), and ultimately to improvements in cardiac myofiber architecture, cardiac fibrosis, and papillary muscle contractility. Recently, Amoasii et al. (11) showed an

increased expression of cardiac and skeletal muscle dystrophin in a dog model of DMD after treatment with intravenous AAV9 that contained Cas9 and gRNA. These findings demonstrated that, in cases such as DMD, partial effectiveness also has a significant potential to improve symptoms and clinical outcome. Additional studies will be required to evaluate long-term safety and efficacy in larger animals, and ultimately, humans.

OTHER NONISCHEMIC CARDIOMYOPATHIES. A wide variety of additional causes of nonischemic cardiomyopathy will likely one day be treatable via either germline or somatic genome editing. For example, phospholamban regulates intracellular calcium concentrations through its inhibitory actions on sarcoplasmic reticulum calcium–adenosine triphosphatase (SERCA2), and mutations in the gene for phospolamban (*PLN*) have been identified as a cause of dilated nonischemic cardiomyopathy (12). Kaneko et al. (13) performed germline genome editing via CRISPR-Cas9 to knockout the *PLN* gene in a mouse model of severe heart failure (calsequestin [*CSQ*] overexpressing mice). Compared with control heart failure mice, *PLN* knockout mice survived longer and had improved cardiac size and function (13).

DYSLIPIDEMIA AND ATHEROSCLEROTIC CARDIOVASCULAR DISEASE. Lipid metabolism is an attractive target for somatic genome editing for several reasons. Editing of genes involved in the development of dyslipidemia has the potential to affect not only individuals with monogenic disorders (e.g., familial hypercholesterolemia) but also the large population of individuals without monogenic lipid disorders who have established atherosclerotic disease or elevated risk for cardiovascular events. In addition, although progress in somatic gene editing has thus far been hampered by challenges in gene delivery to tissues of interest, the liver is one particular tissue where success has already been achieved. For instance, AAV vectors have been used successfully in human trials for gene transfer and treatment of hemophilia A and B (14,15), and additional preclinical studies have used them for somatic genome editing for lipid disorders.

Proprotein convertase subtilisin/kexin type 9 (PCSK9) became a novel therapeutic target for prevention of atherosclerotic cardiovascular disease when it was observed that loss-of-function mutations in PCSK9 were associated with reduced low-density lipoprotein cholesterol and reduced risk for coronary heart disease, with no clear adverse clinical consequences (16). Pharmacological inhibition of PCSK9 in vivo also dramatically lowers low-density lipoprotein cholesterol and reduces cardiovascular events in subjects with an elevated baseline risk (17). Ding et al. (18) showed that when Cas9 and gRNA targeting *Pcsk9* was delivered in vivo to mice via an adenovirus vector, approximately 50% of the *Pcsk9* alleles in the liver tissue were successfully edited, with a wide variety of loss-of-function indels generated via NHEJ (**Figure 1**). No significant off-target effects were seen. Furthermore, this experiment resulted in substantially (~90%) lower levels of plasma PCSK9 levels and total plasma cholesterol (35% to 40% reduction) in the edited mice (18). Similar results were achieved using mice with transplanted human hepatocytes using an adenovirus vector (19). Although these studies used adenovirus vectors to deliver Cas9 and gRNA to the liver, adenovirus is not a suitable vector for use in human therapies because of its substantial immunogenicity. Because of its size, *S. pyogenes* Cas9 cannot be packaged in smaller, less immunogenic vectors such as AAV. However, Ran et al. (20) produced knockout of *Pcsk9* in a mouse liver using an AAV vector packaged with *S. aureus* Cas9, which resulted in ~95% decrease in blood PCSK9 and ~40% decrease in blood cholesterol levels with no major off-target effects. These studies provided proof-of-concept that it might soon be possible to immunize patients against atherosclerotic cardiovascular disease by using somatic genome editing to permanently lower plasma lipid levels. Additional work will need to ensure these methods are safe and effective in humans.

Although some of the results of these early investigations in somatic genome editing in cardiovascular disease have been encouraging, most of these studies have depended on NHEJ-mediated DSB repair (**Figure 1**). Because HDR tends to be inefficient and to only operate in proliferating cells, these techniques would not be useful for producing gain-of-function genome edits in mature cardiac or vascular tissues. In addition, off-target effects have the potential to be more damaging if NHEJ is used (potentially producing activating or inactivating indel mutations in proto-oncogenes or tumor suppressor genes, or producing loss of function mutations in other essential genes).

One promising technique that may be able to overcome this limitation is in vivo base editing (21,22). Base editors are CRISPR-Cas9 systems that have been modified to alter single base pairs rather than induce DSBs. For example, base editor 3 (BE3) is a *S. pyogenes* Cas9 mutated to induce only a single-strand break, and it is attached to a cytosine deaminase domain that exchanges a cytosine base at the nick site for a uracil base. This modified Cas9

enzyme then removes the corresponding guanine base, and the result is a C-G pair replaced with a U-A pair; the uracil is ultimately permanently replaced with thymine. Chadwick et al. (23) used an adenovirus vector and BE3 to show that this method could also be used to disrupt mouse *Pcsk9*, and again found significant reductions in plasma PCSK9 and cholesterol levels in treated mice.

These techniques were extended to modification of *ANGPTL3* (angiopoietin-like 3), which codes for a protein that regulates blood lipid levels. Loss-of-function mutations in *ANGPTL3* are associated with reduced low-density lipoprotein cholesterol and triglycerides, as well as a reduced risk for coronary heart disease (24,25). Chadwick et al. (26) again used BE3, introduced via an adenovirus vector, to produce cytosine-to-thymine nonsense mutations in *Angptl3* in mice. Treated mice had a 31% decline in plasma triglycerides and a 19% decline in plasma cholesterol. There were no significant signs of off-target mutagenesis (26). Although the current usefulness of base-editing techniques is limited to generating specific point mutations largely confined to the generation of knockouts, and further limited by challenges in packaging larger components into small viral vectors, future advances may ameliorate some of these problems. In addition to *PCSK9* and *ANGPTL3*, somatic genome editing may be useful in addressing cardiovascular risk carried by *LPA*, *APOB*, or other genetic mutations. Germline genome editing may also be useful in treating heritable monogenic dyslipidemias.

AGE-RELATED CLONAL HEMATOPOIESIS. Somatic genome editing has the additional potential of providing treatment for diseases that are only now beginning to be understood. Clonal hematopoiesis (of indeterminate potential, CHIP), which is also known as age-related clonal hematopoiesis (ARCH), has recently become widely appreciated as a possible contributor to cardiovascular disease. It refers to the clonal amplification of hematopoietic cells due to the accumulation of somatic mutations that confer competitive advantages to these cells at the expense of other cell types (27). Its prevalence increases with age, and it is associated with increased risk for atherosclerotic cardiovascular disease, stroke, and death (28). Although mutations in a large variety of driver genes have been implicated in the development of ARCH, *TET2* and *DNMT3A* are believed to play a major role.

Sano et al. (29) used lentivirus vectors carrying Cas9 and gRNA to inactivate *Tet2* and *Dnmt3a* (via indel mutations) in mouse bone marrow cells and then implanted those cells into irradiated mice. Mice with *Tet2* or *Dnmt3a* inactivation displayed a greater decline in cardiac function as well as increased cardiac size and fibrosis when challenged with angiotensin II infusion compared with those without inactivation of those genes. In addition, inactivation of both genes led to increased expression of pro-inflammatory cytokines (29). These results further implicated these genes in ARCH–mediated cardiovascular disease, and potentially suggest a future therapy. If methods can be developed to reliably knock in somatic gene mutations, it may be possible to reverse driver gene mutations using a vector that targets hematopoietic stem and/or progenitor cells. Consequently, somatic genome editing may be a useful approach to treating ARCH in humans, thus reducing cardiovascular risk. These approaches may be preferable to bone marrow transplantation.

TRANSTHYRETIN CARDIAC AMYLOIDOSIS. One of the challenges of somatic genome editing has been defining the optimal method for delivery of the CRISPR-Cas9 components to the cells of interest. Viral vectors are not optimal for this purpose. Finn et al. (30) demonstrated that, under the right conditions, nonviral vectors may be able to successfully deliver somatic genome editing tools to desired tissues. Transthyretin (TTR) cardiac amyloidosis is an infiltrative disease of cardiac muscle that results from deposition of abnormal pre-albumin (transthyretin) protein and is caused by either heritable *TTR* gene mutations or accumulation of wild-type transthyretin. It may be an attractive candidate for somatic genome editing because most transthyretin is produced in the liver.

Finn et al. (30) administered a lipid nanoparticle packaged with Cas9 mRNA and gRNA targeted to the *Ttr* gene in mice and found a significant (>97%) drop in serum TTR levels. It is unclear whether this approach will translate into disease phenotype rescue or prevention. Additional studies will be needed to investigate the effects on cardiac tissue and to determine whether the lipid nanoparticle vector can be used successfully for other conditions. Other nonviral vectors (e.g., microbubbles) that can be selectively destroyed in the tissue of interest by ultrasound to introduce the vector locally also hold promise (31).

INHERITED ARRHYTHMIC DISORDERS. Channelopathies and other inherited arrhythmic disorders are another area of potential therapeutic application of genome editing. Although CRISPR-Cas9 is already proving useful in the characterization of ion channel protein function and drug–gene interactions in induced pluripotent stem cell–based cell cultures,

genome editing will also likely provide the opportunity to treat these rare disorders.

PRKAG2 syndrome is a rare familial disorder characterized by abnormal glycogen storage, ventricular pre-excitation, recurrent arrhythmias, and cardiac hypertrophy. It is caused by mutations in the *PRKAG2* gene coding for a regulatory subunit of the adenosine monophosphate-activated protein kinase (AMPK) (32). Xie et al. (33) showed that post-natal correction of the disorder was achieved in mice via a single administration of Cas9 and gRNA in an AAV9 vector, with significant reduction in left ventricular wall thickness, decreased myocardial glycogen content, normalization of the QRS width and PR intervals, and improvements in myofibril organization and ventricular function. Further work is required to translate these results to different types of *PRKAG2* mutations and to larger animals to better define the corrected phenotype.

Long QT syndrome (LQTS), which predisposes individuals to life-threatening cardiac arrhythmias, would potentially be an attractive candidate for germline and somatic genome editing. Rare cases of LQTS are caused by mutations in genes that code for calmodulin (*CALM1*, *CALM2*, and *CALM3*), a protein that binds calcium and interacts closely with L-type calcium channels in cardiomyocytes. When this protein is over-expressed, it causes action potential prolongation. CRISPR interference is a novel method of modulating gene expression without permanently modifying the genome; gene expression is modified by using dCas9 ("dead" Cas9, which lacks endonuclease activity) along with a transcriptional activator or suppressor. Limpitikul et al. (34) cultured cardiomyocytes from induced pluripotent stem cells derived from a patient with a disease-causing *CALM2* mutation, and demonstrated that these cells recapitulated the cellular phenotype of LQTS. Treatment with CRISPR interference significantly lowered levels of *CALM2* mRNA, and calmodulin protein, and also reduced action potential duration. In addition, these investigators showed that expression of *CALM1* or *CALM3* could also be selectively reduced in this way (34). It remains to be seen whether this approach might be effective in vivo or applicable to other variants of LQTS or other cardiac conditions.

MARFAN SYNDROME. Base editing techniques may be one way of more precisely correcting pathogenic single nucleotide mutations with perhaps fewer concerns about the inefficiencies of HDR and about off-target effects. Marfan syndrome is a connective tissue disorder associated with abnormalities in multiple organ systems, but for which morbidity and mortality are most closely tied to the risk of thoracic aortic aneurysm and aortic dissection. It is most often caused by autosomal dominant mutations in the gene *FBN1*, which codes for the extracellular matrix protein fibrillin-1 (35). Zeng et al. (36) recently identified an individual with Marfan syndrome who was heterozygous for a pathogenic T7498C mutation in the *FBN1* gene and cultured human cells with an identical mutation in *FBN1*. After those cells were transfected with gRNA and BE3, sequencing revealed that 10 of 20 clones had been edited, 8 with a desirable C-to-T correction and 2 others with unwanted base pair conversions. The investigators then tested the technique in human embryos; zygotes produced via in vitro fertilization of donor oocytes with sperm from the same Marfan syndrome patient were subsequently microinjected with BE3 and gRNA. In 100% of the 7 treated embryos, the *FBN1* T7498C mutation was corrected, compared with 50% of control embryos, although there was 1 unwanted base conversion in 1 of the treated embryos. No unintended corrections were discovered via screening of potential off-target sites in corrected embryos (36). The results provided proof-of-concept that base editing techniques might be applicable to the correction of pathogenic gene mutations in the human germline, especially if problems of off-target conversions could be more thoroughly resolved.

ETHICAL CONSIDERATIONS

Several ethical concerns must be considered with germline gene editing because any intended and unintended changes would be transmitted to subsequent generations. Mosaicism is also a cause of major concern. However, as shown by Ma et al. (6), mosaicism can be largely prevented if CRISPR is introduced before cell division starts. Furthermore, detailed analysis demonstrated no off-target effects. However, the gene edited in this case was only 4 base pairs long, and more off-target effects may occur when editing larger genes (37). Whether these off-target effects are automatically recognized and corrected in the human embryo is not known. Consequently, more studies need to confirm the absence of off-target effects in human genome editing, and to further develop novel techniques such as base editing that might allow for more precise mutation correction in select cases.

One can argue that as long as we have preimplantation genetic diagnosis we do not need germline gene editing because we can select the unaffected embryos for implantation. However, this argument does not hold for polygenic diseases,

or when both parents are homozygous for a gene variant. It has also been argued that applications of germline gene editing could widen inappropriately and be used for purposes other than therapy. However, we must address these concerns with effective policies rather than prevention of the development of potential therapies. International consensus and tight regulation will be critical to ensure that this technology is only used for necessary treatment purposes rather than creating "designer" babies or providing nonessential treatment. Indeed, recent reports suggest that CRISPR-Cas9 has already been used to create babies in China, sparking an international debate and stressing the immediate importance of setting up such regulatory systems (38). The earlier these deliberations begin, the better prepared society will be for such treatments when they become available.

Another concern is that the expense associated with germline gene editing and in vitro fertilization will result in the treatment only benefiting wealthy patients. Coverage by insurance could mitigate this concern, and governmental health care services should take this possibility into account when instituting future policies. In many instances, the cost of germline gene editing and in vitro fertilization would be significantly less than the lifelong pharmacological treatment of the condition, therefore making these treatments economically more attractive.

Finally, objections to germline gene editing on religious grounds will continue to exist and people with such objections can decline this therapy. Accordingly, the National Academy of Medicine has recommended that attempts to make gene therapy safe should continue (39).

CONCLUSIONS

It is rapidly becoming apparent that a wide variety of cardiovascular diseases may one day be curable using CRISPR-Cas9 or similar technology, including many that heretofore have been entirely untreatable. Germline genome editing promises to permanently resolve monogenic cardiovascular disorders for the offspring and subsequent generations of affected individuals. Although technically easier and likely to be ready for implementation in humans in the near future, this approach remains ethically controversial. Public debate and public policy determinations will need to proceed rapidly to allow decisions to be made regarding how and when these therapies may be used clinically. In addition, further technical matters will need to be more fully resolved, including those of long-term risks, off-target effects, mosaicism, and applicability to a wider variety of mutations and cardiovascular conditions.

Although currently beset by several technical challenges, and not yet past small animal models, somatic genome editing may also be useful for a variety of cardiovascular disorders. It potentially avoids ethical concerns about permanent editing of the germline and allows treatment of already diseased individuals. If technical challenges of Cas9-gRNA delivery (viral vector immune response, nonviral vector delivery, size of the vector) can be worked out in large animals and humans, then CRISPR-Cas9 may have a significant place in the treatment of a wide variety of disorders in which partial or complete gene knockout is desired (e.g., for *PCSK9* and *DMD*). More challenging (and perhaps unachievable) will be knock in via HDR or base editing in nonproliferating cells. Off-target effects remain a concern in somatic genome editing as well, although small animal studies thus far have been reassuring. Some of the therapies mentioned in this review will be ready for small clinical trials in the near future (perhaps soonest in high-risk patients with hereditary lipid disorders).

ADDRESS FOR CORRESPONDENCE: Dr. Sanjiv Kaul, Knight Cardiovascular Institute, Oregon Health & Science University, UHN 62, 3181 Southwest Sam Jackson Park Road, Portland, Oregon 97239. E-mail: kauls@ohsu.edu.

REFERENCES

1. Mali P, Yang L, Esvelt KM, et al. RNA-guided human genome engineering via Cas9. Science 2013;339:823–6.

2. Anders C, Niewoehner O, Duerst A, Jinek M, et al. Structural basis of PAM-dependent target DNA recognition by the Cas9 endonuclease. Nature 2014;513:569–73.

3. Kleinstiver BP, Prew MS, Tsai SQ, et al. Engineered CRISPR-Cas9 nucleases with altered PAM specificities. Nature 2015;523:481–5.

4. Friedland AE, Baral R, Singhal P, et al. Characterization of Staphylococcus aureus Cas9: a smaller Cas9 for all-in-one adeno-associated virus delivery and paired nickase applications. Genome Biol 2015;16:257.

5. Ribeiro LF, Ribeiro LFC, Barreto MQ, Ward RJ, et al. Protein engineering strategies to expand CRISPR-Cas9 applications. Int J Genomics 2018;2018:1652567.

6. Ma H, Marti-Gutierrez N, Park SW, et al. Correction of a pathogenic gene mutation in human embryos. Nature 2017;548:413–9.

7. Schlossarek S, Mearini G, Carrier L. Cardiac myosin-binding protein C in hypertrophic cardiomyopathy: mechanisms and therapeutic opportunities. J Mol Cell Cardiol 2011;50:613–20.

8. Mearini G, Stimple D, Geertz B, et al. Mybpc3 gene therapy for neonatal cardiomyopathy enables long-term disease prevention in mice. Nat Commun 2014;5:5515.

9. Long C, McAnally JR, Shelton JM, et al. Prevention of muscular dystrophy in mice by CRISPR/Cas9-mediated editing of germline DNA. Science 2014;345:1184–8.

10. El Refaey M, Xu L, Gao Y, et al. In vivo genome editing restores dystrophin expression and cardiac function in dystrophic mice. Circ Res 2017;121:923–9.

11. Amoasii L, Hildyard JCW, Li H, et al. Gene editing restores dystrophin expression in a canine model of Duchenne muscular dystrophy. Science 2018;362:86–91.

12. Schmitt JP, Kamisago M, Asahi M, et al. Dilated cardiomyopathy and heart failure caused by a mutation in phospholamban. Science 2003;299:1410–3.

13. Kaneko M, Hashikami K, Yamamoto S, Matsumoto H, Nishimoto T. Phospholamban ablation using CRISPR/Cas9 system improves mortality in a murine heart failure model. PLoS One 2016;11:e0168486.

14. George LA, Sullivan SK, Giermasz A, et al. Hemophilia B gene therapy with a high-specific-activity factor IX variant. N Engl J Med 2017;377:2215–27.

15. Rangarajan S, Walsh L, Lester W, et al. AAV5-factor VIII gene transfer in severe hemophilia A. N Engl J Med 2017;377:2519–30.

16. Cohen JC, Boerwinkle E, Mosley TH Jr., Hobbs HH. Sequence variations in PCSK9, low LDL, and protection against coronary heart disease. N Engl J Med 2006;354:1264–72.

17. Sabatine MS, Giugliano RP, Keech AC, et al. Evolocumab and clinical outcomes in patients with cardiovascular disease. N Engl J Med 2017;376:1713–22.

18. Ding Q, Strong A, Patel KM, et al. Permanent alteration of PCSK9 with in vivo CRISPR-Cas9 genome editing. Circ Res 2014;115:488–92.

19. Wang X, Raghavan A, Chen T, et al. CRISPR-Cas9 targeting of PCSK9 in human hepatocytes in vivo-brief report. Arterioscler Thromb Vasc Biol 2016;36:783–6.

20. Ran FA, Cong L, Yan WX, et al. In vivo genome editing using Staphylococcus aureus Cas9. Nature 2015;520:186–91.

21. Komor AC, Kim YB, Packer MS, Zuris JA, Liu DR. Programmable editing of a target base in genomic DNA without double-stranded DNA cleavage. Nature 2016;533:420–4.

22. Gaudelli NM, Komor AC, Rees HA, et al. Programmable base editing of A*T to G*C in genomic DNA without DNA cleavage. Nature 2017;55:464–71.

23. Chadwick AC, Wang X, Musunuru K. In vivo base editing of PCSK9 (proprotein convertase subtilisin/kexin type 9) as a therapeutic alternative to genome editing. Arterioscler Thromb Vasc Biol 2017;37:174–7.

24. Musunuru K, Pirruccello JP, Do R, et al. Exome sequencing, ANGPTL3 mutations, and familial combined hypolipidemia. N Engl J Med 2010;363:2220–7.

25. Dewey FE, Gusarova V, Dunbar RL, et al. Genetic and pharmacologic inactivation of ANGPTL3 and cardiovascular disease. N Engl J Med 2017;377:211–21.

26. Chadwick AC, Evitt NH, Lv W, Musunuru K. Reduced blood lipid levels with in vivo CRISPR-Cas9 base editing of ANGPTL3. Circulation 2018;137:975–7.

27. Fuster JJ, Walsh K. Somatic mutations and clonal hematopoiesis: unexpected potential new drivers of age-related cardiovascular disease. Circ Res 2018;122:523–32.

28. Jaiswal S, Natarajan P, Silver AJ, et al. Clonal hematopoiesis and risk of atherosclerotic cardiovascular disease. N Engl J Med 2017;37:111–21.

29. Sano S, Oshima K, Wang Y, Katanasaka Y, Sano M, Walsh K. CRISPR-mediated gene editing to assess the roles of Tet2 and Dnmt3a in clonal hematopoiesis and cardiovascular disease. Circ Res 2018;123:335–41.

30. Finn JD, Smith AR, Patel MC, et al. A single administration of CRISPR/Cas9 lipid nanoparticles achieves robust and persistent in vivo genome editing. Cell Rep 2018;22:2227–35.

31. Christiansen JP, French BA, Klibanov AL, Kaul S, Lindner JR. Targeted tissue transfection with ultrasound destruction of plasmid-bearing cationic microbubbles. Ultrasound Med Biol 2003;29:1759–67.

32. Porto AG, Brun F, Severini GM, et al. Clinical spectrum of PRKAG2 syndrome. Circ Arrhythm Electrophysiol 2016;9:e003121.

33. Xie C, Zhang YP, Song L, et al. Genome editing with CRISPR/Cas9 in postnatal mice corrects PRKAG2 cardiac syndrome. Cell Res 2016;26:1099–111.

34. Limpitikul WB, Dick IE, Tester DJ, et al. A precision medicine approach to the rescue of function on malignant calmodulinopathic long-QT syndrome. Circ Res 2017;120:39–48.

35. Landis BJ, Veldtman GR, Ware SM. Genotype-phenotype correlations in Marfan syndrome. Heart 2017;103:1750–2.

36. Zeng Y, Li J, Li G, et al. Correction of the Marfan syndrome pathogenic FBN1 mutation by base editing in human cells and heterozygous embryos. Mol Ther 2018;26:2631–7.

37. Fu Y, Foden JA, Khayter C, et al. High-frequency off-target mutagenesis induced by CRISPR-Cas nucleases in human cells. Nat Biotechnol 2013;31:822–6.

38. How to respond to CRISPR babies? Available at: https://www.nature.com/magazine-assets/d41586-018-07634-0/d41586-018-07634-0.pdf. Accessed January 9, 2019.

39. Human Genome Editing. Available at: https://www.nap.edu/catalog/24623/human-genome-editing-science-ethics-and-governance. Accessed January 2019.

KEY WORDS CRISPR, gene editing, germline gene correction

JACC: BASIC TO TRANSLATIONAL SCIENCE VOL. 4, NO. 1, 2019

EDITOR'S PAGE

What Are the Off-Target Effects of Plan "S" For Translational Investigators?

Douglas L. Mann, MD, *Editor-in-Chief JACC: Basic to Translational Science*

"There are known knowns; there are things we know we know. We also know there are known unknowns; that is to say we know there are some things we do not know. But there are also unknown unknowns—the ones we don't know we don't know."

—Donald H. Rumsfeld (1)

On September 4, 2018, a coalition of European and national research funding agencies announced the cOAlition S initiative, which will require all of the investigators they fund to make their papers free to read immediately upon publication by 2020. This ambitious plan, termed Plan "S," has the noble goal of maximizing the impact of research by allowing new research findings to be freely accessible to the public. Under the proposed framework of this plan, researchers will be required to publish their findings in pure open access (OA) journals (referred to as Gold OA). Plan "S" will specifically prohibit researchers from publishing in subscription journals (referred to as paywalled or toll access), and after a transition period, will also prohibit investigators from publishing in so-called hybrid journals that have both subscription and free content. Currently, the majority of scientific journals employ a hybrid business model, which allows authors to pay an additional fee if they want to publish their research OA immediately. Plan "S" will also preclude investigators from archiving their research in data repositories sponsored by universities or professional societies that allows the investigators to make their research OA after a prespecified period of time has passed (referred to as Green OA). Although some green OA journals permit immediate public archiving, many high-impact journals, such as *Nature*, *Cell*, and *Science*, do not permit public archiving until at least 6 months after the date of publication. Last, Plan "S" proposes that all gold OA research papers will have a liberal publishing license that allows anyone to download, translate, or otherwise reuse their work. As might be expected, publishing companies have pushed back on Plan "S," which they feel will undermine their business model and disrupt the entire research publishing system (2). Aside from the negative impact of Plan "S" on the publishing world, Plan "S" also has a less obvious, but potentially equally disruptive effect on investigators, particularly those investigators who engage in translational research, as will be discussed in the following text.

The most obvious concern is that Plan "S" will restrict the academic freedom of investigators by preventing them from publishing their research findings in the journals of their choice. As currently written, Plan "S" will bar researchers from publishing in ~85% of the existing journals, including high-impact journals such as *Cell*, *Nature,* or *Science*. Apart from the issue of publishing in high impact factor journals, Plan "S" may also prevent investigators from reaching their intended audience. As a translational investigator, I have had the liberty of publishing my research in journals that have either a clinical readership or a basic science readership, depending on the scope of the research project. It is unclear at the time of this writing whether this flexibility will exist under Plan "S." Plan "S" may also disrupt the collaborative nature of science, insofar as the publishing restrictions imposed by the plan may isolate European investigators by preventing them from publishing their findings with investigators who are not restricted to publishing in gold OA journals. As we have emphasized previously on these pages, translational research is, by its nature, team science (3).

From the Center for Cardiovascular Research, Cardiovascular Division, Washington University School of Medicine, St. Louis, Missouri.

ISSN 2452-302X https://doi.org/10.1016/j.jacbts.2019.01.005

Plan "S" may also ultimately increase the cost of publication for investigators. Although the architects of Plan "S" have indicated that they would pay for reasonable article-processing charges for gold OA journals, it is: 1) not clear how long this commitment will last; and 2) highly unlikely that this type support will last in perpetuity. Moreover, having lived through the painful research cuts to the National Institutes of Health budget following the 2007 to 2008 global financial crisis, it is not clear whether Plan "S" will be able to support publication charges when the next financial crisis comes. It is also not apparent, absent the economic margins provided by subscription fees and copyright licensing, that OA journals will be able to develop a sustainable business model without raising their article-processing fees. When the cOAlition S funding agencies withdraw their commitment to pay for article processing charges, these escalating costs will, by necessity, shift to the investigators.

However, the most potentially devastating aspect of Plan "S" from the perspective of investigators is that it may negatively affect the quality of scientific publishing. High-quality peer review and scientific rigor remains the cornerstone of subscription, hybrid, and pure OA publishing. Currently, many print and hybrid journals publish a limited number of papers with each issue, which allows the Editorial board to be selective with respect to the quality of the scientific papers that they publish. The economics of this model are possible because of the margins provided by subscription, advertising, and licensing fees. Given that Plan "S" will cap the article-processing charges, OA journals will need to publish more papers to remain financially viable. This poses a serious risk that the increase in the number of papers may lead to publication of papers that are of lower quality and originality. Further, it will be difficult to maintain the high quality of external peer reviewers and editorial boards if the reviewers and editors are asked to place finances before rigorous scientific review. Gold OA publishing may give new meaning to the expression publish or perish. Last, it is unclear what will happen to the research that is archived in the servers of gold OA journals that go out of business. Will the archived research disappear if the gold OA journal cannot sustain itself, or will the cOAlition S funding agencies agree to pay for the research to be publicly archived indefinitely?

IS PLAN "S" A STEP FORWARD OR A MISSTEP?

As the editor-in-chief of an OA journal, I would be completely hypocritical if I did not acknowledge the benefits of the OA publishing format. The pace of scientific discovery has increased so rapidly over the past decade that the transition to some form of OA publishing for print journals is inevitable. Indeed, this is the reason why most journals have adopted a hybrid publishing model. Plan "S" will, undoubtedly further hasten the transition to full OA publishing, and thus has the appearance of being a step forward for science. However, as I have tried to articulate in the foregoing Editor's Page, there are too many "unknown unknowns" with respect to the potential off-target effects of Plan "S," particularly for translational scientists. Given this uncertainty, perhaps the smart move would be to hit the pause button on the roll-out for Plan "S" until after we have a clearer understanding of the full societal impact of this ambitious plan. As always, we welcome comments and suggestions from investigators in academia and industry, patients, societies, and all of the governmental regulatory agencies to share your thoughts about the best models for scientific publishing, either through social media (*#JACC:BTS*) or by e-mail (jaccbts@acc.org).

ADDRESS FOR CORRESPONDENCE: Dr. Douglas L. Mann, *Editor-in-Chief JACC: Basic to Translational Science,* American College of Cardiology, 2400 N. Street NW, Washington, DC 20037. E-mail: JACC@acc.org.

REFERENCES

1. Rumsfeld DH. DoD News Briefing—Secretary Rumsfeld and Gen. Myers, February 12, 2002. Available at: http://archive.defense.gov/Transcripts/Transcript.aspx?TranscriptID=2636. Accessed January 20, 2019.

2. Else H. Radical open-access plan could spell end to journal subscriptions. Nature 2018;561:17–8.

3. Mann DL, Annex BH, Bishopric NH, et al. Introducing JACC: Basic to Translational Science: why now? J Am Coll Cardiol Basic Trans Science 2016;1:1–2.

JACC: BASIC TO TRANSLATIONAL SCIENCE
VOL. 4, NO. 1, 2019
ISSN 2452-302X

CORRECTION

Li Z, Organ CL, Kang J, Polhemus DJ, Trivedi RK, Sharp III TE, Jenkins JS, Tao Y, Xian M, Lefer DJ

Hydrogen Sulfide Attenuates Renin Angiotensin and Aldosterone Pathological Signaling to Preserve Kidney Function and Improve Exercise Tolerance in Heart Failure

J Am Coll Cardiol Basic Trans Science 2018;3:796–809.

In the section "Delayed treatment with JK-1 ameliorates renal dysfunction and reduces renal fibrosis in HF" the citations for Figure 4 were incorrectly identified.

The corrected section is below.

DELAYED TREATMENT WITH JK-1 AMELIORATES RENAL DYSFUNCTION AND REDUCES RENAL FIBROSIS IN HF. The effect of JK-1 on renal function in HF was assessed at 18 weeks post TAC by plasma creatinine measurements. Mice treated with Control exhibited impaired renal function as shown by elevated plasma creatinine levels that were compared to Sham mice. Mice treated with JK-1 initiated at 3 weeks post TAC and 10 weeks post TAC displayed significant reductions in plasma creatinine levels, indicating preserved renal function (Figure 4A). In addition, histological assessment of Picro Sirius red-stained kidney sections revealed increased renal fibrosis in mice subjected to the TAC procedure and those that received Control treatment. Contrary to our observation in cardiac fibrosis, we saw significantly lessened amounts of renal fibrosis in mice that received 3-week-delayed or 10-week-delayed JK-1 treatment (Figures 4B and 4C). Furthermore, both 3-week- and 10-week-delayed JK-1 treatment significantly mitigated the transcription of interleukin-6 and connective tissue growth factor in the kidney, whereas only 3-week-delayed treatment significantly reduced the transcription of collagen 1a1 and fibronectin (Figure 4D).

The authors apologize for this error.

The current online version has been corrected.

https://doi.org/10.1016/j.jacbts.2019.01.001